Transformable Deterministic Sampling

Daniel Frisch

Transformable Deterministic Sampling

Zur Erlangung des akademischen Grades eines

Doktors der Ingenieurwissenschaften

von der KIT-Fakultät für Informatik
des Karlsruher Instituts für Technologie (KIT)

genehmigte

Dissertation

von

Daniel Frisch

aus Freudenstadt

Tag der mündlichen Prüfung:	19.02.2024
Erster Gutachter:	Prof. Dr.-Ing. Uwe D. Hanebeck
Zweiter Gutachter:	Professor Simon Maskell

Acknowledgment

This work was written as part of my research activities carried out at the Intelligent Sensor-Actuator-Systems (ISAS) laboratory, Institute for Anthropomatics and Robotics (IAR), Karlsruhe Institute of Technology (KIT), led by Prof. Uwe Hanebeck.

Thinking back, my interest in technical things started early in childhood, facilitated by my parents informally and also formally with e.g. Fischertechnik construction kits. It went on through dissecting and repairing (sometimes irreparably) all kinds of appliances with Philips screws. Later during my school career, certain teachers, like Dr. Wolfgang Brandenbusch, also a KIT graduate, were able to convey a glimpse of the depth of knowledge waiting beyond the curriculum. Like him, I studied Electrical Engineering and Information Technology (ETIT) at KIT, being exposed to lecturers like Fernando Puente, Friedrich Jondral, Gert Trommer, and Olaf Dössel, perpetuating the spark of interest in understanding technical relationships. I am very grateful to my parents, Karl-Heinz and Annette, for making this possible with their support.

After that, Prof. Hanebeck gave me the opportunity to work in his lab. I am very grateful for his constant support and motivation by proposing, whenever needed, interesting research questions rich in variety. He is not just an organizer, but always fully aware of the entirety of technical details of all research going on at his institute. Especially fun are the mutual technical conversations where new ideas seem to spark on both sides every time. I once read that Nobel laureate Klaus Hasselmann saw his institute as a kind of greenhouse with lots of growing plants and that his role was to water and fertilize here and there, but otherwise let the “plants” – i.e.

his employees – flourish undisturbed. This comforting experience is also what I feel at ISAS.

Finally, the friendly and cooperative atmosphere of like-minded, research-interested, capable colleagues was and is very pleasant. I want to express my gratitude to all of them, especially Kailai Li, whom I had a lot of casual conversations with, Gerhard Kurz, who introduced me to various topics in the very beginning, the late Christian Tesch as my first office colleague, Benjamin Noack, Florian Rosenthal, Johannes Westermann, Jana Mayer, Susanne Radtke, Marcel Reith-Braun, Michael Fennel, Dominik Prossel, and Jiachen Zhou. I also want to thank our team of technicians who know how to get "real things" done, Alexander Riffel, Sascha Faber, Achim Langendörfer, the meanwhile retired secretary Dagmar Gambichler, and the new secretary Pia Haberlag.

Karlsruhe, March 2025 Daniel Frisch

Contents

Notation

General Conventions

x	scalar value
$\underline{x}$	vector
$\boldsymbol{x}$	random variable
$\mathbf{A}$	matrix

Abbreviations

1D	one-dimensional / univariate
2D	two-dimensional
3D	three-dimensional
4D	four-dimensional
CKF	Cubature Kalman Filter
CLT	Central Limit Theorem
EM	expectation–maximization
iid	independent identically distributed
LCD	Localized Cumulative Distribution
LRKF	Linear Regression Kalman filter
ODE	ordinary differential equation
PCD	projected cumulative distribution
S^{2}KF	Smart Sampling Kalman Filter
SND	standard normal density
UKF	Unscented Kalman Filter
vMF	von Mises–Fisher
wce	worst-case error

CHAPTER 1

Introduction

Contents

> The generation of random numbers
> is too important to be left to chance.
>
> Robert R. Coveyou (1915 – 1996)

This thesis describes methods for drawing deterministic samples from non-uniform multivariate densities. These methods are not yet widely used. Instead, people use independent identically distributed (iid) (pseudo-)random samples that are locally very inhomogeneous. In deviation from this, we deal with deterministically placed samples, aiming for a high degree of local homogeneity of the samples (or the gaps between them). Depending on the use case, this leads to faster convergence of calculations, more consistent fulfillment of requirements, or better space use.

Supplementary material, like presentations, figures tables, and code can be found online[1] or will be added on request.

1.1 Terminology

Because sampling is a natural part of our everyday lives in various contexts, extensive terminology refers to it.

Sampling may also be called placing, selecting locations, stacking, arranging, building, designing, distributing, drawing, packing, or covering.

Samples may also be called objects, points, sigma points, particles, vertices, nodes, knots, or abscissas.

Sample sets may also be called vertex arrangements, point clouds, ensembles, groups, arrangements, patterns, or clusters.

[1] `https://github.com/KIT-ISAS/Dissertation_Frisch_Supplementary`

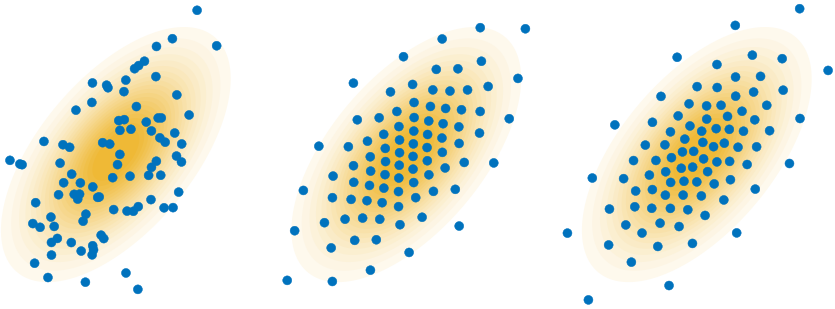

(a) Random **(b)** Fibonacci **(c)** LCD

Figure 1.1: Not all Gaussian sampling is the same. Different methods to draw samples from the same 2D Gaussian density. Showing iid samples (a) and deterministic sampling methods (b+c).

1.2 Applications of Sampling. Why Deterministic Sampling?

Here are some examples where sampling is used, with reference to the advantages that deterministic sampling brings.

1.2.1 Short Examples

1.2.1.A (State Estimation) In nonlinear recursive state estimation or filtering, the occurring probability densities cannot be represented in closed form. Standard approximation methods involve discrete representations of the densities using samples. This simplifies density representation and state propagation [O2], [145]. Deterministic sampling yields faster convergence (with respect to the number of samples) to the true result.

1.2.1.B (Control) In control problems, on top of the state estimation problem, an appropriate control trajectory has to be found. This can be done by sampling from the space of control trajectories and implementing the one with the best outcome. Deterministic sampling facilitates a more

(a) Spotlight (concentric circular arrangement).

(b) Spotlight (square arrangement).

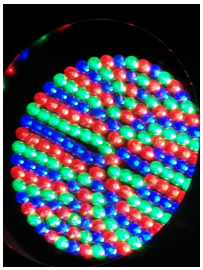

(c) RGB spotlight (unstructured arrangement).

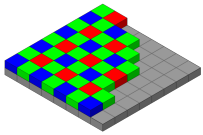

(d) RGB Bayer filter (square arrangement) [22].

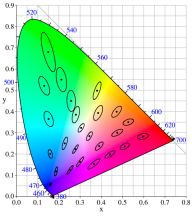

(e) MacAdam diagram [23].

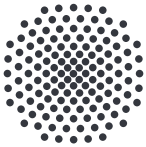

(f) Logo Uni Stuttgart [165].

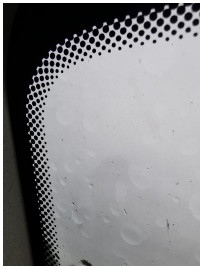

(g) Frits on car window.

(h) Shower head [62].

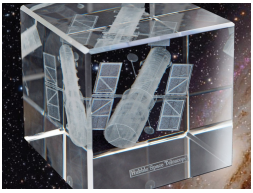

(i) Subsurface Laser Engraving [119]

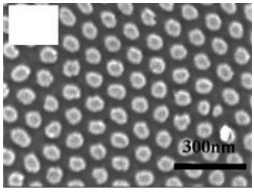

(j) Ferroelectric nanoislands as capacitors [56].

(k) Concentrated solar power [24].

Figure 1.2: Object arrangement in technology and everyday life.

homogeneous space coverage, thereby improving efficiency. See for example [54], [71], [53], [81].

1.2.1.C (Integration) An elementary method for quadrature, i.e., numerically solving 1D integrals, is the rectangle rule. It uses equidistant samples. Choosing an appropriate ensemble in the higher-dimensional equivalent is not trivial. More about this below, in Section 1.2.2.

1.2.1.D (Partial Differential Equations) Partial differential equations can often not be solved in closed form, only numerically in a discretized form, e.g., via the Finite Difference Method or the Finite Element Method. Deterministic samples are one possibility to achieve an efficient, homogeneous coverage of the considered domain with a numerically beneficial shape of the Delaunay simplices of the mesh [101].

1.2.1.E (Optimization) To find the global extremum of a multivariate, multimodal, and nonconvex function, it can be evaluated on a set of samples that uniformly cover the relevant area, narrowing the search space. Deterministic samples cover the space more homogeneously, thereby making the search more efficient [121].

1.2.1.F (Representation of Densities) Sample sets can be used as a discrete representation of probability densities. In this form, it is straightforward to propagate them through state transition models and to compute expectation values. Deterministic samples yield a more locally homogeneous space coverage according to the probability mass, thereby increasing the expressiveness (see Figure 1.1).

1.2.1.G (Modulation) Digital information transmission using high-frequency signals requires encoding the information stream into signal properties like phase and amplitude. Such modulated signals can be represented in the 2D constellation diagram, where several regions with their corresponding symbols must be defined. For example, the Quadrature

amplitude modulation (QAM) scheme uses a square arrangement. Deterministic samples have always been used here to maximize the efficiency of the communication channel.

1.2.1.H (Color Palettes) To show figures with many different plot lines that should be distinguishable by color (e.g., Figure 8.12), we need a set of distinguishable discrete colors as a color palette. The MacAdam ellipse gives the perceived color distance in a chromaticity diagram [115], where the ellipse size depends on the respective color (see Figure 1.2e). A sound palette would place the colors more densely in regions where the MacAdam ellipses are small and vice versa. With deterministic sampling, the selected colors will be locally homogeneous, e.g., no two colors are randomly much more similar than all the other neighboring pairs.

1.2.1.I (Subsurface Laser Engraving) In subsurface laser engraving (SSLE), microcracks are introduced inside a transparent object [96], [168]. Each of these cracks is visible as a small dot. By varying the point density, 3D probability densities and also objects like construction plans can be visualized with this technology. Since the microcracks must be discrete, separated points, the object to be visualized first has to be converted into a discrete representation via sampling (see Figure 1.2i).

1.2.1.J (Arrangement of Objects) A sampling strategy also has to be decided on whenever it is necessary to arrange multiple similar objects side by side. Examples are LEDs in a spotlight, photodetectors and color filters on CCDs, frits on a car window, boreholes in sieves and shower heads, capacitors in computer memory, and mirrors in concentrated solar power plants (see Figure 1.2). Furthermore, think of packing cannonballs, distributing seats in a hall, placing surveillance cameras and weather stations, designing a network of buoys for water temperature observation. Even finding a place on the sunbathing lawn and choosing a locker at the gym is a sampling problem – it is solved deterministically as soon as one tries to maximize the distance to the neighbors.


(a) Centaurea.


(b) Dipsacus.


(c) Brassica.

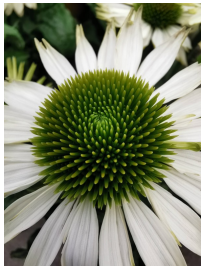
(d) Echinacea.

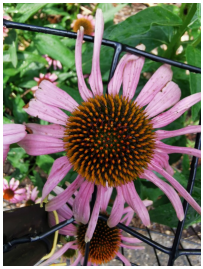
(e) Echinacea.

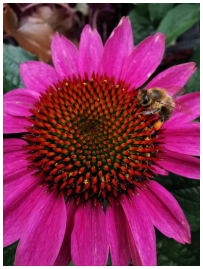
(f) Echinacea.


(g) Bellis perennis.


(h) Leucanthemum.


(i) Leucanthemum.


(j) Helianthus.


(k) Wasp nest [25].

Figure 1.3: Object placement in nature, often exhibiting Fibonacci lattices for growing objects and hexagonal arrangements for fixed-size objects.

Some of these application scenarios involve reproducing a desired non-uniform density function, while others just strive for an efficient packing of identical objects. The latter is a special case and will concern us more on the periphery.

1.2.1.K (In Nature) In plant life, clusters of flowers or seeds, called inflorescences, are often arranged to maximize space utilization under the constraint of continuous radial growth – this is discussed further in Section 3.3.1.D. Due to the size and number of seeds, the pattern is especially striking in the Helianthus but is also visible in many other plants (see Figures 1.3 and 1.4).

Honey bees must arrange clusters of objects fixed in size, tubes to raise new brood, and store honey and pollen. They do it in a hexagonal pattern that maximizes space utilization (without the growth constraint as in inflorescences). Similarly, social wasps build nests with hexagonal cells made of paper instead of wax (see Figure 1.3k).

1.2.2 Cubature

We focus especially on multivariate numerical integration or cubature as application area of (deterministic) sampling, so we highlight it in detail here. Cubature is the multivariate equivalent of 1D integration or quadrature that can be solved, e.g., with the rectangular or midpoint rule.

In general, to solve the integral

$$I_s(g) = \int_{[0,1]^s} g(\underline{x}) \, \mathrm{d}\underline{x} \ ,$$

it is discretized as

$$Q_s(g; \mathcal{P}_L) = \frac{1}{L} \sum_{\underline{x} \in \mathcal{P}_L} g(\underline{x}) \ ,$$

using a point set $\mathcal{P}_L$ consisting of L points $\underline{x} \in [0,1]^s$. We are particularly interested in how the integration error

$$\epsilon_{L,g} = |I_s(g) - Q_s(g; \mathcal{P}_L)| \tag{1.1}$$

depends on the number L as well as the construction method of the samples $\mathcal{P}_L$.

Figure 1.4: Leucanthemum versus Fibonacci–Kronecker lattice in polar coordinates.

1.2.2.A (The Common Method: iid Random Samples or Monte Carlo) Most commonly, iid random samples are chosen. In that case, the behavior of the integration error $\epsilon_{L,g}$ is given by the Central Limit Theorem (CLT)

[16, Sec. 2.1], [41, p. 244]. It states that the Monte Carlo integration error $\epsilon_{L,g}$ of an arbitrary square-integrable function $g(\cdot)$ over the s-dimensional unit cube $[0,1]^s$, using a large number L of iid uniform random samples $\underline{x}_n \in [0,1]^s$, is normally distributed with standard deviation $\sigma_g \cdot L^{-1/2}$, where

$$\sigma_g^2 = \int_{[0,1]^s} \left(g(\underline{x}) - \left(\int_{[0,1]^s} g(\underline{\tilde{x}}) \, \mathrm{d}\underline{\tilde{x}} \right) \right)^2 \mathrm{d}\underline{x} \ . \tag{1.2}$$

Thus, $\epsilon_{L,g}$ depends only on the standard deviation σ_g but not on the smoothness of g. Indeed, for general square-integrable integrands g, which could be white noise, the convergence rate of $L^{-1/2}$ is the best we can get [7].

- Advantages
  - Unbiased estimator.
  - Convergence rate does not depend on dimension s.
  - Convergence rate does not depend on smoothness of f.
  - Practical error estimate [35, pp. 139f].
- Disadvantages
  - Slow convergence rate of $L^{-1/2}$.

1.2.2.B (The Deterministic Method: Low-Discrepancy Sampling or Quasi–Monte Carlo) For smooth integrands, convergence can be vastly improved (compared to iid random samples) by using quasi-random or low-discrepancy samples. This is also called quasi–Monte Carlo method. The relevant cubature error $\epsilon_{\mathcal{P}_L,g}$ estimation is the Koksma-Hlawka identity

$$\epsilon_{\mathcal{P}_L,g} \leq \mathrm{discr}^*_\infty(\mathcal{P}_L) \cdot V(g) \ , \tag{1.3}$$

for point set $\mathcal{P}_L$ consisting of L samples $\underline{x} \in [0,1]^s$ and its discrepancy $\mathrm{discr}^*_\infty(\mathcal{P}_L)$. The smoothness of the integrand is incorporated via its variation in the sense of Hardy and Krause $V(g)$. This is discussed further in Section 5.1.1. The important point here is that for all integrands g with finite variation $V(g)$, we obtain good integration results by choosing point sets $\mathcal{P}_L$ with low discrepancy $\mathrm{discr}^*_\infty(\mathcal{P}_L)$. It is known that point sets with

a discrepancy of $(\log(L))^{s-1}L^{-1}$ do exist [11]. This implies a cubature convergence rate of the same order.

- Advantages
  - Superior convergence rate of $(\log(L))^{s-1}L^{-1}$.
  - Reproducible.
- Disadvantages
  - Best low-discrepancy point set not always known, especially in higher dimensions.
  - Convergence rate gets worse with higher dimensions.
  - Randomization needed for unbiasedness and error estimate [35, pp. 155ff].

1.2.3 Gaussian Density Representation

Another important application of sampling is density representation, e.g., for propagation through state transition models. The most important density function is the Gaussian or normal density.

1.2.3.A (Independent Random Samples) The most commonly used discrete density representation involves iid samples again. These Gaussian samples can be produced, e.g., by transforming iid uniform samples with the Box-Muller method [12]. The independence of the samples inevitably leads to locally uneven coverage, with colliding samples on the one hand and uncovered holes on the other (see Figure 1.1 a). Computations on random ensembles, like expectation value computations, have slow convergence, as described in Section 1.2.2.A.

- Advantages
  - Arbitrary number of samples.
  - Fast computation.
- Disadvantages
  - Locally inhomogeneous distribution.

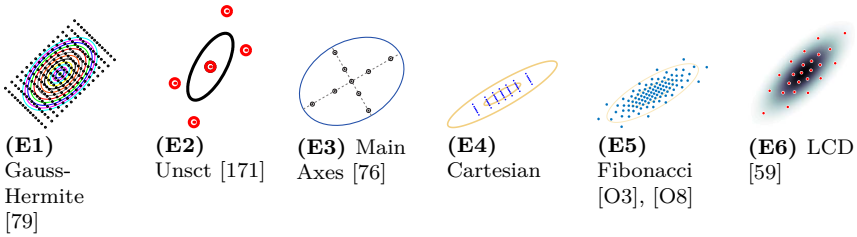

(E1) Gauss-Hermite [79]
(E2) Unsct [171]
(E3) Main Axes [76]
(E4) Cartesian
(E5) Fibonacci [O3], [O8]
(E6) LCD [59]

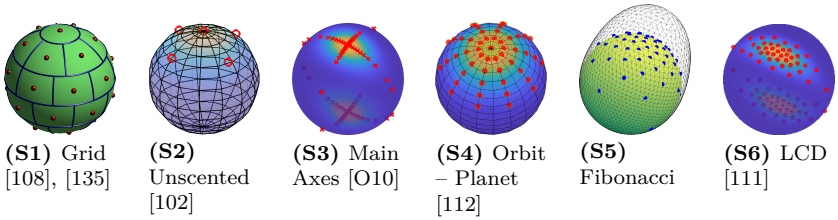

(S1) Grid [108], [135]
(S2) Unscented [102]
(S3) Main Axes [O10]
(S4) Orbit – Planet [112]
(S5) Fibonacci
(S6) LCD [111]

Figure 1.5: Different types of deterministic Gaussian sampling in Euclidean space (top, E) and von Mises–Fisher (vMF) and Bingham sampling on the spherical domain (bottom, S). Figures are captured from the stated references. First column (E1, S1) shows uniform-grid-based filters with individually weighted samples, second column (E2, S2) moment matching, other columns equally weighted samples. Note that LCD samples (E5, S6) are much slower to compute than all others. This work focuses on low-discrepancy sampling with Fibonacci lattices on the sphere (S5), as it produces high-quality results *and* is fast.

1.2.3.B (Deterministic: Moment Matching) The most commonly used deterministic Gaussian samples are based on moment matching, yielding a finite set of weighted samples. For example, Gauss-Hermite quadrature uses a certain set of weighted samples and is ideally suited for scalar integrals of polynomial-like functions that are multiplied with a 1D Gaussian density function [159]. In higher dimensions, this requires the Cartesian product of the evaluation points [78, Eq. 3.3], [79] (see Figure 1.5 E1). Thus, the number of required points increases exponentially with the number of dimensions.

To avoid this "curse of dimensionality", one can place samples on the main axes only [75] (see Figure 1.5 E3). A more radical variant is the Unscented Kalman Filter (UKF), where only two samples, "sigma points", are placed

on each coordinate axis [84], [87], plus optionally one in the center, i.e., the number of samples is $L = 2s$ or $L = 2s + 1$ for dimension s (see Figure 1.5 E2). The coordinates are chosen such that mean and covariance match. Very similarly, the 3rd order Cubature Kalman Filter (CKF) places two samples on each coordinate axis, without the sample at the mode, hence $L = 2s$ [5]. The 5th order CKF employs instead $L = 2s^2 + 1$ weighted samples [82], see also [29, Sec. 7], [136, Eq. 48+49]. The smallest possible sample set suitable to propagate mean and covariance has been explored in [85], [130] – it takes only $L = s + 1$ or $L = s + 2$ samples.

- Advantages
  - Simple and fast (only the methods with few samples).
- Disadvantages
  - Weighted samples mostly.
  - Fixed number of samples.
  - Ideal only for certain types of integrands (e.g., polynomials).

1.2.3.C (Deterministic: Nonlinear Optimization of a Metric) Now, we focus on methods that allow the number of samples to be flexibly adapted to the problem and the desired accuracy. Given a suitable distance or optimality measure such as the Localized Cumulative Distribution (LCD) [60], optimal deterministic Gaussian sample sets can be computed using gradient optimization [59], [48] (see Figures 1.1 c, 1.5 E6 and 2.2 c). As this kind of sampling process is itself computationally expensive, for practical filtering, it is necessary to compile a library of *standard* normally distributed samples beforehand and transform them to the desired arbitrary Gaussian density online using the Cholesky factorization of the covariance matrix [161], [162], [164]. After such transformation, however, the samples are no longer optimal as before (see Figure 2.2 a). One contribution of this work is conditional deterministic sampling, which somewhat improves the transformability of LCD-based Gaussian samples.

- Advantages
  - Very locally homogeneous.
  - Arbitrary number of samples.

  - Computational load does not increase exponentially with dimension.
- Disadvantages
  - Expensive computation.
  - Badly transformable (e.g., to other density parameters).

1.2.3.D (Deterministic: Orthogonal Inverse Transform of Low-Discrepancy Point Sets) One main contribution of this work is the orthogonal inverse transform of low-discrepancy samples. It can produce locally homogeneous samples of density functions with an orthogonal inverse transform. Discussed further in Section 6.7. For visual examples of Gaussian samples, see Figures 1.1 b and 1.5 E5.

- Advantages
  - Very locally homogeneous.
  - Arbitrary number of samples.
  - Fast computation.
  - Well transformable.
- Disadvantages
  - Need orthogonal inverse transform.
  - Need suitable uniform low-discrepancy point set.

1.3 Riemannian Manifolds

The above examples are usually considered in Euclidean spaces. However, their treatment in Riemannian manifolds becomes more and more critical.

1.3.1 Applications

For example, in modern wireless communications, the angle of arrival (AoA) distribution is modeled with spherical densities to facilitate highly efficient data transmission using multiple input multiple output (MIMO) techniques [116]. Wind directions in weather simulations [66] can only be truthfully represented via a vector field with vectors from Riemannian manifolds.

Robotic design, kinematics, and path planning require optimization, state estimation, and control on hyperspheres and hypertori [42], [17]. Aircraft require sophisticated balancing control. Their state is best represented via quaternions that, in turn, require a hyperhemispherical manifold [176].

Computations are often performed on linearized Euclidean tangent spaces of the underlying Riemannian manifolds. This works well if uncertainties are small. However, with greater uncertainty, performing the calculations directly on the nonlinear manifold becomes increasingly essential. If a significant part of the probability mass protrudes beyond periodicity limits, the result will be distorted even with an optimally selected linearization point. Drones and robots have become smaller and more versatile. Therefore, the predictions of the internal motion models (that must reflect the physical capabilities) become more uncertain: a small drone can make sudden changes in direction and speed that a passenger aircraft would not be physically capable of. Weather simulations get more fine-grained, and the individual forecasts, limited to smaller areas, are more unstable. Products are pushing into the mass market, equipped with more but cheaper sensors that provide unreliable measurement data. In summary, processing uncertain sensor data on nonlinear manifolds becomes increasingly essential.

1.3.2 Spherical Sampling Methods

Just as with the Euclidean space [87], the most widely used deterministic sampling method is based on moment matching. Transferred to hyperspheres, trigonometric moments are to be matched [102] (see Figure 1.5 S2). Again, the major limitation is that the number of samples is fixed and cannot be adapted to the problem's difficulty. Furthermore, how many and which moments should be considered is usually unclear. The number of samples may be increased somewhat by placing more samples on the spherical "main axes" [O10], [109] (see Figure 1.5 S3).

However, this approach still misses the areas apart from the main axes, so the probability mass there is not adequately represented. This can be improved by using an "orbit-planet" sample arrangement [110], [112] (see Figure 1.5 S4). It can be seen as mapping a regular Cartesian lattice to the sphere. However, this leads to the "concatenation" of samples to circular rings near the pole and lines near the equator, yielding locally bad space coverage. By using, instead of the regular lattice, a low-discrepancy point set (a main contribution of this work), we get a much more locally homogeneous result (see Figure 1.5 S5). And it is likewise cheap to compute.

Another contribution of this work is applying the LCD directly in the spherical domain [O9], [111] (see Figure 1.5 S6) without using a tangent space. These samples also provide very locally homogeneous state space coverage according to the desired density, arguably the best. However, one must solve a nonlinear optimization problem to obtain the samples, which might be too expensive for real-time applications.

1.4 State of Art

1.4.1 Variance Reduction

Deterministic sampling falls into the broader class of variance reduction techniques [107]. Variance reduction techniques for expectation value computation include antithetic variates [55], control variates [117], [150], importance sampling [169], stratified sampling [131], low-discrepancy or quasi-random sampling [156], [35], moment matching [87], [86], [118], [149], LCD based sampling [60], [59], [162], and Projected Cumulative Distribution (PCD) based sampling [58], [139]. These methods can also be combined, e.g., LCD based sampling with moment matching and antithetic variates [164].

Combinations of probability density functions and system equations such that the Bayesian inference problem can be solved analytically, are called conjugate priors [44]. In such cases, sample-based approximation (Section 1.2.2) is of course neither necessary nor advisable. Sometimes, a

part of the dependencies described by the system equations is tractable and another part intractable. In such case, we ideally take advantage of available closed form solutions and employ sample-based approximations only to the densities involved in the intractable dependencies. This is also referred to as Rao-Blackwellization [14].

1.4.2 Low-Discrepancy Point Sets

The most well-known and widely used low-discrepancy point set for higher dimensions is probably the Sobol sequence [83], [158]. It is readily available (for $s \leq 1111$) in numerous programming languages like Matlab (`sobolset` class), Julia (`Sobol` module), Python (`scipy.stats.qmc.Sobol` class), and R (`runif.sobol` function in `fOptions` package). Other choices are the Faure sequence [6], [40], and the Niederreiter sequence [122]. All of these are so-called (t-s)-sequences.

Since the globally optimal 2D point set, the Fibonacci lattice, and related variants of it, come not as (t-s)-sequence but as rank-1 lattice, Kronecker lattice, and Frolov lattice, we focus on the latter types of low-discrepancy point sets in the remainder of this work.

1.4.3 Open Questions

The LCD has been applied in the Euclidean space and, for Riemannian manifolds, in their Euclidean tangent spaces, but it has not been adapted and defined directly in a Riemannian manifold before this work. Furthermore, a subsequent transformation of LCD samples to adjust, e.g., second order moments, is not anticipated and often reduces their local homogeneity.

The local homogeneity of uniform point sets is often quantified by dispersion, i.e., the radius of the largest point-free circle (ball, hyperball) that can be placed in there. While the discrepancy has already been extended to non-uniform measures, the dispersion has not.

Transforming uniform low-discrepancy into non-uniform low-dispersion point sets is known only for product-type densities.

There are three types of 2D Fibonacci lattices: a rank-1 lattice, a Kronecker lattice, and a Frolov lattice, all with very similar appearance and properties. While the formal connection between the Fibonacci–rank-1 and –Kronecker lattice coordinates is trivial and obvious, a connection to the Fibonacci–Frolov lattice coordinates has not been established.

There is a reproducing kernel Hilbert space with associated worst-case integration error whose minimization yields precisely the 2D Fibonacci–rank-1 lattice. This has not been explored in higher dimensions or adapted to Kronecker lattices.

Constructions of globally optimal low-discrepancy point sets, like the Fibonacci lattice in 2D, are not available in higher dimensions. Even non-constructive statements on the "lowest-possible-discrepancy" point sets regarding the precise order with respect to L is considered the "Grand Open Problem" of discrepancy theory [3], [64, p. 418].

1.5 Overview

1.5.1 About Sampling

1.5.1.A (What is Sampling?) The goal of sampling is to obtain point locations or samples such that the resulting point cloud exhibits certain properties. The space of possible such properties includes the probability density, independence, smoothness or local homogeneity, dimension, number of samples, and convergence rate for numerical approximations.

1.5.1.B (Not All Sampling Is the Same) Most people are aware only of iid sampling and unscented sampling and use only those two, despite the poor local homogeneity and convergence rate of the former and the fixed and often too small number of samples of the latter. We present alternatives (see Figures 1.1 and 1.5) that allow for more efficient and accurate computations in many fields of application.

1.5.1.C (Fibonacci Spirals) For more than hundred years, people have wondered about the "Fibonacci spirals" ubiquitous in nature (especially striking in the sunflower) and their relation to the golden ratio and Fibonacci numbers. This work contributes some little-known and some novel puzzle pieces to this fascinating topic.

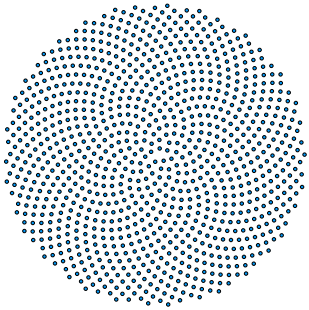

1.5.2 About This Thesis

1.5.2.A (Structure) Chapter 2 presents three deterministic sampling methods (LCD, PCD, and PoVuD) and variations thereof. All are based on computationally expensive numerical optimization; therefore, caching is necessary for real-time applications. However, caching is complicated by the fact that these samples degrade in local homogeneity when transformed.

Chapter 3 introduces four basic types (rank-1 lattice, Kronecker sequence, Kronecker lattice, and Frolov lattice) of uniform point sets in $[0,1]^s$, $s \in \mathbb{N}$, detailing their mathematical representation, various ways of construction, and practical methods of enumeration. Special attention is given to relationships between the well-known Fibonacci–rank-1 lattice, the well-known Fibonacci–Kronecker lattice, and the little-known Fibonacci–Frolov lattice in 2D.

Chapter 4 gives a deep insight into the Fibonacci–Frolov lattice. This is a fascinating topic because Fibonacci-based constructions are ubiquitous in plant life. We also present a possible generalization to higher dimensions.

Chapter 5 treats optimality measures and consequent optimization-based construction of rank-1 lattices and Kronecker sequences. This leads to a number of superior, novel point sets.

Chapter 6 constitutes the main contribution of this work. An optimality measure (dispersion) for uniform point sets is generalized to non-uniform continuous densities. Furthermore, the known relation between two optimality measures (dispersion and discrepancy) for uniform point sets is generalized to non-uniform and transformed point sets. This enables a sampling strategy for non-uniform densities using a uniform reference point set (Chapters 3 to 5) and an orthogonal transformation, yielding locally homogeneous samples if the reference point set is low-discrepancy.

Chapter 7 describes the above sampling method (orthogonal transform of low-discrepancy samples) concretely for various multivariate densities. We cover arbitrary independent densities, the Gaussian density, the hyperspherical uniform density, the hyperspherical von Mises–Fisher density, and arbitrary densities using acceptance-rejection.

Chapter 8 gives a quantitative evaluation of the presented sampling methods based on a number of optimality measures.

Chapter 9 summarizes and concisely lists the contributions and novelties in this work.

Appendix A contains the same plots as Chapter 8 but with a greater range of samples.

Appendix B contains an extensive compilation of figures showing the sample sets of all the uniform construction methods presented in Chapters 3 to 5 for various numbers of samples.

Appendix C contains numerical tables with rank-1 lattice and Kronecker sequence generators obtained via brute force numerical optimization from Chapter 5. The content is such that it can be copy-pasted directly into program code.

1.5.2.B (Reading Paths) Any direct sampling method in Chapter 2 is self-contained, with more details given in the specified references of the original works.

Chapters 4 to 5 presuppose the definitions brought forward in Chapter 3.

Interesting insights regarding Fibonacci–based construction are located in Sections 3.3.1.D, 3.3.2.A, 3.3.3.A, 3.3.4.D, 5.1.5.C, 5.2.2.B, 6.8.1, 8.1.4.B, 8.2.1.B, 8.2.2.A and 8.3.1.B, Chapter 4, and Appendix B.1.

Chapter 6 presupposes the definitions brought forward in Section 5.1.

Chapter 7 presupposes the insights brought forward in Chapter 6.

1.6 Summary

In this introduction, we have discussed how deterministic sampling is part of our everyday lives in many ways without us even thinking about it. Then, we compared random sampling, widely used in engineering, with deterministic sampling. Furthermore, the necessity of sampling on Riemannian manifolds has been discussed. We concluded with an overview of this work and an indication of which chapters build on each other.

CHAPTER 2

Direct Deterministic Sampling

Contents

We are all special cases.

Albert Camus (1913 – 1960)

In this chapter, we compute locally homogeneous, deterministic samples for a specific density function. The general procedure is to minimize a distance measure D between a given density $\tilde{f}(x)$ and a sought density $f(\underline{x})$ of a different type, particularly a Dirac mixture density. As there are no further restrictions, we can potentially reach the best sampling quality that can be attained. However, computation is quite costly and has to be repeated for every different set of density parameters. In Section 2.2.2, we take a first step towards transformable sampling. In the following chapters, transformable sampling will become the central theme of this work.

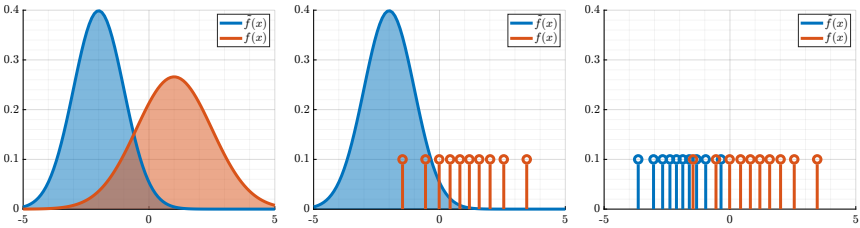

(a) Continuous vs Continuous **(b)** Continuous vs Discrete **(c)** Discrete vs Discrete

Figure 2.1: Pairs of continuous and discrete densities, to be compared with suitable distance measures. Simple distance measures like the Kullback-Leibler-divergence only work if both densities are continuous (a).

2.1 Simple Density Distances

Continuous densities can be easily compared via distance functions that, for every $\underline{x}$, take into account only the two scalar values $\tilde{f}(\underline{x})$ and $f(\underline{x})$, yielding a "local distance function" d of the two densities $\tilde{f}, f$,

$$d\big(\underline{x}; \tilde{f}, f\big) = d\big(\underline{x}; \tilde{f}(\underline{x}), f(\underline{x})\big) \ , \tag{2.1}$$

that is then integrated over the entire support $\Omega \subseteq \mathbb{R}^s$

$$D\big(\tilde{f}, f\big) = \int_{\Omega} d\big(\underline{x}; \tilde{f}(\underline{x}), f(\underline{x})\big) \, \mathrm{d}\underline{x} \ . \tag{2.2}$$

Continuous densities (see Figure 2.1 a) can be compared very well with these methods. Common examples are the Kullback-Leibler-divergence [98]

$$d^{\mathrm{KLD}}\big(\underline{x}; \tilde{f}, f\big) = f(\underline{x}) \cdot \log\left(\frac{\tilde{f}(\underline{x})}{f(\underline{x})}\right) \ , \tag{2.3}$$

the Hellinger distance [65]

$$d^{\mathrm{BC}}\big(\underline{x}; \tilde{f}, f\big) = \frac{1}{2}\left(\sqrt{\tilde{f}(\underline{x})} - \sqrt{f(\underline{x})}\right)^2 \ , \tag{2.4}$$

or simply the L^2 norm of the difference of the density functions [153]

$$d^{\mathrm{L2}}\big(\underline{x}; \tilde{f}, f\big) = \big(\tilde{f}(\underline{x}) - f(\underline{x})\big)^2 \ . \tag{2.5}$$

If at least one of the densities is a Dirac mixture density on continuous support

$$f(\underline{x}|\mathcal{P}_L) = \frac{1}{L} \sum_{\underline{y} \in \mathcal{P}_L} \delta(\underline{x} - \underline{y}) \ , \tag{2.6}$$

where $\mathcal{P}_L$ is a set of L samples (see Figure 2.1 b and 2.1 c), the distance measures above cannot be applied anymore. In these cases, the local *concentration* of samples must be involved in some way in the distance measure. The Cramér-von Mises distance [32], [21], i.e., the (weighted) L^2 norm of the difference of the *cumulative* distribution functions $\tilde{F}(x)$ and $F(x)$

$$D_{\mathrm{CDF}}^{\mathrm{CvM}}\big(\tilde{f}, f\big) = \int_{\Omega} \big(\tilde{F}(x) - F(x)\big)^2 \, \mathrm{d}x \tag{2.7}$$

is, however, well suited as a distance of density functions, including Dirac mixtures. Therefore, we can compute the desired samples $\mathcal{P}_L$ that constitute Dirac mixture density $f(\cdot|\mathcal{P}_L)$ via numerical optimization

$$\mathcal{P}_L = \arg\min_{\mathcal{P}_L} \big\{ D(\tilde{f},\ f(\cdot|\mathcal{P}_L)) \big\} \ . \tag{2.8}$$

Note the general "workflow" (that we will revisit and improve in the following sections): first, we propagate $\tilde{f}$ and f through an integral transform, yielding (in this case) their respective cumulative distributions $\tilde{F}$ and F that are continuous even for discrete densities. Then, we apply the L^2 norm on the difference of the transformed densities (2.7). Yet there is an ambiguity in the definition of the cumulative distribution; it could be either F_1 or F_2

$$F_1(x) = \int_{-\infty}^{x} f(t) \, \mathrm{d}t \ , \tag{2.9}$$

$$F_2(x) = \int_{x}^{\infty} f(t) \, \mathrm{d}t \ . \tag{2.10}$$

In the one-dimensional case, this ambiguity is irrelevant since both variants are linearly dependent, $F_1(x) + F_2(x) = 1$. However, in the multivariate case,

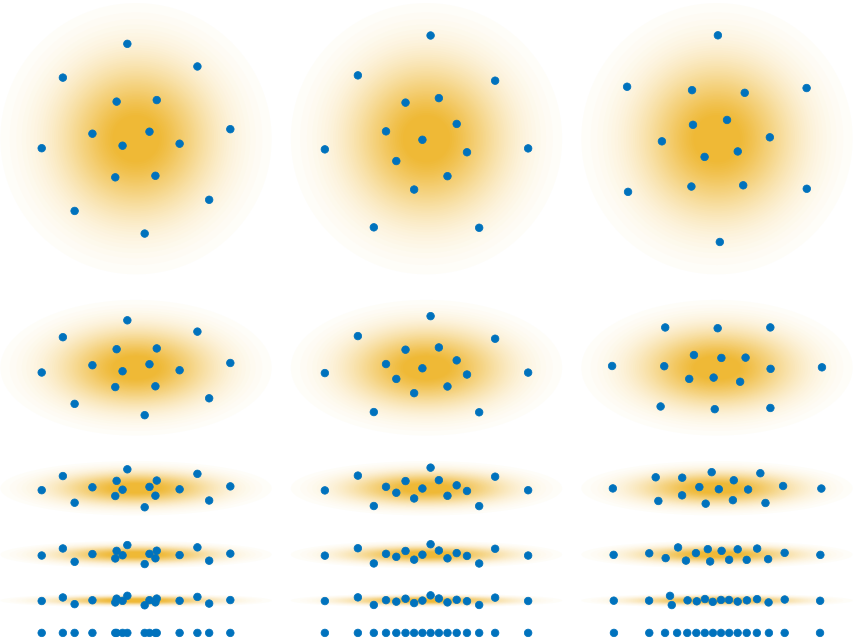

(a) Standard normal density (SND), rescaled.

(b) Conditional, rescaled.

(c) High-Quality, individually optimized

Figure 2.2: Gaussian sampling via minimizing LCD-based distance measure (2.14) with nonlinear optimization. (a) Standard normal density (SND) reference samples (top) rescaled to arbitrary Gaussians without further optimization, yielding S^2KF, (b) conditional sampling with built-in transformability, (c) new optimization for every Gaussian parameter change (high quality but slower). Standard deviation along horizontal axis is always 1, and along vertical axis 1 (standard normal density (SND), top), 0.5, 0.2, 0.1, 0.05, and 0 (bottom), respectively.

there are $2^s - 1$ independent variants of defining cumulative distributions [133, p. 617], [60, Fig. 1], making a unique Cramér-von Mises distance based on all possible cumulative distributions intractable for $s \gg 1$.

2.2 Localized Cumulative Distribution

The LCD is a special cumulative distribution uniquely defined even in higher dimensions. It is given as [60]

$$F(\underline{m}, b) = \int_{\Omega} f(\underline{x}) \cdot K(\underline{x}; \underline{m}, b) \, \mathrm{d}\underline{x} \ , \tag{2.11}$$

where $K(\cdot\,; \underline{m}, b)$ is a kernel function, e.g., an unnormalized Gaussian

$$K^{\mathrm{G}}(\underline{x}; \underline{m}, b) = \exp\left(-\frac{\|\underline{x} - \underline{m}\|_2^2}{2\,b} \right) \ . \tag{2.12}$$

In other words, the localized cumulative distribution $F(\underline{m}, b)$ is the convolution of f with kernel $K(\cdot\,, \underline{m}, b)$. It is a continuous representation of discrete and continuous densities that is unique even in higher dimensions. Now we can apply the same workflow as above and compute a distance measure with the Cramér-von Mises Distance

$$D_{\mathrm{LCD}}^{\mathrm{CvM}}(\tilde{f}, f, b) = \int_{\Omega} \left(\tilde{F}(\underline{m}, b) - F(\underline{m}, b) \right)^2 \mathrm{d}\underline{m} \ . \tag{2.13}$$

Finally, averaging over the kernel size b, we obtain the *modified* Cramér-von Mises Distance as proposed in [60]

$$D_{\mathrm{LCD}}^{\mathrm{mCvM}}(\tilde{f}, f) = \int_{b=0}^{\infty} w(b) \int_{\Omega} \left(\tilde{F}(\underline{m}, b) - F(\underline{m}, b) \right)^2 \mathrm{d}\underline{m} \, \mathrm{d}b \ , \tag{2.14}$$

with suitable weighting function $w(b)$. The triple-nested integral (2.14) can be solved in closed form if both densities, $\tilde{f}$ and f are Dirac mixtures, yielding a method for optimal sample reduction while keeping the most relevant information [57]. For Gaussian $\tilde{f}$ and Dirac mixture f, i.e., the Gaussian sampling application, (2.14) can be simplified analytically such that a one-dimensional integral (the one over b) remains to be solved numerically [59]. The resulting samples look well-placed and locally homogeneous (see Figure 2.2c).

- Advantages

  - Resulting point sets are subjectively visually appealing.
  - Numerical results are very good as well.
  - Arbitrarily high dimensions are no problem.
- Disadvantages
  - Seldom closed form solution of triple-nested integral (2.14).
  - Numerical optimization necessary for sampling.
  - Badly transformable; new samples should be generated for every change in $\tilde{f}$.

2.2.1 Spherical Manifolds

The sampling method just described for the Euclidean space $\mathbb{R}^s$ was extended to non-Euclidean manifolds, especially the sphere $\mathbb{S}^2$ and also hyperspheres $\mathbb{S}^s$. Riemannian manifolds have an Euclidean tangent space where samples can be placed via "standard" Euclidean LCD and then mapped to the sphere with a suitable nonlinear transformation [109]. However, this introduces distortions that become noticeable in the case of large uncertainties.

The LCD (2.11) and its modified Cramér-von Mises distance (2.7) can also be defined directly on the sphere [O9]. Therefore we have to i) change the domain Ω from $\mathbb{R}^2$ to $\mathbb{S}^2$ and ii) find a suitable kernel function

$$K(\underline{x}; \underline{m}, b) \ , \qquad \underline{x},\ \underline{m} \in \mathbb{S}^2 \ . \tag{2.15}$$

An obvious choice is the von Mises–Fisher kernel

$$K^{\mathrm{VMF}}(\underline{x}; \underline{m}, b) = \exp\{b \cdot \underline{x}^\top \underline{m}\} \ . \tag{2.16}$$

Interestingly, we can show that Gaussian and von Mises–Fisher kernels become identical if the uncertainty tends to zero and the curvature of the space is therefore negligible: introducing d as the shortest distance between $\underline{x}$ and $\underline{m}$ in the respective space, we obtain

$$K^{\mathrm{G}}(d, \sigma) = \exp\left\{\frac{1}{\sigma} \cdot \left(-\frac{d^2}{2}\right)\right\} \qquad d = \|\underline{x} - \underline{m}\|_2 \tag{2.17}$$

$$K^{\mathrm{VMF}}(d, b) = \exp\{b \cdot \cos(d)\} \qquad d = \cos^{-1}\left(\underline{x}^\top \underline{m}\right) \ . \tag{2.18}$$

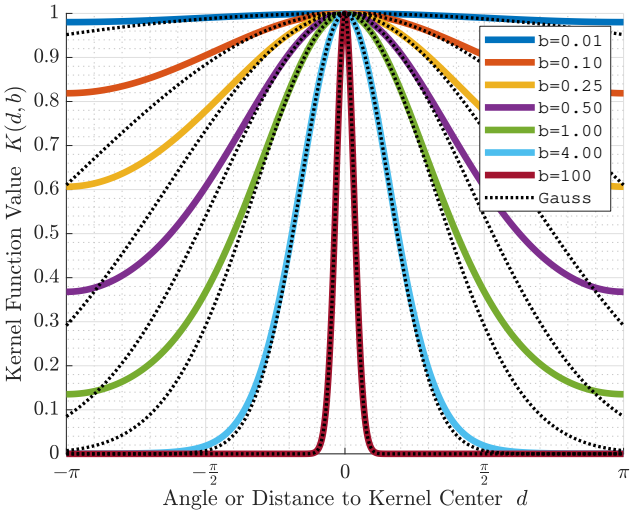

Figure 2.3: Comparison of von Mises–Fisher (vMF) kernel (colored lines) and Gaussian kernel (dashed black lines). Note that both kernels are very similar near the kernel center, and the narrow kernels (small σ, large b) are nearly identical everywhere. Taken from [O9, Fig. 2].

Kernel width parameters b and σ can be matched via

$$\sigma = b^{-\frac{1}{2}} \quad . \tag{2.19}$$

The similarity can now be seen mathematically as $\left(-d^2/2\right)$ and $(\cos(d)-1)$ have identical Taylor polynomials up to the second order, and visually in Figure 2.3.

For the sample reduction problem, i.e.,

$$\tilde{f}(\underline{x}) = \frac{1}{M}\sum_{k=1}^{M}\delta(\underline{x}-\underline{y}_j) \quad , \tag{2.20}$$

$$f(\underline{x}) = \frac{1}{L}\sum_{i=1}^{L}\delta(\underline{x}-\underline{x}_i) \quad , \tag{2.21}$$

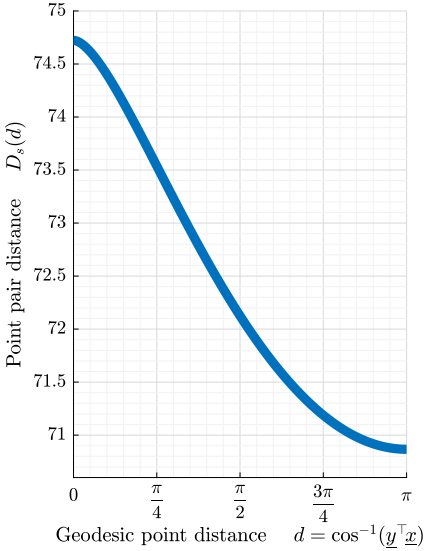

Figure 2.4: Sample-pair distance function $D_s(d)$ from (2.27). Used to compute the distance between two Dirac mixture densities on the $\mathbb{S}^2$ sphere by applying it to all pairs of samples and summing it up according to (2.23).

we can solve the triple-nested integral defining the distance measure

$$D^2 = \int_{\mathbb{R}_+} w(b) \int_{\mathbb{S}^2} \left(\tilde{F}(\underline{m}, b) - F(\underline{m}, b)\right)^2 \mathrm{d}\underline{m} \, \mathrm{d}b \ , \tag{2.22}$$

with weighting function $w(b) = b^{-1}e^{-2b}$, in closed form [O9]

$$D^2 = D_{xx} - 2D_{xy} + D_{yy} \ , \tag{2.23}$$

$$D_{xx} = \frac{1}{L^2} \sum_{i=1}^{L} \sum_{j=1}^{L} D_s(\underline{x}_i, \underline{x}_j) \ , \tag{2.24}$$

$$D_{xy} = \frac{1}{LM} \sum_{i=1}^{L} \sum_{j=1}^{M} D_s(\underline{x}_i, \underline{y}_j) \ , \tag{2.25}$$

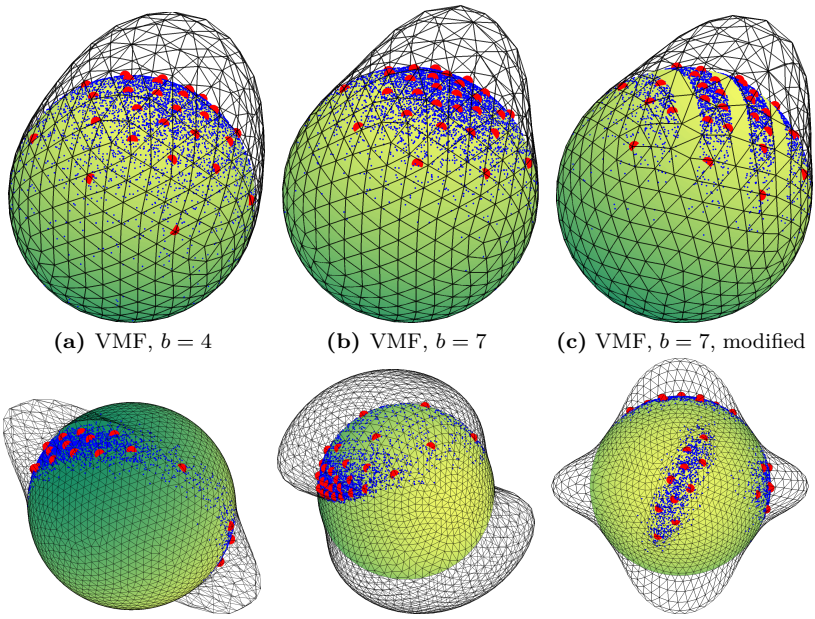

(a) VMF, $b = 4$ **(b)** VMF, $b = 7$ **(c)** VMF, $b = 7$, modified

(d) Bingham **(e)** Projected Gaussian **(f)** Mixture

Figure 2.5: Sample reduction on the 2-sphere $\mathbb{S}^2$. Random samples (blue) are, by minimizing (2.22), reduced to few deterministic samples (red) representing nearly the same information about the density. Modified from [O9, Fig. 3].

$$D_{yy} = \frac{1}{M^2} \sum_{j=1}^{M} D_s(\underline{y}_i, \underline{y}_j) \ , \tag{2.26}$$

with sample-pair distance function $D_s(\underline{x}, \underline{y})$. Due to symmetry, its arguments $(\underline{x}, \underline{y})$ can be reduced to one single argument, the geodesic distance $d = \cos^{-1}(\underline{x}^\top \underline{y})$ between them, yielding $D_s(d)$

$$D_s(d) = \tag{2.27}$$

$$\begin{cases} \pi\left[4\,\mathrm{Ei}(-4b) + \frac{1}{b}\left(e^{-4b} - 1\right)\right]_{b_1}^{b_2}, & d = 0 \ , \\ \frac{\pi}{\cos\left(d/2\right)}\left[c_1\mathrm{Ei}(c_1 b) - c_2\mathrm{Ei}(c_2 b) + \frac{1}{b}\left(e^{c_2 b} - e^{c_1 b}\right)\right]_{b_1}^{b_2}, & d \in (0, \pi) \ , \\ \left[4\,\pi\,\mathrm{Ei}(-2b)\right]_{b_1}^{b_2} \ , & d = \pi \ , \end{cases}$$

where

$$\begin{aligned} c_1 &= +2\cos(d/2) - 2 \ , \\ c_2 &= -2\cos(d/2) - 2 \ , \end{aligned} \tag{2.28}$$

and bounds of integration (b_1, b_2) that can be set to $b_1 = 0.001$ and $b_2 \to \infty$. Ei denotes the exponential integral

$$\mathrm{Ei}(x) = \int_{-\infty}^{x} \frac{e^t}{t}\,\mathrm{d}t \ . \tag{2.29}$$

Note that D_s is a scalar function on bounded domain (see Figure 2.4)

$$D_s \colon [0, \pi] \to \mathbb{R}_+ \ , \tag{2.30}$$

that can also be tabulated and interpolated instead of repeatedly evaluating the expression (2.27). Either way, we can reduce many (random) samples of an arbitrary density on the $\mathbb{S}^2$ sphere to fewer nicely arranged, deterministic samples (see Figure 2.5). The code of the presented method has been published as part of `libDirectional` [104] and can be found in the class `AbstractHypersphericalDistribution`. This method for deterministic sampling on the $\mathbb{S}^2$ sphere [O9] has subsequently been generalized to hyperspheres $\mathbb{S}^s$ in [111].

2.2.2 Conditional or Component-by-Component Sampling for Transformability

The main disadvantage of LCD sampling in conjunction with cheap Gaussian filters is that its computation is too expensive for real-time application.

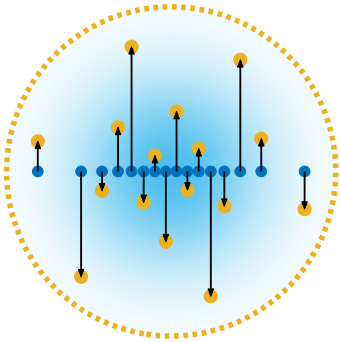

Figure 2.6: Transformable conditional LCD sampling of 2D standard normal density (SND) (blue shade), as explained in Section 2.2.2. First, a one-dimensional standard normal density (SND) is sampled on the x-axis (blue points). Second, a two-dimensional standard normal density (SND) (yellow points) is sampled by adding y-coordinates (black arrows) to the existing samples. Subsequent rescaling against the arrows to obtain arbitrary Gaussians (not shown here) retains much of the uniformity of sample distribution. Taken from [O1, Fig. 1].

One way to circumvent this is computing *standard* normal samples $\underline{x}_i$ in advance (for the respective dimension s and number of samples L) and store them in a matrix $\mathbf{X}^{\mathrm{SN}} \in \mathbb{R}^{s \times L}$

$$\mathbf{X}^{\mathrm{SN}} = \left[\underline{x}_1^{\mathrm{SN}}, \underline{x}_2^{\mathrm{SN}}, \ldots, x_L^{\mathrm{SN}}\right] \quad . \tag{2.31}$$

During run-time, these "template" samples can then be transformed from standard normal density (SND) to arbitrary Gaussian (with covariance $\mathbf{C}$, its Cholesky decomposition $\mathbf{C} = \mathbf{L} \cdot \mathbf{L}^\top$, and mean $\underline{\mu}$) at very low cost with a simple linear transform

$$\mathbf{X}^{\mathrm{G}} = \mathbf{L} \cdot \mathbf{X}^{\mathrm{SN}} + \underline{\mu} \tag{2.32}$$

(see Figure 2.2a).

Proof.

$$\underline{\boldsymbol{x}} = \underline{\boldsymbol{x}}^{\mathrm{SN}} \Rightarrow \mathrm{Cov}\{\underline{\boldsymbol{x}}\} = \mathrm{E}\{\underline{\boldsymbol{x}} \cdot \underline{\boldsymbol{x}}^\top\} = \mathbf{I} \tag{2.33}$$

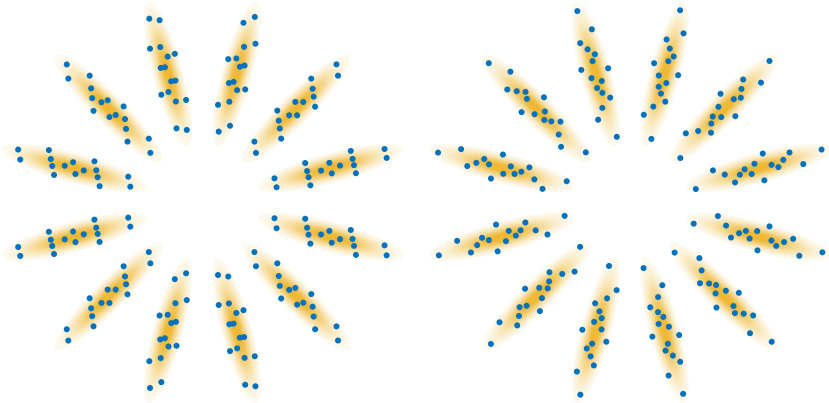

(a) LCD & Cholesky.

(b) Conditional LCD & Eigendecomposition.

Figure 2.7: (a) Gaussian samples produced via LCD-based standard normal density (SND) sampling (2.14), subsequently transformed via Cholesky decomposition (2.32). (b) Standard normal density (SND) LCD-based conditional sampling, subsequently transformed via eigenvalues and eigenvectors (2.32). Quality of samples in (a) depends on the rotation angle of the density, and in (b) not. Modified from [O1, Fig. 5].

$$\Rightarrow \mathrm{Cov}\{\underline{\boldsymbol{x}}^{\mathrm{G}}\} = \mathrm{Cov}\{\mathbf{L} \cdot \underline{\boldsymbol{x}}\} \tag{2.34}$$

$$= \mathrm{E}\{(\mathbf{L} \cdot \underline{\boldsymbol{x}}) \cdot (\mathbf{L} \cdot \underline{\boldsymbol{x}})^{\top}\} \tag{2.35}$$

$$= \mathrm{E}\{\mathbf{L} \cdot \underline{\boldsymbol{x}} \cdot \underline{\boldsymbol{x}}^{\top} \cdot \mathbf{L}^{\top}\} \tag{2.36}$$

$$= \mathbf{L} \cdot \mathrm{E}\{\underline{\boldsymbol{x}} \cdot \underline{\boldsymbol{x}}^{\top}\} \cdot \mathbf{L}^{\top} \tag{2.37}$$

$$= \mathbf{C} \ . \tag{2.38}$$

□

This makes it possible to implement a practical Linear Regression Kalman filter (LRKF), called the Smart Sampling Kalman Filter (S^2KF) [162], [164], and also (progressive) Gaussian filters [163], [61].

However, the LCD samples are not *designed* to be transformable and thus potentially lose some of their optimality (see Figures 2.2a and 2.7a).

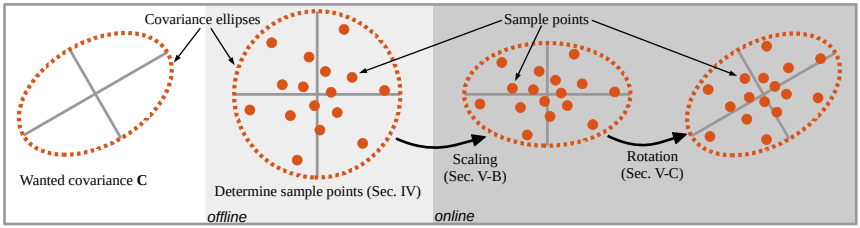

Figure 2.8: For obtaining deterministic conditional samples with arbitrary covariance $\mathbf{C}$, at first, the sample points for the SND are determined offline. Performing the scaling and rotation operations based on eigendecomposition online completes the approximation. Taken from [O1, Fig. 2], a similar figure for Gaussian sampling only on principal axes appeared in [76].

Therefore, a conditional sampling scheme is introduced that mitigates this problem to some degree [O1]. The key idea is a recursive sampling procedure: start with the one-dimensional problem, sampling only x-coordinates to 1D SND by minimizing (2.14) via numerical optimization (see blue samples in Figure 2.6). Then, add random y-coordinates and start numerical optimization again, targeting the 2D SND. However, let it optimize and modify only the y-coordinates, keeping the x-coordinates in place (see yellow samples in Figure 2.6). Then add random z-coordinates and optimize them towards three-dimensional SND, keeping the x- and y-coordinates in place, and so on. Refer to [O1, Sec. IV] for more details.

Decompositions of covariance matrices, like the Cholesky decomposition $\mathbf{C} = \mathbf{L} \cdot \mathbf{L}^\top$, are ambiguous in terms of a transformation matrix $\mathbf{Q}$ that is orthonormal, i.e.,

$$\mathbf{Q}^\top \cdot \mathbf{Q} = \mathbf{Q} \cdot \mathbf{Q}^\top = \mathbf{I} \ .$$

Proof.

$$(\mathbf{L} \cdot \mathbf{Q}) \cdot (\mathbf{L} \cdot \mathbf{Q})^\top = \mathbf{L} \cdot \mathbf{Q} \cdot \mathbf{Q}^\top \cdot \mathbf{L}^\top = \mathbf{L} \cdot \mathbf{L}^\top = \mathbf{C}$$

□

Hence, there is an ambiguity in the transformation from SND to arbitrary Gaussian

$$\mathrm{Cov}\{\underline{\boldsymbol{x}}\} = \mathbf{I} \quad \Rightarrow \quad \mathrm{Cov}\{\mathbf{L}\cdot\underline{\boldsymbol{x}}\} = \mathrm{Cov}\{\mathbf{L}\cdot\mathbf{Q}\cdot\underline{\boldsymbol{x}}\} = \mathbf{C} \ .$$

This also makes sense intuitively: the density of the SND random variable $\underline{\boldsymbol{x}}$ is rotationally symmetric; therefore, an orthonormal transformation $\mathbf{Q}\cdot\underline{\boldsymbol{x}}$ will not change anything. However, in conditional Gaussian sampling, there is one preferred direction, the y-axis, along which the anisotropic compression should occur to preserve the sampling quality. Therefore, in this case, one should *not* employ the Cholesky decomposition (2.32) as it does not allow control over the directions along which compression or stretching takes place. Instead, we propose a transform based on the eigendecomposition of the covariance matrix

$$\mathbf{C} = \mathbf{V}\cdot\mathbf{D}\cdot\mathbf{V}^{\top} \tag{2.39}$$

with orthogonal matrix $\mathbf{V}$ containing the eigenvectors as columns and diagonal matrix $\mathbf{D}$ containing the eigenvalues. The linear transform

$$\mathbf{X}^{\mathrm{G}} = \mathbf{V}\cdot\sqrt{\mathbf{D}}\cdot\mathbf{X}^{\mathrm{SN}} + \underline{\mu} \ , \tag{2.40}$$

also maps SND samples $\mathbf{X}^{\mathrm{SN}}$ to arbitrary Gaussian samples $\mathbf{X}^{\mathrm{G}}$ (see Figure 2.8).

Proof.

$$\underline{\boldsymbol{x}} = \underline{\boldsymbol{x}}^{\mathrm{SN}} \tag{2.41}$$

$$\Rightarrow \mathrm{Cov}\{\underline{\boldsymbol{x}}^{\mathrm{G}}\} = \mathrm{Cov}\Big\{\mathbf{V}\cdot\sqrt{\mathbf{D}}\cdot\underline{\boldsymbol{x}}\Big\} \tag{2.42}$$

$$= \mathrm{E}\Big\{(\mathbf{V}\cdot\sqrt{\mathbf{D}}\cdot\underline{\boldsymbol{x}})\cdot(\mathbf{V}\cdot\sqrt{\mathbf{D}}\cdot\underline{\boldsymbol{x}})^{\top}\Big\} \tag{2.43}$$

$$= \mathrm{E}\Big\{\mathbf{V}\cdot\sqrt{\mathbf{D}}\cdot\underline{\boldsymbol{x}}\cdot\underline{\boldsymbol{x}}^{\top}\cdot\sqrt{\mathbf{D}}^{\top}\cdot\mathbf{V}^{\top}\Big\} \tag{2.44}$$

$$= \mathbf{V}\cdot\mathbf{D}\cdot\mathbf{V}^{\top} \tag{2.45}$$

$$= \mathbf{C} \ . \tag{2.46}$$

□

Thereby, all anisotropic rescalings occur only along the coordinate axes.

Proof. In (2.40), the first operation $\sqrt{\mathbf{D}} \cdot \underline{\boldsymbol{x}}^{\mathrm{SN}}$ rescales the components of $\underline{\boldsymbol{x}}^{\mathrm{SN}}$ with the diagonal values of $\mathbf{D}$, respectively, i.e., an anisotropic rescaling along the coordinate axes. The second operation, multiplication from left with orthonormal $\mathbf{V}$, represents a rigid mapping consisting of rotations and reflections only. □

The SND samples generated by this method (see Figure 2.2b, top) are somewhat inferior to the other two where the SND samples are more freely optimized – without the constraint that only y coordinates can be changed. In strongly anisotropic Gaussians, e.g., $\sigma_y = 0.1$, the conditional samples (see Figure 2.2b, lower area) have a higher quality than $\mathrm{S}^2\mathrm{KF}$ samples, though. In summary, conditional sampling produces a tradeoff and can give a benefit for strongly anisotropic Gaussian densities. The consistent choice of the otherwise ambiguous rotational part in the covariance decomposition removes the undesired dependence of the sampling quality on the covariance orientation (see Figure 2.7b).

2.3 Projected Cumulative Distribution (PCD)

Computation of the LCD distance measure is reasonably efficient only in special cases like comparing two discrete densities (for sample reduction) or comparing a Gaussian with a discrete density (for Gaussian sampling). Even then, minimizing this distance measure with respect to the desired sample locations is computationally expensive. This motivates a search for other distance measures.

The projected cumulative distribution (PCD) [58] is a promising candidate. It is equivalent to the Radon transform. Thus, we consider projections $f_r(r|\underline{u})$ of density f

$$f_r(r|\underline{u}) = \int_{\mathbb{R}^s} f(\underline{t}) \cdot \delta(r - \underline{u}^\top \underline{t}) \, \mathrm{d}\underline{t} \ . \tag{2.47}$$

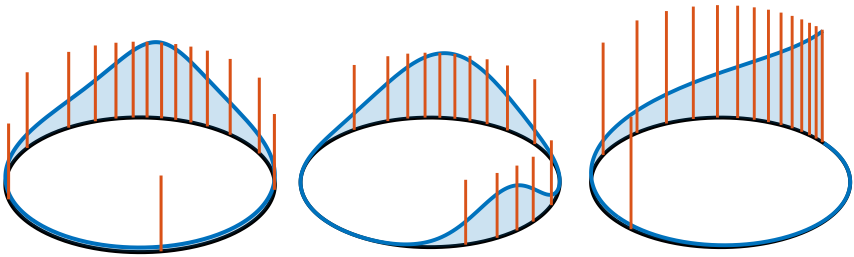

(a) wrapped Cauchy **(b)** von Mises–Fisher (vMF) mixture **(c)** wrapped exponential

Figure 2.9: Density function (blue), defined on the angular domain $\mathbb{S}^1$ (black), approximated with $L = 15$ samples using the projected cumulative distribution (PCD) method. For better visualization, the length of the red lines representing the unweighted samples has been set to the maximum density function value (mode) instead of the sample weight $1/L$. Taken from [O4].

Note that for $\underline{u} = \underline{e}_i$, these projections $f_r(r|\underline{e}_i)$ are precisely the marginal densities. Yet we consider projections along all directions $\underline{u} \in \mathbb{S}^{s-1}$, or equivalently, marginal densities of the rigidly rotated density. With the cumulative projected density

$$F_r(r|\underline{u}) = \int_{-\infty}^{r} f_r(q|\underline{u}) \, \mathrm{d}q \ , \tag{2.48}$$

we define a distance measure between two PCDs $\tilde{F}_r$ and F_r

$$D(\tilde{F}_r, \ F_r) = \int_{\mathbb{S}^{s-1}} \int_{\mathbb{R}^s} \left[\tilde{F}_r(r|\underline{u}) - F_r(r|\underline{u})\right]^2 \mathrm{d}r \, \mathrm{d}\underline{u} \ . \tag{2.49}$$

By fixing $\tilde{f}$ to a specific density and choosing $f(\cdot|\mathcal{P}_L)$ as a Dirac mixture with variable sample locations $\mathcal{P}_L$, said distance measure yields an optimality measure of how well the samples $\mathcal{P}_L$ match $\tilde{f}$. Minimizing this yields a gradient-free optimization similar to expectation–maximization (EM). This method has been applied to Gaussian and Gaussian mixture sampling [58],

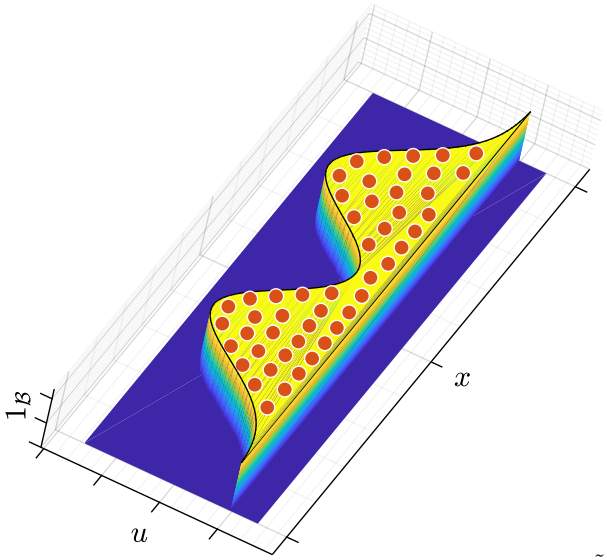

Figure 2.10: Given the state space x, some density function $u = \tilde{f}(x)$, and the joint space $\underline{\xi} = [x, u]^\top$, we obtain the area $\mathcal{B}$ under the density function, i.e., the area between the x axis and $\tilde{f}(x)$. Now, we draw samples from $1_{\mathcal{B}}$, i.e., the indicator function of that area interpreted as density. After projection to the x axis, we obtain the desired samples from $\tilde{f}(x)$ (not shown here).

sample reduction [139], and sampling of arbitrary continuous densities on the circle [O4] (see Figure 2.9a).

- Advantages
  - EM-style, gradient-free optimization.
  - Integrals in the quality measure are simpler than for LCD.
  - Ensembles are somewhat transformable.
- Disadvantages
  - Still requires iterative optimization.
  - 1D marginals of rotated density needed.

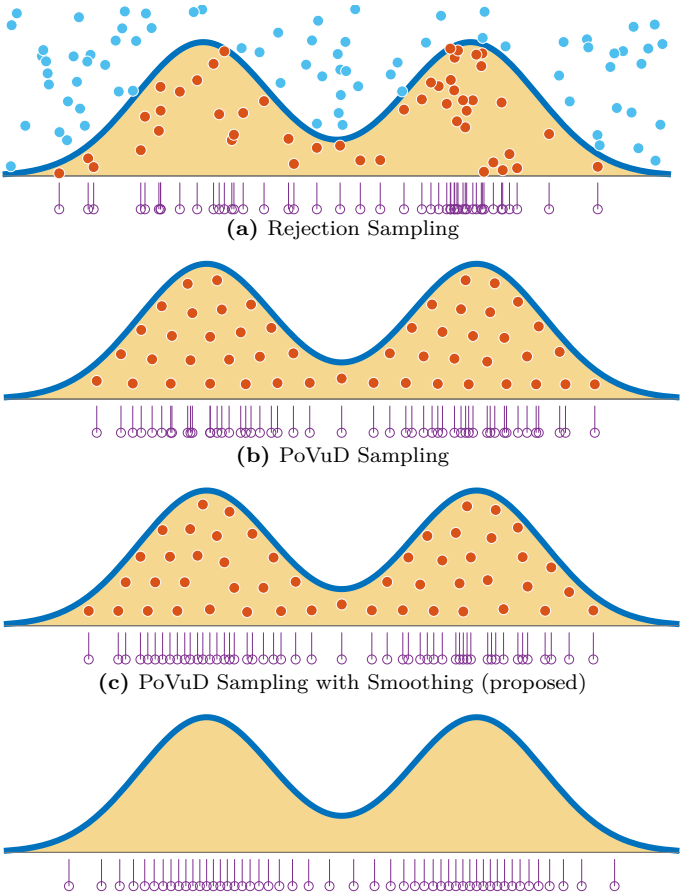

(a) Rejection Sampling

(b) PoVuD Sampling

(c) PoVuD Sampling with Smoothing (proposed)

(d) Inverse Transform Sampling [73, p. 14] of Equidistant Samples

Figure 2.11: Four methods to draw 50 1D samples (purple) from an arbitrary density function (blue line): classical rejection sampling (a), our proposed methods (b,c), and inverse transform sampling (d) of equidistant samples as "gold standard". Note that random samples as in (a) can also be obtained, e.g., via Markov Chain Monte Carlo sampling methods for arbitrary density functions. Note also that inverse transform sampling (d) for arbitrary densities is only available in the 1D case.

2.4 Sphere Packing in Volume Under Density (PoVuD)

This section presents a method to draw samples $x_i \in \mathbb{R}$ from an arbitrary, not necessarily normalized density function $\tilde{f}(x)$, $x \in \mathbb{R}$. The first step is to compute augmented uniform samples $\underline{\xi}_i \in \mathbb{R}^2$ from "under the density function" as shown in Figure 2.10. In particular, we augment the scalar sample space $x \in \mathbb{R}$ with a second auxiliary dimension u, yielding a two-dimensional vector $\underline{\xi}$,

$$\underline{\xi} = (u, x) \in \mathbb{R}^2 \ , \tag{2.50}$$

$$u = \tilde{f}(x) \ . \tag{2.51}$$

The auxiliary variable u accounts for the sample's density function value. Now define the domain $\mathcal{B}$ as the region under the density function (or likelihood)

$$\mathcal{B} = \left\{ \underline{\xi} \mid u \leq \gamma \cdot \tilde{f}(x) \right\} \ , \tag{2.52}$$

and solve the corresponding equal hypersphere packing problem

$$\underline{\xi}_{1:L}^{\text{opt}} = \arg\min_{\underline{\xi}_{1:L}} \left\{ \Theta(\underline{\xi}_{1:L}) \right\} \tag{2.53}$$

$$\text{w.r.t} \quad \underline{\xi}_i \in \mathcal{B} \quad \forall\, i \ .$$

Hence the name "Packing of Volume under Density" (PoVuD). In the examples shown here, we employ the objective function Θ

$$\Theta(\underline{\xi}_{1:L}) = \sum_{i=1}^{L} \frac{1}{\min\left\{ \min_{\substack{j \\ j \neq i}} \left\{ \left\| \underline{x}_i - \underline{x}_j \right\| \right\}, \dfrac{\tilde{f}(x_i) - u_i}{2}, \dfrac{u_i}{2} \right\}} \ , \tag{2.54}$$

which worked best in practice. Alternative objective functions are

$$\Theta(\underline{\xi}_{1:L}) = \sum_{i=1}^{L} \frac{1}{\min\left\{ \min\limits_{\substack{j \\ j \neq i}} \{\|\underline{x}_i - \underline{x}_j\|\}, \tilde{f}(x_i) - u_i \right\}} \quad , \tag{2.55}$$

$$\Theta(\underline{\xi}_{1:L}) = \sum_{i=1}^{L} \frac{1}{\min\limits_{\substack{j \\ j \neq i}} \{\|\underline{x}_i - \underline{x}_j\|\}} \quad , \tag{2.56}$$

where the latter leads to many samples sitting directly on the boundary, yielding a systematic bias (random samples are arranged irrespective of the boundary, giving some average distance to the boundary, which we have to reproduce here). Refer to [O6, Sec. II+IV] for more information.

After solving the constrained nonlinear optimization problem, we project the samples back to the original scalar domain. Then, the resulting samples will have a higher density in regions with higher density function values and vice versa (see Figure 2.11 b). The samples now represent a discrete and deterministic approximation of $\tilde{f}(x)$. A second objective can be included to make the samples better than random, considering the projected density's smoothness (see Figure 2.11 c). Refer to [O6, Sec. V] for more details.

Computational burden is the computation of an approximate close packing of equal hyperspheres under the density function, i.e., a constrained optimization problem. This method is related to rejection sampling, explained in Section 7.3.

- Advantages
  - Only requires unnormalized density function handle.
  - No integral needed.
- Disadvantages
  - Numerical optimization necessary.
  - Density support should be simply connected.
  - Badly transformable, new samples should be generated for every change in $\tilde{f}$.

2.5 Summary

In the beginning, we presented common distance measures for densities and their shortcomings, motivating the search for integral-transform-based distances. Two integral transforms and associated distances have been introduced, followed by the resulting deterministic sampling methods using numerical optimization. Finally, we presented a deterministic variant of acceptance-rejection sampling.

CHAPTER 3

Uniform Point Sets

Contents

> Die ganzen Zahlen hat der liebe Gott gemacht,
> alles andere ist Menschenwerk.
>
> Leopold Kronecker (1823 – 1891)

In this chapter, we will describe state-of-art representations, enumerations, and constructions of uniform point sets that exhibit low discrepancy, i.e., are suitable for multivariate numerical integration (cubature). We focus on the rank-1 lattice, the Kronecker sequence, and the Frolov lattice and the relations between them. Furthermore we focus on dimensions $s \in \{1, 2, 3\}$, yet some low-discrepancy constructions are available for thousands of dimensions.

3.1 Representations

The term "countable point set" applies very generally, but often, these point sets have a special inner structure that allows for a more memory-efficient representation. We will focus on rank-1-lattices, Kronecker sequences, and Frolov lattices as representations (see Figure 3.1 for an overview). Furthermore, the next section will describe construction methods for particularly good point sets.

3.1.1 Lattice

A **lattice** is a point set

- that is closed under addition and subtraction,
- that exhibits a minimum distance between any two lattice points
- and a maximum distance between any point in space and its nearest lattice point.

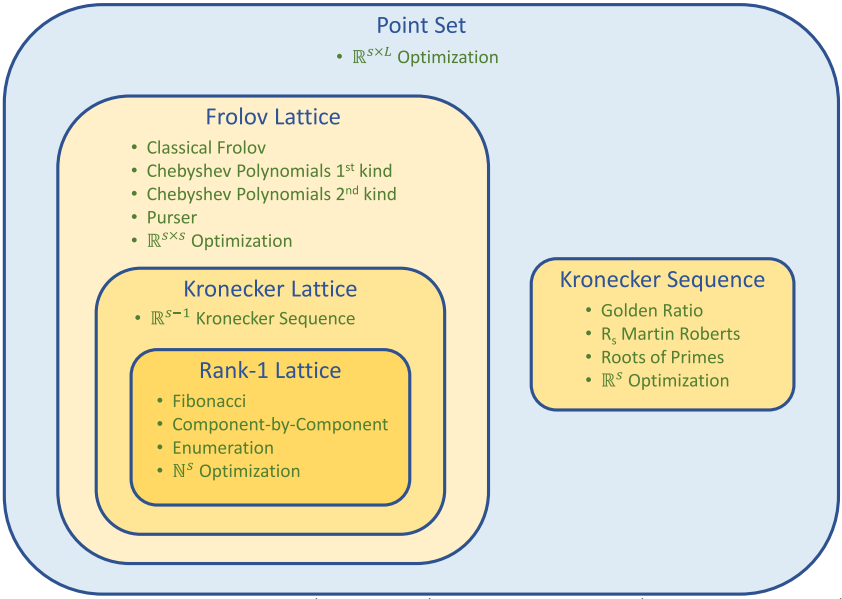

Figure 3.1: Representations (blue boxes) and constructions (green bullet points) of low-discrepancy point sets for cubature.

Individual lattice points on $\mathbb{R}^s$ can be represented as a linear combination (with integer coefficients a_i) of **generating vectors** or **generators** $\underline{g}_i$

$$\sum_{i=1}^{t} a_i \cdot \underline{g}_i \ , \quad a_i \in \mathbb{Z} \ , \tag{3.1}$$

and the entire lattice point set $\mathcal{P}_L$ as the union over all these points

$$\mathcal{P}_L = \bigcup_{a_1\in\mathbb{Z}} \cdots \bigcup_{a_t\in\mathbb{Z}} \sum_{i=1}^{t} a_i \cdot \underline{g}_i \ . \tag{3.2}$$

For a domain of $[0,1)^s$ instead of $\mathbb{R}^s$, take (3.2) modulo 1. The lattice is fully characterized by a set of generators, though different sets of generators and different numbers t of generators can produce the same lattice. In $[0,1)^s$, the number of generators is always smaller than or equal to the

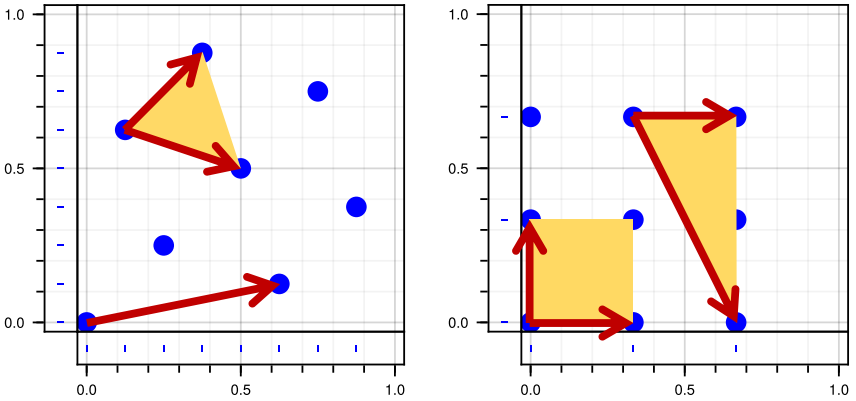

(a) Fibonacci–rank-1 Lattice. **(b)** Regular Lattice.

Figure 3.2: Lattices (blue points) in $[0,1)^2$ with two possible choices of generating vectors (red) and corresponding unit cells (orange), respectively.

dimension, i.e., $t \leq s$. The smallest possible number of generators to represent a given lattice is called the **rank** of that lattice. In $\mathbb{R}^s$, we always have $t \geq s$.

For $t = s$, the set of generators spans a **unit cell**, and the lattice can be seen as regular **tiling or tessellation** by one primitive cell that is identical to said unit cell. A special case are the **regular lattices** $\mathbb{Z}^s \subset \mathbb{R}^s$, with generating vectors $\underline{g}_i = \underline{e}_i$, and rank s. Its unit cells are squares, cubes, or hypercubes of unit volume (see Figure 3.2). Lattices that contain the regular lattice as a subset are called **integration lattices**.

Lattices always contain the origin. Sometimes, an offset vector is added to every lattice point, yielding a new point set that is a shifted variant of the lattice.

A numerical integration rule that uses lattice points as evaluation points or abscissas is called a **lattice rule**. A very good and accessible introduction to these can be found in [34].

3.1.2 Rank-1 Lattice

Of special interest are rank-1 lattice rules. Thereby a single integral generating vector $\underline{g} = \underline{z} \in \mathbb{Z}^s$ produces L rank-1 lattice points $\underline{x}_i \in [0,1)^s$ inside the unit cube

$$\underline{x}_i = \frac{i \cdot \underline{z}}{L} \mod 1 \ , \qquad i \in \{0, 1, \ldots, L-1\} \ . \tag{3.3}$$

Applied to approximate integration of function $f(\underline{x})$ [94], [35, p. 143], we obtain the **rank-1 lattice rule**

$$\int_{[0,1]^s} f(\underline{x}) \, \mathrm{d}\underline{x} \approx \frac{1}{L} \sum_{i=1}^{L} f\left(\frac{i \cdot \underline{z}}{L} \mod 1 \right) \ . \tag{3.4}$$

Rank-1 lattices are in general **closed** point sets, i.e., a subsequent adding of samples is not possible because the generator $\underline{z}$ depends on L. They are also **periodic** along each coordinate axis, i.e., the mod 1–unit squares (cubes, hypercubes) can be tiled without visible irregularities at the transitions.

3.1.3 Kronecker Sequence

A **Kronecker sequence** is produced by taking the fractional part of repeated additions of an irrational generating vector $\underline{\alpha} \in \mathbb{R}^s$ [35, p. 142]

$$\underline{x}_i = i \cdot \underline{\alpha} \mod 1 \ , \qquad i \in \{0, 1, \ldots, L-1\} \ . \tag{3.5}$$

They are named after Leopold Kronecker, who showed that any number can be approximated by linear combinations of irrational numbers with integer coefficients [95]. Hermann Weyl later showed that the sequence (3.5), and more complicated polynomials modulo one, produce uniformly distributed points, given the variable is irrational [174]. Therefore, the Kronecker sequence is sometimes also referred to as *Weyl sequence*. Applying this to numerical integration, we obtain the **Kronecker sequence rule**

$$\int_{[0,1]^s} f(\underline{x}) \, \mathrm{d}\underline{x} \approx \frac{1}{L} \sum_{i=1}^{L} f(i \cdot \underline{\alpha} \mod 1) \ . \tag{3.6}$$

The Kronecker sequence with all-irrational generating vector $\underline{\alpha}$ is not a lattice, and it is – other than lattices – an **open** point set. This means in our context that more points can be generated and used without discarding the previously generated points. (This has nothing to do with openness of sets in topology.) Kronecker sequences are, like rank-1 lattices, periodic along each coordinate axis.

3.1.4 Kronecker Lattice

A Kronecker sequence can, however, be turned into a lattice by combining a simple equidistant lattice rule ($g = \frac{1}{L}$) along the first dimension with a Kronecker sequence along the other dimensions (irrational entries α_i)

$$\underline{g} = \begin{bmatrix} \frac{1}{L} & \alpha_1 & \alpha_2 & \dots & \alpha_{s-1} \end{bmatrix}^\top \quad . \tag{3.7}$$

The resulting point set

$$\underline{x}_i = i \cdot \underline{g} \mod 1 \ , \qquad\qquad i \in \{0, 1, \dots, L-1\} \ . \tag{3.8}$$

is again a lattice and is called the **Kronecker lattice** [36, p. 119]. Applying this to cubature, we obtain the **Kronecker lattice rule**

$$\int_{[0,1]^s} f(\underline{x}) \, \mathrm{d}\underline{x} \approx \frac{1}{L} \sum_{i=1}^{L} f\big(i \cdot \underline{g} \mod 1\big) \ . \tag{3.9}$$

Kronecker lattices are closed point sets. They are periodic only along the "Kronecker sequence axes" but not along the axis with the equidistant coordinates.

3.1.5 Frolov Lattice

Given a bijective linear map $\varphi\colon \mathbb{R}^s \to \mathbb{R}^s$, the image $\varphi(\mathbb{Z}^s)$ of the regular integer lattice $\mathbb{Z}^s$ through φ is again a lattice. Let the linear map φ be described via matrix $\mathbf{T}$

$$\varphi\colon \underline{x} \to \mathbf{T}\,\underline{x} \ . \tag{3.10}$$

Now define the **Frolov lattice** $\mathbf{T}(\mathbb{Z}^s)$ generated by representation matrix $\mathbf{T} \in \mathbb{R}^{s\times s}$ [36, p. 110], [90, Sec. 4.1]

$$\mathbf{T}(\mathbb{Z}^s) = \{\mathbf{T}\,\underline{z} \colon \underline{z} \in \mathbb{Z}^s\} \ . \tag{3.11}$$

The columns of $\mathbf{T}$ can be seen as lattice generators (3.2). Usually, the infinite lattice $\mathbf{T}(\mathbb{Z}^s)$ is cropped to a point set that is confined within a hypercube of unit volume, i.e., $\mathbf{T}(\mathbb{Z}^s) \cap \mathcal{Q}^s$, with cube $\mathcal{Q}^s = [0,1]^s$ or $\mathcal{Q}^s = \left[-\frac{1}{2}, \frac{1}{2}\right]^s$, or the respective open sets, depending on the use case. Frolov lattices that are cropped to the unit hypercube are generally not periodic along any coordinate axis. Therefore, while being lattices in $\mathbb{R}^s$, their cropped variant on $[0,1]^s$ is no lattice anymore.

The exact number of resulting points inside the unit hypercube is, in general, not known in advance, but for $\det T < 1$, an often reasonable estimate is, of course, $|\det(\mathbf{T})|^{-1}$ due to the relation of volumes.

Proof. The determinant of a square matrix can be defined as the volume of the parallelotope spanned by its column vectors [51]

$$\mathrm{vol}(\mathbf{T}([0,1]^s)) = |\det \mathbf{T}| \ . \tag{3.12}$$

In the integer lattice $\mathbb{Z}^s$, every lattice point can be associated with an enclosing Voronoi cell with hypercubic shape and unit volume. These cells are transformed via $\mathbf{T}$ to parallelotopes with volume $|\det \mathbf{T}|$. If such a parallelotope is a subset of $\mathcal{Q}^s$, then the corresponding integer lattice point is part of $\mathbf{T}(\mathbb{Z}^s)$. (If the intersection between parallelotope and $\mathcal{Q}^s$ is empty, it is not. Cases in between become less important for higher numbers of samples). Therefore, as a first approximation, $\mathcal{Q}^s$ can fit $|\det \mathbf{T}|^{-1}$ parallelotopes. Results on the convergence rate of this estimation are given in [114]. □

A Frolov lattice is a lattice with s generators that are the columns of the representation matrix. The standard or regular lattice is the Frolov lattice with identity representation matrix $\mathbf{T} = \mathbf{I}$. Due to the concept of representation matrices, Frolov lattices are very general and in fact, up to

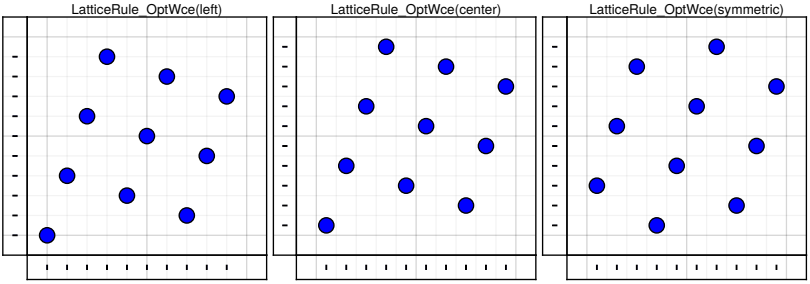

Figure 3.3: Centering rank-1 lattices. Left aligned with zero offset (left), centered version (center), and symmetric variant (right).

the crop operation, equivalent to the definition of lattice via generators (3.2). Thus, rank-1 lattices [36, p. 123] as well as Kronecker lattices [36, p. 119] can be represented as Frolov lattices.

3.2 Enumerating and Centering

This section describes how to actually obtain the sample coordinates given a representation.

3.2.1 Rank-1 Lattice and Similar

Enumeration of lattice rule cubature points for given generator $\underline{z}_L$ is obviously very cheap

$$\underline{x}_i = \frac{i \cdot \underline{z}_L}{L} \mod 1 \ , \qquad i \in \{0, 1, \ldots, L-1\} \ . \tag{3.13}$$

Instead of this left-aligned point set, we often need a centered point set

$$\underline{x}_i = \left(\frac{i \cdot \underline{z}_L}{L} \mod 1 \right) + \frac{1}{2L} \ , \qquad i \in \{0, 1, \ldots, L-1\} \ . \tag{3.14}$$

that does not contain the all-zero vector and is therefore not a lattice. As a third option, we define a symmetric variant

$$\underline{x}_i = \left(\left(\frac{i \cdot \underline{z}_{L+1}}{L} \mod 1\right) + \frac{1}{2L} - \frac{1}{2}\right) \cdot \frac{L+1}{L} + \frac{1}{2} \ , \quad i \in \{0, \ldots, L-1\} \tag{3.15}$$

that is, however, not anymore periodic along the coordinate axes.

For visualization, see Figure 3.3.

3.2.2 Kronecker Sequence

Enumeration of Kronecker sequences, given the generating vector $\underline{\alpha}$, is also very easy

$$\underline{x}_i = i \cdot \underline{\alpha} \mod 1 \ , \qquad i \in \{0, 1, \ldots, L-1\} \ . \tag{3.16}$$

A "centering" can be performed by simply counting $i \in \{1, \ldots, L\}$ instead of $i \in \{0, \ldots, L-1\}$. This does not make the point set mean-free, but it avoids the all-zero vector.

For high L, the numeric cancellation introduced by the modulus operation becomes relevant. Suppose we require a numeric precision of at least $\frac{1}{10 \cdot L}$ for the sample coordinates, i.e.,

$$\frac{1}{10 \cdot L} \leq \mathrm{eps}(L \cdot \alpha) \ , \tag{3.17}$$

with machine epsilon $\mathrm{eps}(\cdot)$. For generator $\alpha = 1$ in single-precision floating-point format (binary32) [120], this is satisfied only until $L_{\max} = 1023$, and until $L_{\max} = 26\,843\,545$ in double-precision (binary64). Each generator α has different representations that are equivalent mathematically but not

numerically. For example, three different generators for the golden sequence and their double-precision $L_{\max}$ are

$$\alpha = \varphi = 1.618033\ldots \qquad L_{\max} = 20\,737\,779 \ , \tag{3.18}$$

$$\alpha = \varphi - 1 = \frac{1}{\varphi} = 0.618033\ldots \qquad L_{\max} = 27\,146\,105 \ , \tag{3.19}$$

$$\alpha = 1 - (\varphi - 1) = \frac{1}{\varphi^2} = 0.381966\ldots \qquad L_{\max} = 43\,923\,321 \ , \tag{3.20}$$

where the third generator produces the reflected point set.

Using an unsigned integer data type with wraparound behavior, a fixed-point arithmetic over $[0, 1)$ can implicitly compute the mod 1 operation via overflow. For n-bit unsigned integer and again

$$\frac{1}{10 \cdot L} \leq \frac{L}{2^n} \ , \tag{3.21}$$

we obtain $L_{\max} = 20\,724$ and $L_{\max} = 1\,358\,187\,913$ for α represented as a 32-bit and 64-bit unsigned integer, respectively.

3.2.3 Kronecker Lattice

The Kronecker lattice points are computed by combining equidistant points for the first coordinate with an $(s-1)$-dimensional Kronecker sequence in the other coordinates. The equidistant points are computed as a rank-1 lattice with generator $z = 1$. Centering can be performed as described above for rank-1 lattices and Kronecker sequence, i.e., adding $\frac{1}{2L}$ to the equidistant coordinate and skipping the all-zero vector of the Kronecker sequence.

3.2.4 Frolov Lattice

Enumeration of Frolov lattices is, in general, computationally difficult. It can be done by enumerating lattice points inside a larger set that has a shape that simplifies enumeration, e.g., a hypercube [O5, Fig. 3], [O8, Sec. IV-A] or a hyperellipsoid [90, Sec. 4.1], [89, Sec. 5]. Alternatively,

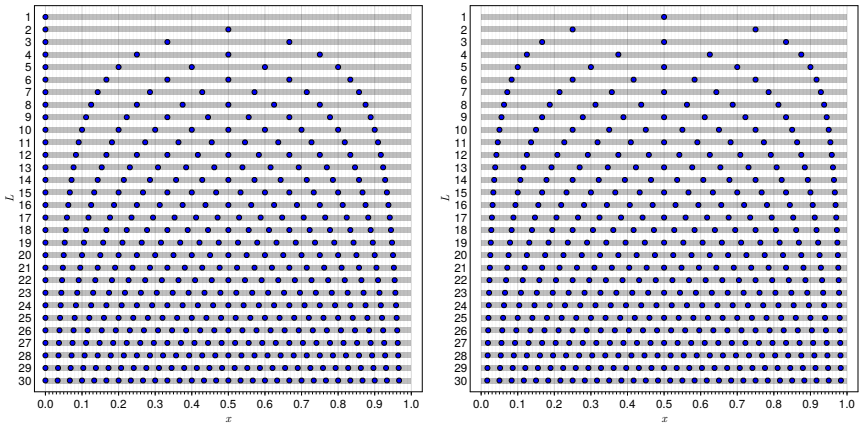

(a) Left-aligned equidistant. **(b)** Centered equidistant.

Figure 3.4: Equidistant 1D rank-1 lattices for various numbers of samples L (vertical axis).

the points can be enumerated recursively [O8, Sec. IV-B], [166, Sec. 3]. All these algorithms for enumerating Frolov lattices have a computational complexity linear in L and exponential in s. Frolov lattices can be centered by enumerating the points in $\left[-\frac{1}{2}, \frac{1}{2}\right]^s$ and adding $\frac{1}{2}$ to move them to the standard hypercube $[0,1]^s$, instead of enumerating them in $[0,1]^s$ directly.

3.3 Constructions

Having introduced various representations and enumerations, we now turn to the question of how to construct particularly good point sets, respectively their representations, that can be then used to enumerate the actual points.

3.3.1 Rank-1 Lattice

3.3.1.A (Brute Force Search) Elements of the generating vector $\underline{g}$ should have no factor in common with L, i.e., be relatively prime or

coprime. Otherwise, the points repeat. For example, with $L = 12$ and $g = 4$, we obtain (3.3)

$$\mathcal{P}_L = \{0, 1, 2, 3, \ldots, 11\} \cdot \frac{4}{12} \mod 1 \tag{3.22}$$

$$= \left\{0, \frac{1}{4}, \frac{1}{2}, \frac{3}{4}\right\} , \tag{3.23}$$

i.e., only four points (repeated three times, respectively) while computing with $L = 12$ points. This leads to unnecessarily poor coverage of the integrand. This restriction of the search space is however not much help as the number of integers coprime to L, given by Euler's totient function $\varphi(L)$ [127, A000010], has an average order of about L [151, § I.24]

$$\mathrm{E}\{\varphi(L)\} \approx \frac{6}{\pi^2} \cdot L \ , \tag{3.24}$$

therefore the complexity enumerating all admissible rank-1 lattices is $\mathcal{O}(L^s)$. In addition, we must evaluate a quality measure for each generator to identify the best one. Quality measures will be described in Chapter 5.

3.3.1.B (Component-by-Component Construction) Constructing generators for globally minimum discrepancy lattices is still subject to active research. One simplification is component-by-component construction [37], [30], [39]. Further dimensions are added to existing point sets, similar to the conditional sampling described in Section 2.2.2. However, this results in samples of varying quality along the different dimensions and combinations of dimensions.

3.3.1.C (Equidistant for $s = 1$) The best 1D rank-1 lattice is, trivially, the equidistant point set

$$x_i = i \cdot \frac{1}{L} \ , \qquad i \in \{0, 1, \ldots, L-1\} \ . \tag{3.25}$$

Sometimes, it is advantageous to use a centered version (that is however not a lattice)

$$x_i = \frac{2\,i+1}{2L} \ , \qquad i \in \{0, 1, \ldots, L-1\} \ . \tag{3.26}$$

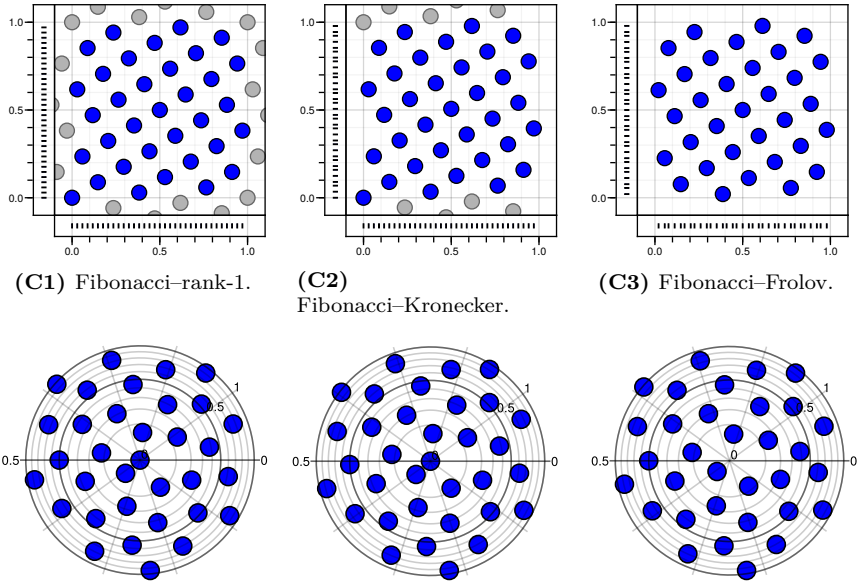

(C1) Fibonacci–rank-1.

(C2) Fibonacci–Kronecker.

(C3) Fibonacci–Frolov.

(P1) Transformed to Polar.

(P2) Transformed to Polar.

(P3) Transformed to Polar.

Figure 3.5: Fibonacci construction of rank-1 lattice, Kronecker lattice, and Frolov lattice, respectively. First row in Cartesian coordinates, second row mapped to polar coordinate system. Grey points indicate periodic repetition, if available. $L = 34$ in first two columns and $L = 33$ in last column. Polar representations show degraded local homogeneity near the pole. Discussed further in Section 6.6.4.

Visualization: Figure 3.4.

3.3.1.D (Fibonacci–Rank-1 Lattice for $s = 2$) In two dimensions, the optimal construction is well known: the **Fibonacci–rank-1 lattice**

$$\underline{x}_i = \frac{i}{F_{k+1}} \cdot \begin{bmatrix} 1 \\ F_k \end{bmatrix} \mod 1 \ , \qquad i \in \{0, 1, \ldots, F_{k+1} - 1\} \ , \tag{3.27}$$

where F_k is the k-th Fibonacci number [35, Ex. 2.8]. Note that the total number of lattice points must be a Fibonacci number, i.e., $L = F_{k+1}$.

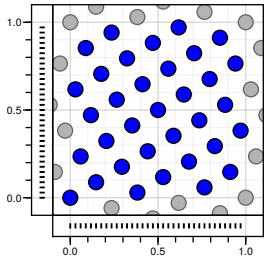

(C1) Fibonacci–rank-1.

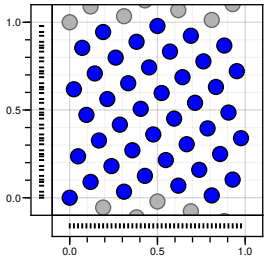

(C2) Fibonacci–Kronecker.

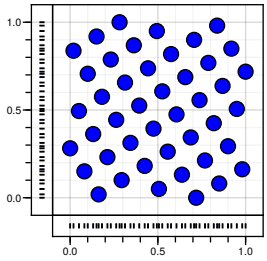

(C3) Fibonacci–Frolov.

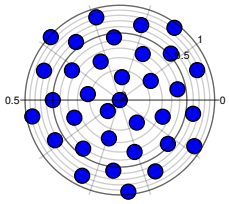

(P1) Transformed to Polar.

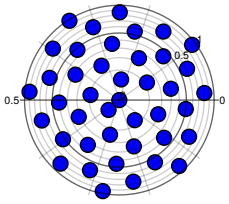

(P2) Transformed to Polar.

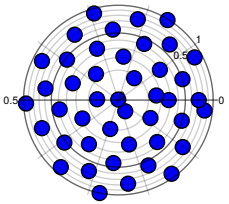

(P3) Transformed to Polar.

Figure 3.6: Same as Figure 3.5 but non-Fibonacci number of samples where applicable (Kronecker and Frolov). $L = 34 = F_9$ in first column and $L = 42$ last two columns. Contrary to Figure 3.5 where all point sets are very similar, they look rather different here. The non-periodicity of the Frolov lattice is visible in (P3) at the transition between 0° and 360° (line from center to right).

Visualization: Figures 3.5 C1 and B.1.

Both marginals, i.e., the x and the y coordinates, are equidistant point sets. The point set is periodic along both main axes.

Transformed to polar coordinates, this yields the well-known, conspicuous "sunflower pattern" (see Figures 1.4 and 3.5 P1). It is well known that the Fibonacci–rank-1 lattice belongs to the best possible point sets for cubature under very general conditions [177, p. 186], [123, p. 66], [35, p. 143], [38, p. 744], [68, Sec. 5], [90, p. 186]. In particular, for $L \in \{1, 2, 3, 5, 8, 13\}$,

it has been shown that the Fibonacci–rank-1 lattice is the unique global minimizer of the worst-case integration error of periodic functions in a Sobolev space [68]. It provides nearly equal-area packing with relatively high packing efficiency – about 70 % of that of a hexagonal close packing [144].

Arrangements of organs on plant stems or flower heads follow the Fibonacci–rank-1 lattice, showing striking spiral patterns in their phyllotaxis. Detailed studies targeting these arrangements date back more than 100 years [77]. The behavior can even be reproduced experimentally using a "magnetic cactus" [125]. The ubiquitous appearance of spiral phyllotaxis and its resilience to internal, environmental, and genetic variations suggests a connection to mathematics [49].

Several models have been proposed that try to explain the biological processes in the meristem that create the spiral phyllotaxis, e.g., the Hofmeister hypothesis and Snow hypothesis [74]. Investigations on a molecular level in plants showed the plant hormone auxin is triggering organ initiation. This activator is then consumed by the growing organ, effectively inhibiting the initiation of an adjacent organ [49]. In summary, opportunistic organ initiation constitutes an entirely local mechanism and explains phyllotaxis, just as stated in the Hofmeister hypothesis [49]. The occurrence of spirals and the golden angle as the divergence angle is, therefore, probably an emergent by-product rather than the mechanistic principle of the morphogenetic process [49].

According to [123, Theorem 3], the unit cell of the Fibonacci–rank-1 lattice is square for Fibonacci numbers $L = F_k$ where k is odd, and the generating vectors representing these cells are

$$\underline{g}_1 = \begin{bmatrix} \frac{F_t}{F_{2t+1}} \\ \frac{(-1)^{t-1} F_{t+1}}{F_{2t+1}} \end{bmatrix} \quad , \quad \underline{g}_2 = \begin{bmatrix} \frac{F_{t+1}}{F_{2t+1}} \\ \frac{(-1)^{t} F_{t}}{F_{2t+1}} \end{bmatrix} \quad , \quad k = 2\,t + 1 \ , \quad t \in \mathbb{N} \ . \tag{3.28}$$

For example, with ($k = 9$) odd, we have $L = F_9 = 34$, therefore the Fibonacci–rank-1 lattice with $L = 34$ has square unit cells (see Figure 3.5 C1).

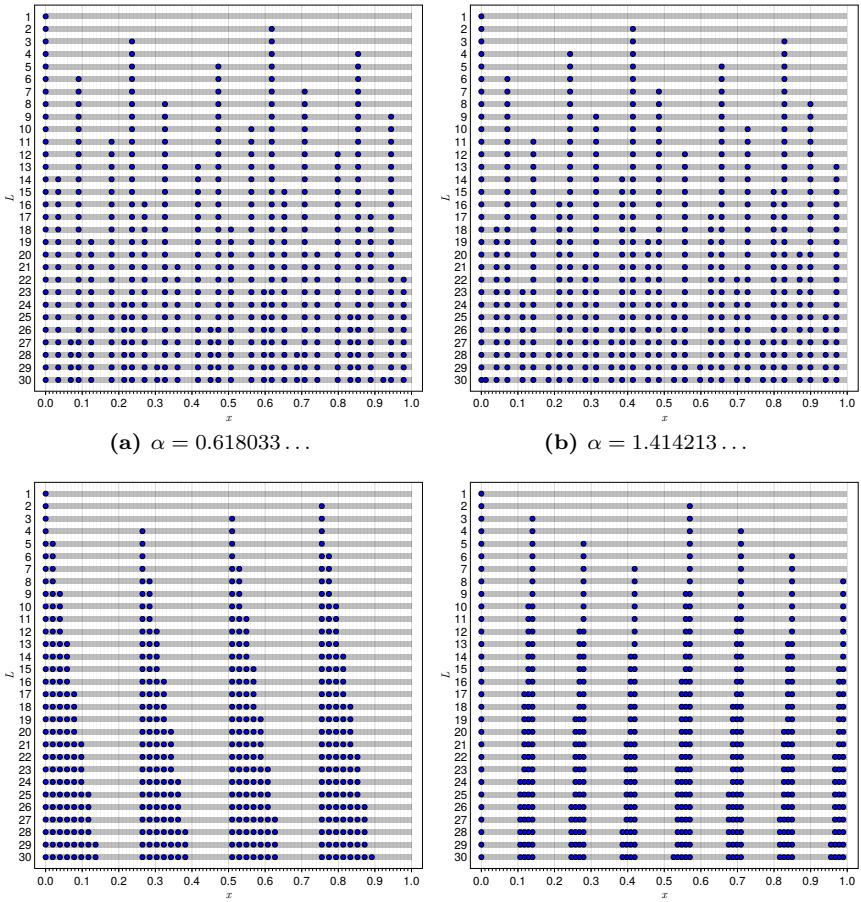

(a) $\alpha = 0.618033\ldots$ **(b)** $\alpha = 1.414213\ldots$

(c) $\alpha = 0.754877\ldots$ **(d)** $\alpha = 0.569840\ldots$

Figure 3.7: 1D Kronecker sequences with various generators α: (a) inverse golden ratio, (b) silver ratio, (c) inverse plastic ratio, (d) inverse square plastic ratio.

3.3.2 Kronecker Sequence

A current overview of Kronecker sequence constructions is given in [132, pp. 57–58]. We present some state-of-art constructions in detail so that we can later discuss how they relate to each other and to the newly developed methods.

3.3.2.A (Golden Sequence / Fibonacci–Kronecker Sequence for $s = 1$) A well-known 1D Kronecker sequence is the **Fibonacci–Kronecker sequence** or **Golden sequence**, with irrational generator $\alpha = \frac{1}{\Phi}$

$$x_i = i \cdot \frac{1}{\Phi} \mod 1 \ , \qquad i \in \{0, 1, \ldots, L-1\} \ , \tag{3.29}$$

with the golden ratio [127, A001622], [127, A094214],

$$\Phi = \frac{\sqrt{5}+1}{2} = 1.618033\ldots \ , \tag{3.30}$$

$$\frac{1}{\Phi} = \frac{\sqrt{5}-1}{2} = 0.618033\ldots \ . \tag{3.31}$$

Visualization: Figure 3.7a.

This is believed to be the best possible 1D Kronecker sequence, as the golden ratio is the worst approximable regarding continued fraction expansion. In higher dimensions, no explicit generating vector is known where the same strict discrepancy bound holds [124, p. 222].

3.3.2.B (Plastic Ratio for $s = 2$) The so-called plastic ratio $\gamma = 1.324717\ldots$ [127, A060006], i.e., the unique real root of $x^3 - x - 1$, is suggested as a basis for deriving 2D Kronecker sequences. The vector

$$\underline{\alpha} = \begin{bmatrix} \gamma^{-1} \\ \gamma^{-2} \end{bmatrix} = \begin{bmatrix} 0.754877\ldots \\ 0.569840\ldots \end{bmatrix}$$

is badly approximable, similar to the golden ratio in the 1D case [67, p. 6]. In addition, $1 + \gamma^{-1} = 1.754877\ldots$ [127, A109134] (only the fractional part

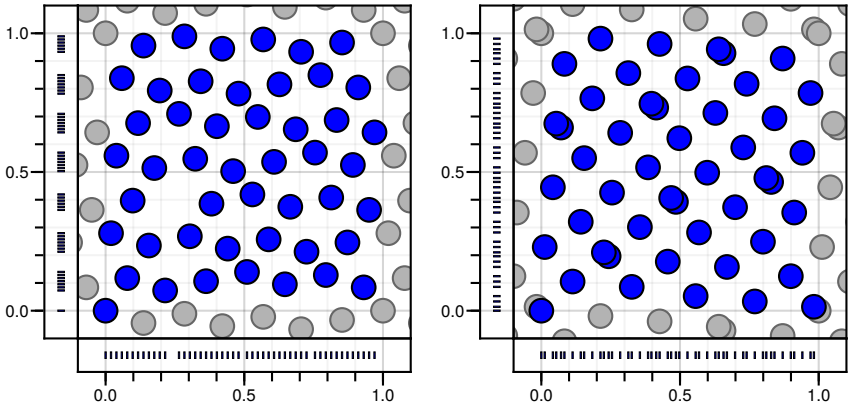

(a) $\underline{\alpha} = \begin{bmatrix} 0.754877\ldots \\ 0.569840\ldots \end{bmatrix}$ **(b)** $\underline{\alpha} = \begin{bmatrix} 1.414213\ldots \\ 1.732050\ldots \end{bmatrix}$

Figure 3.8: 2D Kronecker sequences, $L = 48$, with different generators $\underline{\alpha}$, (a) derived from plastic number and (b) square roots of primes, equivalent to R_2 sequence. Note that in (a) the 2D plane looks very homogeneous, but the marginals show point collisions, whereas in (b), it is vice versa. Grey points indicate periodic repetition. See also Figures B.9 and B.10.

is relevant in Kronecker sequences), the real root of $x^3 - 2x^2 + x - 1$ is, just like the golden ratio, a limit point of Pisot numbers [13, p. 1251].

Visualization: Figures 3.8a and B.9.

While the point distribution in the 2D plane looks locally homogeneous, the one-dimensional projections or marginals are significantly less homogeneous than the 1D Kronecker sequences from the golden ratio or a square root (see Figure 3.7).

3.3.2.C (R_s-Sequence) The concept of the plastic ratio has been extended to higher dimensions by Martin Roberts [146], see also [155]. According to this, a "generalized version of the golden ratio" Φ_s is defined as the unique positive root of the polynomial $x^{s+1} - x - 1 = 0$, in particular,

$$\Phi = \Phi_1 = 1.618033\ldots \tag{3.32}$$

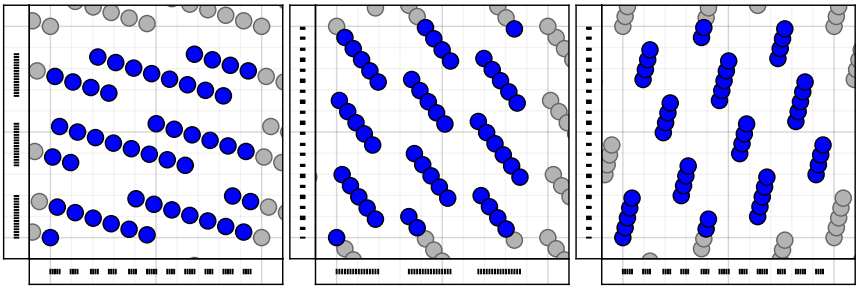

(a) $\underline{\alpha} = \begin{bmatrix} 0.819172\ldots \\ 0.671043\ldots \\ 0.549700\ldots \end{bmatrix}$

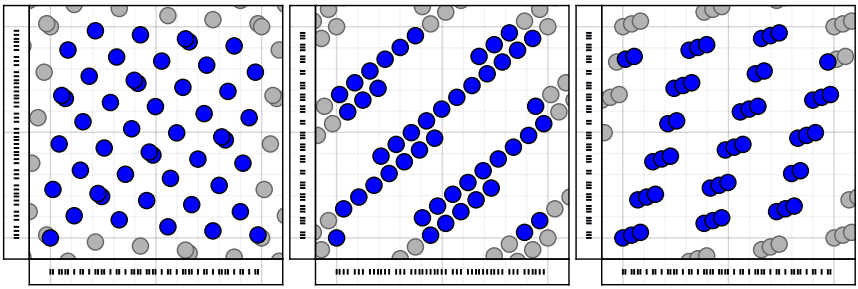

(b) $\underline{\alpha} = \begin{bmatrix} 1.414213\ldots \\ 1.732050\ldots \\ 2.236067\ldots \end{bmatrix}$

Figure 3.9: 3D Kronecker sequences, $L = 48$, visualized as xy, xz, and yz projection, respectively. (a) shows the R_3-sequence and (b) the square roots of primes sequence. Grey points indicate periodic repetition. See also Figures B.23 and B.24.

$$\gamma = \Phi_2 = 1.324717\ldots \tag{3.33}$$
$$\Phi_3 = 1.220744\ldots \tag{3.34}$$
$$\Phi_4 = 1.167303\ldots \tag{3.35}$$
$$\Phi_5 = 1.134724\ldots \tag{3.36}$$
$$\vdots \tag{3.37}$$

and the generating vector of the R_s-sequence is defined as

$$\underline{\alpha} = \begin{bmatrix} \frac{1}{\Phi_s} & \frac{1}{\Phi_s^2} & \cdots & \frac{1}{\Phi_s^s} \end{bmatrix}^\top \quad . \tag{3.38}$$

The R_s-sequence is identical to the golden ratio-based Fibonacci–Kronecker sequence for $s = 1$ and the plastic ratio-based sequence for $s = 2$.

Visualization: R_2 sequence, Figures 3.8 a and B.9; R_3 sequence, Figures 3.9 a and B.23.

3.3.2.D (Roots of Primes) A generating vector for higher-dimensional point sequences can also be constructed from the roots of pairwise coprime numbers [124, p. 209], like, for example, succeeding prime numbers [35, p. 142],

$$\underline{x}_i = i \cdot \begin{bmatrix} \sqrt{2} \\ \sqrt{3} \\ \sqrt{5} \\ \vdots \\ \sqrt{p_s} \end{bmatrix} \mod 1 \ , \qquad i \in \{0, 1, \ldots, L-1\} \ , \tag{3.39}$$

where p_s is the s-th prime number.

Visualization: 1D (note that $1 + \sqrt{2}$ is called the silver ratio), Figure 3.7 b; 2D, Figures 3.8 b and B.10; 3D, Figures 3.9 b and B.24.

Noticeably, the marginals, i.e., the 1D Kronecker sequences with roots of primes as generators, look relatively homogeneous, while point collisions occur in the 2D joint space.

3.3.2.E (Optimization) Using a suitable quality measure, numerical optimization can also obtain good candidates for the generating vector $\underline{\alpha}$. This is discussed further in Chapter 5.

3.3.3 Kronecker Lattice

Kronecker sequences are closely related to Kronecker lattices. The former are open point sets, the latter closed point sets but with somewhat better discrepancy.

3.3.3.A (From Kronecker Sequence) Every $(s-1)$-dimensional Kronecker sequence from above can be turned into a s-dimensional Kronecker lattice with generator

$$\underline{g} = \begin{bmatrix} \frac{1}{L} & \alpha_1 & \alpha_2 & \dots & \alpha_{s-1} \end{bmatrix}^\top \quad . \tag{3.40}$$

Note that this point set is not periodic anymore.

3.3.3.B (Fibonacci–Kronecker Lattice for $s = 2$) A famous example is the Fibonacci–Kronecker sequence with

$$\underline{g} = \begin{bmatrix} \frac{1}{L} & \frac{1}{\Phi} \end{bmatrix}^\top \quad . \tag{3.41}$$

Visualization: Figures 3.5 C2, 3.6 C2 and B.2.

3.3.4 Frolov Lattice

3.3.4.A (Classical Frolov) The representation matrix of classical Frolov lattices is derived from so-called admissible polynomials. In principle, any polynomial is admissible if it 1) has integer coefficients, 2) has leading coefficient one, 3) is irreducible over $\mathbb{Q}$, and 4) has s different real roots ξ_j

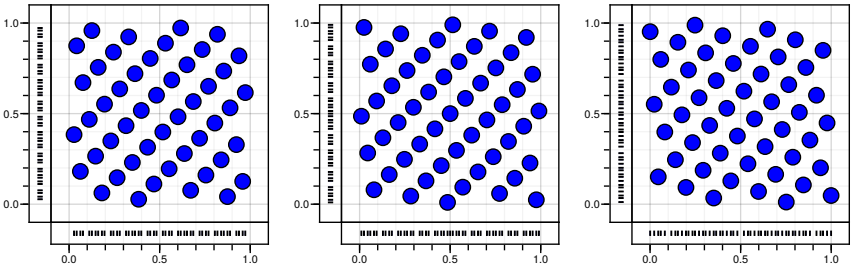

(a) Classical Frolov **(b)** Chebyshev First Kind **(c)** Chebyshev Second Kind

Figure 3.10: 2D Frolov lattices, with $L \approx 50$.

[90, Proposition 1]. Frolov's original admissible polynomial is [46, Eq. 5], [90, Eq. 1.5]

$$P(x) = -1 + \prod_{j=1}^{s}(x - (2 \cdot j - 1)) \tag{3.42}$$
$$= \prod_{j=1}^{s}(x - \xi_j) \ .$$

From the polynomial's roots, ξ_j, we construct a Vandermonde matrix [90, Eq. 1.6]

$$\mathbf{V}^{\mathrm{Cls}} = \begin{bmatrix} 1 & \xi_1 & \xi_1^2 & \cdots & \xi_1^{s-1} \\ 1 & \xi_2 & \xi_2^2 & \cdots & \xi_2^{s-1} \\ \vdots & \vdots & \vdots & \ddots & \vdots \\ 1 & \xi_s & \xi_s^2 & \cdots & \xi_s^{s-1} \end{bmatrix} \ . \tag{3.43}$$

The classical Frolov lattice is then produced via $\mathbf{V}^{\mathrm{Cls}}(\mathbb{Z}^s) \cap \mathcal{Q}^s$, i.e., using $\mathbf{V}^{\mathrm{Cls}}$, or a rescaled version, as representation matrix and enumerating the respective points. A general limitation of Frolov lattices defined via Vandermonde matrices is that one generating vector of the lattice's basis system, i.e., the columns of $\mathbf{V}^{\mathrm{Cls}}$, is always $\underline{1}$, i.e., the diagonal of the

Euclidean basis system, due to the column of ones in (3.43). For example, we have in

$$s = 2: \quad \mathbf{V}^{\mathrm{Cls}} = \begin{bmatrix} 1 & 0.585786\ldots \\ 1 & 3.414213\ldots \end{bmatrix} , \tag{3.44}$$

$$s = 3: \quad \mathbf{V}^{\mathrm{Cls}} = \begin{bmatrix} 1 & 1.139194\ldots & 1.297763\ldots \\ 1 & 2.745898\ldots & 7.539957\ldots \\ 1 & 5.114907\ldots & 26.162279\ldots \end{bmatrix} , \tag{3.45}$$

$$s = 4: \quad \mathbf{V}^{\mathrm{Cls}} = \begin{bmatrix} 1 & 0.979552\ldots & 0.959522\ldots & 0.939902\ldots \\ 1 & 3.063573\ldots & 9.385483\ldots & 28.753118\ldots \\ 1 & 4.936426\ldots & 24.368305\ldots & 120.292345\ldots \\ 1 & 7.020447\ldots & 49.286688\ldots & 346.014632\ldots \end{bmatrix} . \tag{3.46}$$

The magnitudes of the roots ξ_n grow for higher dimensions. In conjunction with the high powers in the last columns of (3.43), this leads to numerical problems.

Visualization: 2D, Figures 3.10a and B.3; 3D, Figure B.12.

3.3.4.B (Chebyshev Polynomials of the First Kind for $s = 2^n$) Admissible polynomials can also be constructed from Chebyshev polynomials.

Definition 3.1. Chebyshev polynomials of the first kind $T_s(x)$ are recursively defined as

$$T_0(x) = 1 \ , \tag{3.47}$$

$$T_1(x) = x \ , \tag{3.48}$$

$$T_s(x) = 2 \cdot x \cdot T_{s-1}(x) - T_{s-1}(x) \ , \quad s \geq 2 \ . \tag{3.49}$$

For dimensions that are powers of two, i.e., $s = 2^n$, the rescaled Chebyshev polynomial of the first kind

$$\widetilde{T}_s(x) = 2 \cdot T_s(x/2)$$

is an admissible polynomial [89, p. 427]. The roots are

$$t_{n,k} = 2 \cdot \cos\left(\pi \cdot \frac{2 \cdot k - 1}{2 \cdot s}\right) \ , \quad k \in \{1, 2, \ldots, s\} \ , \tag{3.50}$$

and with the corresponding Vandermonde matrix $\mathbf{V}^{\mathrm{Cheb1}}$, we can construct the Chebyshev1–Frolov lattice $\mathbf{V}^{\mathrm{Cheb1}}(\mathbb{Z}^s) \cap \mathcal{Q}^s$. For example, we have in

$$s = 2\colon \quad \mathbf{V}^{\mathrm{Cheb1}} \approx \begin{bmatrix} 1 & 1.414213\ldots \\ 1 & -1.414213\ldots \end{bmatrix} \ , \tag{3.51}$$

$$s = 3\colon \quad s \neq 2^n \ , \tag{3.52}$$

$$s = 4\colon \quad \mathbf{V}^{\mathrm{Cheb1}} \approx \begin{bmatrix} 1 & 1.847759\ldots & 3.414213\ldots & 6.308644\ldots \\ 1 & 0.765366\ldots & 0.585786\ldots & 0.448341\ldots \\ 1 & -0.765366\ldots & 0.585786\ldots & -0.448341\ldots \\ 1 & -1.847759\ldots & 3.414213\ldots & -6.308644\ldots \end{bmatrix} . \tag{3.53}$$

Visualization: Figure 3.10 b.

3.3.4.C (Chebyshev Polynomials of the Second Kind for $(2 \cdot s + 1)$ prime) Chebyshev polynomials of the second kind also give rise to a Frolov lattice.

Definition 3.2. Chebyshev polynomials of the second kind $U_s(x)$ are recursively defined as

$$U_0(x) = 1 \ , \tag{3.54}$$

$$U_1(x) = 2 \cdot x \ , \tag{3.55}$$

$$U_s(x) = 2 \cdot x \cdot U_{s-1}(x) - U_{s-1}(x) \ , \quad s \geq 2 \ . \tag{3.56}$$

After some transforms of variables [90, Lemma 3, Lemma 5], it gives rise to a polynomial that is admissible if $(2 \cdot s + 1)$ is a prime. Its roots are

$$\xi_j = 2 \cos\left(\pi \cdot \frac{2j}{2s+1}\right) \ , \quad j \in \{1, 2, \ldots, s\} \ , \tag{3.57}$$

yielding its corresponding Vandermonde matrix $\mathbf{V}^{\mathrm{Chb2}}$. An equivalent but numerically more suitable and not-Vandermonde representation matrix $\mathbf{T}^{\mathrm{Chb2T}}$ can be obtained via a transformation [90, Lemma 1], resulting in

$$\left[\mathbf{T}^{\mathrm{Chb2T}}\right]_{i,j} = \cos\left(\pi \cdot \frac{2i \cdot (j-1)}{2s+1}\right) \cdot c(j) \ , \tag{3.58}$$
$$c(j) = \begin{cases} 1 \ , & j = 1 \\ 2 \ , & j > 1 \end{cases} \ .$$

For example, we have

$$s = 2\colon \qquad \mathbf{T}^{\mathrm{Cheb2T}} \approx \begin{bmatrix} 1 & 0.618033\ldots \\ 1 & -1.618033\ldots \end{bmatrix} \ , \tag{3.59}$$

$$s = 3\colon \qquad \mathbf{V}^{\mathrm{Cheb2T}} = \begin{bmatrix} 1 & 1.246979\ldots & -0.445041\ldots \\ 1 & -0.445041\ldots & -1.801937\ldots \\ 1 & -1.801937\ldots & 1.246979\ldots \end{bmatrix} \ , \tag{3.60}$$

$$s = 4\colon \qquad 2 \cdot s + 1 = 9, \text{ not prime} \ . \tag{3.61}$$

Visualization: 2D, Figures 3.10 c and B.4; 3D, Figure B.12.

3.3.4.D (Fibonacci–Frolov Lattice for $s = 2$) Every rank-1 lattice and Kronecker lattice can be represented as a Frolov lattice. For example, the Fibonacci–rank-1 lattice (3.27) can be represented as [36, Eq. 15]

$$\{\underline{x}_i\} = \mathbf{T}\left(\mathbb{Z}^2\right) \cap \mathcal{Q}^2 \ , \quad \mathbf{T} = \begin{bmatrix} 0 & \frac{1}{F_{k+1}} \\ 1 & \frac{F_k}{F_{k+1}} \end{bmatrix} \ , \quad i \in \{1, 2, \ldots, F_{k+1}\} \ , \tag{3.62}$$

and the Fibonacci–Kronecker lattice (3.41) as [36, Eq. 11]

$$\{\underline{x}_i\} = \mathbf{T}\left(\mathbb{Z}^2\right) \cap \mathcal{Q}^2 \ , \quad \mathbf{T} = \begin{bmatrix} 0 & \frac{1}{L} \\ 1 & \Phi \end{bmatrix} \ , \quad i \in \{1, 2, \ldots, F_{k+1}\} \ . \tag{3.63}$$

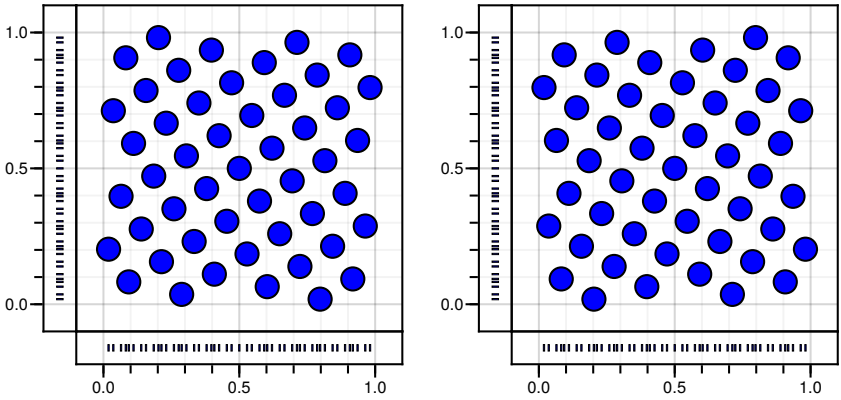

(a) Fibonacci–Frolov lattice with $\mathbf{T}^{\mathrm{FibS1}}$ **(b)** Fibonacci–Frolov lattice with $\mathbf{T}^{\mathrm{FibS2}}$

Figure 3.11: 2D Frolov lattices, with $L = 49$.

In particular, the square-unit-cell representation (3.28) from [123, Theorem 3] of certain Fibonacci–rank-1 lattices gives rise to a Frolov-type representation matrix of the respective rank-1 lattice

$$\mathbf{T}^{\mathrm{FibRk1}} = \begin{bmatrix} \frac{F_t}{F_{2t+1}} & \frac{F_{t+1}}{F_{2t+1}} \\ \frac{(-1)^{t-1}F_{t+1}}{F_{2t+1}} & \frac{(-1)^t F_t}{F_{2t+1}} \end{bmatrix}, \qquad t \in \mathbb{N} \ . \tag{3.64}$$

Note that, unlike the Frolov lattices mentioned before, this is an integration lattice, i.e., it contains $\mathbb{Z}^2$ as a subset and periodically extends into every unit cell of the $\mathbb{Z}^2$ lattice.

We can, however, derive an aperiodic Fibonacci–Frolov representation matrix as follows. The length of the vectors in (3.64) is exactly the length of the corresponding square lattice cell, getting smaller for higher numbers of samples. Hence, we can obtain the corresponding unit-absolute-determinant matrix by multiplying with $\sqrt{L}$

$$\mathbf{T}^{\mathrm{FibRk1}} = \begin{bmatrix} \frac{F_t}{\sqrt{F_{2t+1}}} & \frac{F_{t+1}}{\sqrt{F_{2t+1}}} \\ \frac{(-1)^{t-1}F_{t+1}}{\sqrt{F_{2t+1}}} & \frac{(-1)^t F_t}{\sqrt{F_{2t+1}}} \end{bmatrix} .$$

The ratios for the limit $t \to \infty$ are

$$\lim_{t\to\infty} \frac{F_t}{\sqrt{F_{2t+1}}} = \frac{1}{\sqrt{1+\Phi^2}} \approx 0.525731 \tag{3.65}$$

$$\lim_{t\to\infty} \frac{F_{t+1}}{\sqrt{F_{2t+1}}} = \frac{\Phi}{\sqrt{1+\Phi^2}} \approx 0.850650 \ . \tag{3.66}$$

Proof. Starting from the identity [19], [72, p. 107]

$$F_n = F^2_{\frac{n+1}{2}} + F^2_{\frac{n-1}{2}} \ ,$$

that holds for odd n, we substitute $n \to 2t+1$, see also [123, Eq. 2.2]

$$F_{2t+1} = F^2_{t+1} + F^2_t \ ,$$

rearrange for $\frac{F_t^2}{F_{2t+1}}$

$$\frac{F_t^2}{F_{2t+1}} = \left(\frac{F^2_{t+1}}{F^2_t} + 1\right)^{-1} \ ,$$

and obtain

$$\lim_{t\to\infty} \frac{F_t}{\sqrt{F_{2t+1}}} = \left(\Phi^2+1\right)^{-\frac{1}{2}} \ ,$$

using the relationship

$$\lim_{t\to\infty} \frac{F_{t+1}}{F_t} = \Phi \ .$$

□

Now we can state the representation matrices $\mathbf{T}^{\mathrm{FibS1}}$, $\mathbf{T}^{\mathrm{FibS2}}$ of the two aperiodic, square Fibonacci–Frolov lattices

$$\mathbf{T}^{\mathrm{FibS1,2}} = \begin{bmatrix} \frac{1}{\sqrt{1+\Phi^2}} & \frac{\Phi}{\sqrt{1+\Phi^2}} \\ \frac{\mp\Phi}{\sqrt{1+\Phi^2}} & \frac{\pm 1}{\sqrt{1+\Phi^2}} \end{bmatrix} \ , \tag{3.67}$$

$$\mathbf{T}^{\mathrm{FibS1}} = \begin{bmatrix} 0.525731\ldots & 0.850650\ldots \\ -0.850650\ldots & 0.525731\ldots \end{bmatrix} \ , \tag{3.68}$$

$$\mathbf{T}^{\mathrm{FibS2}} = \begin{bmatrix} 0.525731\ldots & 0.850650\ldots \\ 0.850650\ldots & -0.525731\ldots \end{bmatrix} \ . \tag{3.69}$$

Visualization: Figure 3.11.

Both marginals of this lattice are not equidistant but much more homogeneous than, e.g., random samples (see Figure 3.5 C3). It cannot be periodically extended along any main axis (see Figure 3.6 C3). However, it can be expanded by increasing the area $\mathcal{Q}^2$ over which the cut is made in $\mathcal{P}_L = \mathbf{T}^{\mathrm{Fib}}(\mathbb{Z}^2) \cap \mathcal{Q}^2$. The polar representation (see Figure 3.6 P3), shows the conspicuous "Fibonacci spirals" as well, but due to non-periodicity, the pattern has a disruption where the angle switches from 0 to 2π (line from center to right). The Fibonacci–Frolov lattice will be further explained and extended in Chapter 4.

3.4 Summary

We have become familiar with the sample representations rank-1 lattice, Kronecker lattice, Frolov lattice, and Kronecker sequence. Furthermore, various known construction methods were listed, respectively, that generate uniform samples with desirable properties. We saw that each 2D lattice representation has a Fibonacci construction and identified the connections between them.

CHAPTER 4

Fibonacci–Frolov Construction and Higher-Dimensional Extensions

Contents

> Look at the lilies and how they grow. They don't work or make their clothing, yet Solomon in all his glory was not dressed as beautifully as they are. And if God cares so wonderfully for flowers that are here today and thrown into the fire tomorrow, he will certainly care for you. Why do you have so little faith?
>
> *Luke 12:27-28 NLT*
> Jesus of Nazareth (c. 4 BC – AD 31)

We have just explained the relationship between the Fibonacci–rank-1 lattice and an aperiodic Fibonacci–Frolov lattice (3.67). This Fibonacci–Frolov construction allows for some interesting and intuitive insights on why the 2D Fibonacci lattices have superior properties. The concept was introduced 15 years ago by James Purser in a non-peer-reviewed publication [140], but has not received attention elsewhere. It involves a set of unimodular matrices giving rise to a lattice of transformations all of which transform a square lattice into a square lattice. Relaxation of the lattice into a continuous space of transformations enables the generation of non-uniform point sets with a local homogeneity similar to that of square lattices everywhere. A possible extension to higher dimensions is also presented.

4.1 2D Fibonacci–Frolov Lattice

The Fibonacci matrix $\mathbf{M}$, sometimes also referred to as Fibonacci $\mathbf{Q}$ matrix [50], is defined as

$$\mathbf{M} = \begin{bmatrix} 1 & 1 \\ 1 & 0 \end{bmatrix} \quad . \tag{4.1}$$

This matrix produces the Fibonacci numbers F_k according to the recurrence

$$\mathbf{M} \cdot \begin{bmatrix} F_k \\ F_{k-1} \end{bmatrix} = \begin{bmatrix} F_{k+1} \\ F_k \end{bmatrix} \quad . \tag{4.2}$$

The eigenvalue decomposition of $\mathbf{M}$ is

$$\begin{bmatrix} 1 & 1 \\ 1 & 0 \end{bmatrix} = \mathbf{V} \cdot \mathbf{D} \cdot \mathbf{V}^\top \ , \tag{4.3}$$

$$\mathbf{D} = \begin{bmatrix} \Phi & 0 \\ 0 & -\frac{1}{\Phi} \end{bmatrix} \ , \tag{4.4}$$

$$\mathbf{V} = \begin{bmatrix} \cos(\gamma) & -\sin(\gamma) \\ \sin(\gamma) & \cos(\gamma) \end{bmatrix} \cdot \begin{bmatrix} 0 & 1 \\ 1 & 0 \end{bmatrix} \ , \tag{4.5}$$

$$\gamma = \tan^{-1}(-\Phi) = 58.282525\ldots^\circ \ , \tag{4.6}$$

$$\mathbf{V} = \begin{bmatrix} 0.850650\ldots & 0.525731\ldots \\ 0.525731\ldots & -0.850650\ldots \end{bmatrix} \ . \tag{4.7}$$

Note that there are many relationships between the Fibonacci–rank-1 lattice (3.27), the Fibonacci–Kronecker lattice (3.41), and the Fibonacci matrix $\mathbf{M}$ (4.5), via the Fibonacci numbers and the golden ratio. In particular, the eigenvector matrix $\mathbf{V} = \mathbf{V}^\top$ is equivalent to the Fibonacci–Frolov representation matrix we obtained in (3.67).

Therefore, we can use the orthogonal eigenvector matrix $\mathbf{V}$ or $\mathbf{V}^\top$ as Frolov lattice representation matrix $\mathbf{T}$ in (3.11), yielding an orthogonal Fibonacci–Frolov lattice

$$\mathcal{P}_L = \mathbf{T}\left(\mathbb{Z}^2\right) \cap \mathcal{Q}^2 \ , \tag{4.8}$$

$$\mathbf{T} = \frac{1}{\alpha}\,\mathbf{V}^\top \ ,$$

where α is a scaling parameter that decides the number of samples, $L \approx \alpha^s$ since $|\det(\mathbf{V})| = 1$.

4.2 Towards Higher Dimensions with Purser's Extension

A novel theory of good Frolov lattices has been formalized [140] that covers the two-dimensional Fibonacci–Frolov lattice and extends to higher dimensions.

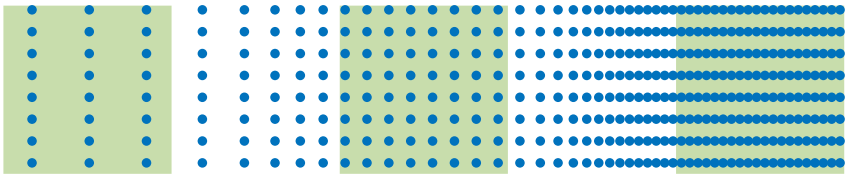

(a) Regular lattice.

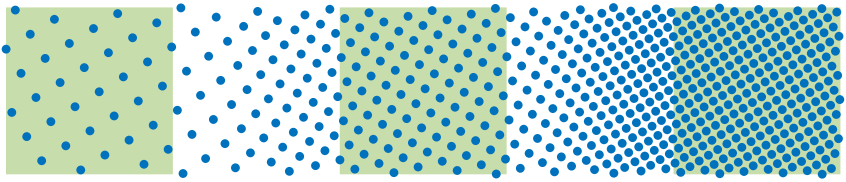

(b) Fibonacci lattice.

Figure 4.1: Regular or square configuration (center), stretching of horizontal coordinate (left), and compression of horizontal coordinate (right). If anisotropically rescaled, the Fibonacci lattice (b) returns to square configurations periodically (green boxes), but the regular lattice (a) does not.

It is based on sets of commuting ($\mathbf{A} \cdot \mathbf{B} = \mathbf{B} \cdot \mathbf{A}$) and unimodular ($\mathbf{A} \in \mathbb{Z}^s$, $|\det \mathbf{A}| = 1$) matrices $\mathbf{M}_0, \mathbf{M}_1, \ldots, \mathbf{M}_{s-1}$ and their powers $\mathbf{M}_d^k$, $k \in \mathbb{Z}$. They form a basis system spanning a "lattice" of linear transformations. Each lattice point (in the transformation domain) is an unimodular transform and therefore maps the s-dimensional regular integer lattice $\mathbb{Z}^s$ (the lattice in the state domain where we want to obtain low-discrepancy point sets) into itself. Due to the lattice structure, "intermediate" transformations (between lattice points denoting unimodular transformations) can never be far away from an unimodular neighbor and, therefore, the original square regular lattice configuration where all the points have approximately equal distances to their neighbors. This means that it is not possible for points lumping together or string together to form "lines" with empty space in between, as would happen when deforming a regular lattice along a single coordinate axis (see Figure 4.1 a). Instead, the points periodically change their neighborhood relationships, forming

regular lattices with new neighbors (see Figure 4.1b). We explain this theory in detail, exemplarily in the two-dimensional case.

4.2.1 Exemplary Demonstration in Two Dimensions

We review the two-dimensional Fibonacci–Frolov lattice in light of this theory. Starting from the diagonalization of $\mathbf{M}$

$$\mathbf{M} = \mathbf{M}_0 = \mathbf{V} \cdot \mathbf{D} \cdot \mathbf{V}^\top \tag{4.9}$$

in (4.5), we demonstrate how to produce a different but commuting matrix. We do this in two different ways and will see that both are equivalent for the special case of the Fibonacci matrix.

First, we create the matrix $\mathbf{M}_1^{\mathrm{PD}}$ that shares eigenvectors and eigenvalues and thus necessarily commutes with $\mathbf{M}_0$ by interchanging (or circularly shifting) the eigenvalues in $\mathbf{D}$ with respect to the eigenvectors, i.e., the columns in $\mathbf{V}$. Therefore we define the unsigned permutation matrix $\mathbf{P}^{\mathrm{u}}$

$$\mathbf{P}^{\mathrm{u}} = \begin{bmatrix} 0 & 1 \\ 1 & 0 \end{bmatrix} \tag{4.10}$$

and use it to permute the eigenvalues in $\mathbf{D}$ or, equivalently, the columns in $\mathbf{V}$

$$\begin{aligned} \mathbf{M}_1^{\mathrm{PD}} &= \mathbf{V} \cdot \left(\mathbf{P}^{\mathrm{u}} \cdot \mathbf{D} \cdot (\mathbf{P}^{\mathrm{u}})^\top\right) \cdot \mathbf{V}^\top \ , \\ &= (\mathbf{V} \cdot \mathbf{P}^{\mathrm{u}}) \cdot \mathbf{D} \cdot (\mathbf{V} \cdot \mathbf{P}^{\mathrm{u}})^\top \ . \end{aligned} \tag{4.11}$$

Numerically, we obtain (digits truncated to two decimal places)

$$\mathbf{M}_0 = \begin{bmatrix} 1 & 1 \\ 1 & 0 \end{bmatrix} \approx \underbrace{\begin{bmatrix} 0.85 & 0.52 \\ 0.52 & -0.85 \end{bmatrix}}_{\mathbf{V}} \cdot \underbrace{\begin{bmatrix} 1.61 & 0 \\ 0 & -0.61 \end{bmatrix}}_{\mathbf{D}} \cdot \underbrace{\begin{bmatrix} 0.85 & 0.52 \\ 0.52 & -0.85 \end{bmatrix}}_{\mathbf{V}^\top} \ , \tag{4.12}$$

$$\mathbf{M}_1^{\mathrm{PD}} = \begin{bmatrix} 0 & -1 \\ -1 & 1 \end{bmatrix} \approx \underbrace{\begin{bmatrix} 0.85 & 0.52 \\ 0.52 & -0.85 \end{bmatrix}}_{\mathbf{V}} \cdot \underbrace{\begin{bmatrix} -0.61 & 0 \\ 0 & 1.61 \end{bmatrix}}_{\mathbf{P}^{\mathrm{u}} \cdot \mathbf{D} \cdot (\mathbf{P}^{\mathrm{u}})^\top} \cdot \underbrace{\begin{bmatrix} 0.85 & 0.52 \\ 0.52 & -0.85 \end{bmatrix}}_{\mathbf{V}^\top} \ . \tag{4.13}$$

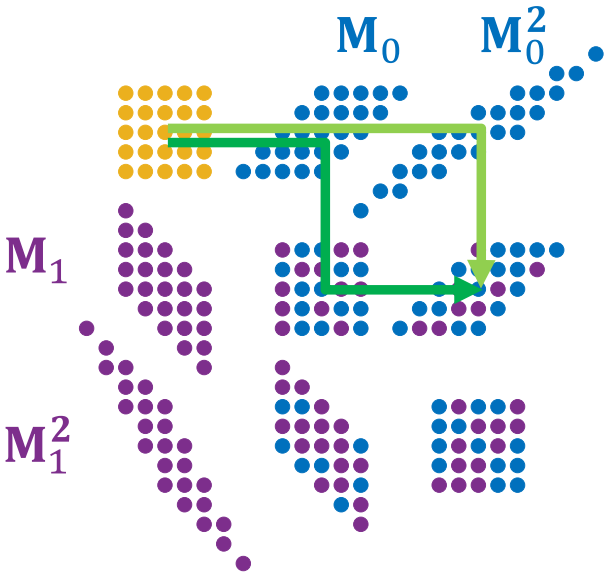

Figure 4.2: Lattice of transformations via the "basis system" of commuting unimodular matrices $\mathbf{M}_0, \mathbf{M}_1$. A convex set of integer vectors $\underline{z} \in \mathbb{Z}^2$ (yellow) is transformed in eight ways, yielding other convex sets of integer vectors. Traced with arrows are $\mathbf{M}_0 \cdot \mathbf{M}_1 \cdot \mathbf{M}_0$ (dark green) and $\mathbf{M}_0^2 \cdot \mathbf{M}_1$ (light green), both equivalent.

Note that $\mathbf{M}_1^{\mathrm{PD}}$ is, interestingly, integer-valued just like $\mathbf{M}_0$.

Alternatively, with the signed permutation matrix $\mathbf{P}^{\mathrm{s}}$

$$\mathbf{P}^{\mathrm{s}} = \begin{bmatrix} 0 & 1 \\ -1 & 0 \end{bmatrix} \quad , \tag{4.14}$$

we can generate a necessarily integer-valued matrix $\mathbf{M}_1^{\mathrm{PV}}$

$$\mathbf{M}_1^{\mathrm{PV}} = \mathbf{P}^{\mathrm{s}} \cdot \mathbf{M}_0 \cdot (\mathbf{P}^{\mathrm{s}})^{-1} = \begin{bmatrix} 0 & -1 \\ -1 & 1 \end{bmatrix} \quad . \tag{4.15}$$

Note that this is equivalent to permuting the rows of $\mathbf{V}$

$$\begin{aligned}\mathbf{M}_1^{\mathrm{PV}} &= \mathbf{P}^{\mathrm{s}} \cdot \mathbf{M}_0 \cdot (\mathbf{P}^{\mathrm{s}})^{-1} \\ &= \mathbf{P}^{\mathrm{s}} \cdot \left(\mathbf{V} \cdot \mathbf{D} \cdot \mathbf{V}^{\top}\right) \cdot (\mathbf{P}^{\mathrm{s}})^{\top} \\ &= (\mathbf{P}^{\mathrm{s}} \cdot \mathbf{V}) \cdot \mathbf{D} \cdot (\mathbf{P}^{\mathrm{s}} \cdot \mathbf{V})^{\top} \end{aligned} \tag{4.16}$$

Interestingly, we obtain $\mathbf{M}_1^{\mathrm{PD}} = \mathbf{M}_1^{\mathrm{PV}} = \mathbf{M}_1$, therefore $\mathbf{M}_0$ and $\mathbf{M}_1$ both are integer-valued *and* do commute. This equivalence is due to the unique structure of $\mathbf{V}$: the absolute values of the entries in the columns of $\mathbf{V}$ are s different numbers. Therefore, the signed permutation of rows (4.16) is equivalent to the permutation of columns (4.11).

$\mathbf{M}_0$ and $\mathbf{M}_1$ are unimodular. Unimodularity of $\mathbf{M}$ means 1) $\mathbf{M} \in \mathbb{Z}^{2\times 2}$, thus $\mathbf{M}$ transforms integer vectors $\underline{z} \in \mathbb{Z}^2$ into other integer vectors $\mathbf{M} \cdot \underline{z} \in \mathbb{Z}^2$, and 2) $|\det(\mathbf{M})| = 1$. The latter implies that convex sets of integer vectors are transformed into other convex sets of integer vectors with no holes in between, as the density of points is not changed (see Figure 4.2). In summary, if the infinite integer lattice $\mathbb{Z}^2$ is entirely mapped through $\mathbf{M}_0$ or $\mathbf{M}_1$, the same infinite integer lattice will result as lattice points are indistinguishable

$$\begin{aligned}\mathbf{M}_0\left(\mathbb{Z}^2\right) &= \mathbb{Z}^2 \ , \\ \mathbf{M}_1\left(\mathbb{Z}^2\right) &= \mathbb{Z}^2 \ . \end{aligned} \tag{4.17}$$

This also holds for any sequence of transformations like $\mathbf{M}_0 \cdot \mathbf{M}_1 \cdot \mathbf{M}_0$. Due to commutativity, we can sort these transformations and write them as $\mathbf{M}_0^2 \cdot \mathbf{M}_1$ (see green arrows in Figure 4.2) or in general $\mathbf{M}_0^{k_1} \cdot \mathbf{M}_1^{k_2}$. This constitutes a two-dimensional lattice of linear transformations with indices $k_1, k_2 \in \mathbb{Z}$.

With diagonalization of $\mathbf{M}_i$

$$\mathbf{M}_i = \mathbf{V} \cdot \mathbf{D}_i \cdot \mathbf{V}^{\top} \ , \tag{4.18}$$

we obtain

$$\mathbf{M}_i^k = \mathbf{V} \cdot \mathbf{D}_i^k \cdot \mathbf{V}^{\top} \tag{4.19}$$

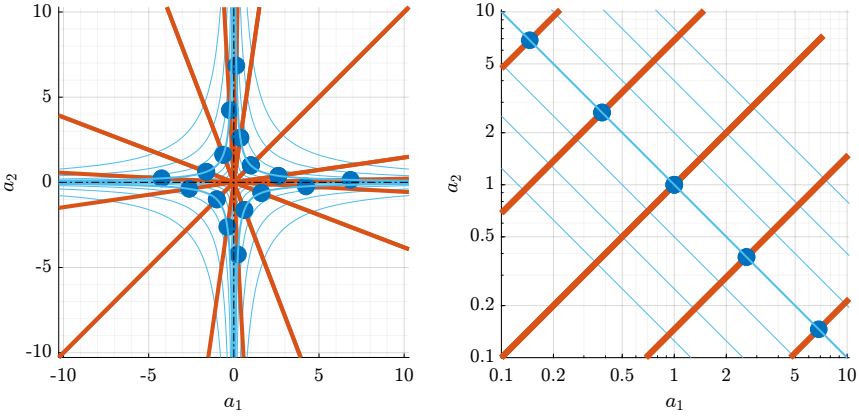

(a) Linear. **(b)** Logarithmic.

Figure 4.3: Eigenvalues a_1, a_2 of linear transformation (4.20) for $k_1, k_2 \in [-2, 2] \cap \mathbb{Z}$ plotted as blue points. Red lines show scalings of these points corresponding to isotropic stretching or compression in the linear transformation. Thicker blue line indicates $|a_1 \cdot a_2| = 1$, i.e., unit determinant transformations, thinner blue lines in background the respective scalings $\left\{\frac{1}{8}, \frac{1}{4}, \frac{1}{2}, 2, 4, 8\right\}$. All-positive quadrant of (a) shown in (b) in logarithmic scale.

and can write

$$\mathbf{M}_0^{k_1} \cdot \mathbf{M}_1^{k_2} = \mathbf{V} \cdot \mathbf{D}_0^{k_1} \cdot \mathbf{D}_1^{k_2} \cdot \mathbf{V}^\top \tag{4.20}$$

$$= \mathbf{V} \cdot \begin{bmatrix} a_1 & 0 \\ 0 & a_2 \end{bmatrix} \cdot \mathbf{V}^\top \ , \tag{4.21}$$

with suitable values for $a_1, a_2 \in \mathbb{R}$, depending on k_1, k_2.

While for any $k_1, k_2 \in \mathbb{Z}$, the mapping $\mathbf{M}_0^{k_1} \cdot \mathbf{M}_1^{k_2}$ is unimodular, we now relax this restriction and freely choose $a_1, a_2 \in \mathbb{R}$. According to Figure 4.3, especially the logarithmic version Figure 4.3 b, for arbitrary a_1, a_2, none of the resulting point sets is far away from a square configuration of unit size (blue dots) or a square configuration of arbitrary size (red lines). The configurations in between are not square but homogeneous to a high degree (see regions with white background in Figure 4.1 b).

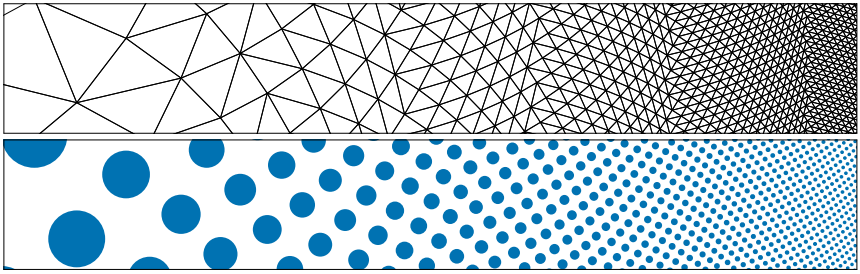

Figure 4.4: Fibonacci–Kronecker lattice, exponentially rescaled along horizontal axis. Visualized as Delaunay triangulation (top) and dots (bottom). Note the repeated transition between square and near-hexagonal pattern.

We notice in (4.21) that if the reference point set $\mathbb{Z}^2$ is transformed according to

$$\underline{z} \to \mathbf{M}_0^{k_1} \cdot \mathbf{M}_1^{k_2} \cdot \underline{z} = \mathbf{V} \cdot \begin{bmatrix} a_1 & 0 \\ 0 & a_2 \end{bmatrix} \cdot \mathbf{V}^\top \cdot \underline{z} \ , \tag{4.22}$$

it is first transformed (rotated and reflected) by $\mathbf{V}^\top$, then rescaled along the coordinate axes by a_1, a_2, then transformed back by $\mathbf{V}$

$$\underline{z} \to \mathbf{V} \cdot \begin{bmatrix} a_1 & 0 \\ 0 & a_2 \end{bmatrix} \cdot \mathbf{V}^\top \cdot \underline{z} \ . \tag{4.23}$$

Thus, as a final step, if we do not require the resulting square lattice to be axis-aligned, we keep $\mathbf{V}^\top$ inside the lattice, i.e., take $\mathbf{T}\big(\mathbb{Z}^2\big) \cap \mathcal{Q}^2$, $\mathbf{T} = \frac{1}{\alpha}\mathbf{V}^\top$ as reference point set instead of $\mathbb{Z}^2$ and henceforth can rescale the coordinate values directly

$$\begin{aligned} &\underline{x} \to \begin{bmatrix} a_1 & 0 \\ 0 & a_2 \end{bmatrix} \cdot \underline{x} \ , \\ &\underline{x} \in \mathbf{T}\big(\mathbb{Z}^2\big) \cap \mathcal{Q}^2 \ , \\ &\mathbf{T} = \frac{1}{\alpha} \cdot \mathbf{V}^\top \ . \end{aligned} \tag{4.24}$$

See Figures 4.1 b and 4.4 for visualizations where a_1 is altered along the horizontal axis.

This theory about Fibonacci–Frolov lattices is also deep enough to be applied in higher dimensions. It allows for high-dimensional Frolov lattices arising, e.g., from the Fibonacci formalism, with optimality properties analogous to the two-dimensional case [140]. We continue explaining some aspects of the higher-dimensional case.

4.2.2 A Higher-Dimensional Extension

The s-dimensional quasi-Fibonacci matrix $\mathbf{M}$ according to Purser [140, Appendix A] is given by

$$[\mathbf{M}]_{i,j} = \begin{cases} 1, & i+j \leq s+1 \\ 0, & i+j > s+1 \end{cases} , \tag{4.25}$$

i.e., for example,

$$\mathbf{M}^{s=2} = \begin{bmatrix} 1 & 1 \\ 1 & 0 \end{bmatrix} , \quad \mathbf{M}^{s=3} = \begin{bmatrix} 1 & 1 & 1 \\ 1 & 1 & 0 \\ 1 & 0 & 0 \end{bmatrix} , \quad \mathbf{M}^{s=4} = \begin{bmatrix} 1 & 1 & 1 & 1 \\ 1 & 1 & 1 & 0 \\ 1 & 1 & 0 & 0 \\ 1 & 0 & 0 & 0 \end{bmatrix} . \tag{4.26}$$

An eigenvalue decomposition

$$\mathbf{M} = \mathbf{V} \cdot \mathbf{D} \cdot \mathbf{V}^{\top} , \tag{4.27}$$

splits $\mathbf{M}$ into unitary $\mathbf{V}$ and diagonal $\mathbf{D}$. The matrix of eigenvectors $\mathbf{V}$ can be obtained by [140, Eq. A.4]

$$[\mathbf{V}]_{i,j} = \cos\left(\frac{\pi}{2} \cdot \frac{(2i-1)\,(2j-1)}{2s+1}\right) \cdot \frac{2}{\sqrt{2s+1}} , \tag{4.28}$$
$$i,j \in \{1,2,\ldots,s\} .$$

The matrix $\mathbf{V}$ is not only unitary, i.e., $\mathbf{V}^{-1} = \mathbf{V}^{\top}$, as expected, but also involutory, i.e., $\mathbf{V}^{-1} = \mathbf{V}^{\top} = \mathbf{V}$ and $\mathbf{V}^2 = \mathbf{I}$. Note that some of the aspects of $\mathbf{M}$ have also been explored in [142, Eq. 2], [88, Eq. 3], [4, Eq. 2].

4.2.3 Dimensions Where $(2s + 1)$ Prime

In dimensions where $(2s + 1)$ is prime, $\mathbf{M}$ and its commuting variants (obtained by circularly shifting the eigenvalues with respect to the eigenvectors, or via $\mathbf{P} \cdot \mathbf{M} \cdot \mathbf{P}^{-1}$, where $\mathbf{P}$ is a signed permutation matrix) form a set of matrices that guarantee the existence of an orthogonal Frolov lattice [140] that we call Purser–Frolov lattice. Due to the properties of the cosine and primes, the absolute values of the entries of $\mathbf{V}$ (4.28) consist of exactly s different values, where each column of $\mathbf{V}$ contains them in a different order [140, p. 25]. Now, if a regular lattice is rescaled along any of the eigenvectors of $\mathbf{M}$, i.e., the columns of $\mathbf{V}$, the lattice remains uniform and locally homogeneous. It periodically returns to regular (square, cubic, hypercubic) lattice configurations of different scales. In the same way, we can rotate a regular lattice with $\mathbf{V}^\top$ and subsequently easily apply deformations along the principal axes (see Figure 4.1).

For example, in $s = 3$, we obtain

$$\begin{aligned}
\mathbf{M} &= \mathbf{V} \cdot \mathbf{D} \cdot \mathbf{V}^\top \ , \\
\mathbf{V} &= \begin{bmatrix} 0.736976\ldots & 0.591009\ldots & 0.327985\ldots \\ 0.591009\ldots & -0.327985\ldots & -0.736976\ldots \\ 0.327985\ldots & -0.736976\ldots & 0.591009\ldots \end{bmatrix} \ , \\
\mathbf{D} &= \begin{bmatrix} 2.246979\ldots & 0 & 0 \\ 0 & -0.801937\ldots & 0 \\ 0 & 0 & 0.554958\ldots \end{bmatrix} \ .
\end{aligned} \tag{4.29}$$

The columns of $\mathbf{V}$ contain $s = 3$ different numerical absolute values exactly once each. With unsigned $\mathbf{P}^{\mathrm{u}}$ and signed $\mathbf{P}^{\mathrm{s}}$ permutation matrices

$$\mathbf{P}^{\mathrm{u}} = \begin{bmatrix} 0 & 0 & 1 \\ 1 & 0 & 0 \\ 0 & 1 & 0 \end{bmatrix} \ , \qquad \mathbf{P}^{\mathrm{s}} = \begin{bmatrix} 0 & 0 & -1 \\ 1 & 0 & 0 \\ 0 & -1 & 0 \end{bmatrix} \ , \tag{4.30}$$

we define

$$\mathbf{M}_i^{\mathrm{PD}} = \mathbf{V} \cdot (\mathbf{P}^{\mathrm{u}})^i \cdot \mathbf{D} \cdot \left(\mathbf{V} \cdot (\mathbf{P}^{\mathrm{u}})^i\right)^\top \tag{4.31}$$

$$\mathbf{M}_i^{\mathrm{PV}} = (\mathbf{P}^{\mathrm{s}})^i \cdot \mathbf{M}_0 \cdot (\mathbf{P}^{\mathrm{s}})^{-i} \ , \tag{4.32}$$

and obtain

$$\mathbf{M}_0^{\mathrm{PD}} = \begin{bmatrix} 1 & 1 & 1 \\ 1 & 1 & 0 \\ 1 & 0 & 0 \end{bmatrix} \qquad \mathbf{M}_0^{\mathrm{PV}} = \begin{bmatrix} 1 & 1 & 1 \\ 1 & 1 & 0 \\ 1 & 0 & 0 \end{bmatrix}$$

$$\mathbf{M}_1^{\mathrm{PD}} = \begin{bmatrix} 1 & 0 & -1 \\ 0 & 0 & 1 \\ -1 & 1 & 1 \end{bmatrix} \qquad \mathbf{M}_1^{\mathrm{PV}} = \begin{bmatrix} 0 & -1 & 0 \\ -1 & 1 & -1 \\ 0 & -1 & 1 \end{bmatrix}$$

$$\mathbf{M}_2^{\mathrm{PD}} = \begin{bmatrix} 0 & -1 & 0 \\ -1 & 1 & -1 \\ 0 & -1 & 1 \end{bmatrix} \qquad \mathbf{M}_2^{\mathrm{PV}} = \begin{bmatrix} 1 & 0 & -1 \\ 0 & 0 & 1 \\ -1 & 1 & 1 \end{bmatrix}$$

$$\mathbf{M}_3^{\mathrm{PD}} = \begin{bmatrix} 1 & 1 & 1 \\ 1 & 1 & 0 \\ 1 & 0 & 0 \end{bmatrix} \qquad \mathbf{M}_3^{\mathrm{PV}} = \begin{bmatrix} 1 & 1 & 1 \\ 1 & 1 & 0 \\ 1 & 0 & 0 \end{bmatrix}$$

As we can see, (4.31) and (4.32) for $i \in \{0, 1, s-1\}$ both produce the same set of matrices and repeat for $i \geq s$. The permutation $\mathbf{M}_1^{\mathrm{PD}} = \mathbf{M}_2^{\mathrm{PV}}$ and $\mathbf{M}_2^{\mathrm{PD}} = \mathbf{M}_1^{\mathrm{PV}}$ is purely due to the choice of permutation matrices (4.30). Summarizing, we obtained a set of s matrices that, analogous to Section 4.2.1, provide a basis system of a three-dimensional lattice of unimodular transformations, and after relaxation of the unimodularity, we know how to anisotropically rescale a three-dimensional lattice such that it returns to cubic configurations (of different size and with other neighbors) again and again. This is what we call Purser–Frolov lattice.

4.2.4 Other Dimensions

In dimensions where $(2s+1)$ is not prime, (4.25) is not well suited [140]. For example, in $s = 4$, we have $(2s+1) = 9$, which is not prime. As we can see in the corresponding $\mathbf{V}$ matrix

$$\mathbf{V} = \begin{bmatrix} 0.656538\ldots & 0.577350\ldots & 0.428525\ldots & 0.228013\ldots \\ 0.577350\ldots & 0.000000\ldots & -0.577350\ldots & -0.577350\ldots \\ 0.428525\ldots & -0.577350\ldots & -0.228013\ldots & 0.656538\ldots \\ 0.228013\ldots & -0.577350\ldots & 0.656538\ldots & -0.428525\ldots \end{bmatrix}, \tag{4.33}$$

the second column does not exhibit unique entries. Looking at the argument of the cosine in (4.28), here in degrees

$$\mathbf{V} = \cos\left(\frac{\pi}{180} \cdot \begin{bmatrix} 10 & 30 & 50 & 70 \\ 30 & 90 & 150 & -150 \\ 50 & 150 & -110 & -10 \\ 70 & -150 & -10 & 130 \end{bmatrix}\right) , \tag{4.34}$$

we notice the cycle in the second column that produces repeating absolute values. Closer examination of the argument in (4.28), focusing on an individual column, i.e., fixed j

$$\frac{\pi}{2} \cdot \frac{(2i-1)\,(2j-1)}{2s+1} = \underbrace{\pi \cdot \frac{i \cdot (2j-1)}{2s+1}}_{\text{should be acyclic}} - \underbrace{\frac{\pi}{2} \cdot \frac{2j-1}{2s+1}}_{\text{offset}} \tag{4.35}$$

reveals that $\left[\frac{i\cdot(2j-1)}{2s+1} \mod 2\right]$ should result in s different values in any column. This is given only if $(2j-1)$ does not divide the denominator $(2s+1)$, i.e.,

$$\begin{aligned} &\gcd(2j-1,\ 2s+1) \overset{!}{=} 1 \\ &\forall \quad j \in \{1, 2, \ldots, s\} \ . \end{aligned} \tag{4.36}$$

Note that $(2j-1)$, for the individual columns, "tries out" all odd numbers from 1 to $(2s-1)$. Now, in case the denominator $(2s+1)$, which is also odd, is not prime, then one of the $(2j-1) \in \{1, 3, 5, \ldots, 2s-1\}$ will divide it, resulting in a cycle and repeated absolute values in a single column in $\mathbf{V}$. Therefore, $(2s+1)$ must be prime to fulfill (4.36). In particular, in our $s = 4$ example, we have

$$\frac{i \cdot (2j-1)}{2s+1} = \begin{bmatrix} \frac{1\cdot1}{9} & \frac{1\cdot3}{9} & \frac{1\cdot5}{9} & \frac{1\cdot7}{9} \\ \frac{2\cdot1}{9} & \frac{2\cdot3}{9} & \frac{2\cdot5}{9} & \frac{2\cdot7}{9} \\ \frac{3\cdot1}{9} & \frac{3\cdot3}{9} & \frac{3\cdot5}{9} & \frac{3\cdot7}{9} \\ \frac{4\cdot1}{9} & \frac{4\cdot3}{9} & \frac{4\cdot5}{9} & \frac{4\cdot7}{9} \end{bmatrix}_{i,j} , \tag{4.37}$$

and in the second column, $(2j-1) = 3$ divides the denominator $(2s+1) = 9$ and thus creates the repetitions.

It is, however, possible to search for alternative candidates. A candidate for $s = 4$ is given in [140, Sec. 7]

$$\mathbf{M}_0^{s=4} = \begin{bmatrix} 1 & 1 & 0 & 0 \\ 1 & 0 & 0 & 0 \\ 0 & 0 & 1 & 1 \\ 0 & 0 & 1 & 0 \end{bmatrix}, \qquad \mathbf{M}_1^{s=4} = \begin{bmatrix} 1 & -1 & 1 & 0 \\ -1 & 2 & 0 & 1 \\ 1 & 0 & 0 & 0 \\ 0 & 1 & 0 & 0 \end{bmatrix}, \tag{4.38}$$

$$\mathbf{M}_2^{s=4} = \begin{bmatrix} 1 & 0 & -1 & -1 \\ 0 & 1 & -1 & 0 \\ -1 & -1 & 1 & 1 \\ -1 & 0 & 1 & 0 \end{bmatrix}. \tag{4.39}$$

It comprises two block-diagonal replications of $\mathbf{M}^{(s=2)}$.

The theory presented in this chapter provides a satisfying explanation for the genuine optimality of two-dimensional Fibonacci grids. Furthermore, it can be extended to higher dimensions, giving rise to high-quality orthogonal Frolov lattices.

4.3 Summary

We formally and intuitively explained the interesting properties of the 2D Fibonacci–Frolov lattice: any anisotropic rescaling along the coordinate axes produces locally homogeneous samples and, for certain scaling factors, square arrangements. (This directly enables deterministic sampling of product-type densities, as their variability is described in terms of the individual coordinate axes. This is formalized and exploited in Chapter 6.) The described formalism can be extended to higher dimensions. We explicitly presented the 3D and 4D lattices as well as a generic expression for $(2s + 1)$ prime.

CHAPTER 5

Optimization-Based Construction

Contents

> The trouble is that, except for easy low-dimensional cases, no explicit constructions of good lattice points modulo L are available. Finding such explicit constructions in arbitrary dimensions is indeed *the* outstanding open problem in the theory of good lattice points, and it seems to be a hard nut to crack.
>
> *Applied Number Theory: Quasi-Monte Carlo Methods (2015)*
> Harald Niederreiter (*1944)

> I have had my results for a long time:
> but I do not yet know how I am to arrive at them.
>
> Carl Friedrich Gauss (1777 – 1855)

This chapter lists various measures to quantify the quality of uniform point sets. We then proceed to calculate samples that minimize these quality measures.

5.1 Quality Measures

We introduce measures that quantify the uniformity and homogeneity of point sets to later find point sets that minimize them.

5.1.1 Discrepancy

Intuitively, the discrepancy $\text{discr}(\mathcal{P}_L)$ of a point set

$$\mathcal{P}_L = \{\underline{x}_i\}_{i=1}^{L}, \quad \underline{x}_i \in [0,1]^s$$

is the average or maximum mismatch between the volume of certain sets $A \subset [0,1]^s$ and the proportion of points of $\mathcal{P}_L$ that lie inside A. Formally, define the **local discrepancy** $\Delta(A, \mathcal{P}_L)$ [35, p. 165]

$$\Delta(A, \mathcal{P}_L) = \frac{\#(A, \mathcal{P}_L)}{L} - \lambda(A) \ , \tag{5.1}$$

where $\#(A, \mathcal{P}_L)$ counts the points of $\mathcal{P}_L$ that lie in A and $\lambda(A)$ is the s-dimensional Lebesgue measure of A, e.g., the area in $s = 2$ and the volume in

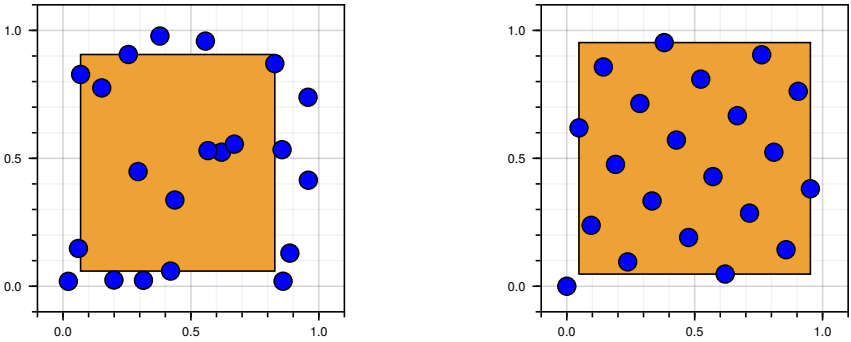

(a) Random samples. **(b)** Fibonacci–rank-1 lattice.

Figure 5.1: Visualization of discrepancy measure. High-discrepancy samples (a) with yellow box area corresponding to 13.5 samples, yielding $\text{discr}(\mathcal{P}_L) = 0.36$. Low-discrepancy samples (b) with box area corresponding to 17.2 samples, yielding $\text{discr}(\mathcal{P}_L) = 0.13$.

$s = 3$. Note that $\Delta(A, \mathcal{P}_L)$ is the integration error of the indicator function of the set A using cubature points $\mathcal{P}_L$ [35, p. 165]. Usually, A is an axes-aligned hyperrectangle or cuboid $A(\underline{a}, \underline{b})$ that can be described by the two diagonally opposite corners $(\underline{a}, \underline{b})$ where $0 \leq a_i < b_i \leq 1 \quad \forall\, i \in \{1, 2, \ldots, s\}$ (see Figure 5.1). The **extreme discrepancy** of point set $\mathcal{P}_L$ is the supremum of the local discrepancy [97, p. 92–93]

$$\text{discr}(\mathcal{P}_L) = \sup_{\underline{a}, \underline{b}} |\Delta(A(\underline{a}, \underline{b}), \mathcal{P}_L)| \ . \tag{5.2}$$

Often this is simplified to the **extreme star discrepancy** $\text{discr}^*(\mathcal{P}_L)$

$$\text{discr}^*(\mathcal{P}_L) = \sup_{\underline{x}} |\Delta^*(A(\underline{x}), \mathcal{P}_L)| \ , \tag{5.3}$$

$$\Delta^*(A(\underline{x}), \mathcal{P}_L) = \Delta(A(\underline{0}, \underline{x}), \mathcal{P}_L) \ , \tag{5.4}$$

where one vertex of the cuboid is fixed to the origin; this simplifies computation. It is well known that point sets with an extreme star discrepancy of $\mathcal{O}\big((\log(L))^{s-1} L^{-1}\big)$ do exist [2].

Instead of the L_∞-norm, the local discrepancies can also be accumulated via an arbitrary L_p norm

$$\mathrm{discr}_p^*(\mathcal{P}_L) = \sqrt[p]{\int_{\underline{x}\in[0,1]^s} |\Delta^*(A(\underline{x}),\mathcal{P}_L)|^p \,\mathrm{d}\underline{x}} \ . \tag{5.5}$$

For the L_2 norm, there is a closed-form result [126, p. 7], [172]

$$\mathrm{discr}_2^*(\mathcal{P}_L) = \tag{5.6}$$
$$\sqrt{\left(\frac{4}{3}\right)^s - \frac{2}{L}\sum_{\underline{x}\in\mathcal{P}_L}\prod_{j=1}^{s}\frac{3-x_j^2}{2} + \frac{1}{L^2}\sum_{\underline{x}\in\mathcal{P}_L}\sum_{\underline{y}\in\mathcal{P}_L}\prod_{j=1}^{s}(2-\max\{x_j,y_j\})} \ .$$

The merit of low-discrepancy point sets is shown by the Koksma-Hlawka identity [93], [70], [92]

$$\left|\frac{1}{L}\sum_{\underline{x}\in\mathcal{P}_L}^{L} g(\underline{x}) - \int_{[0,1]^s} g(\underline{x})\,\mathrm{d}\underline{x}\right| \le \mathrm{discr}_\infty^*(\mathcal{P}_L)\cdot V(g) \ . \tag{5.7}$$

In words, the integration error (left-hand side) for integrand $g(\cdot)$ is bounded by the discrepancy $\mathrm{discr}_\infty(\mathcal{P}_L)$ of the point set $\mathcal{P}_L$, times the variation in the sense of Hardy and Krause $V(g)$ of the integrand (right-hand side). This constant depends on the smoothness of $g(\cdot)$. Hence, point sets with low discrepancy produce better cubature results for a given number of samples. There exist theoretical lower bounds for the asymptotic behavior of the discrepancy for large L [11, Sec. 1].

Low-discrepancy point sets $\mathcal{P}_L$ are therefore well suited for cubature, i.e., approximate integration of functions $f(\underline{x})$ in higher dimensions $\underline{x}\in\mathbb{R}^s$ based on samples $\underline{x}_i\in[0,1]^s,\ \ i\in[1,2,\ldots,L]$

$$\int_{[0,1]^s} f(\underline{x})\,\mathrm{d}\underline{x} \approx \frac{1}{L}\sum_{\underline{x}\in\mathcal{P}_L}^{L} f(\underline{x}) \ . \tag{5.8}$$

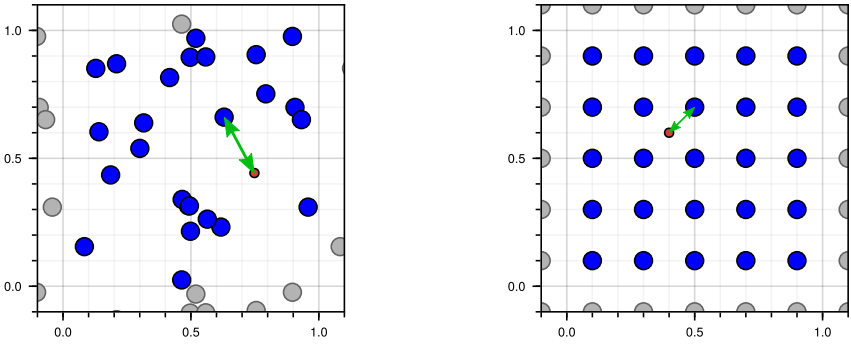

(a) High dispersion. **(b)** Low dispersion.

Figure 5.2: Dispersion (green arrow) of sample set (blue) with periodic continuation samples (grey), and most isolated point / deep hole (red).

A disadvantage is that many simple functions g have very large or infinite variation $V(g)$. Therefore, the error bound given by the Koksma-Hlawka identity is often too wide for direct practical use.

5.1.2 Dispersion

Definition 5.1 (Dispersion)**.** The **dispersion** of a point set $\mathcal{P}_L$ in $[0,1]^s$ is defined as [121, p. 524]

$$\operatorname{dispr}(\mathcal{P}_L) = \max_{\underline{x}\in[0,1]^s} \left\{ \min_{\underline{y}\in\mathcal{P}_L} \left\| \underline{x} - \underline{y} \right\|_2 \right\} . \tag{5.9}$$

It is also called “fill distance” [43, Eq. 36] or “fill-distance” [91, Eq. 3.9].

Intuitively, dispersion quantifies the **resolution** with which the points cover the space. The points furthest away from any samples are also called **deep holes** (see Figure 5.2). For infinite point sets on $\mathbb{R}^s$ instead of $[0,1]^s$, deep holes are necessarily vertices of Voronoi cells, where the distance to the nearest sample, also called **covering radius**, is identical to the largest **circumradius** of a Delaunay triangulation [27, p. 33]. Low-dispersion point sets are therefore well suited, e.g., for searching the global optimum of multimodal nonlinear functions.

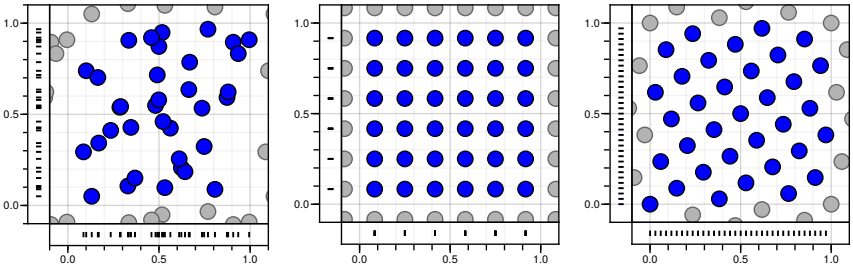

(a) Random samples. **(b)** Regular lattice, shifted. **(c)** Fibonacci–rank-1 lattice.

Figure 5.3: High-discrepancy high-dispersion point set (a), high-discrepancy low-dispersion point set (b) and low-discrepancy low-dispersion point set (c). Note that in (c), every sample has individual x- and y-coordinates. Therefore, separable integrands $g(x, y) = g(x) \cdot g(y)$ are evaluated at far more different positions in (c).

The relationship between discrepancy and dispersion is [121, Theorem 3]

$$\operatorname{dispr}(\mathcal{P}_L) \leq \sqrt{s} \cdot [\operatorname{discr}_\infty(\mathcal{P}_L)]^{1/s} \quad . \tag{5.10}$$

In words, low discrepancy implies low dispersion, but not vice versa. For example, a scaled regular grid has very low dispersion but very high discrepancy (see Figure 5.3).

5.1.3 Packing Density

Equal circles (spheres, hyperspheres) being tiled as a lattice without overlap in the infinite $\mathbb{R}^s$ space is called a **lattice packing**. This results in a certain packing density ρ_s depending on the lattice. The highest packing densities, achieved by the most efficient lattice packings of (hyper-)spheres, are [147, p. 3]

$$\rho_2^{\max} = \frac{\pi}{2 \cdot \sqrt{3}} = 0.906899\ldots \quad , \tag{5.11}$$

$$\rho_3^{\max} = \frac{\pi}{3 \cdot \sqrt{2}} = 0.740480\ldots \quad , \tag{5.12}$$

$$\rho_4^{\max} = \frac{\pi^2}{16} = 0.616850\ldots \quad , \tag{5.13}$$

$$\rho_5^{\max} = \frac{\pi^2}{15 \cdot \sqrt{2}} = 0.465257\ldots \quad . \tag{5.14}$$

$$\tag{5.15}$$

5.1.4 Covering Density

Equal circles (spheres, hyperspheres) being tiled as a lattice *with* overlap and fully covering the infinite $\mathbb{R}^s$ space is called a **lattice covering**. The lowest covering densities, achieved by the most efficient lattice coverings of spheres, are [147, p. 17]

$$\rho_2^{\min} = \frac{2\pi}{3 \cdot \sqrt{3}} = 1.209199\ldots \quad , \tag{5.16}$$

$$\rho_3^{\min} = \frac{5 \cdot \sqrt{5}\pi}{24} = 1.463503\ldots \quad . \tag{5.17}$$

5.1.5 Worst Case Errors

5.1.5.A (Reproducing Kernel Hilbert Space) Reproducing kernel Hilbert spaces provide an elegant formalism for sets of nonlinear functions. The result that is very useful for us is a closed-form expression for the worst-case integration error of a set of cubature points.

Definition 5.2 (reproducing kernel Hilbert space [35, p. 167])**.** A Hilbert space $\mathcal{H}(K)$ with the inner product $\langle \cdot, \cdot \rangle_{\mathcal{H}}$ is a **reproducing kernel Hilbert space** with kernel K,

$$K \colon [0,1]^s \times [0,1]^s \to \mathbb{R} \ ,$$

if the kernel with one argument fixed is a function contained in $\mathcal{H}$

$$K(\cdot, \underline{x}) \in \mathcal{H} \quad \forall \underline{x} \in [0,1]^s \ ,$$

and the reproducing property holds

$$f(\underline{x}) = \langle f(\cdot),\ K(\cdot, \underline{x}) \rangle_{\mathcal{H}} \quad \forall \underline{x} \in [0,1]^s \ .$$

Each kernel function gives rise to a unique reproducing kernel Hilbert space, and each reproducing kernel Hilbert space has a unique kernel function.

Definition 5.3 (tensor product Hilbert space [35, p. 167])**.** An s-dimensional **tensor product Hilbert space** $\mathcal{H}_s$ of functions $f \colon [0,1]^s \to \mathbb{R}$ is a tensor product

$$\mathcal{H}_s = \mathcal{H}_{1,1} \otimes \mathcal{H}_{1,2} \otimes \cdots \otimes \mathcal{H}_{1,s}$$

of one-dimensional Hilbert spaces $\mathcal{H}_{1,j}$. It is the completion of

$$\sum_{i \in \mathbb{N}} \lambda_i \prod_{j=1}^{s} f(x_j) \ , \quad \lambda_i \in \mathbb{R}$$

under the norm in $\mathcal{H}_s$.

The reproducing kernel of a tensor product Hilbert space is the product of the individual kernels.

Definition 5.4 (worst-case error [35, p. 169])**.** The **worst-case error** (wce) of a cubature rule using unweighted points $\mathcal{P}_L$ in a normed space H (not necessarily a Hilbert space) is

$$\operatorname{wce}(\mathcal{P}_L; H) = \sup_{\|f\|_H \leq 1} \left| \int_{[0,1]^s} f(\underline{x}) \, \mathrm{d}x - \frac{1}{L} \sum_{\underline{x} \in \mathcal{P}_L} f(\underline{x}) \right| \ .$$

In general, wces are difficult to compute, except for reproducing kernel Hilbert spaces. There, the wce can be easily expressed in terms of the reproducing kernel.

Theorem 5.5 (formula for the wce [35, p. 169])**.** *Let kernel* $K \colon [0,1]^s \times [0,1]^s \to \mathbb{R}$ *satisfy*

$$\int_{[0,1]^s} \int_{[0,1]^s} K(\underline{x}, \underline{y}) \, \mathrm{d}\underline{x} \, \mathrm{d}\underline{y} < \infty \ .$$

Then in a reproducing kernel Hilbert space $\mathcal{H}(K)$ *with reproducing kernel* K*, cubature using unweighted points* $\mathcal{P}_L$ *for any integrand* $f(\cdot) \in \mathcal{H}(K)$ *is subject to squared wce*

$$\operatorname{wce}^2(\mathcal{P}_L; \mathcal{H}(K)) = \int_{[0,1]^s} \int_{[0,1]^s} K(\underline{x}, \underline{y}) \, \mathrm{d}\underline{x} \, \mathrm{d}\underline{y} \tag{5.18}$$

$$- \frac{2}{L} \sum_{\underline{x} \in \mathcal{P}_L} \int_{[0,1]^s} K(\underline{x}, \underline{y}) \, \mathrm{d}\underline{y} \tag{5.19}$$

$$+ \frac{1}{L^2} \sum_{\underline{x} \in \mathcal{P}_L} \sum_{\underline{y} \in \mathcal{P}_L} K(\underline{x}, \underline{y}) \ . \tag{5.20}$$

In addition to the wce, the mean of the wce over all possible evaluation points $\mathcal{P}_L = \{\underline{x}_1, \ldots, \underline{x}_L\}$,

$$\mathrm{E}_{\mathcal{P}_L}\left\{\operatorname{wce}^2(\mathcal{P}_L; \mathcal{H}(K))\right\} \tag{5.21}$$

$$= \int_{[0,1]^s} \cdots \int_{[0,1]^s} \operatorname{wce}(\{\underline{x}_1, \ldots, \underline{x}_L\}; \mathcal{H}(K)) \, \mathrm{d}\underline{x}_1 \cdots \mathrm{d}\underline{x}_L \ , \tag{5.22}$$

can also easily be computed.

Theorem 5.6 (mean squared wce [35, p. 171])**.** *Let kernel* $K\colon [0,1]^s \times [0,1]^s \to \mathbb{R}$ *satisfy*

$$\int_{[0,1]^s} \int_{[0,1]^s} K(\underline{x}, \underline{y}) \, \mathrm{d}\underline{x} \, \mathrm{d}\underline{y} < \infty \ .$$

The mean squared wce in a reproducing kernel Hilbert space $\mathcal{H}(K)$ *is*

$$\mathrm{E}_{\mathcal{P}_L} \left\{ \mathrm{wce}^2(\mathcal{P}_L; \mathcal{H}(K)) \right\} \tag{5.23}$$

$$= \frac{1}{L} \left(\int_{[0,1]^s} K(\underline{x}, \underline{x}) \, \mathrm{d}\underline{x} - \int_{[0,1]^s} \int_{[0,1]^s} K(\underline{x}, \underline{y}) \, \mathrm{d}\underline{x} \, \mathrm{d}\underline{y} \right) \ . \tag{5.24}$$

Thus, the average squared wce for arbitrarily chosen evaluation points $\mathcal{P}_L$ is of order $\mathcal{O}(L^{-1})$ and, according to Jensen's inequality, the average non-squared wce of order $\mathcal{O}(L^{-1/2})$. That is the same convergence rate as Monte Carlo. Therefore, if there is a non-null set of worse-than-average evaluation points, then there must be better ones as well, and the latter is what we are looking for. For example, consider sets of evaluation points where all points are very close to each other. They form a set of positive measure and are yielding an integration performance that reflects merely that of a single evaluation point.

5.1.5.B (Sobolev Space of Functions with Square-Integrable Mixed First Derivatives) The one-dimensional reproducing kernel Hilbert space

$$\mathcal{H}_1 = \{ f\colon [0,1] \to \mathbb{R} \mid f \text{ absolutely continuous and } \|f\| < \infty \}$$

has reproducing kernel [35, p. 166]

$$K(x, y) = 2 - \max(x, y) \ .$$

Therefore, its multi-dimensional tensor product space $\mathcal{H}_s$ has the kernel

$$K(\underline{x}, \underline{y}) = \prod_{j=1}^{s} (2 - \max(x_j, y_j)) \ .$$

$\mathcal{H}_s$ contains real-valued functions on $[0,1]^s$ with square-integrable mixed first derivatives. It is an anchored Sobolev space. The squared wce is [35, p. 171]

$$\mathrm{wce}^2(\mathcal{P}_L;\mathcal{H}_s) = \tag{5.25}$$

$$\left(\frac{4}{3}\right)^s - \frac{2}{L}\sum_{\underline{x}\in\mathcal{P}_L}\prod_{j=1}^{s}\frac{3-x_j^2}{2} + \frac{1}{L^2}\sum_{\underline{x}\in\mathcal{P}_L}\sum_{\underline{y}\in\mathcal{P}_L}\prod_{j=1}^{s}(2-\max\{x_j,y_j\}) \ . \tag{5.26}$$

Note that this wce is identical to the L_2-discrepancy (5.6).

5.1.5.C (Sobolev Space of 1-periodic Functions with Square-Integrable Mixed First Derivatives) A Hilbert space of 1-periodic functions on the torus with bounded mixed first derivatives has reproducing kernel [68, p. 388]

$$K_1(x,y) = 1 + \sum_{n\in\mathbb{Z}\setminus 0} |2\pi n|^{-2} e^{2\pi\cdot i\cdot n\cdot(x-y)} \tag{5.27}$$

$$= 1 + \gamma\cdot k(|x-y|) \ , \tag{5.28}$$

$$k(t) = \frac{1}{2}\cdot\left(t^2 - t + \frac{1}{6}\right) \ , \tag{5.29}$$

with parameter γ. The kernel of the corresponding tensor product spaces is again

$$K_s(\underline{x},\underline{y}) = \prod_{j=1}^{s} K_1(x_j,y_j) \ . \tag{5.30}$$

The squared wce is [68, p. 389]

$$\mathrm{wce}^2(\mathcal{P}_L) = -1 + \frac{1}{L^2}\sum_{\underline{x}\in\mathcal{P}_L}\sum_{\underline{y}\in\mathcal{P}_L} K_s(\underline{x},\underline{y}) \ . \tag{5.31}$$

This particular wce is very interesting as for $\gamma = 1$ it is minimized by the rank-1 Fibonacci lattice (see Section 5.2.2.B). On the other hand, for $\gamma = 6$, it has a monotonic relation to the periodic L_2-discrepancy $\mathring{\mathrm{discr}}_2(\mathcal{P}_L)$ [68,

p. 390], therefore both have the same minimizer. Due to its periodicity, this wce is best suited for 1-periodic point sets like rank-1 lattices and Kronecker sequences.

5.1.5.D (Sobolev-Space of Functions with Square-Integrable Mixed First Derivatives and Homogeneous Boundary Conditions) A Hilbert space of square-integrable mixed first derivatives, defined on compact support $(0,1)^s$ with homogeneous boundary conditions, has the reproducing kernel [90, Sec. 5.2]

$$K_1(x,y) = \min\{x,y\} - x \cdot y$$

and squared wce

$$\begin{aligned}\operatorname{wce}^2 \mathcal{P}_L = &\left(\frac{1}{12}\right)^s - \frac{2}{L} \sum_{\underline{x} \in \mathcal{P}_L} \prod_{j=1}^{s} \left[\frac{x_j - x_j^2}{2}\right] \\ &+ \frac{1}{L^2} \sum_{\underline{x} \in \mathcal{P}_L} \sum_{y \in \mathcal{P}_L} \prod_{j=1}^{s} [\min\{x_j, y_j\} - x_j \cdot y_j] \ . \end{aligned} \tag{5.32}$$

It is well suited to compare Frolov lattices that are not periodic on $(0,1)^s$ [90].

5.2 Global Search for Closed Point Sets

5.2.1 State of Art

For $L \leq 6$ and $s = 2$, point sets with globally minimal extreme star discrepancy $\operatorname{discr}^*_\infty(\mathcal{P}_L)$ (5.5) have been determined [175].

For $L \leq 16$ and $s = 2$, points sets with globally minimal worst case error (5.31) have been determined [68]. It turned out that for Fibonacci numbers $L \in \{1, 2, 3, 5, 8, 13\}$, this best lattice is the Fibonacci–rank-1 lattice (3.27). Optimal point sets for $L \in \{7, 12\}$ were lattices as well, and for $L \in \{4, 6, 9, 10, 11, 14, 15, 16\}$, the best lattice was only slightly inferior to the best point set.

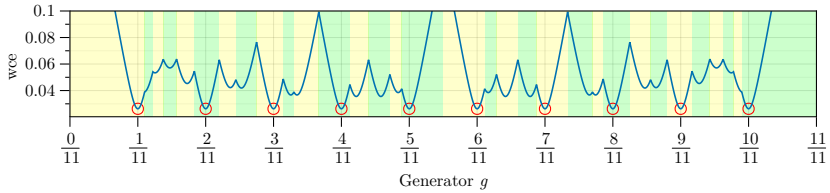

(a) $L = 11$. Global optima are $g \in \left\{\frac{1}{11}, \frac{2}{11}, \ldots, \frac{10}{11}\right\}$.

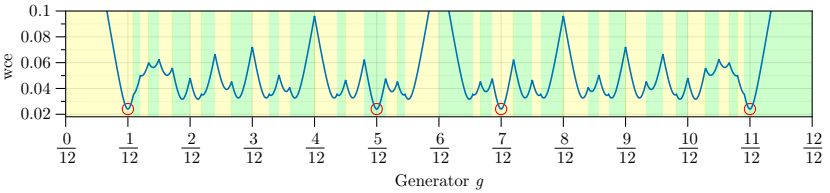

(b) $L = 12$. Global optima are $g \in \left\{\frac{1}{12}, \frac{5}{12}, \frac{7}{12}, \frac{11}{12}\right\}$.

Figure 5.4: Global search for 1D rank-1 lattice generators g_L. It turns out that the global optima g_L^{opt} (red circles) are rational numbers where the numerator is relatively prime to the number of samples L. Then we obtain L equidistant points, which is the best 1D low-discrepancy point set (3.25). Alternating background colors indicate piecewise square sections in (5.31).

5.2.2 Rank-1 Lattices

In this section, we determine the rank-1 lattice generator that is best in terms of wce of the periodic function space from Section 5.1.5.C. Therefore, we insert the rank-1 lattice point set (with variable generator $\underline{g}$)

$$\mathcal{P}_L(\underline{g}) = \left\{ i \cdot \underline{g} \mod 1 \right\}_{i=1}^{L} \tag{5.33}$$

into the wce formula (5.31) and obtain the quality measure

$$\Theta_L(\underline{g}) = \text{wce}\left(\left\{ i \cdot \underline{g} \mod 1 \right\}_{i=1}^{L} \right) . \tag{5.34}$$

Minimizing it yields the optimal generator $\underline{g}_L^{\text{opt}}$

$$\underline{g}_L^{\text{opt}} = \arg\min_{\underline{g}} \left\{ \Theta_L(\underline{g}) \right\} . \tag{5.35}$$

The search space for the best generator is $\underline{g} \in [0,1]^s$.

5.2.2.A $(s = 1)$ For $s = 1$, the quality measure $\Theta_L(\cdot)$ is a piecewise quadratic. Boundaries between quadratic segments are

$$\left\{0, \frac{1}{2}, \frac{1}{3}, \frac{2}{3}, \frac{1}{4}, \frac{2}{4}, \frac{3}{4}, \frac{1}{5}, \frac{2}{5}, \frac{3}{5}, \frac{4}{5}, \ldots, \frac{1}{L-1}, \frac{2}{L-1}, \ldots, \frac{L-2}{L-1}, 1\right\} \ , \quad (5.36)$$

which is (after sorting and discarding multiple identical entries) the Farey sequence of order L [127, A006842], [127, A006843]. The number of terms $N(L)$ in the Farey sequence F_L is [127, A005728]

$$N(L) = 1 + \sum_{k=1}^{L} \phi(k) \ , \quad (5.37)$$

with an asymptotic limit [173], [170, p. 155]

$$N(L) \sim \frac{3L^2}{\pi^2} \ . \quad (5.38)$$

With optimality measure $\Theta(\cdot)$ implemented in Julia [10], we can easily determine its exact first and second derivative in every segment by evaluating it, e.g., in the middle of each interval, using automatic differentiation [143] combined with rational arithmetic. We then determine the minimum of each segment with a single Newton step and, by comparing the local minima of all the segments, finally identify the global minimum g_L^{opt}.

We find that g_L^{opt} is always a rational number where the denominator is the number of samples L and the numerator is any integer relatively prime to L. See Figure 5.4 for a visualization of the quality measure and its local and global minima. Since a number coprime to L is a generator of the

cyclic group $\mathbb{Z}/(L \cdot \mathbb{Z})$, the resulting 1D rank-1 lattice is a set of L different, equidistant points on $[0, 1]$. In particular, we have

$$
\begin{aligned}
L = 2\colon &\qquad g^{\mathrm{opt}} = \frac{1}{2} \\
L = 3\colon &\qquad g^{\mathrm{opt}} = \left\{\frac{1}{3}, \frac{2}{3}\right\} \\
L = 4\colon &\qquad g^{\mathrm{opt}} = \left\{\frac{1}{4}, \frac{3}{4}\right\} \\
L = 5\colon &\qquad g^{\mathrm{opt}} = \left\{\frac{1}{5}, \frac{2}{5}, \frac{3}{5}, \frac{4}{5}\right\} \\
L = 6\colon &\qquad g^{\mathrm{opt}} = \left\{\frac{1}{6}, \frac{5}{6}\right\} \\
L = 7\colon &\qquad g^{\mathrm{opt}} = \left\{\frac{1}{7}, \frac{2}{7}, \frac{3}{7}, \frac{4}{7}, \frac{5}{7}, \frac{6}{7}\right\} \\
L = 8\colon &\qquad g^{\mathrm{opt}} = \left\{\frac{1}{8}, \frac{3}{8}, \frac{5}{8}, \frac{7}{8}\right\} \\
L = 9\colon &\qquad g^{\mathrm{opt}} = \left\{\frac{1}{9}, \frac{2}{9}, \frac{4}{9}, \frac{5}{9}, \frac{7}{9}, \frac{8}{9}\right\} \\
L = 10\colon &\qquad g^{\mathrm{opt}} = \left\{\frac{1}{10}, \frac{3}{10}, \frac{7}{10}, \frac{9}{10}\right\} \\
L = 11\colon &\qquad g^{\mathrm{opt}} = \left\{\frac{1}{11}, \frac{2}{11}, \frac{3}{11}, \frac{4}{11}, \frac{5}{11}, \frac{6}{11}, \frac{7}{11}, \frac{8}{11}, \frac{9}{11}, \frac{10}{11}\right\} \\
L = 12\colon &\qquad g^{\mathrm{opt}} = \left\{\frac{1}{12}, \frac{5}{12}, \frac{7}{12}, \frac{11}{12}\right\} \\
&\vdots
\end{aligned}
$$

The most straightforward construction is always to take

$$
g_L^{\mathrm{opt}} = \frac{1}{L} \ . \tag{5.39}
$$

This is precisely the rather obvious and trivial equidistant rank-1 lattice (3.25) (see Figure 3.4a).

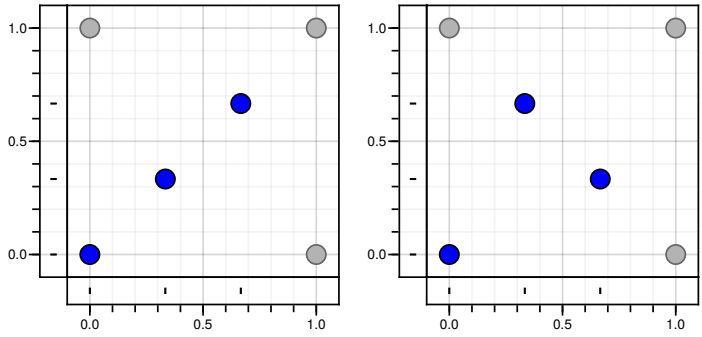

(a) $\underline{g} = \begin{bmatrix} \frac{1}{3} & \frac{1}{3} \end{bmatrix}^\top$ **(b)** $\underline{g} = \begin{bmatrix} \frac{1}{3} & \frac{2}{3} \end{bmatrix}^\top$

(c) $\underline{g} = \begin{bmatrix} \frac{1}{5} & \frac{2}{5} \end{bmatrix}^\top$ **(d)** $\underline{g} = \begin{bmatrix} \frac{1}{5} & \frac{3}{5} \end{bmatrix}^\top$

Figure 5.5: Two optimal point sets with $L = 3$ and $L = 5$, respectively. They are identical under periodicity considerations and symmetry considerations.

5.2.2.B ($s = 2$) We can apply the same approach in two dimensions. The worst case error (5.31) is again a piecewise polynomial, where the individual regions are rectangular and are given by the Cartesian product of two Farey sequences. Therefore, we count $\mathcal{O}(L^4)$ such rectangular regions. Each of these rectangles contains a 2D polynomial of order four (5.31). It can be minimized either numerically with several Newton steps or exactly with computer algebra methods for exact polynomial system solving [8]. In this work, we compute Newton steps until reaching numerical precision[1]. When the optimality measure no longer changes or reaches a cycle, we approximate the resulting floating-point number with a rational number and insert the latter into the objective function derivative. If this last step, entirely done in rational arithmetic, results in the fraction $0/1$, we know that our rational number exactly represents the minimizer.

Interestingly, it turns out that the globally optimal generator $\underline{g}_L^{\text{opt}}$ again consists of rational numbers where L is the denominator, i.e., we obtain a rank-1 lattice rule. Even more interestingly, if L is a Fibonacci number, we obtain precisely the Fibonacci-rank-1 lattice (3.27) (indicated below in red). This has already been conjectured and proven up to $L = 16$ [68].

$$L = 2: \quad \underline{g}^{\text{opt}} = \begin{bmatrix} \frac{1}{2} \\ \frac{1}{2} \end{bmatrix}$$

$$L = 3: \quad \underline{g}^{\text{opt}} \in \left\{ \begin{bmatrix} \frac{1}{3} \\ \frac{1}{3} \end{bmatrix}, \begin{bmatrix} \frac{1}{3} \\ \frac{2}{3} \end{bmatrix}, \begin{bmatrix} \frac{2}{3} \\ \frac{1}{3} \end{bmatrix}, \begin{bmatrix} \frac{2}{3} \\ \frac{2}{3} \end{bmatrix} \right\}$$

$$L = 4: \quad \underline{g}^{\text{opt}} \in \left\{ \begin{bmatrix} \frac{1}{4} \\ \frac{1}{4} \end{bmatrix}, \begin{bmatrix} \frac{1}{4} \\ \frac{3}{4} \end{bmatrix}, \begin{bmatrix} \frac{3}{4} \\ \frac{1}{4} \end{bmatrix}, \begin{bmatrix} \frac{3}{4} \\ \frac{3}{4} \end{bmatrix} \right\}$$

$$L = 5: \quad \underline{g}^{\text{opt}} \in \left\{ \begin{bmatrix} \frac{1}{5} \\ \frac{2}{5} \end{bmatrix}, \begin{bmatrix} \frac{1}{5} \\ \frac{3}{5} \end{bmatrix}, \begin{bmatrix} \frac{2}{5} \\ \frac{1}{5} \end{bmatrix}, \begin{bmatrix} \frac{2}{5} \\ \frac{4}{5} \end{bmatrix}, \begin{bmatrix} \frac{3}{5} \\ \frac{1}{5} \end{bmatrix}, \begin{bmatrix} \frac{3}{5} \\ \frac{4}{5} \end{bmatrix}, \begin{bmatrix} \frac{4}{5} \\ \frac{2}{5} \end{bmatrix}, \begin{bmatrix} \frac{4}{5} \\ \frac{3}{5} \end{bmatrix} \right\}$$

$$L = 6: \quad \underline{g}^{\text{opt}} \in \left\{ \begin{bmatrix} \frac{1}{6} \\ \frac{1}{6} \end{bmatrix}, \begin{bmatrix} \frac{1}{6} \\ \frac{5}{6} \end{bmatrix}, \begin{bmatrix} \frac{5}{6} \\ \frac{1}{6} \end{bmatrix}, \begin{bmatrix} \frac{5}{6} \\ \frac{5}{6} \end{bmatrix} \right\}$$

[1] 64-bit floating point arithmetic (binary64) according to the IEEE 754 standard [120]

$$L = 7\colon \quad \underline{g}^{\text{opt}} \in \left\{ \begin{bmatrix} \frac{1}{7} \\ \frac{2}{7} \end{bmatrix}, \begin{bmatrix} \frac{1}{7} \\ \frac{3}{7} \end{bmatrix}, \begin{bmatrix} \frac{1}{7} \\ \frac{4}{7} \end{bmatrix}, \begin{bmatrix} \frac{1}{7} \\ \frac{5}{7} \end{bmatrix}, \begin{bmatrix} \frac{2}{7} \\ \frac{1}{7} \end{bmatrix}, \begin{bmatrix} \frac{2}{7} \\ \frac{3}{7} \end{bmatrix}, \begin{bmatrix} \frac{2}{7} \\ \frac{4}{7} \end{bmatrix}, \begin{bmatrix} \frac{2}{7} \\ \frac{6}{7} \end{bmatrix}, \begin{bmatrix} \frac{3}{7} \\ \frac{1}{7} \end{bmatrix}, \begin{bmatrix} \frac{3}{7} \\ \frac{2}{7} \end{bmatrix}, \begin{bmatrix} \frac{3}{7} \\ \frac{5}{7} \end{bmatrix}, \begin{bmatrix} \frac{3}{7} \\ \frac{6}{7} \end{bmatrix}, \dots \right\}$$

$$L = 8\colon \quad \underline{g}^{\text{opt}} \in \left\{ \begin{bmatrix} \frac{1}{8} \\ \frac{3}{8} \end{bmatrix}, \begin{bmatrix} \frac{1}{8} \\ \frac{5}{8} \end{bmatrix}, \begin{bmatrix} \frac{3}{8} \\ \frac{1}{8} \end{bmatrix}, \begin{bmatrix} \frac{3}{8} \\ \frac{7}{8} \end{bmatrix}, \begin{bmatrix} \frac{5}{8} \\ \frac{1}{8} \end{bmatrix}, \begin{bmatrix} \frac{5}{8} \\ \frac{7}{8} \end{bmatrix}, \begin{bmatrix} \frac{7}{8} \\ \frac{3}{8} \end{bmatrix}, \begin{bmatrix} \frac{7}{8} \\ \frac{5}{8} \end{bmatrix} \right\}$$

$$L = 9\colon \quad \underline{g}^{\text{opt}} \in \left\{ \begin{bmatrix} \frac{1}{9} \\ \frac{2}{9} \end{bmatrix}, \begin{bmatrix} \frac{1}{9} \\ \frac{4}{9} \end{bmatrix}, \begin{bmatrix} \frac{1}{9} \\ \frac{5}{9} \end{bmatrix}, \begin{bmatrix} \frac{1}{9} \\ \frac{7}{9} \end{bmatrix}, \begin{bmatrix} \frac{2}{9} \\ \frac{1}{9} \end{bmatrix}, \begin{bmatrix} \frac{2}{9} \\ \frac{4}{9} \end{bmatrix}, \begin{bmatrix} \frac{2}{9} \\ \frac{5}{9} \end{bmatrix}, \begin{bmatrix} \frac{2}{9} \\ \frac{8}{9} \end{bmatrix}, \begin{bmatrix} \frac{4}{9} \\ \frac{1}{9} \end{bmatrix}, \begin{bmatrix} \frac{4}{9} \\ \frac{2}{9} \end{bmatrix}, \begin{bmatrix} \frac{4}{9} \\ \frac{7}{9} \end{bmatrix}, \begin{bmatrix} \frac{4}{9} \\ \frac{8}{9} \end{bmatrix}, \dots \right\}$$

$$L = 10\colon \quad \underline{g}^{\text{opt}} \in \left\{ \begin{bmatrix} \frac{1}{10} \\ \frac{3}{10} \end{bmatrix}, \begin{bmatrix} \frac{1}{10} \\ \frac{7}{10} \end{bmatrix}, \begin{bmatrix} \frac{3}{10} \\ \frac{1}{10} \end{bmatrix}, \begin{bmatrix} \frac{3}{10} \\ \frac{9}{10} \end{bmatrix}, \begin{bmatrix} \frac{7}{10} \\ \frac{1}{10} \end{bmatrix}, \begin{bmatrix} \frac{7}{10} \\ \frac{9}{10} \end{bmatrix}, \begin{bmatrix} \frac{9}{10} \\ \frac{3}{10} \end{bmatrix}, \begin{bmatrix} \frac{9}{10} \\ \frac{7}{10} \end{bmatrix} \right\}$$

$$L = 11\colon \quad \underline{g}^{\text{opt}} \in \left\{ \begin{bmatrix} \frac{1}{11} \\ \frac{3}{11} \end{bmatrix}, \begin{bmatrix} \frac{1}{11} \\ \frac{4}{11} \end{bmatrix}, \begin{bmatrix} \frac{1}{11} \\ \frac{7}{11} \end{bmatrix}, \begin{bmatrix} \frac{1}{11} \\ \frac{8}{11} \end{bmatrix}, \begin{bmatrix} \frac{2}{11} \\ \frac{3}{11} \end{bmatrix}, \begin{bmatrix} \frac{2}{11} \\ \frac{5}{11} \end{bmatrix}, \begin{bmatrix} \frac{2}{11} \\ \frac{6}{11} \end{bmatrix}, \begin{bmatrix} \frac{2}{11} \\ \frac{8}{11} \end{bmatrix}, \begin{bmatrix} \frac{3}{11} \\ \frac{1}{11} \end{bmatrix}, \dots \right\}$$

$$L = 12\colon \quad \underline{g}^{\text{opt}} \in \left\{ \begin{bmatrix} \frac{1}{12} \\ \frac{5}{12} \end{bmatrix}, \begin{bmatrix} \frac{1}{12} \\ \frac{7}{12} \end{bmatrix}, \begin{bmatrix} \frac{5}{12} \\ \frac{1}{12} \end{bmatrix}, \begin{bmatrix} \frac{5}{12} \\ \frac{11}{12} \end{bmatrix}, \begin{bmatrix} \frac{7}{12} \\ \frac{1}{12} \end{bmatrix}, \begin{bmatrix} \frac{7}{12} \\ \frac{11}{12} \end{bmatrix}, \begin{bmatrix} \frac{11}{12} \\ \frac{5}{12} \end{bmatrix}, \begin{bmatrix} \frac{11}{12} \\ \frac{7}{12} \end{bmatrix} \right\}$$

$$\vdots$$

In reduced form, globally optimal rank-1 lattice generators $\underline{g}_L^{\text{opt}}$ for $L \in [13, 65]$ in $s = 2$ are

$$\begin{bmatrix} 1 \\ 13 \\ \{5,8\} \\ 13 \end{bmatrix}, \begin{bmatrix} 1 \\ 14 \\ \{3,5,9,11\} \\ 14 \end{bmatrix}, \begin{bmatrix} 1 \\ 15 \\ \{4,11\} \\ 15 \end{bmatrix}, \begin{bmatrix} 1 \\ 16 \\ \{7,9\} \\ 16 \end{bmatrix}, \begin{bmatrix} 1 \\ 17 \\ \{5,7,10,12\} \\ 17 \end{bmatrix}, \begin{bmatrix} 1 \\ 18 \\ \{5,7,11,13\} \\ 18 \end{bmatrix},$$
$$\begin{bmatrix} 1 \\ 19 \\ \{7,8,11,12\} \\ 19 \end{bmatrix}, \begin{bmatrix} 1 \\ 20 \\ \{9,11\} \\ 20 \end{bmatrix}, \begin{bmatrix} 1 \\ 21 \\ \{8,13\} \\ 21 \end{bmatrix}, \begin{bmatrix} 1 \\ 22 \\ \{5,9,13,17\} \\ 22 \end{bmatrix}, \begin{bmatrix} 1 \\ 23 \\ \{7,10,13,16\} \\ 23 \end{bmatrix}, \begin{bmatrix} 1 \\ 24 \\ \{7,17\} \\ 24 \end{bmatrix},$$
$$\begin{bmatrix} 1 \\ 25 \\ \{7,18\} \\ 25 \end{bmatrix}, \begin{bmatrix} 1 \\ 26 \\ \{7,11,15,19\} \\ 26 \end{bmatrix}, \begin{bmatrix} 1 \\ 27 \\ \{8,10,17,19\} \\ 27 \end{bmatrix}, \begin{bmatrix} 1 \\ 28 \\ \{5,11,17,23\} \\ 28 \end{bmatrix}, \begin{bmatrix} 1 \\ 29 \\ \{12,17\} \\ 29 \end{bmatrix},$$
$$\begin{bmatrix} 1 \\ 30 \\ \{11,19\} \\ 30 \end{bmatrix}, \begin{bmatrix} 1 \\ 31 \\ \{12,13,18,19\} \\ 31 \end{bmatrix}, \begin{bmatrix} 1 \\ 32 \\ \{7,9,23,25\} \\ 32 \end{bmatrix}, \begin{bmatrix} 1 \\ 33 \\ \{10,23\} \\ 33 \end{bmatrix}, \begin{bmatrix} 1 \\ 34 \\ \{13,21\} \\ 34 \end{bmatrix},$$
$$\begin{bmatrix} 1 \\ 35 \\ \{8,13,22,27\} \\ 35 \end{bmatrix}, \begin{bmatrix} 1 \\ 36 \\ \{11,13,23,25\} \\ 36 \end{bmatrix}, \begin{bmatrix} 1 \\ 37 \\ \{10,11,26,27\} \\ 37 \end{bmatrix}, \begin{bmatrix} 1 \\ 38 \\ \{9,17,21,29\} \\ 38 \end{bmatrix}, \begin{bmatrix} 1 \\ 39 \\ \{16,17,22,23\} \\ 39 \end{bmatrix},$$

$$\left[\begin{matrix}\frac{1}{40}\\ \{11,29\}\\ 40\end{matrix}\right], \left[\begin{matrix}\frac{1}{41}\\ \{12,17,24,29\}\\ 41\end{matrix}\right], \left[\begin{matrix}\frac{1}{42}\\ \{13,29\}\\ 42\end{matrix}\right], \left[\begin{matrix}\frac{1}{43}\\ \{12,18,25,31\}\\ 43\end{matrix}\right], \left[\begin{matrix}\frac{1}{44}\\ \{13,17,27,31\}\\ 44\end{matrix}\right],$$
$$\left[\begin{matrix}\frac{1}{45}\\ \{19,26\}\\ 45\end{matrix}\right], \left[\begin{matrix}\frac{1}{46}\\ \{17,19,27,29\}\\ 46\end{matrix}\right], \left[\begin{matrix}\frac{1}{47}\\ \{13,18,29,34\}\\ 47\end{matrix}\right], \left[\begin{matrix}\frac{1}{48}\\ \{11,13,35,37\}\\ 48\end{matrix}\right],$$
$$\left[\begin{matrix}\frac{1}{49}\\ \{18,19,30,31\}\\ 49\end{matrix}\right], \left[\begin{matrix}\frac{1}{50}\\ \{19,21,29,31\}\\ 50\end{matrix}\right], \left[\begin{matrix}\frac{1}{51}\\ \{11,14,20,23,28,31,37,40\}\\ 51\end{matrix}\right], \left[\begin{matrix}\frac{1}{52}\\ \{11,19,33,41\}\\ 52\end{matrix}\right],$$
$$\left[\begin{matrix}\frac{1}{53}\\ \{23,30\}\\ 53\end{matrix}\right], \left[\begin{matrix}\frac{1}{54}\\ \{17,19,35,37\}\\ 54\end{matrix}\right], \left[\begin{matrix}\frac{1}{55}\\ \{21,34\}\\ 55\end{matrix}\right], \left[\begin{matrix}\frac{1}{56}\\ \{17,23,33,39\}\\ 56\end{matrix}\right],$$
$$\left[\begin{matrix}\frac{1}{57}\\ \{13,16,22,25,32,35,41,44\}\\ 57\end{matrix}\right], \left[\begin{matrix}\frac{1}{58}\\ \{17,41\}\\ 58\end{matrix}\right], \left[\begin{matrix}\frac{1}{59}\\ \{18,23,36,41\}\\ 59\end{matrix}\right], \left[\begin{matrix}\frac{1}{60}\\ \{13,23,37,47\}\\ 60\end{matrix}\right],$$
$$\left[\begin{matrix}\frac{1}{61}\\ \{17,18,43,44\}\\ 61\end{matrix}\right], \left[\begin{matrix}\frac{1}{62}\\ \{23,27,35,39\}\\ 62\end{matrix}\right], \left[\begin{matrix}\frac{1}{63}\\ \{17,26,37,46\}\\ 63\end{matrix}\right], \left[\begin{matrix}\frac{1}{64}\\ \{19,27,37,45\}\\ 64\end{matrix}\right],$$
$$\left[\begin{matrix}\frac{1}{65}\\ \{19,24,41,46\}\\ 65\end{matrix}\right]. \tag{5.40}$$

Fibonacci–rank-1 lattices in the form (3.27) are again colored in red. Note that for each L, the different global minimizers are identical under symmetry and periodicity considerations (see Figure 5.5).

Visualization: Figure B.6 to B.8. Complete list: Appendix C.1.1.

5.2.2.C ($s = 3$) Similarly, we can search for rank-1 lattices in $s = 3$ that are optimal with respect to the wce (5.31). For most L, including Fibonacci numbers, we obtain again rank-1 lattice rules. In some cases ($L \in \{10, 12, 15, 26, 28\}$), we obtain irrational generating vectors (and therefore non-lattice point sets) as global optima but rank-1 lattice rules as local optima.

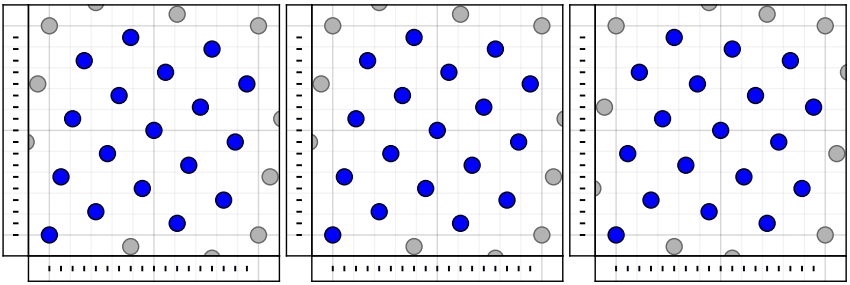

Figure 5.6: Rank-1 lattice with $L = 18$ in $s = 3$ that globally minimizes the wce (5.31). Shown are xy, xz, and yz-projection, respectively.

$$
\begin{bmatrix} \frac{1}{2} \\ \frac{1}{2} \\ \frac{1}{2} \end{bmatrix}, \begin{bmatrix} \frac{1}{3} \\ \frac{1}{3} \\ \frac{1}{3} \end{bmatrix}, \begin{bmatrix} \frac{1}{4} \\ \frac{1}{4} \\ \frac{1}{4} \end{bmatrix}, \begin{bmatrix} \frac{1}{5} \\ \frac{1}{5} \\ \frac{2}{5} \end{bmatrix}, \begin{bmatrix} \frac{1}{6} \\ \frac{1}{6} \\ \frac{1}{6} \end{bmatrix}, \begin{bmatrix} \frac{1}{7} \\ \frac{2}{7} \\ \frac{3}{7} \end{bmatrix}, \begin{bmatrix} \frac{1}{8} \\ \frac{1}{8} \\ \frac{3}{8} \end{bmatrix}, \begin{bmatrix} \frac{1}{9} \\ \frac{2}{9} \\ \frac{4}{9} \end{bmatrix}, \begin{bmatrix} \frac{1}{10} \\ \frac{1}{10} \\ \frac{3}{10} \end{bmatrix}, \begin{bmatrix} \frac{1}{11} \\ \frac{2}{11} \\ \frac{3}{11} \end{bmatrix}, \begin{bmatrix} \frac{1}{12} \\ \frac{1}{12} \\ \frac{5}{12} \end{bmatrix}, \begin{bmatrix} \frac{1}{13} \\ \frac{3}{13} \\ \frac{4}{13} \end{bmatrix}, \begin{bmatrix} \frac{1}{14} \\ \frac{3}{14} \\ \frac{5}{14} \end{bmatrix},
$$

$$
\begin{bmatrix} \frac{1}{15} \\ \frac{2}{15} \\ \frac{4}{15} \end{bmatrix}, \begin{bmatrix} \frac{1}{16} \\ \frac{3}{16} \\ \frac{5}{16} \end{bmatrix}, \begin{bmatrix} \frac{1}{17} \\ \frac{3}{17} \\ \frac{5}{17} \end{bmatrix}, \begin{bmatrix} \frac{1}{18} \\ \frac{5}{18} \\ \frac{7}{18} \end{bmatrix}, \begin{bmatrix} \frac{1}{19} \\ \frac{7}{19} \\ \frac{8}{19} \end{bmatrix}, \begin{bmatrix} \frac{1}{20} \\ \frac{3}{20} \\ \frac{7}{20} \end{bmatrix}, \begin{bmatrix} \frac{1}{21} \\ \frac{4}{21} \\ \frac{5}{21} \end{bmatrix}, \begin{bmatrix} \frac{1}{22} \\ \frac{3}{22} \\ \frac{5}{22} \end{bmatrix}, \begin{bmatrix} \frac{1}{23} \\ \frac{4}{23} \\ \frac{10}{23} \end{bmatrix}, \begin{bmatrix} \frac{1}{24} \\ \frac{5}{24} \\ \frac{7}{24} \end{bmatrix}, \begin{bmatrix} \frac{1}{25} \\ \frac{4}{25} \\ \frac{11}{25} \end{bmatrix}, \begin{bmatrix} \frac{1}{26} \\ \frac{3}{26} \\ \frac{7}{26} \end{bmatrix},
$$

$$
\begin{bmatrix} \frac{1}{27} \\ \frac{8}{27} \\ \frac{10}{27} \end{bmatrix}, \begin{bmatrix} \frac{1}{28} \\ \frac{3}{28} \\ \frac{5}{28} \end{bmatrix}, \begin{bmatrix} \frac{1}{29} \\ \frac{8}{29} \\ \frac{12}{29} \end{bmatrix}, \begin{bmatrix} \frac{1}{30} \\ \frac{7}{30} \\ \frac{11}{30} \end{bmatrix}, \begin{bmatrix} \frac{1}{31} \\ \frac{7}{31} \\ \frac{9}{31} \end{bmatrix}, \begin{bmatrix} \frac{1}{32} \\ \frac{5}{32} \\ \frac{7}{32} \end{bmatrix}, \begin{bmatrix} \frac{1}{33} \\ \frac{4}{33} \\ \frac{10}{33} \end{bmatrix}, \begin{bmatrix} \frac{1}{34} \\ \frac{9}{34} \\ \frac{13}{34} \end{bmatrix}, \begin{bmatrix} \frac{1}{35} \\ \frac{6}{35} \\ \frac{8}{35} \end{bmatrix},
$$

$$
\begin{bmatrix} \frac{1}{36} \\ \frac{11}{36} \\ \frac{13}{36} \end{bmatrix}, \begin{bmatrix} \frac{1}{37} \\ \frac{8}{37} \\ \frac{10}{37} \end{bmatrix}, \begin{bmatrix} \frac{1}{38} \\ \frac{7}{38} \\ \frac{11}{38} \end{bmatrix}, \begin{bmatrix} \frac{1}{39} \\ \frac{16}{39} \\ \frac{17}{39} \end{bmatrix}, \begin{bmatrix} \frac{1}{40} \\ \frac{7}{40} \\ \frac{9}{40} \end{bmatrix}, \begin{bmatrix} \frac{1}{55} \\ \frac{12}{55} \\ \frac{21}{55} \end{bmatrix}, \tag{5.41}
$$

Visualization: Figure 5.6 and Figure B.15 to B.22. Complete list: Appendix C.1.2.

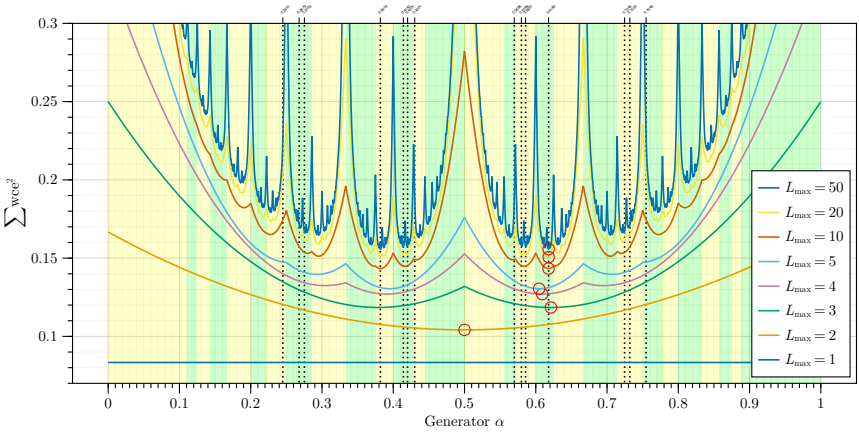

Figure 5.7: Global search for best 1D Kronecker sequence generator α, for various values of $L_{\max}$ in (5.42). Red circles indicate global optima, apparently converging to the inverse golden ratio $\frac{1}{\Phi} = 0.618033\ldots$. Some irrationals from Section 3.3.2 indicated by vertical dashed lines. The quality measure is symmetric around $\alpha = 0.5$ because mirrored point sets have identical wces. Piecewise quadratic segments are indicated by alternating background color for $L_{\max} = 10$.

5.3 Global Search for Open Point Sets

5.3.1 State of Art

Kronecker sequences with low periodic L_2 discrepancy, also called diaphony, are computed in [132]. Furthermore, it is possible to construct rank-1 lattices where the same generating vector can be used for a range of L, effectively representing an open point set. Such "lattice sequences" can be efficiently obtained via component-by-component construction of embedded lattice rules [28], [100].

5.3.2 Kronecker Sequences

The Kronecker sequence is distinctive in that a generator is not specific to a certain number of samples, but additional samples can always be added using the same generator. Hence, we sum up the squared wces (5.31) for a range of numbers of samples L and attempt to minimize that

$$\underline{\alpha}^{\text{opt}}_{L_{\max}} = \arg\min_{\underline{\alpha}} \left\{ \sum_{L=1}^{L_{\max}} \text{wce}^2\big(\{i \cdot \underline{\alpha} \mod 1\}_{i=0}^{L-1}\big) \right\} . \tag{5.42}$$

It is a piecewise polynomial of order $2s$ with s variables and $\mathcal{O}(L_{\max}^{2s})$ (5.38) piecewise regions. It may be possible to determine the global minimum for $L_{\max} \to \infty$ with arbitrary precision by alternately increasing $L_{\max}$ and restricting the search range.

5.3.2.A ($s = 1$) In the 1D case, we obtain

$$\begin{aligned}
\alpha_2^{\text{opt}} &= {}^1\!/_2 = 0.500000\ldots \\
\alpha_3^{\text{opt}} &= {}^{41}\!/_{66} = 0.621212\ldots \\
\alpha_4^{\text{opt}} &= {}^{95}\!/_{156} = 0.608974\ldots \\
\alpha_5^{\text{opt}} &= {}^{907}\!/_{1500} = 0.604666\ldots \\
\alpha_{10}^{\text{opt}} &= {}^{12261601}\!/_{19845000} = 0.617868\ldots \\
\alpha_{20}^{\text{opt}} &= {}^{12749201923299811}\!/_{20626104644145000} = 0.618110\ldots \\
\alpha_{30}^{\text{opt}} &= \tfrac{72336848387458919263771 13}{11704991633539654700250000} = 0.618000\ldots \\
\alpha_{40}^{\text{opt}} &= \tfrac{10603776964101375196451425648375859455097794489}{17157283103536350082369152434117495811090000000} = 0.618033\ldots
\end{aligned}$$

This possibly converges towards the inverse golden ratio ${}^1\!/_\Phi$.

Visualization: Figure 5.7. Complete list: Appendix C.2.1.

5.3.2.B ($s = 2$) It is now an extremely interesting problem finding a globally optimal Kronecker sequence for $s = 2$ (and thereby also a globally optimal 3D Kronecker lattice for $s = 3$). The wce (5.31) for $s = 2$ is a

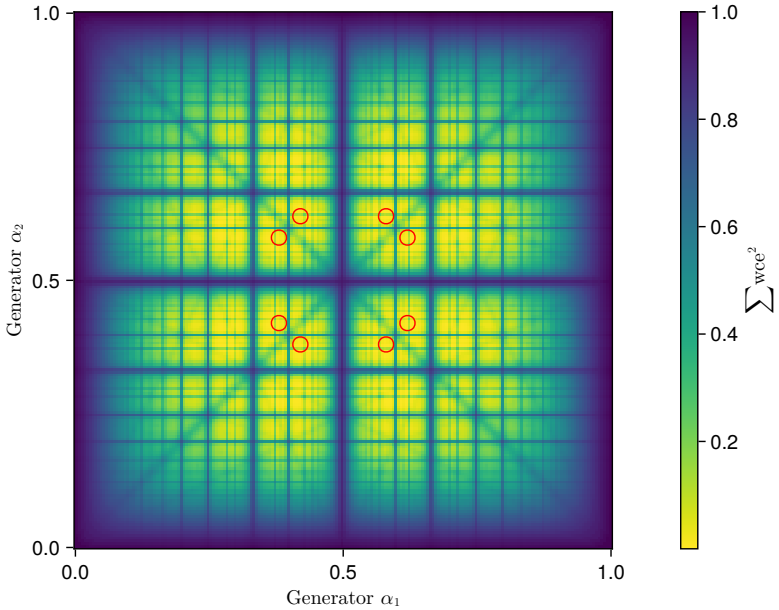

Figure 5.8: Global search for best 2D Kronecker sequence generator $\underline{\alpha} \in [0,1]^2$, for $L_{\max} = 50$ in (5.42). Red circles indicate global optima $\underline{\alpha}_{50}^{\text{opt}} \approx [0.58, 0.61]^\top$, compare (5.43). The quality measure is mirror-symmetric at 0.5 (both axes), because mirrored point sets have identical wces.

piecewise 2D quartic polynomial. Rational approximations do not seem to be helpful here, so we compute the result to double precision and print the decimal approximation

$$\begin{aligned}
\underline{\alpha}_{5}^{\text{opt}} &= \begin{bmatrix} 0.394945\ldots & 0.394945\ldots \end{bmatrix}^\top \widehat{=} \begin{bmatrix} 0.605054\ldots & 0.605054\ldots \end{bmatrix}^\top , \\
\underline{\alpha}_{10}^{\text{opt}} &= \begin{bmatrix} 0.380493\ldots & 0.417969\ldots \end{bmatrix}^\top \widehat{=} \begin{bmatrix} 0.619506\ldots & 0.582030\ldots \end{bmatrix}^\top , \\
\underline{\alpha}_{20}^{\text{opt}} &= \begin{bmatrix} 0.368534\ldots & 0.420105\ldots \end{bmatrix}^\top \widehat{=} \begin{bmatrix} 0.631465\ldots & 0.579894\ldots \end{bmatrix}^\top , \\
\underline{\alpha}_{50}^{\text{opt}} &= \begin{bmatrix} 0.381914\ldots & 0.419879\ldots \end{bmatrix}^\top \widehat{=} \begin{bmatrix} 0.618085\ldots & 0.580120\ldots \end{bmatrix}^\top , \\
\underline{\alpha}_{100}^{\text{opt}} &= \begin{bmatrix} 0.381988\ldots & 0.419810\ldots \end{bmatrix}^\top \widehat{=} \begin{bmatrix} 0.618011\ldots & 0.580189\ldots \end{bmatrix}^\top ,
\end{aligned}$$

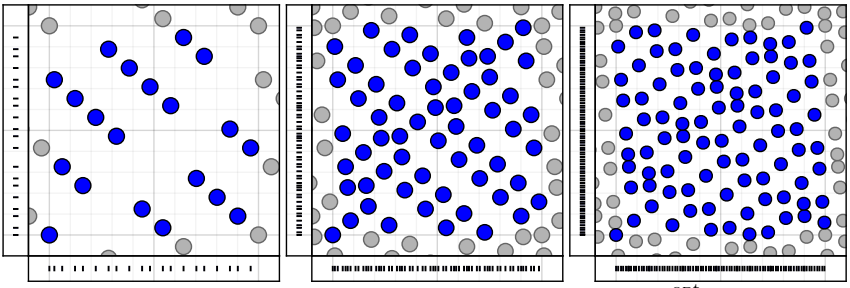

Figure 5.9: Kronecker Sequence in $s = 2$ using generator $\underline{\alpha}_{90}^{\text{opt}}$ that globally minimizes the wce (5.31). Shown for $L \in \{20, 60, 90\}$.

$$\underline{\alpha}_{150}^{\text{opt}} = \begin{bmatrix} 0.381967\ldots & 0.420190\ldots \end{bmatrix}^\top \widehat{=} \begin{bmatrix} 0.618032\ldots & 0.579809\ldots \end{bmatrix}^\top . \tag{5.43}$$

Visualization: Figures 5.8, 5.9 and B.11. Complete list: Appendix C.2.2. Interrelationships: Figure 5.10.

5.3.2.C ($s = 3$) The wce (5.31) for $s = 3$ is a piecewise polynomial of order six with three variables. We obtain (cropped after six digits)

$$\begin{aligned}
\underline{\alpha}_{10}^{\text{opt}} &= \begin{bmatrix} 0.294271 & 0.381780 & 0.417900 \end{bmatrix}^\top \widehat{=} \begin{bmatrix} 0.705728 & 0.618219 & 0.582099 \end{bmatrix}^\top , \\
\underline{\alpha}_{20}^{\text{opt}} &= \begin{bmatrix} 0.276840 & 0.381487 & 0.419937 \end{bmatrix}^\top \widehat{=} \begin{bmatrix} 0.723159 & 0.618512 & 0.580062 \end{bmatrix}^\top , \\
\underline{\alpha}_{50}^{\text{opt}} &= \begin{bmatrix} 0.276464 & 0.381970 & 0.418922 \end{bmatrix}^\top \widehat{=} \begin{bmatrix} 0.723535 & 0.618029 & 0.581077 \end{bmatrix}^\top , \\
\underline{\alpha}_{70}^{\text{opt}} &= \begin{bmatrix} 0.275319 & 0.381972 & 0.418920 \end{bmatrix}^\top \widehat{=} \begin{bmatrix} 0.724680 & 0.618027 & 0.581079 \end{bmatrix}^\top .
\end{aligned} \tag{5.44}$$

Complete list: Appendix C.2.3. Interrelationships: Figure 5.10.

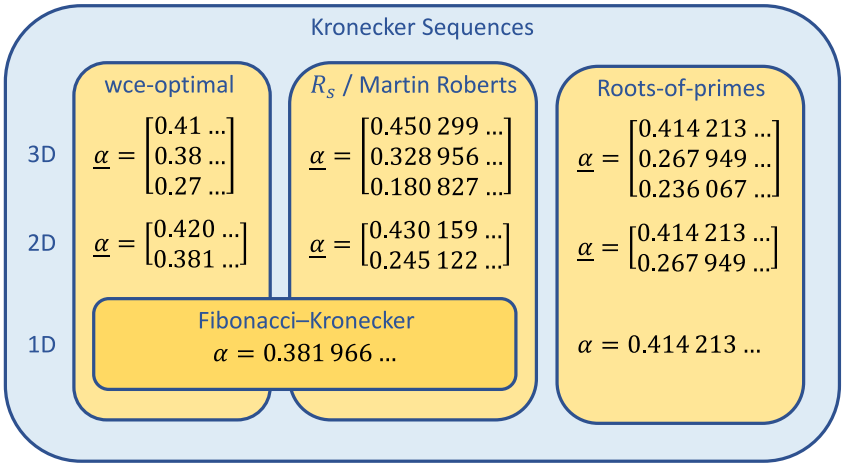

(a) $\alpha \in [0, 0.5]$

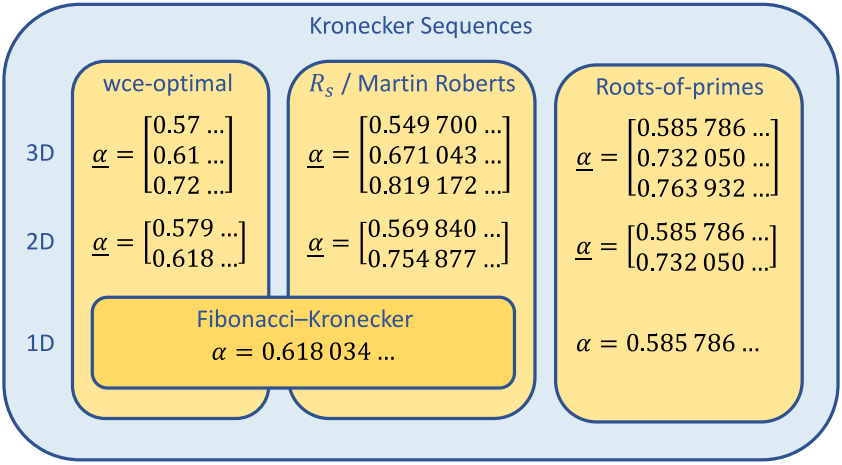

(b) $\alpha \in [0.5, 1]$

Figure 5.10: Overview of Kronecker sequence constructions. Both equivalent representations, $\alpha \in [0, 0.5]$ and $\alpha \in [0.5, 1]$ are shown.

5.4 Summary

This chapter introduced discrepancy, dispersion, packing density, covering density, and various worst-case integration errors, allowing us to quantify the quality of uniform point sets. We then computed wce-optimal 1D, 2D, and 3D rank-1 lattice rules and Kronecker sequences via brute force search. These wce-optimal constructions were found to be consistent with the respective 1D Fibonacci–Kronecker and 2D Fibonacci–rank-1 lattice construction but novel in the higher-dimensional versions.

CHAPTER 6

Transformations

Contents

> The systematic representation of all or part
> of the surface of a round body, especially the earth,
> onto a flat or plane surface is called a *map projection*.
> Literally an infinite number of map projections are
> possible, and several hundred have been published.
>
> *Flattening the Earth:*
> *Two Thousand Years of Map Projections*
> John P. Snyder (1926–1997)

In this chapter, we introduce discrepancy and dispersion for non-uniform densities. We close gaps in the state of art with novel definitions. We examine the relationship between discrepancy and dispersion of transformed point sets depending on the properties of the particular mapping. Overall, the result is a method for low-dispersion sampling of non-uniform densities using an orthogonal inverse transform of low-discrepancy reference samples.

6.1 General Attributes of Transformations

Transformations $T\colon \underline{x} \to T(\underline{x})$, $\underline{x} \in \mathbb{R}^s$, are characterized by specific properties of their Jacobian matrix $\mathbf{J}_T(\cdot)$ and its determinant. We list a few of these characteristics that we will need later in this chapter.

Rigid transformations or **isometries** preserve distances (and thereby also angles). They can be represented with translation vector $\underline{v}$ and orthogonal matrix $\mathbf{R}$ representing rotations ($\det \mathbf{R} = 1$) or reflections ($\det \mathbf{R} = -1$)

$$T\colon \mathbb{R}^s \to \mathbb{R}^s \ , \tag{6.1}$$

$$T(\underline{x}) = \mathbf{R} \cdot \underline{x} + \underline{v} \ , \quad \underline{v} \in \mathbb{R}^s \ , \tag{6.2}$$

$$\mathbf{R}^\top = \mathbf{R}^{-1} \ , \tag{6.3}$$

$$|\det \mathbf{R}| = 1 \ . \tag{6.4}$$

Conformal maps preserve angles locally. Their Jacobian matrix is an orthogonal matrix multiplied by a scalar.

$$T\colon \mathbb{R}^s \to \mathbb{R}^s \ , \tag{6.5}$$

$$\mathbf{J}_T(\underline{x}) = \alpha(\underline{x}) \cdot \mathbf{R}(\underline{x}) \quad , \tag{6.6}$$

$$\alpha(\underline{x}) > 0 \quad \forall \underline{x} \ , \tag{6.7}$$

$$\mathbf{R}^\top(\underline{x}) = \mathbf{R}^{-1}(\underline{x}) \quad \forall \underline{x} \ . \tag{6.8}$$

Equiareal maps preserve the area ($s = 2$) or volume ($s > 2$) of subsets of arbitrary shape and size. Their absolute Jacobian determinant is one.

$$T\colon \mathbb{R}^s \to \mathbb{R}^s \ , \tag{6.9}$$

$$|\det \mathbf{J}_T(\underline{x})| = 1 \quad \forall \underline{x} \ . \tag{6.10}$$

Component-wise transformations are arbitrary transformations of the individual coordinates, respectively. They preserve the orthogonality of the coordinate axes. Their Jacobian matrices are diagonal matrices with different positive entries.

$$T\colon \mathbb{R}^s \to \mathbb{R}^s \ , \tag{6.11}$$

$$T(\underline{x}) = \begin{bmatrix} T_1(x_1) & T_2(x_2) & \cdots & T_s(x_s) \end{bmatrix} \ , \tag{6.12}$$

$$\mathbf{J}_T(\underline{x}) = \mathbf{D}(\underline{x}) \ , \tag{6.13}$$

with $\mathbf{D}(\cdot)$ diagonal.

Orthogonal coordinate system transformations preserve the right angles between coordinate axes. Columns of their Jacobian matrix are orthogonal, with individual, arbitrary norms. We may call such matrices column-orthogonal.

$$T\colon \mathbb{R}^s \to \mathbb{R}^s \ , \tag{6.14}$$

$$\mathbf{J}_T(\underline{x})^\top \cdot \ \mathbf{J}_T(\underline{x}) = \mathbf{D}(\underline{x}) \ , \tag{6.15}$$

with $\mathbf{D}(\cdot)$ diagonal. Furthermore, it holds

$$\mathbf{J}_T(\underline{x}) \cdot \mathbf{D}^{-1}(\underline{x}) \cdot \mathbf{J}_T(\underline{x})^\top = \mathbf{I} \ , \tag{6.16}$$

$$\mathbf{J}_T^{-1}(\underline{x}) = \mathbf{D}^{-1}(\underline{x}) \cdot \mathbf{J}_T(\underline{x})^\top \ . \tag{6.17}$$

Diffeomorphic maps are bijective transformations, where both the forward and inverse transformation are differentiable.

$$T\colon \mathbb{R}^s \to \mathbb{R}^s \ , \tag{6.18}$$

$$T(\underline{x}) \text{ differentiable bijection} \ , \tag{6.19}$$

$$T^{-1}(\underline{x}) \text{ differentiable bijection} \ . \tag{6.20}$$

Rigid maps are conformal, equiareal, and diffeomorphic. Conformal maps are orthogonal and diffeomorphic. Component-wise maps are orthogonal. The stated properties are preserved in concatenations. For conformal, equiareal, and orthogonal maps, differentiability is a prerequisite.

6.2 Discrepancy for Non-Uniform Densities

Following [3], we define a discrepancy measure for non-uniform densities. Starting from the **local discrepancy** for uniform densities (5.1),

$$\Delta(A, \mathcal{P}_L) = \frac{\#(A, \mathcal{P}_L)}{L} - \lambda(A) \ , \tag{6.21}$$

with Lebesgue measure λ, we can generalize this to the **local discrepancy with respect to density** $f(\cdot)$

$$\Delta(A, \mathcal{P}_L; f) = \frac{\#(A, \mathcal{P}_L)}{L} - \int_A f(\underline{x}) \, \mathrm{d}x \ , \tag{6.22}$$

and, by applying the L_p norm over all axes-parallel rectangular boxes $A(\cdot)$ anchored at $\underline{0}$, obtain the star discrepancy with respect to $f(\cdot)$.

Definition 6.1. The **star discrepancy with respect to** f is defined as [3, Eq. 4]

$$\mathrm{discr}_p^*(\mathcal{P}_L; f) = \sqrt[p]{\int_{\underline{x}\in[0,1]^s} |\Delta(A(\underline{x}), \mathcal{P}_L; f)|^p \, \mathrm{d}\underline{x}} \ . \tag{6.23}$$

Similarly, we can define, e.g., the **extreme discrepancy with respect to** $f(\cdot)$ with $p = \infty$ and arbitrary axes-parallel rectangular boxes $A(\underline{a}, \underline{b})$ [69, Eq. 1]

$$\mathrm{discr}(\mathcal{P}_L; f) = \sup_{\underline{a},\underline{b} \in [0,1]^s} |\Delta(A(\underline{a}, \underline{b}), \mathcal{P}_L; f)| \ . \tag{6.24}$$

The existence of point sets achieving an order of $(\log(L))^{s-\frac{1}{2}} L^{-1}$ or better in the extreme star discrepancy with respect to non-uniform densities $f(\cdot)$ has been proven [2].

Now we can state the **Koksma-Hlawka inequality for non-uniform densities** [3, Thm. 1]

$$\left| \frac{1}{L} \sum_{\underline{x} \in \mathcal{P}_L}^{L} g(\underline{x}) - \int_{[0,1]^s} g(\underline{x}) f(\underline{x}) \, \mathrm{d}\underline{x} \right| \leq \mathrm{discr}^*_\infty(\mathcal{P}_L; f) \cdot V(g) \ . \tag{6.25}$$

It tells us that the expectation value of $g(\underline{\boldsymbol{x}})$, $\underline{\boldsymbol{x}} \sim f(\underline{x})$,

$$\mathrm{E}\{g(\underline{\boldsymbol{x}})\} = \int_{[0,1]^s} g(\underline{x}) \cdot f(\underline{x}) \, \mathrm{d}\underline{x} \ , \tag{6.26}$$

can be approximated using a quasi-Monte Carlo method

$$\mathrm{E}\{g(\underline{\boldsymbol{x}})\} \approx \frac{1}{L} \sum_{\underline{x} \in \mathcal{P}_L}^{L} g(\underline{x}) \ , \tag{6.27}$$

and that the accuracy is higher i) if the variation of the integrand $V(g)$ is smaller or ii) if $\mathcal{P}_L$ has a lower extreme star discrepancy with respect to f.

6.3 Dispersion for Non-Uniform Densities

Here, we define a novel dispersion measure for non-uniform densities. It generalizes the well-known dispersion for the uniform density (5.9) to arbitrary densities $f(\cdot)$.

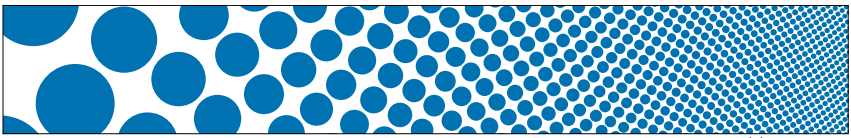

Figure 6.1: Samples $\underline{x}_i$, low-dispersion with respect to density $f(\cdot)$ that is exponential along horizontal and uniform along vertical axis. Radii are chosen proportional to $[f(\underline{x}_i)]^{-1/2}$ according to (6.29).

Definition 6.2 (Dispersion with respect to f)**.** For a point set $\mathcal{P}_L$ in $[0,1]^s$, and density function f being nonnegative and normalized, the **dispersion with respect to** f is

$$\mathrm{dispr}(\mathcal{P}_L; f) = \max_{\underline{x} \in [0,1]^s \setminus \mathcal{P}_L} \left\{ \left[\frac{\int_{B(\underline{x}, r(\underline{x})) \cap [0,1]^s} f(\underline{u}) \, \mathrm{d}\underline{u}}{\lambda(B(\underline{x}, r(\underline{x})) \cap [0,1]^s)} \right]^{\frac{1}{s}} \cdot \, r(\underline{x}) \right\} \ , \quad (6.28)$$

with $r(\underline{x})$ being the distance between $\underline{x}$ and the closest point in $\mathcal{P}_L$,

$$r(\underline{x}) = \min_{\underline{y} \in \mathcal{P}_L} \left\| \underline{x} - \underline{y} \right\|_2 \ ,$$

and ball $B(\underline{x}, r)$ with radius r around $\underline{x}$

$$B(\underline{x}, r) = \{ \underline{u} \mid \|\underline{u} - \underline{x}\|_2 \leq r \} \ .$$

A convenient approximation of the dispersion with respect to f, for sufficiently smooth f and/or large enough L, is

$$\mathrm{dispr}(\mathcal{P}_L; f) \approx \max_{\underline{x} \in [0,1]^s} \left\{ [f(\underline{x})]^{1/s} \cdot \min_{\underline{y} \in \mathcal{P}_L} \left\| \underline{x} - \underline{y} \right\|_2 \right\} \ . \quad (6.29)$$

For the uniform density, $f(\underline{x}) = 1$, $\underline{x} \in [0,1]^s$, (6.28) and (6.29) are identical and equivalent to the usual definition of dispersion (5.9).

Example 6.3 (Plotting 2D Samples with Adaptive Radius)**.** To plot 2D samples $\underline{x}_i \in \mathcal{P}_L$ with radii adapted to the local density $f(\cdot)$, the radii should be chosen proportional to $[f(\underline{x}_i)]^{-1/2}$ (see Figure 6.1). This scales

the size of the samples relative to the distance to their neighbors in the same way as low-dispersion points are doing, i.e., where the maximization argument $\left([f(\underline{x})]^{1/s} \cdot \min_{\underline{y}\in\mathcal{P}_L} \left\|\underline{x}-\underline{y}\right\|_2\right)$ in (6.29) is constant.

Lemma 6.4. *The dispersion with respect to f of a 1D point set obtained via inverse transform sampling $F^{-1}(\mathcal{P}_L)$, where $F(x) = \int_{-\infty}^{t} f(t)\,\mathrm{d}t$, is identical to the dispersion of the point set $\mathcal{P}_L$ before the transform*

$$s = 1\colon \qquad \mathrm{dispr}(F^{-1}(\mathcal{P}_L), f) = \mathrm{dispr}(\mathcal{P}_L)\ . \tag{6.30}$$

Proof. Consider the case where $\{0,1\} \subseteq \mathcal{P}_L$ and $\{0,1\} \subseteq F^{-1}(\mathcal{P}_L)$. Then we have

$$\begin{aligned}
\mathrm{dispr}(F^{-1}(\mathcal{P}_L); f) &= \max_{x\in[0,1]\setminus\mathcal{P}_L} \left\{ \frac{\displaystyle\int_{B(x,r(x))\cap[0,1]} f(u)\,\mathrm{d}u}{\lambda(B(x,r(x))\cap[0,1])} \cdot r(x) \right\} \\
&= \max_{x\in[0,1]\setminus\mathcal{P}_L} \left\{ \frac{\displaystyle\int_{B(x,r(x))} f(u)\,\mathrm{d}u}{2\cdot|x-y(x)|} \cdot |x-y(x)| \right\} \\
&= \max_{x\in[0,1]} \left\{ \frac{1}{2} \cdot \int_{B(x,r(x))} f(u)\,\mathrm{d}u \right\}\ ,
\end{aligned}$$

where $y(x)$ is the nearest neighbor sample of x. Now, we can limit the search space of the maximization from $x \in [0,1]$ to the centers between neighboring samples

$$x \in \left\{ \frac{x_i + x_{i+1}}{2}\ \ ,\quad i \in \mathbb{N}\cap[1, L-1] \right\}\ , \tag{6.31}$$

where x_i are the samples of $F^{-1}(\mathcal{P}_L)$ in sorted order. Therefore, we have

$$\begin{aligned}
\mathrm{dispr}(F^{-1}(\mathcal{P}_L); f) &= \max_{i\in\mathbb{N}\cap[1,L-1]} \left\{ \frac{1}{2} \cdot \int_{x_i}^{x_{i+1}} f(u)\,\mathrm{d}u \right\} && (6.32) \\
&= \max_{i\in\mathbb{N}\cap[1,L-1]} \left\{ \frac{1}{2} \cdot \int_{F^{-1}(p_i)}^{F^{-1}(p_{i+1})} f(u)\,\mathrm{d}u \right\} && (6.33)
\end{aligned}$$

$$= \max_{i \in \mathbb{N} \cap [1, L-1]} \left\{ \frac{1}{2} \cdot \int_{p_i}^{p_{i+1}} 1 \, \mathrm{d}v \right\} \tag{6.34}$$

$$= \mathrm{dispr}(\mathcal{P}_L; 1) \tag{6.35}$$

$$= \mathrm{dispr}(\mathcal{P}_L) \ , \tag{6.36}$$

where p_i are the samples of $\mathcal{P}_L$ in sorted order. Note that F^{-1} is monotonous.

In the case where $\{0,1\} \notin \mathcal{P}_L$ or $\{0,1\} \notin F^{-1}(\mathcal{P}_L)$, we can, instead of (6.32), write

$$\mathrm{dispr}(F^{-1}(\mathcal{P}_L); f) = \max_{i \in \mathbb{N} \cap [1, L+1]} \{M_i\} \ , \tag{6.37}$$

where

$$M_i = \begin{cases} \frac{1}{2} \cdot \int_{x_i}^{x_{i+1}} f(u) \, \mathrm{d}u \ , & i \in [1, L-1] \ , \\ \int_0^{x_1} f(u) \, \mathrm{d}u \ , & i = L \ , \\ \int_{x_L}^{1} f(u) \, \mathrm{d}u \ , & i = L+1 \ , \end{cases} \tag{6.38}$$

and the following lines accordingly, and therefore still obtain

$$\mathrm{dispr}(F^{-1}(\mathcal{P}_L); f) = \mathrm{dispr}(\mathcal{P}_L) \ .$$

□

6.4 Component-Wise Transformation of Product-Type Densities

Let density $f(\underline{x})$, $\underline{x} \in [0,1]^s$, be of **product type**, i.e., **separable** in the coordinate axes, describing independent random variables associated with the individual coordinate axes, respectively,

$$f(\underline{x}) = f_1(x_1) \cdot f_2(x_2) \cdots f_s(x_s) \ . \tag{6.39}$$

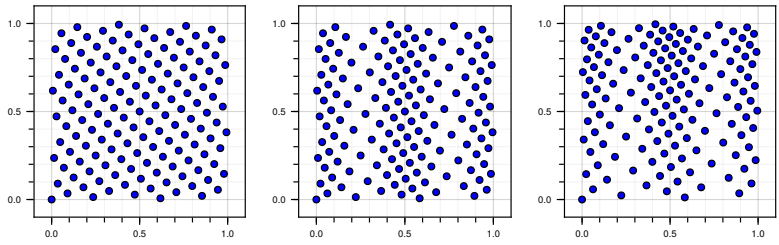

(a) Low Discrepancy

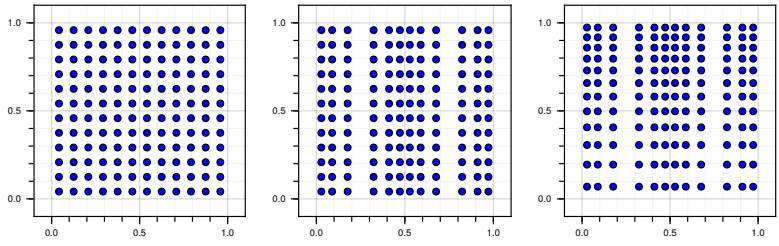

(b) Low Dispersion

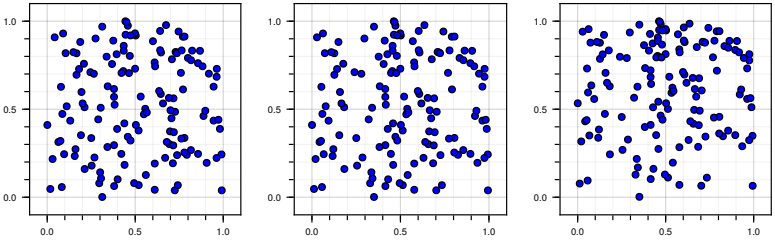

(c) Random

Figure 6.2: Inverse transform sampling with product-type density from Example 6.6 using low-discrepancy (a), low-dispersion (b), and random point sets (c) as reference, respectively. Uniform reference point set (left), transformation of the x_1 coordinate (middle), and complete transformation (right).

The mapping for **inverse transform sampling** of $f(\cdot)$ is then a component-wise nonlinear rescaling

$$Q(\underline{p}) = \begin{bmatrix} F_1^{-1}(p_1) & F_2^{-1}(p_2) & \cdots & F_s^{-1}(p_s) \end{bmatrix}^\top = \underline{x} \ , \tag{6.40}$$

$$f_p(p) = 1 \quad \rightarrow \quad Q(\underline{\boldsymbol{p}}) \sim f_x(\underline{x}) \ , \tag{6.41}$$

where $F(\cdot)$ is the cumulative distribution of $f(\cdot)$. This is essentially a change of parametrization of the coordinate curves.

Theorem 6.5. *If a low-discrepancy point set $\mathcal{P}_L$ is transformed via component-wise $Q(\cdot)$, the resulting point set $Q(\mathcal{P}_L)$ is low-discrepancy with respect to $f(\cdot)$ [3, Thm. 4]*

$$\text{discr}^*_\infty(Q(\mathcal{P}_L); f) \leq \text{discr}^*_\infty(\mathcal{P}_L) \ . \tag{6.42}$$

Equality holds if all cumulative distributions $F_i(\cdot)$ are invertible.

In summary, component-wise transformations preserve a point set's discrepancy. Intuitively, this is because component-wise transformations map axes-parallel boxes into axes-parallel boxes of different aspect ratio, and the definition of discrepancy considers axes-parallel boxes of any aspect ratio.

Example 6.6. We define a 2D product-type density function

$$f(\underline{x}) = c \cdot (2 + \cos(4\pi \cdot x_1)) \cdot e^{x_2} \ , \tag{6.43}$$

with cumulative distributions

$$F_1(x) = x + \frac{\sin(4\pi \cdot x)}{8\pi} \ , \tag{6.44}$$

$$F_2(x) = \frac{e^x - 1}{e - 1} \ . \tag{6.45}$$

According to (6.40) we evaluate $F_1^{-1}(x)$ with a bisection algorithm, and $F_2^{-1}(x)$ via the analytical solution. We can transform any uniformly distributed point set to $f(\underline{x})$. See Figure 6.2 for a visualization using a low-discrepancy, low-dispersion, and random uniform point set, respectively.

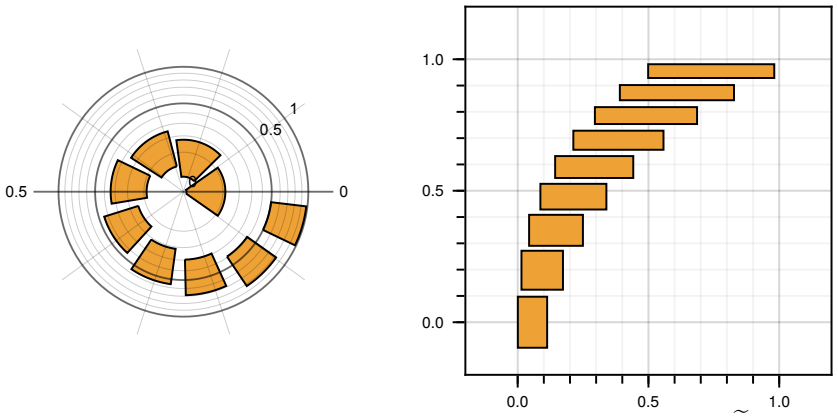

Figure 6.3: Polar coordinate mapping T (left), with polar grid cells $\widetilde{A}$ (orange) that are chosen such that they cover an enclosing circle with best efficiency (see also Figure 6.6). The corresponding Cartesian grid cells (right) are rectangles of various aspect ratios. Note that the polar grid cells become more square-like at larger radii where T has a lower curvature.

A more general but wrong proof is claimed in [20], which has also been taken up several times. It suggests that the preservation of discrepancy observed in component-wise inverse transforms, Theorem 6.5, actually holds for arbitrary density functions using the Rosenblatt transformation as inverse transform. A detailed explanation of the error is given in [3, Sec. 5].

In Section 6.7, we will describe a transformation method that preserves the dispersion for a more general class of density functions than product-type density functions, in particular, density functions that are product-type in any orthogonal coordinate system.

6.5 Non-Cartesian Discrepancy

We extend the usual Cartesian definition of discrepancy to a broader class of coordinate systems.

Definition 6.7 (Non-Cartesian Local Discrepancy)**.** Let transformation T

$$T\colon [0,1]^s \to M$$

describe a coordinate transform with unit absolute Jacobian determinant, i.e., an equiareal map, between the two s-dimensional unit-volume and simply connected domains $[0,1]^s$ and M

$$\begin{aligned} &[0,1]^s && M \\ &\lambda([0,1]^s) = 1 && \lambda(M) = 1 \ . \end{aligned}$$

Furthermore, let domain A be an axes-parallel box in $[0,1]^s$, i.e., a grid cell in Cartesian coordinates, and domain $\widetilde{A}$ the corresponding, potentially non-rectangular and curvilinear, grid cell in the coordinate system described by T

$$\begin{aligned} &A \subseteq [0,1]^s && \widetilde{A} \subseteq M \\ &A = \{\underline{x} \mid \underline{a} \leq \underline{x} \leq \underline{b}\} && \widetilde{A} = \{\widetilde{\underline{x}} = T(\underline{x}) \mid \underline{x} \in A\} \ . \end{aligned}$$

See Figure 6.3 for a visualization with polar coordinates. Now for point set

$$\widetilde{\mathcal{P}_L} = \{\widetilde{\underline{x}}_i\}_{i=1}^L \ , \quad \widetilde{\underline{x}}_i \in M \ ,$$

and grid cell $\widetilde{A}$, we define the **non-Cartesian local discrepancy** $\widetilde{\Delta}(\widetilde{A}, \widetilde{\mathcal{P}_L})$

$$\widetilde{\Delta}(\widetilde{A}, \widetilde{\mathcal{P}_L}) = \frac{\#\left(\widetilde{A}, \widetilde{\mathcal{P}_L}\right)}{L} - \lambda\left(\widetilde{A}\right) \ .$$

Lemma 6.8. *Given point sets $\mathcal{P}_L$ and $\widetilde{\mathcal{P}_L}$*

$$\mathcal{P}_L = \{\underline{x}_i\}_{i=1}^L \ , \qquad \widetilde{\mathcal{P}_L} = \{T(\underline{x}_i)\}_{i=1}^L \ ,$$

and T as in Definition 6.7, it holds

$$\widetilde{\Delta}(\widetilde{A}, \widetilde{\mathcal{P}_L}) = \Delta(A, \mathcal{P}_L) \ .$$

Proof. Since T is equiareal, both grid cells have the same volume

$$\lambda(A) = \lambda\left(\widetilde{A}\right) \ ,$$

and since the samples are transformed in the same way as the grid cell, both have the same number of samples

$$\#\left(\widetilde{A}, \widetilde{\mathcal{P}_L}\right) = \#(A, \mathcal{P}_L) \ .$$

□

Definition 6.9 (Non-Cartesian Discrepancy)**.** For equiareal transformation $T\colon [0,1]^s \to M$ and point set $\widetilde{\mathcal{P}_L}$ with points $\underline{x} \in M$, we define the **non-Cartesian extreme discrepancy in map** T as

$$\operatorname{discr}^T(\mathcal{P}_L) = \sup_{\underline{a},\underline{b}\in M} \left|\Delta(\widetilde{A}(\underline{a},\underline{b}), \widetilde{\mathcal{P}_L})\right| \ , \tag{6.46}$$

where $\widetilde{A}(\underline{a},\underline{b}) = T(A(\underline{a},\underline{b}))$ is a potentially non-rectangular and curvilinear grid cell in M.

It is straightforward to extend this, analogous to (6.22), to the **non-Cartesian discrepancy in map** T **with respect to density** $f(\cdot)$

$$\operatorname{discr}^T(\mathcal{P}_L; f) = \sup_{\underline{a},\underline{b}\in M} \left|\Delta(\widetilde{A}(\underline{a},\underline{b}), \widetilde{\mathcal{P}_L}; f)\right| \ . \tag{6.47}$$

6.6 Dispersion and Discrepancy

We repeat the well-known relation between dispersion and discrepancy for uniform densities and generalize in several steps to arbitrary densities and the effect of mappings.

6.6.1 Uniform Density

We reiterate the theorem relating dispersion and extreme discrepancy [121, p. 528, Theorem 3].

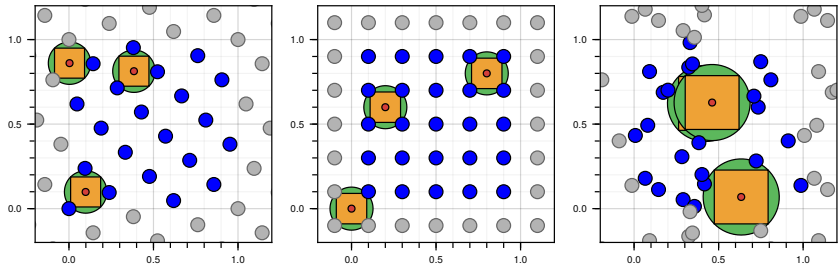

(a) Low Discrepancy **(b)** Low Dispersion **(c)** Random

Figure 6.4: Visualization of proof in Section 6.6.1. Samples $\mathcal{P}_L$ (blue) in $[0,1]^2$, periodic continuation (grey), points $\underline{x}$ (red), $\epsilon = 0.1 \cdot \mathrm{dispr}(\mathcal{P}_L)$, ball $B(\underline{x}, 0.9 \cdot \mathrm{dispr}(\mathcal{P}_L))$ (green), and inscribed cube (yellow). Shown for low-discrepancy (a), low-dispersion but high-discrepancy (b), and random point set (c), respectively.

Theorem 6.10. *For any point set $\mathcal{P}_L$ in $[0,1]^s$, it holds*

$$\mathrm{dispr}(\mathcal{P}_L) \leq \sqrt{s} \cdot [\mathrm{discr}(\mathcal{P}_L)]^{1/s} \quad . \tag{6.48}$$

That is, intuitively speaking, all low-discrepancy point sets are also low-dispersion. We add the assumption that the point set $\mathcal{P}_L$ is tiled periodically, or equivalently, that the domain $[0,1)^s$ has toroidal connectivity. Thereby, we simplify the proof and also achieve a tighter bound.

Definition 6.11 (Periodic L_p distance)**.** Starting from the conventional L_p distance, $d_p(\underline{x}, \underline{y}) = \|\underline{x} - \underline{y}\|_p$, $\underline{x}, \underline{y} \in \mathbb{R}^s$, we define a periodic equivalent, $\mathring{d}_p(\cdot,\cdot)$, on the domain $[0,1)^s$ being considered as 1-periodic or having toroidal connectivity

$$\mathring{d}_p(\underline{x}, \underline{y}) = \sqrt[p]{\sum_{i=1}^{s} (\min\{|x_i - y_i|,\ 1 - |x_i - y_i|\})^p} \quad , \quad \underline{x}, \underline{y} \in [0,1]^s \quad .$$

Definition 6.12 (Periodic dispersion)**.** Starting from the conventional dispersion, Definition 5.1, the periodic dispersion $\mathring{\text{dispr}}(\mathcal{P}_L)$ of a point set $\mathcal{P}_L$ in $[0,1]^s$ is

$$\mathring{\text{dispr}}(\mathcal{P}_L) = \max_{\underline{x}\in[0,1)^s} \left\{ \min_{\underline{y}\in\mathcal{P}_L} \mathring{d}_2(\underline{x},\underline{y}) \right\} \ .$$

Intuitively, the periodic dispersion equals the radius of the largest hyperball not containing $\mathcal{P}_L$ in its interior, i.e., the circumradius of the largest circumhypersphere in a periodic Delaunay triangulation without refinements of $\mathcal{P}_L$ (see green circles in Figure 6.4).

Definition 6.13 (Periodic discrepancy)**.** Following [33, pp. 1f], we define the 1-periodic "interval"

$$\mathring{I}(x,y) = \begin{cases} [x,y) \ , & x \le y \ , \\ [0,y)\cup[x,1) \ , & x > y \ , \end{cases} \tag{6.49}$$

for $x, y \in [0,1]$. Extending this to $s > 1$ and $\underline{x},\underline{y} \in [0,1]^s$, we obtain periodic "boxes"

$$\mathring{A}(\underline{x},\underline{y}) = \mathring{I}(x_1,y_1) \times \mathring{I}(x_2,y_2) \times \cdots \times \mathring{I}(x_s,y_s) \ . \tag{6.50}$$

This leads to the periodic extreme discrepancy

$$\mathring{\text{discr}}(\mathcal{P}_L) = \sup_{\underline{a},\underline{b}} \left| \Delta\Big(\mathring{A}(\underline{a},\underline{b}), \mathcal{P}_L \Big) \right| \ . \tag{6.51}$$

Intuitively, the periodic discrepancy $\mathring{\text{discr}}(\mathcal{P}_L)$ takes into account boxes or hyperrectangles $\mathring{A}(\underline{x},\underline{y})$ that protrude the boundary of $[0,1]^s$ and continue on the opposite side.

Theorem 6.14. *For any point set $\mathcal{P}_L$ in $[0,1]^s$, it holds*

$$\mathring{\text{dispr}}(\mathcal{P}_L) \le \frac{1}{2} \cdot \sqrt{s} \cdot \left[\mathring{\text{discr}}(\mathcal{P}_L) \right]^{1/s} \ , \tag{6.52}$$

where $\mathring{\text{dispr}}(\mathcal{P}_L)$ and $\mathring{\text{discr}}(\mathcal{P}_L)$ are the periodic dispersion and periodic extreme discrepancy of $\mathcal{P}_L$, respectively.

Proof. Following [121, p. 528]. For any ϵ with $0 < \epsilon < \mathring{\text{disp}}\text{r}(\mathcal{P}_L)$, there are points $\underline{x} \in [0,1]^s$ such that

$$\min_{\underline{y} \in \mathcal{P}_L} \mathring{d}_2(\underline{x}, \underline{y}) > \mathring{\text{disp}}\text{r}(\mathcal{P}_L) - \epsilon \ .$$

(These points $\underline{x}$ are located around the circumcenters of the largest circumhyperspheres of the periodic Delaunay triangulation of $\mathcal{P}_L$.) Then the periodic ball $\mathring{B}(\underline{x}, r)$, centered at $\underline{x}$ with radius $r = \mathring{\text{disp}}\text{r}(\mathcal{P}_L) - \epsilon$, contains none of the points in $\mathcal{P}_L$. It is easy to see that the largest possible cube that can be inscribed into a ball $\mathring{B}(\underline{x}, r)$ has edge length $2 \cdot r/\sqrt{s}$. Therefore, into the former ball,

$$\mathring{B}(\underline{x}, \mathring{\text{disp}}\text{r}(\mathcal{P}_L) - \epsilon) \ ,$$

we can inscribe $\mathring{C}$, a cube that can periodically wrap around the boundary of $[0,1)^s$, with maximum edge length

$$2 \cdot \frac{\mathring{\text{disp}}\text{r}(\mathcal{P}_L) - \epsilon}{\sqrt{s}} \ ,$$

and it follows that

$$\mathring{\text{discr}}_\infty(\mathcal{P}_L) \geq \left| \frac{\#\left(\mathring{C}, \mathcal{P}_L\right)}{L} - \lambda\left(\mathring{C}\right) \right| = \lambda\left(\mathring{C}\right) = \left(2 \cdot \frac{\mathring{\text{disp}}\text{r}(\mathcal{P}_L) - \epsilon}{\sqrt{s}} \right)^s \ , \tag{6.53}$$

which, for $\epsilon \to 0_+$, implies (6.52). Refer to Figure 6.4 for a visualization. □

6.6.2 Non-Uniform Densities

We have shown in Section 6.6.1 that low-discrepancy point sets are also low-dispersion,

$$\mathring{\text{disp}}\text{r}(\mathcal{P}_L) \leq \frac{1}{2} \cdot \sqrt{s} \cdot \left[\mathring{\text{discr}}(\mathcal{P}_L) \right]^{1/s} \ .$$

In this section, we will show a similar relationship between the non-uniform discrepancy from Section 6.2 and non-uniform dispersion from Section 6.3.

Definition 6.15 (Asymptotically dense point set)**.** Consider point sets $\mathcal{P}_L$, with variable L, produced by a given construction method. If for every $\xi > 0$ there is an L such that

$$\mathring{\text{dispr}}(\mathcal{P}_K) \leq \xi \quad \text{for all} \quad K \geq L \ , \tag{6.54}$$

then we call these point sets **asymptotically dense**. For example, uniform point sets are asymptotically dense. Point sets that contain only a finite set of points (e.g., just the origin) repeatedly, are not asymptotically dense.

Definition 6.16 (Equality within relative tolerance range)**.** We define equality within a relative tolerance range

$$a \overset{\cdot(1\pm\xi)}{=\!=} b \quad \Longleftrightarrow \quad a \cdot (1-\xi) \leq b \leq a \cdot (1+\xi) \ . \tag{6.55}$$

For example,

$$\pi \overset{\cdot(1\pm 0.05)}{=\!=} 3 \ .$$

Theorem 6.17. *Let $\mathcal{P}_L$ be an asymptotically dense point set in $[0,1]^s$ and $f(\cdot)$ a density function that is uniformly continuous on 1-periodic $[0,1)^s$. Then, for every $\xi > 0$, there is an L such that*

$$\mathring{\text{dispr}}(\mathcal{P}_L; f) \leq \frac{1}{2} \cdot \sqrt{s} \cdot \Big[\mathring{\text{discr}}(\mathcal{P}_L; f)\Big]^{1/s} \cdot (1+\xi) \ .$$

Proof. Since $\mathcal{P}_L$ is asymptotically dense, for every $\xi_1 > 0$ there is an L such that $\mathring{\text{dispr}}(\mathcal{P}_L) \leq \xi_1$, i.e., the remaining balls not covering any points

$$\mathring{B}\left(\underline{x}, \ \min_{\underline{y} \in \mathcal{P}_L} \mathring{d}_2(\underline{x}, \underline{y}) - \epsilon\right) \ , \quad \epsilon > 0 \ , \tag{6.56}$$

all have a radius smaller than or equal to ξ_1. And since f is uniformly continuous, for every $\xi_2 > 0$ there is a $\xi_1 > 0$ such that, for all $\underline{x} \in [0,1]^s$,

$$\left[\frac{\displaystyle\int_{\mathring{B}(\underline{x},\xi_1)} f(\underline{u})\,\mathrm{d}\underline{u}}{\lambda\Big(\mathring{B}(\underline{x},\xi_1)\Big)}\right]^{1/s} \overset{\cdot(1\pm\xi_2)}{=\!=} [f(\underline{x})]^{1/s} \ , \tag{6.57}$$

and

$$\left[\int_{\mathring{C}} f(\underline{u})\,\mathrm{d}u\right]^{1/s} \overset{\cdot(1\pm\xi_2)}{=\!=} \left[f(\underline{x})\cdot\lambda(\mathring{C})\right]^{1/s} , \tag{6.58}$$

$$\mathring{C} \subset \mathring{B}(\underline{x},\xi_1) \ . \tag{6.59}$$

We know from the proof of Theorem 6.14 that

$$\min_{\underline{y}\in\mathcal{P}_L}\left\{\mathring{d}_2(\underline{x},\underline{y})\right\} = \frac{1}{2}\cdot\sqrt{s}\cdot\left(\lambda(\mathring{C})\right)^{1/s} , \tag{6.60}$$

for cubes $\mathring{C}$ inscribed in $\mathring{B}$, therefore also

$$[f(\underline{x})]^{1/s}\cdot\min_{\underline{y}\in\mathcal{P}_L}\left\{\mathring{d}_2(\underline{x},\underline{y})\right\} = \frac{1}{2}\cdot\sqrt{s}\cdot\left[f(\underline{x})\cdot\lambda(\mathring{C})\right]^{1/s} , \tag{6.61}$$

and with the above considerations, for every $\xi_3 > 0$, there is a $\xi_2 > 0$ such that

$$\left[\frac{\int_{\mathring{B}} f(\underline{u})\,\mathrm{d}\underline{u}}{\lambda\left(\mathring{B}\right)}\right]^{1/s}\cdot\min_{\underline{y}\in\mathcal{P}_L}\left\{\mathring{d}_2(\underline{x},\underline{y})\right\} \overset{\cdot(1\pm\xi_3)}{=\!=} \frac{1}{2}\cdot\sqrt{s}\cdot\left[\int_{\mathring{C}} f(\underline{u})\,\mathrm{d}u\right]^{1/s} , \tag{6.62}$$

$$\mathring{C} \subset \mathring{B}(\underline{x},\xi_1) \ . \tag{6.63}$$

This holds for every pair of sample-free ball $\mathring{B}$ and inscribed cube $\mathring{C}$ and in particular for the largest sample-free ball and its largest inscribed cube

$$\max_{\underline{x}\in[0,1]^s}\left\{\left[\frac{\int_{\mathring{B}} f(\underline{u})\,\mathrm{d}\underline{u}}{\lambda\left(\mathring{B}\right)}\right]^{1/s}\cdot\min_{\underline{y}\in\mathcal{P}_L}\left\{\mathring{d}_2(\underline{x},\underline{y})\right\}\right\}$$

$$\overset{\cdot(1\pm\xi_3)}{=\!=} \frac{1}{2}\cdot\sqrt{s}\cdot\left[\max_{\mathring{C}}\left\{\frac{\#\left(\mathring{C},\mathcal{P}_L\right)}{L} - \int_{\mathring{C}} f(\underline{u})\,\mathrm{d}u\right\}\right]^{1/s} . \tag{6.64}$$

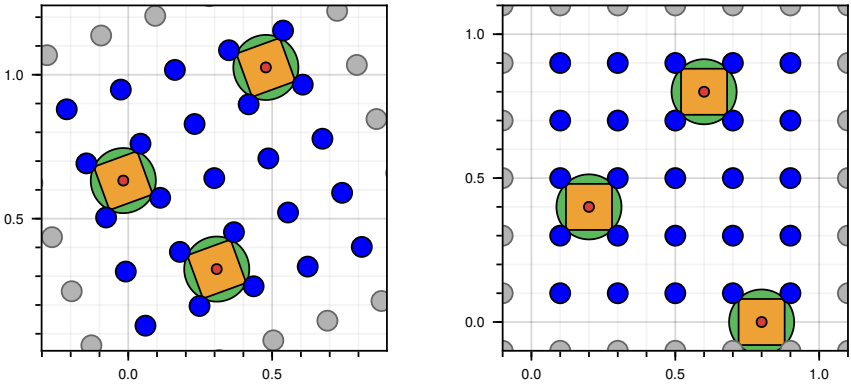

(a) Rigid mapping: rotation by 20°. **(b)** Without transformation.

Figure 6.5: Visualization of proof in Section 6.6.3. Periodic discrepancy is invariant under rigid mapping.

The largest sample-free cube $\mathring{C}$ can be larger than the largest sample-free cube inscribed into a sample-free ball, and the largest sample-free axes-parallel box $\mathring{A}$ (axes-parallel boxes are used in the definition of discrepancy) larger than the largest sample-free cube, therefore the equality turns into an inequality

$$\mathring{\text{dispr}}(\mathcal{P}_L; f) \leq \frac{1}{2} \cdot \sqrt{s} \cdot \left[\mathring{\text{discr}}(\mathcal{P}_L; f)\right]^{1/s} \cdot (1 + \xi_3) \ , \tag{6.65}$$

and for every $\xi_3 > 0$, there is a $\xi_2 > 0$ and in turn a $\xi_1 > 0$ and in turn an L such that this holds. □

6.6.3 Rigid Transformation

We now introduce a rigid transformation T, which includes rotation, translation, and reflection, and investigate the dispersion of the transformed points $\widetilde{\mathcal{P}_L} = T(\mathcal{P}_L)$.

Lemma 6.18. *For any point set $\mathcal{P}_L$ in $[0,1]^s$ and rigid transformation T, it holds*

$$\mathring{\text{dispr}}(T(\mathcal{P}_L)) \leq \frac{1}{2} \cdot \sqrt{s} \cdot \left[\mathring{\text{discr}}(\mathcal{P}_L)\right]^{1/s} . \tag{6.66}$$

Equivalently, using the non-Cartesian discrepancy,

$$\mathring{\text{dispr}}(\widetilde{\mathcal{P}_L}) \leq \frac{1}{2} \cdot \sqrt{s} \cdot \left[\mathring{\text{discr}}^T(\widetilde{\mathcal{P}_L})\right]^{1/s} . \tag{6.67}$$

Proof. The size of the spheres that can be inscribed into the empty space between samples does not change under rigid transformation, hence

$$\mathring{\text{dispr}}(T(\mathcal{P}_L)) = \mathring{\text{dispr}}(\mathcal{P}_L) \ .$$

Furthermore, the size of the squares that can be inscribed into spheres also does not change if the spheres are rigidly rotated, therefore

$$\mathring{\text{dispr}}(T(\mathcal{P}_L)) \leq \frac{1}{2} \cdot \sqrt{s} \cdot \left[\mathring{\text{discr}}(\mathcal{P}_L)\right]^{1/s} .$$

□

See Figure 6.5 for a visualization. This seems trivial and obvious, but we will generalize from rigid to arbitrary maps and obtain a promising and useful result for maps that are orthogonal coordinate transformations.

6.6.4 Dispersion and Discrepancy – Mappings

Theorem 6.19. *Let transformation T*

$$T\colon [0,1]^s \to M$$

be a diffeomorphic and equiareal map between the two s-dimensional unit-volume manifolds $[0,1]^s$ and M. Furthermore, M should form a tiling of $\mathbb{R}^s$ without overlaps and gaps, with T being extended to a diffeomorphism of $\mathbb{R}^s \to \mathbb{R}^s$. We consider an asymptotically dense point set $\mathcal{P}_L$ in $[0,1]^s$,

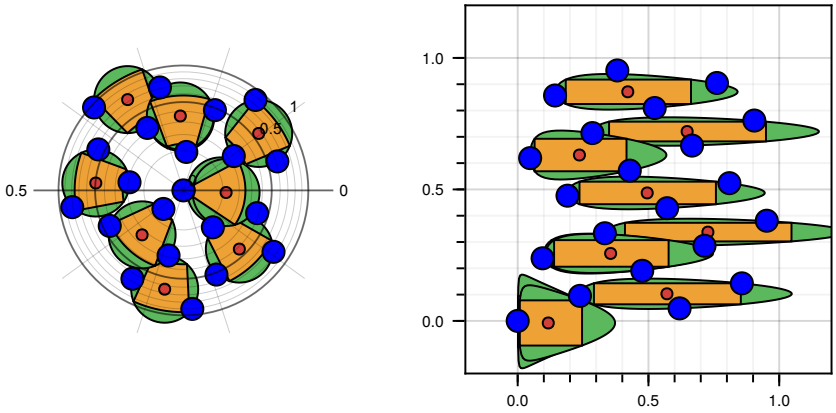

(a) Low-Discrepancy

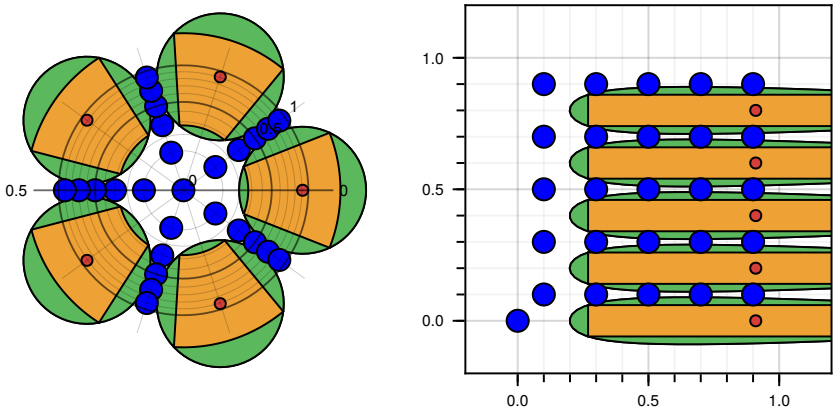

(b) High-Discrepancy

Figure 6.6: A uniform reference point set (right) is transformed (left) using the orthogonal map from the polar coordinate system. In regions away from the pole, polar grid cells (orange) can be made more similar to squares and cover the green balls more efficiently (a), see also Figure 6.3. The high-discrepancy point set (b) cannot preserve its low dispersion in the transformation.

and the transformed points $\widetilde{\mathcal{P}_L} = T(\mathcal{P}_L)$ *in* M*. Then for every* $\xi > 0$*, there is an* L *such that*

$$\mathring{\text{dispr}}(T(\mathcal{P}_L)) \leq \frac{1}{2} \cdot \sqrt{s} \cdot \left[\mathring{\text{discr}}_\infty(\mathcal{P}_L)\right]^{1/s} \cdot \nu \cdot (1+\xi) \ , \tag{6.68}$$

or equivalently, using the non-Cartesian discrepancy,

$$\mathring{\text{dispr}}(\widetilde{\mathcal{P}_L}) \leq \frac{1}{2} \cdot \sqrt{s} \cdot \left[\mathring{\text{discr}}^T_\infty(\widetilde{\mathcal{P}_L})\right]^{1/s} \cdot \nu \cdot (1+\xi) \ , \tag{6.69}$$

where factor ν *depends on the properties of* T*. If* T *is an orthogonal map,* $\nu = 1$*.*

Proof. For any ϵ with $0 < \epsilon < \mathring{\text{dispr}}(\widetilde{\mathcal{P}_L})$, there are points $\widetilde{\underline{x}} \in M$ such that

$$\min_{\underline{y} \in \widetilde{\mathcal{P}_L}} \left\| \widetilde{\underline{x}} - \underline{y} \right\|_2 > \mathring{\text{dispr}}(\widetilde{\mathcal{P}_L}) - \epsilon \ .$$

Then the periodic ball $\mathring{B}(\widetilde{\underline{x}}, r)$, centered at $\widetilde{\underline{x}}$ with radius $r = \mathring{\text{dispr}}(\widetilde{\mathcal{P}_L}) - \epsilon$, contains none of the points in $\widetilde{\mathcal{P}_L}$. Let $\mathring{\widetilde{C}} \subset M$ be a T-grid cell that corresponds to Cartesian grid cell (respectively axes-parallel box or hyper-rectangle) $\mathring{A} \subset [0,1]^s$ via T, both potentially wrapping around the domain boundaries. If we can show that T-grid cell $\mathring{\widetilde{C}}$ with volume

$$\lambda\left(\mathring{\widetilde{C}}\right) = \left(\frac{2 \cdot (\mathring{\text{dispr}}(\widetilde{\mathcal{P}_L}) - \epsilon)}{\sqrt{s} \cdot \nu \cdot (1+\xi)} \right)^s \tag{6.70}$$

can be inscribed into said ball, $\mathring{B}(\widetilde{\underline{x}},\ \mathring{\text{dispr}}(\widetilde{\mathcal{P}_L}) - \epsilon)$, then it follows that

$$\mathring{\text{discr}}_\infty(\mathcal{P}_L) \geq \left| \frac{\#\left(\mathring{H}, \mathcal{P}_L\right)}{L} - \lambda\left(\mathring{H}\right) \right| \tag{6.71}$$

$$= \left| \frac{\#\left(\mathring{\widetilde{C}}, \widetilde{\mathcal{P}_L}\right)}{L} - \lambda\left(\mathring{\widetilde{C}}\right) \right| \tag{6.72}$$

$$= \lambda\left(\mathring{\widetilde{C}}\right) \tag{6.73}$$

$$= \left(\frac{2 \cdot (\mathring{\text{disp}}(\widetilde{\mathcal{P}_L}) - \epsilon)}{\sqrt{s} \cdot \nu \cdot (1+\xi)}\right)^s \ , \tag{6.74}$$

which, for $\epsilon \to 0_+$, implies (6.68).

Therefore, it remains to be shown that if $\mathring{\widetilde{C}}$ is inscribed into $\mathring{B}$, i) ν is a constant depending on the properties of T and ii) for T orthogonal, $\nu = 1$ and iii) ξ approaches zero for large L.

First, we note that an asymptotically dense point set $\mathcal{P}_L$, mapped by transformation T, yields another asymptotically dense point set $\widetilde{\mathcal{P}_L}$ if T is diffeomorphic and has a non-zero functional determinant. This holds especially for our equiareal T with unit functional determinant. Therefore, for every $\xi_1 > 0$ there is an L such that $\mathring{\text{disp}}(\widetilde{\mathcal{P}_L}) \leq \xi_1$, i.e., the remaining balls not covering any points

$$\mathring{B}(\underline{\widetilde{x}},\ \mathring{\text{disp}}(\widetilde{\mathcal{P}_L}) - \epsilon) \ , \quad \epsilon > 0 \ ,$$

all have a radius smaller than or equal to ξ_1.

Second, if T was linear, $\mathring{\widetilde{C}}$ would be a periodic parallelepiped. We define a parallelepiped $\mathring{\widetilde{C}}^{\text{p}}$ inscribed into $\mathring{B}$ and approximating $\mathring{\widetilde{C}}$ by taking the columns of the Jacobian $\mathbf{J}_T(\underline{x})$ of T as basis vectors of the parallepiped

$$\widetilde{C}^{\text{p}} = \{\mathbf{J}_T(\underline{x}) \cdot \underline{u} + \underline{\widetilde{x}} \mid \underline{u} \in [-\underline{\alpha}, \underline{\alpha}]\} \ , \tag{6.75}$$

where $\underline{\alpha}$ is chosen such that $\lambda\left(\widetilde{C}^{\text{p}}\right)$ is maximized while $\mathring{\widetilde{C}}^{\text{p}} \subset \mathring{B}(\underline{\widetilde{x}}, \xi_1)$.

Since T is differentiable, for every ξ_2 and every set function $h(\cdot)$ there is a ξ_1 such that

$$h\left(\mathring{\widetilde{C}}\right) \overset{\cdot(1\pm\xi_2)}{=\!=} h\left(\mathring{\widetilde{C}}^{\text{p}}\right) \ , \tag{6.76}$$

$$\mathring{\widetilde{C}}^{\text{p}} \subset \mathring{B}(\underline{\widetilde{x}}, \xi_1) \ , \quad \mathring{\widetilde{C}} \subset \mathring{B}(\underline{\widetilde{x}}, \xi_1) \ . \tag{6.77}$$

The volume ratio between largest cube and largest parallelepiped inscribed into a ball can be represented by the factor ν^s. It is determined by the angles between the basis vectors of the parallelpiped, in our case the columns of $\mathbf{J}(\cdot)$, as defined by T. If T is orthogonal, the resulting parallelepipeds are rotated boxes, and the largest of these inscribed into a ball is a rotated cube, therefore $\nu = 1$. Note that for this rotated cubic T-grid cell $\mathring{\widetilde{C}}^{\mathrm{p}}$, the corresponding Cartesian grid cell $\mathring{C}$ is not necessarily cubic but a rectangular, axes-parallel box, and therefore, still part of the set of shapes considered in the discrepancy measure.

□

Intuitively, in regions where equiareal and orthogonal T has low curvature inside the individual circumspheres of the Delaunay simplices, any low-discrepancy (and thereby also low-dispersion) point set stays low-dispersion after being propagated through T (see Figures 6.3 and 6.6a).

6.7 Low-Dispersion Sampling with Transformed Low-Discrepancy Point Sets

Now, we have all the tools for low-dispersion sampling of various non-uniform densities using low-discrepancy sequences and suitable mappings.

Theorem 6.20. *Let T be an orthogonal, diffeomorphic coordinate transformation*

$$T\colon \mathbb{R}^s \to M \tag{6.78}$$

$$T(\underline{x}) \to \underline{v} \tag{6.79}$$

defining a "skeleton grid", and $f(\cdot)$ a continuous density function that is product-type in the coordinates defined by T,

$$\begin{aligned} f_x(\underline{x}) &= f_x(T^{-1}(\underline{v})) && (6.80)\\ &= f_v(\underline{v}) && (6.81)\\ &= f_{v,1}(v_1) \cdot f_{v,2}(v_2) \cdots f_{v,s}(v_s)\ . && (6.82) \end{aligned}$$

Then, samples $\mathcal{P}_L^f \sim f(\cdot)$ can be obtained via inverse transform sampling from asymptotically dense uniform samples $\mathcal{P}_L^{\mathrm{u}}$ using the quantile function (6.40)

$$\underline{v} = Q_v(\underline{p}) = \begin{bmatrix} F_{v,1}^{-1}(p_1) & F_{v,2}^{-1}(p_2) & \cdots & F_{v,s}^{-1}(p_s) \end{bmatrix}^\top \ . \tag{6.83}$$

The final samples are usually required in Cartesian coordinates, so they are additionally transformed via T

$$\mathcal{P}_L^f = T(Q_v(\mathcal{P}_L^{\mathrm{u}})) \ .$$

If the uniform samples $\mathcal{P}_L^{\mathrm{u}}$ are low-discrepancy and their number L is sufficiently large, then the resulting samples $\mathcal{P}_L^f$ are low-dispersion with respect to $f(\cdot)$.

More precisely, for every $\xi > 0$, there is an L such that

$$\mathring{\mathrm{disp}}\mathrm{r}(T(\mathcal{P}_L); f) \leq \frac{1}{2} \cdot \sqrt{s} \cdot \left[\mathring{\mathrm{discr}}_\infty(\mathcal{P}_L)\right]^{1/s} \cdot (1+\xi) \ . \tag{6.84}$$

We apply the transformation described in Section 6.4 – only in orthogonal curvilinear coordinates $T(\cdot)$ instead of the Cartesian coordinates.

In practice, this works well not only if the map T is diffeomorphic *and* the number of samples L is high, but also i) if T contains a singularity but L is high, or ii) if L is medium but T is diffeomorphic. Only cases of small L (or medium L combined with singularities) seem to lead to significant losses in dispersion.

Example 6.21 (SND in $s = 2$)**.** The SND is separable both in Cartesian and polar coordinates. In Cartesian coordinates, we have the separable density function

$$f_{x,y}(x,y) = \frac{1}{2\pi} \cdot \exp\left\{-\frac{1}{2} \cdot x^2\right\} \cdot \exp\left\{-\frac{1}{2} \cdot y^2\right\} \tag{6.85}$$

and therefore, the separable cumulative distribution function

$$F_{x,y}(x,y) = \underbrace{\frac{1}{2}\left(1 + \mathrm{erf}\left(\frac{x}{\sqrt{2}}\right)\right)}_{F_x(x)} \cdot \underbrace{\frac{1}{2}\left(1 + \mathrm{erf}\left(\frac{y}{\sqrt{2}}\right)\right)}_{F_y(y)} \ , \tag{6.86}$$

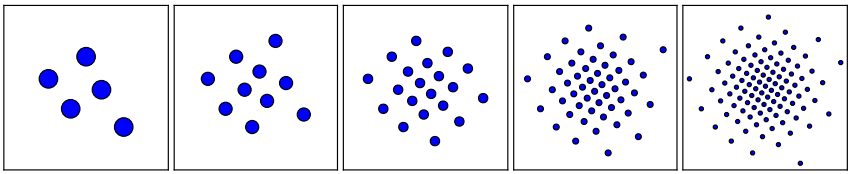

(a) Cartesian / Inverse Transform

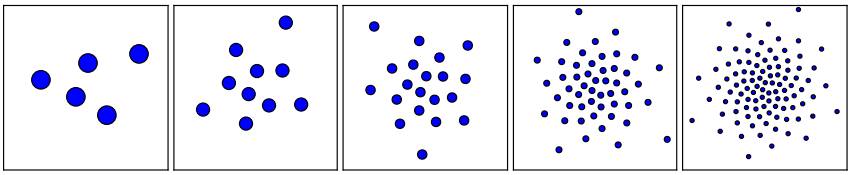

(b) Polar / Box-Muller

Figure 6.7: Orthogonal inverse transform sampling of SND with Fibonacci–Kronecker lattice. Inverse transform via Cartesian map (6.87) (a) and polar map (6.91) (b), respectively. Number of samples $L \in \{5, 10, 20, 50, 100\}$.

which leads to the quantile function

$$Q_{x,y}(p_1, p_2) = \begin{bmatrix} \sqrt{2} \cdot \mathrm{erf}^{-1}(2 \cdot p_1 - 1) \\ \sqrt{2} \cdot \mathrm{erf}^{-1}(2 \cdot p_2 - 1) \end{bmatrix} = \begin{bmatrix} x \\ y \end{bmatrix} \quad , \tag{6.87}$$

where $\mathrm{erf}^{-1}(\cdot)$ is the inverse Gauss error function.

In polar coordinates, the same density function depends only on r and not on φ due to symmetry

$$f_{r,\varphi}(r, \varphi) = \frac{1}{2\pi} \cdot \exp\left\{ -\frac{1}{2} \cdot r^2 \right\} \quad . \tag{6.88}$$

We obtain the cumulative distribution function

$$F_{r,\varphi}(r, \varphi) = \underbrace{\left(1 - \exp\left\{ -\frac{1}{2} \cdot r^2 \right\} \right)}_{F_r(r)} \cdot \underbrace{\frac{\varphi}{2\pi}}_{F_\varphi(\varphi)} \quad , \tag{6.89}$$

which leads to the quantile function

$$Q_{r,\varphi}(p_1, p_2) = \begin{bmatrix} \sqrt{-2 \cdot \log(1 - p_1)} \\ 2\pi \cdot p_2 \end{bmatrix} = \begin{bmatrix} r \\ \varphi \end{bmatrix} \quad , \tag{6.90}$$

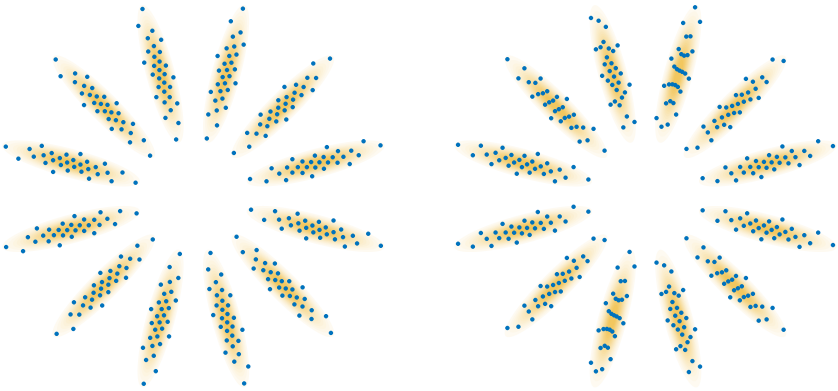

(a) Eigendecomposition **(b)** Cholesky Decomposition

Figure 6.8: Gaussian density, obtained by transforming uniform low-discrepancy point sets, as described in Example 6.22. The eigendecomposition-based transformation is orthogonal; therefore, the resulting samples have low dispersion (a). With the Cholesky decomposition, the low dispersion property can get lost (b).

or, stated in Cartesian coordinates, with mapping $T \circ Q_{r,\varphi}$,

$$Q^{x,y}_{r,\varphi}(p_1, p_2) = \begin{bmatrix} \sqrt{-2 \cdot \log(1-p_1)} \cdot \cos(2\pi \cdot p_2) \\ \sqrt{-2 \cdot \log(1-p_1)} \cdot \sin(2\pi \cdot p_2) \end{bmatrix} = \begin{bmatrix} x \\ y \end{bmatrix} \quad , \tag{6.91}$$

which is essentially the well-known Box-Muller method [12].

With (6.87) and (6.91), we now have two transformations that map from uniform to SND. Both are orthogonal, and one of them has a singularity. We can see that the singularity-free Cartesian version generally leads to a more locally homogeneous arrangement (see Figure 6.7). A similar comparison between inverse transform and Box-Muller SND sampling has been performed in [137].

Example 6.22 (Arbitrary Gaussian Density)**.** The SND sampling method from Example 6.21 with the Cartesian skeleton grid can be adapted to produce low-dispersion samples of arbitrary Gaussian densities. According to Section 6.4, the samples can be rescaled along the Cartesian coordinate axes, yielding non-standard but axes-parallel Gaussian densities. This

can be done by multiplication with a diagonal matrix $\sqrt{\mathbf{D}}$. With an additional rotation, Section 6.6.3, arbitrarily rotated Gaussian densities can be achieved. The required scaling factors $\sqrt{\mathbf{D}}$ and transformation matrix $\mathbf{V}$ are obtained from an eigendecomposition of the desired covariance $\mathbf{C} = \mathbf{V} \cdot \mathbf{D} \cdot \mathbf{V}^\top$. In total, we have

$$\mathcal{P}_L^{\mathrm{u}} \;\to\; Q_{x,y}(\underline{x}) \;\to\; \sqrt{\mathbf{D}} \cdot \underline{x} \;\to\; \mathbf{V} \cdot \underline{x} \;\to\; \underline{x} + \underline{\mu} \;\to\; \mathcal{P}_L^{f} \;. \tag{6.92}$$

Gaussian sampling with low-discrepancy point sets is already known [52], [141], [15, Sec. 3.2]

$$\mathcal{P}_L^{\mathrm{u}} \;\to\; Q_{x,y}(\underline{x}) \;\to\; \mathbf{L} \cdot \underline{x} \;\to\; \underline{x} + \underline{\mu} \;\to\; \mathcal{P}_L^{f} \;, \tag{6.93}$$

but with Cholesky decomposition $\mathbf{C} = \mathbf{L} \cdot \mathbf{L}^\top$ instead of eigenvalue decomposition. Other than the proposed transformation using eigendecomposition, the Cholesky-based transformation is not orthogonal, yielding skew coordinates, and the samples, therefore, lose their low dispersion (see Figure 6.8).

Example 6.23 (Polar and Cartesian Low-Discrepancy and Mappings)**.** We subject a point set that is low-discrepancy in Cartesian coordinates to transformations that affect only i) the horizontal axis, ii) the radial axis, and iii) the angular axis (see Figure 6.9 SC). We find that only the horizontal coordinate mapping preserves the local homogeneity, i.e., the low-dispersion property (with respect to the imprinted density). Conversely, a non-Cartesian, polar low-discrepancy point set preserves its low dispersion not during the mapping of the horizontal coordinate but instead during a mapping of the radial or angular coordinate (see Figure 6.9 SP).

In [140, p. 2+6+22+27], the concept of transforming Fibonacci grids with orthogonal transformations using orthogonal skeleton grids has been introduced and demonstrated with visual examples but not formally elaborated in detail. The intuitive idea of transforming low-discrepancy point sets to polar coordinates is shown in [154, Figure 7]. In [35, p. 162], several possible factorizations for Gaussian inverse transform, including Cholesky and principal components factorization, are mentioned.

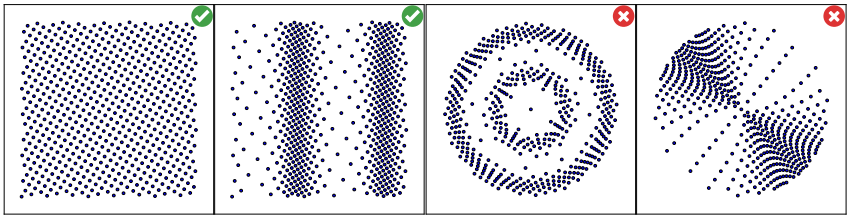

(SC) Samples, Cartesian reference grid.

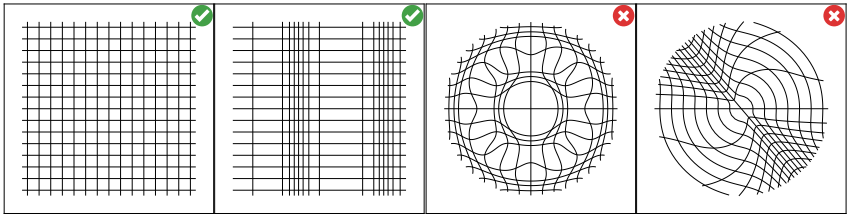

(MC) Mappings, Cartesian reference grid.

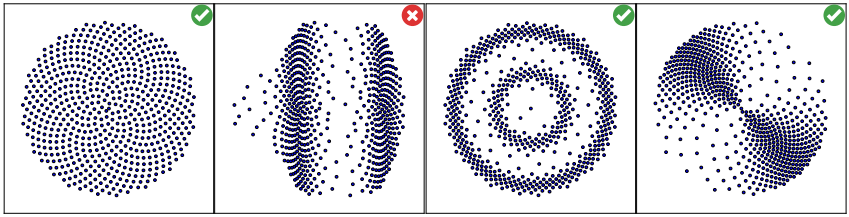

(SP) Samples, polar reference grid.

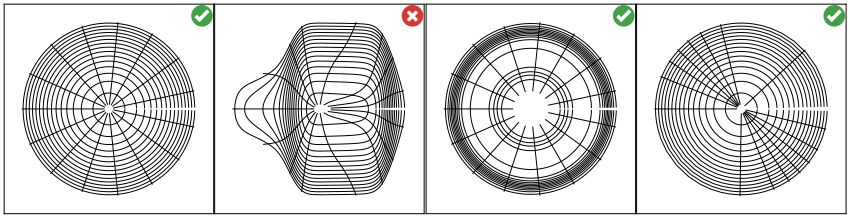

(MP) Mappings, polar reference grid.

Figure 6.9: Cartesian low-discrepancy point set (SC) and non-Cartesian polar low-discrepancy point set (SP) (first column), being transformed along the horizontal axis (second column), the radial axis (third column), and the angular axis (fourth column), respectively. Mappings shown in (MC) and (MP). Low-dispersion samples and orthogonal mappings are indicated with green check marks.

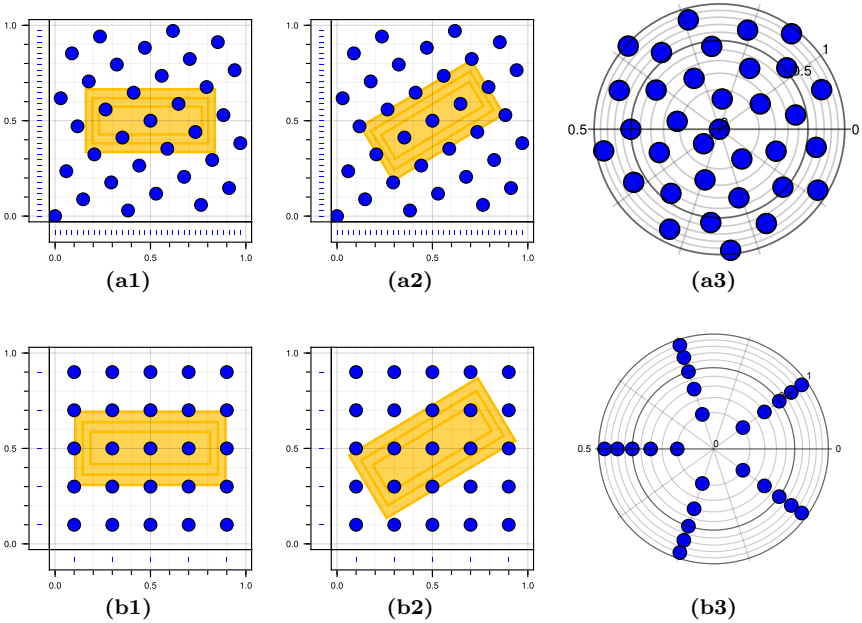

Figure 6.10: Fibonacci–rank-1 lattice (first row) and regular lattice (second row) used for numerical integration of rectangular indicator function (yellow). In (a1) and (b2), integration has high accuracy as all three rectangles give different point counts, in (a2) and (b1) not. Last column shows points after equiareal polar coordinate mapping.

6.8 Transformations of the Integrand

So far, we have looked into the generation and transformation of samples. However, for the accuracy of cubature results, the nature of the integrand is important as well. Suitable transformation of the integrand can contribute to further improvement.

6.8.1 Types of Integrands

One of the virtues of low-discrepancy point sets over low-dispersion point sets is that nearly all samples have unique $x, y, z, \ldots$ coordinates, respectively, compare marginals in Figure 6.10 (a1+b1).

Example 6.24 (Fibonacci Better than Regular)**.** Let integrand $g(\cdot)$ be product-type, $g(x, y) = g_1(x) \cdot g_2(y)$, for example a rectangular indicator function. Clearly, the Fibonacci lattice, Figure 6.10 a1, gives much better integration accuracy than the regular lattice, Figure 6.10 b1.

Proof. The integral of product-type functions can be split into scalar integrals

$$\int g(x, y)\,\mathrm{d}x\,\mathrm{d}y = \left(\int g_1(x)\,\mathrm{d}x\right) \cdot \left(\int g_2(y)\,\mathrm{d}y\right) \ ,$$

therefore, the result is best if each of the abscissa's marginals has unique and equidistant coordinates. □

Of course, cubature of product-type functions can also be done separately in the respective lower-dimensional spaces. Still, the merits of low-discrepancy point sets for cubature extend to many integrands that are not exactly product-type.

However, one can find other examples where Fibonacci and regular lattice give comparable results, or the Fibonacci lattice even giving worse results than the regular lattice.

Example 6.25 (Fibonacci Comparable to Regular)**.** Imagine an integrand that is rotationally symmetric around $[1/2, 1/2]^\top$ in Figure 6.10 (a1+b1), instead of the yellow rectangle. Obviously, both point sets, the Fibonacci lattice and the regular lattice, would be equally well suited for integration, as they are rotated versions of each other. The ideal point set for this integrand would be the Fibonacci lattice with equiareal polar coordinate mapping, Figure 6.10 a3, where all samples have unique radii. This has also been found in a comparison of Gaussian inverse transform sampling and Box-Muller sampling with low-discrepancy sequences, respectively [129].

Example 6.26 (Fibonacci Worse than Regular)**.** A rectangular integrand that is separable into the 30° and −60° axes would flip the outcomes of Fibonacci lattice and regular lattice, respectively, Figure 6.10 (a2+b2), compared to the axes-parallel rectangular integrand from Example 6.24.

Thus, in technical applications where certain sets of coordinates represent, for example, the physical $\mathbb{R}^2$ or $\mathbb{R}^3$ space with no preferred basis vectors, it does not appear to be clear at all why low-discrepancy should be preferred over low-dispersion samples. Perhaps the Fibonacci lattice is also over adapted to the quality measure "discrepancy" that is heavily based on axes-parallel rectangles, Section 5.1.1.

6.8.2 Proposal Density

In addition to minimizing the discrepancy $\mathrm{discr}^*_\infty(\mathcal{P}_L)$ in (5.7), one can also minimize the variation $V(g)$ of the integrand $g(\cdot)$ by using a **proposal density** $p(\cdot)$. Analogous to the equivalence

$$\int_{[0,1]^s} g(\underline{x})\,\mathrm{d}\underline{x} = \int_{[0,1]^s} \frac{g(\underline{x})}{p(\underline{x})} \cdot p(\underline{x})\,\mathrm{d}\underline{x} \ , \tag{6.94}$$

$p(\underline{x}) > 0$, we modify the cubature formula from using uniform samples $\mathcal{P}_L$ to proposal samples $\widetilde{\mathcal{P}_L} \sim p(\cdot)$

$$\frac{1}{L}\sum_{\underline{x}\in\mathcal{P}_L}^{L} g(\underline{x}) \ \ \to \ \ \frac{1}{L}\sum_{\underline{x}\in\widetilde{\mathcal{P}_L}}^{L} \widetilde{g}(\underline{x}) \ , \tag{6.95}$$

with $\widetilde{g}(\underline{x}) = \frac{g(\underline{x})}{p(\underline{x})}$. This is also called **importance sampling** [35, p. 160]. The Koksma-Hlawka equation for importance sampling is [3, Cor. 1]

$$\left|\frac{1}{L}\sum_{\underline{x}\in\mathcal{P}_L}^{L} \frac{g(\underline{x})}{p(\underline{x})} - \int_{[0,1]^s} g(\underline{x})\,\mathrm{d}\underline{x}\right| \le \mathrm{discr}^*_\infty(\mathcal{P}_L; p) \cdot V\left(\frac{g(\underline{x})}{p(\underline{x})}\right) \ . \tag{6.96}$$

If the proposal $p(\cdot)$ is well chosen, then $\frac{g(\underline{x})}{p(\underline{x})}$ can have a much lower variation than $g(\underline{x})$. Thereby, the samples $\mathcal{P}_L$ must be low discrepancy with respect to $p(\cdot)$ instead of uniform in order to minimize the factor $\mathrm{discr}^*_\infty(\mathcal{P}_L; p)$.

6.8.3 Proposal Mapping

Similar to importance sampling (where some of the variability of the integrand is packed into the proposal density and then transferred over to the density function used for sampling the abscissa, Section 6.8.2), it can therefore be advantageous to write the integrand $g(\cdot)$ as two concatenated functions and use the inner one for a coordinate transform $p(\cdot)$ ("proposal mapping") of the abscissa. In particular, it always holds

$$\int_{\underline{x}\in M} g(\underline{x})\,\mathrm{d}\underline{x} = \int_{\underline{x}\in p^{-1}(M)} g(p(\underline{x}))\,\mathrm{d}\underline{x}\ , \tag{6.97}$$

with $p(\cdot)$ being an equiareal map. With this, we replace the quasi-Monte Carlo approximation with a proposal-mapped version

$$\frac{1}{L}\sum_{\underline{x}\in\mathcal{P}_L} g(\underline{x}) \ \rightarrow\ \frac{1}{L}\sum_{\underline{x}\in\mathcal{P}_L} \widetilde{g}(\underline{x}) \ =\ \frac{1}{L}\sum_{\underline{x}\in\widetilde{\mathcal{P}_L}} g(\underline{x})\ , \tag{6.98}$$

either using the **proposal-mapped integrand** $\widetilde{g} = g\circ p$, or, equivalently, the **proposal-mapped samples** $\widetilde{\mathcal{P}_L} = p(\mathcal{P}_L)$, with equiareal $p(\cdot)$. It must thereby however be ensured that the support of $g(\cdot)$ does not exceed $(M\cap p(M))$.

6.8.3.A (Rotation) Take the rotated rectangle integrand $g(\cdot)$ from Figure 6.10 a2 and compute its covariance $\mathbf{C}$. The eigenvector matrix $\mathbf{V}$ of the eigendecomposition of the covariance $\mathbf{C} = \mathbf{V}\cdot\mathbf{D}\cdot\mathbf{V}^\top$ describes the orientation of the rectangle. The proposal mapping

$$p(\underline{x}) = \mathbf{V}\cdot\underline{x}\ ,$$

a rigid map, can then be used to generate i) the axes-parallel proposal-mapped integrand $\widetilde{g} = g\circ p$, as shown in Figure 6.10 a1, or equivalently, the proposal-mapped samples $\widetilde{x}_i = p(\underline{x}_i)$ (see Figure 6.10 b2). An additional translation may be necessary to ensure the integrand's support is covered with samples. Determining the covariance in $s = 2$ entails five numerical integrals similar to the one we actually want to solve: C_{xx}, C_{xy}, C_{yy}, the

mean, and the normalization factor. The latter is precisely the integral we want to solve, and at this stage, we evaluate it rather imprecisely to get a more accurate result later. Therefore, the computational load increases from $\mathcal{O}(L)$ to $\mathcal{O}(6L) = \mathcal{O}(L)$, i.e., just the constant factor changes, so for L large enough we will benefit from the superior convergence rate that low-discrepancy abscissas in conjunction with axes-parallel integrands provide.

6.8.3.B (Linear Mapping) For the absolute integrand, $|g(\cdot)|$, determine the integral

$$I = \int_{[0,1]^s} |g(\underline{x})| \, \mathrm{d}\underline{x} \ , \tag{6.99}$$

the mean vector

$$\underline{m} = \frac{1}{I} \int_{[0,1]^s} \underline{x} \cdot |g(\underline{x})| \, \mathrm{d}\underline{x} \ , \tag{6.100}$$

and the covariance $\mathbf{C}$ and its eigendecomposition

$$\mathbf{C} = \frac{1}{I} \int_{[0,1]^s} (\underline{x} - \underline{m}) \cdot (\underline{x} - \underline{m})^\top \cdot |g(\underline{x})| \, \mathrm{d}\underline{x} \tag{6.101}$$

$$= \mathbf{V} \cdot \mathbf{D} \cdot \mathbf{V}^\top \tag{6.102}$$

as a rough approximation without proposal mapping. Then, with the proposal mapping

$$p_\gamma(\underline{x}) = \gamma \cdot \mathbf{V} \cdot \left(\sqrt{\mathbf{D}} \cdot \left(\underline{x} - \frac{1}{2} \cdot \underline{1} \right) + \underline{m} \right) \ , \tag{6.103}$$

transform the standard cubature formula (with associated abscissa $\mathcal{P}_L$)

$$I(g) = \int_{[0,1]^s} g(\underline{x}) \, \mathrm{d}\underline{x} \approx \frac{1}{L} \cdot \sum_{\underline{x} \in \mathcal{P}_L} g(\underline{x}) \tag{6.104}$$

into the faster converging form

$$I(g) = \frac{1}{\gamma \cdot \sqrt{|\mathbf{D}|}} \int_{p_\gamma^{-1}([0,1]^s)} g(p_\gamma(\underline{x}))\,\mathrm{d}x \tag{6.105}$$

$$\approx \frac{1}{\gamma \cdot \sqrt{|\mathbf{D}|}} \cdot \frac{1}{L} \cdot \sum_{\underline{x} \in \mathcal{P}_L} g(p_\gamma(\underline{x})) \tag{6.106}$$

$$= \frac{1}{\gamma \cdot \sqrt{|\mathbf{D}|}} \cdot \frac{1}{L} \cdot \sum_{\underline{x} \in p_\gamma(\mathcal{P}_L)} g(\underline{x}) \quad . \tag{6.107}$$

Thereby, γ is a safety factor ensuring the relevant support of $g(\cdot)$ being covered with samples. The support of $g(\cdot)$ must be limited to $[0,1]^s$. The entire process can be repeated iteratively.

This is analogous to the whitening process applied in signal processing, here achieved with its inverse formula. A similar transform to improve quasi-Monte Carlo integration is discussed in [99, p. 255].

6.8.3.C (Polar Coordinates) Imagine an integrand whose most variability is separable into an angular and a radial component, e.g., radially symmetric integrands. In this case, an equiareal polar coordinate transform would be a suitable proposal mapping

$$p_\gamma(\underline{x}) = \frac{\gamma}{2\pi} \begin{bmatrix} \sqrt{x_1} \cdot \cos(2\pi \cdot x_2) \\ \sqrt{x_1} \cdot \sin(2\pi \cdot x_2) \end{bmatrix} \quad . \tag{6.108}$$

See Figure 6.10 a3 for proposal-mapped samples $p(\mathcal{P}_L)$ for rank-1 Fibonacci lattice points $\mathcal{P}_L$. They exhibit unique angular and polar coordinates, respectively.

This is the uniform variant of the Box-Muller transform for the SND. The superiority of Box-Muller transformed low-discrepancy samples (over inverse transform samples) for radially symmetric integrands has also been demonstrated in [129].

6.9 Summary

At the beginning of this chapter, we extended the definitions of discrepancy and dispersion from uniform to non-uniform point sets. Similarly, we extended the inequality quantifying the relation between discrepancy and dispersion from uniform to non-uniform and to transformed point sets. The outcome was a low-dispersion sampling method via orthogonal inverse transforms of low-discrepancy samples. Finally, we turned our attention from the samples to the integrand, examining its effects on the integral accuracy and proposing quality-improving transformations of the integrand.

CHAPTER 7

Orthogonal Inverse Transform Sampling

Contents

> The question of how a suitable skeleton system can be constructed to provide the intended resolution enhancements is one that deserves a separate technical discussion and is not further considered here.
>
> *Generalized Fibonacci Grids, Office Note 455, 2008*
> R. James Purser

This chapter states orthogonal transformations that convert uniform reference samples in $[0,1]^s$ to various densities $f(\cdot)$. According to Theorem 6.20, the resulting point sets will be low-dispersion if the mapping is orthogonal and the uniform reference point set is low-discrepancy.

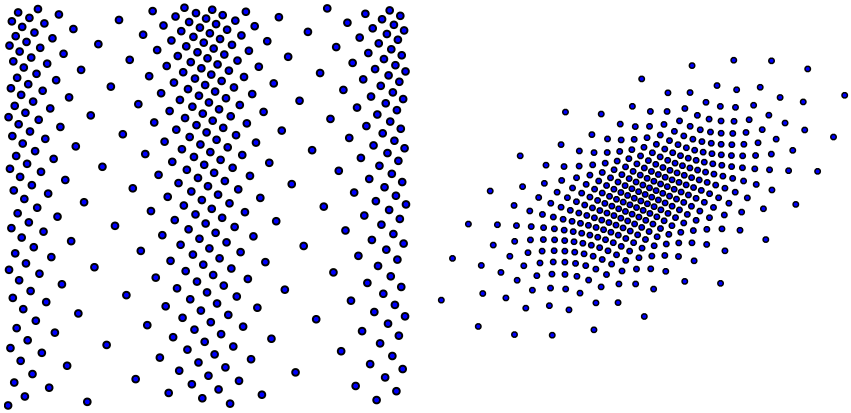

(a) Separable density (sinusoidal and exponential).

(b) Gaussian density.

Figure 7.1: Low-dispersion samples generated via orthogonal inverse transform sampling from the Fibonacci lattice.

7.1 Euclidean Space

7.1.1 Independent Densities

Product-type or separable densities representing the joint density of independent marginals in Cartesian coordinates

$$f(\underline{x}) = f_1(x_1) \cdot f_2(x_2) \cdots f_s(x_s) \ , \tag{7.1}$$

can be obtained by inverse transform sampling of their individual coordinates

$$Q(\underline{p}) = \left[F_1^{-1}(p_1) \quad F_2^{-1}(p_2) \quad \dots \quad F_s^{-1}(p_s)\right]^\top = \underline{x} \ , \tag{7.2}$$

with uniform $\underline{p}$ and $Q(\underline{\boldsymbol{p}}) \sim f_x(\underline{x})$, where F is the cumulative distribution of f. This has already been explained in Section 6.4 (see Figure 7.1 a).

Note that the inverse Rosenblatt Transformation [148], also called the conditional distribution method [18, Sec. 3.1], extends this to arbitrary

densities but does not yield an orthogonal transformation for non-separable densities [3, Sec. 5].

7.1.2 Multivariate Gaussian Density

An arbitrary Gaussian densitiy with covariance and eigendecomposition $\mathbf{C} = \mathbf{V} \cdot \mathbf{D} \cdot \mathbf{V}^\top$ and mean $\underline{\mu}$ can be obtained with the mapping

$$Q(\underline{p}) = \mathbf{V} \cdot \sqrt{\mathbf{D}} \cdot \sqrt{2} \cdot \operatorname{erf}^{-1}(2 \cdot \underline{p}) + \underline{\mu} \ , \tag{7.3}$$

with the Gauss error function

$$\operatorname{erf}(z) = \frac{2}{\sqrt{\pi}} \int_0^z \exp\{-t^2\} \, \mathrm{d}t \ , \tag{7.4}$$

here applied element-wise for vector arguments (see Figure 7.1 b).

This has already been explained in Example 6.22. For more details and various moment-matching methods, refer to [O3], [O8] and also Appendix D.

7.2 Hyperspherical Manifold

7.2.1 Cartography

Map projections have been researched for centuries as they are necessary to produce maps of the entire globe, or larger parts, on flat paper. The main characteristics of map projections are equiareal and conformal [157, p. 4]. **equiareal** means that a coin, or any other object, covers the same area no matter where it is placed on the map. This implies scale, angles, and shapes to be distorted in many parts of the map. **Conformal** maps preserve local angles exactly. Therefore, the shapes of small objects are represented accurately. Maps between sphere and plane can not be equiareal and conformal simultaneously. Conformal maps for 2D manifolds fulfill the Cauchy-Riemann differential equations.

7.2.2 Cylindrical Map Projections

We show the inverse formulas that transform some rectangular domain $\mathcal{R}$ with coordinates (u, v) to the sphere $\mathbb{S}^2 \subset \mathbb{R}^3$, with Cartesian coordinates (x, y, z). Mere linear transformations of the input and the output of the maps are neglected.

7.2.2.A (Equidistant Cylindrical Projection) The Equidistant Cylindrical Projection is one of the simplest and oldest, probably originated by Eratosthenes (c. 276 BC – c. 195/194 BC). It is neither conformal nor equiareal [157, p. 90f]. Its inverse formulas map rectangular coordinates (u, v) to the sphere $\mathbb{S}^2$

$$T\colon \mathcal{R}^2 \to \mathbb{S}^2 \ , \tag{7.5}$$

$$\begin{bmatrix} u \\ v \end{bmatrix} \mapsto \begin{bmatrix} \cos(u) \\ \sin(u) \cdot \sin(v) \\ \sin(u) \cdot \cos(v) \end{bmatrix} = \begin{bmatrix} z \\ y \\ x \end{bmatrix} \ , \tag{7.6}$$

$$\mathcal{R}^2 = [0, \pi] \times \mathbb{T} \ . \tag{7.7}$$

This is precisely the mapping defined by the standard spherical coordinate system.

7.2.2.B (Lambert Cylindrical Equiareal Projection) The Lambert Cylindrical equiareal projection is equiareal and not conformal. Its inverse formula is given by [157, p. 80], [105, Sec. IX]

$$T\colon \mathcal{R}^2 \to \mathbb{S}^2 \ , \tag{7.8}$$

$$\begin{bmatrix} u \\ v \end{bmatrix} \mapsto \begin{bmatrix} \sqrt{1 - u^2} \\ u \cdot \sin(v) \\ u \cdot \cos(v) \end{bmatrix} = \begin{bmatrix} z \\ y \\ x \end{bmatrix} \ , \tag{7.9}$$

$$\mathcal{R}^2 = [-1, 1] \times \mathbb{T} \ . \tag{7.10}$$

Due to the equiareal property, the Lambert Cylindrical equiareal projection can be directly used to transform uniform samples in $\mathcal{R}^2$ into uniform samples in $\mathbb{S}^2$.

7.2.2.C (Mercator Projection) The first map projection that was regularly identified on maps is the Mercator projection [157, p. 38ff]. It is conformal. Inverse formulas in Cartesian coordinates are given by

$$T\colon \mathcal{R}^2 \to \mathbb{S}^2 \ , \tag{7.11}$$

$$\begin{bmatrix} u \\ v \end{bmatrix} \mapsto \begin{bmatrix} \operatorname{sech}(u) \\ \tanh(u) \cdot \sin(v) \\ \tanh(u) \cdot \cos(v) \end{bmatrix} = \begin{bmatrix} z \\ y \\ x \end{bmatrix} \ , \tag{7.12}$$

$$\mathcal{R}^2 = \mathbb{T} \times \mathbb{R} \ . \tag{7.13}$$

The rectangular domain $\mathcal{R}^2$ has infinite size, so the Mercator projection can not project samples from the unit square $[0,1]^2$ to the sphere.

7.2.2.D (Summary) We note that, in all cylindrical map projections, i) the inverse formula is separable in u and v, ii) for constant u and variable v, concentric circles are formed, called "parallels", and iii) for constant v and variable u, arcs between the two poles are formed, called "meridians". A suitable nonlinear rescaling is applied to u, depending on the respective goal to achieve (equidistant, equiareal, or conformal). We will see that we can find another nonlinear rescaling that produces the von Mises–Fisher (vMF) density function on $\mathbb{S}^2$ using uniform samples on $\mathcal{R}^2$.

In other words, the cylindrical map projections are based on two families of differential curves, particularly parallels and meridians. The natural parameterization of these curves gives the Equidistant Cylindrical Projection. The Lambert Cylindrical equiareal and Mercator projections are essentially just other parameterizations of these curves. With suitable parameterizations, we can transform uniform samples on rectangular domains $\mathcal{R}^2$ to represent densities on $\mathbb{S}^2$ – if they are separable into parallels and meridians, i.e., where the density function is independent in the orthogonal coordinate system spanned by parallels and meridians. Examples are the uniform density and the vMF density.

7.2.3 Hyperspherical Coordinate System

The most widely used hyperspherical coordinate system is a generalization of the equidistant cylindrical projection. The transformation is

$$\zeta^{(s)} \colon \mathcal{R}^s_{\mathrm{SC}} \to \mathbb{S}^s \subset \mathbb{R}^{s+1} \tag{7.14}$$

$$\zeta^{(s)} \colon \underline{\varphi} = \begin{bmatrix} \varphi_1 \\ \varphi_2 \\ \vdots \\ \varphi_s \end{bmatrix} \to \begin{bmatrix} \cos(\varphi_1) \\ \sin(\varphi_1)\cos(\varphi_2) \\ \sin(\varphi_1)\sin(\varphi_2)\cos(\varphi_3) \\ \quad\vdots \\ \sin(\varphi_1)\sin(\varphi_2)\cdots\sin(\varphi_{s-1})\cos(\varphi_s) \\ \sin(\varphi_1)\sin(\varphi_2)\cdots\sin(\varphi_{s-1})\sin(\varphi_s) \end{bmatrix} , \tag{7.15}$$

where the domain $\mathcal{R}^s_{\mathrm{SC}}$ of the angular coordinates $\underline{\varphi}$ is

$$\mathcal{R}^s_{\mathrm{SC}} = [0,\pi]^{s-1} \times \mathbb{T} \ .$$

Volume element of this hyperspherical coordinate system is

$$\mathrm{d}V = \prod_{t=1}^{s} \left(\sin^{s-t}(\varphi_t)\,\mathrm{d}\varphi_t\right) \tag{7.16}$$

$$= \sin^{s-1}(\varphi_1)\sin^{s-2}(\varphi_2)\cdots\sin(\varphi_{s-1})\,\mathrm{d}\varphi_1\,\mathrm{d}\varphi_2\cdots\mathrm{d}\varphi_s \ . \tag{7.17}$$

Volume of the entire hypersphere surface is

$$\lambda(\mathbb{S}^s) = \frac{2\cdot\pi^{\frac{s+1}{2}}}{\Gamma\left(\frac{s+1}{2}\right)} \ , \tag{7.18}$$

where Γ is the Euler gamma function [1, pp. 255–258].

7.2.4 Uniform Distribution

The hyperspherical coordinate system (7.15) is an orthogonal transform. A suitable rescaling of the individual coordinates provides an equiareal mapping between unit hypercube and unit hypersphere. The uniform density on the hypersphere $\mathbb{S}^s \subset \mathbb{R}^{s+1}$

$$f^{(s)}(\underline{\varphi}) = \frac{1}{\lambda(\mathbb{S}^s)} \tag{7.19}$$

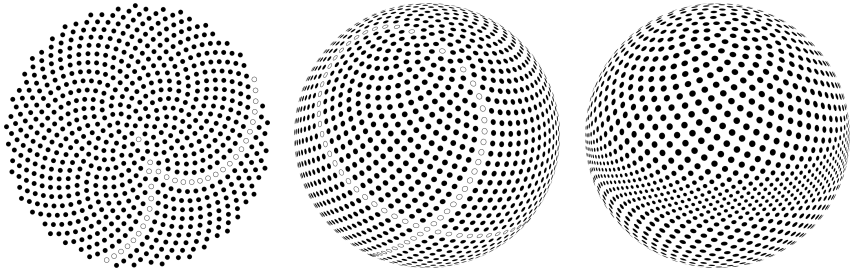

(a) Planar polar Fibonacci grid.

(b) Spherical uniform Fibonacci grid.

(c) Spherical non-uniform Fibonacci grid.

Figure 7.2: State of art regarding the mapping of low-discrepancy point sets to Riemannian manifolds. Taken from [167].

is, of course, separable. We obtain the separable cumulative distribution

$$F^{(s)}(\underline{\varphi}) = \int_{\underline{u}=\underline{0}}^{\underline{\varphi}} f^{(s)}(\underline{\varphi}) \,\mathrm{d}V \tag{7.20}$$

$$= \int_{\underline{u}=\underline{0}}^{\underline{\varphi}} \frac{1}{\lambda(\mathbb{S}^s)} \prod_{t=1}^{s} \left(\sin^{s-t}(u_t) \,\mathrm{d}u_t\right) \tag{7.21}$$

$$= \frac{1}{\lambda(\mathbb{S}^s)} \prod_{t=1}^{s} \left(\int_{u_t=0}^{\varphi_t} \sin^{s-t}(u_t) \,\mathrm{d}u_t \right) \tag{7.22}$$

$$= \prod_{t=1}^{s} F_t^{(s)}(\varphi_t) \tag{7.23}$$

and then the separable inverse cumulative distribution or quantile function

$$Q^{(s)}(\underline{p}) = {F^{(s)}}^{-1}(\underline{p}) = \prod_{t=1}^{s} {F_t^{(s)}}^{-1}(p_t) \ . \tag{7.24}$$

Now, uniform low-discrepancy samples on $[0,1]^s$ inserted into $Q^{(s)}$ yield low-dispersion samples on $\mathbb{S}^s$ – in hyperspherical coordinates. Concatenation with (7.15) yields these samples in Cartesian coordinates.

7.2.4.A (Circle $\mathbb{S}^1$) For the circle $\mathbb{S}^1$, we obtain

$$\lambda(\mathbb{S}^1) = 2\pi \ , \tag{7.25}$$
$$\mathrm{d}V = \mathrm{d}\varphi_1 \ , \tag{7.26}$$
$$F^{(1)}(\varphi) = \frac{\varphi}{2\pi} \ , \tag{7.27}$$
$$Q^{(1)}(p) = 2\pi \cdot p \ . \tag{7.28}$$

Thereby $Q^{(1)}$ maps a 1D uniform point set from $[0,1)$ to $\mathbb{S}^1$, with the result in angular coordinates. Insertion to (7.15) yields the complete representation of the transformation T in Cartesian coordinates

$$T = \zeta^{(1)} \circ Q^{(1)} \colon [0,1] \to \mathbb{S}^1 \ , \tag{7.29}$$
$$T(p) = \begin{bmatrix} \cos(p) \\ \sin(p) \end{bmatrix} \ . \tag{7.30}$$

7.2.4.B (Sphere $\mathbb{S}^2$) For the sphere $\mathbb{S}^2$, we have sphere surface and surface element

$$\lambda\big(\mathbb{S}^2\big) = 4\pi \ , \tag{7.31}$$
$$\mathrm{d}V = \sin(\varphi_1)\,\mathrm{d}\varphi_1\,\mathrm{d}\varphi_2 \ , \tag{7.32}$$

cumulative distribution

$$F_1^{(2)}(\varphi_1) = \frac{1-\cos(\varphi_1)}{2} \ , \tag{7.33}$$
$$F_2^{(2)}(\varphi_2) = \frac{\varphi_2}{2\pi} \ , \tag{7.34}$$

and quantile function

$$Q_1^{(2)}(p_1) = \cos^{-1}(1 - 2 \cdot p_1) \tag{7.35}$$
$$Q_2^{(2)}(p_2) = 2\pi \cdot p_2 \ . \tag{7.36}$$

Back in Cartesian coordinates, this reads

$$T = \zeta^{(2)} \circ Q^{(2)} \colon [0,1]^2 \to \mathbb{S}^2 \ , \tag{7.37}$$

$$T(\underline{p}) = \begin{bmatrix} 1 - 2 \cdot p_1 \\ 2 \cdot \sqrt{p_1 \cdot (1 - p_1)} \cdot \cos(2\pi \cdot p_2) \\ 2 \cdot \sqrt{p_1 \cdot (1 - p_1)} \cdot \sin(2\pi \cdot p_2) \end{bmatrix} \ . \tag{7.38}$$

Over some operations that do not change the essence of the result (scaling, reflection, and coordinate permutation of the input samples, rigid rotation on the sphere), this is identical to the equi-areal Lambert projection (7.9). It is well known that Fibonacci lattices, mapped to the 2-sphere via the Lambert equal-area projection, yield locally homogeneous, uniform point sets [167] (see Figure 7.2b).

7.2.4.C (Hypersphere $\mathbb{S}^3$) For the hypersphere $\mathbb{S}^3$, sphere surface and surface element is

$$\lambda\big(\mathbb{S}^3\big) = 2\pi^2 \ , \tag{7.39}$$

$$\mathrm{d}V = \sin^2(\varphi_1)\sin(\varphi_2)\,\mathrm{d}\varphi_1\,\mathrm{d}\varphi_2\,\mathrm{d}\varphi_3 \ . \tag{7.40}$$

The density function is

$$f_1^{(3)}(\varphi_1) = \frac{2}{\pi}\sin^2(\varphi_1) \ , \tag{7.41}$$

$$f_2^{(3)}(\varphi_2) = \frac{1}{2}\sin(\varphi_2) \ , \tag{7.42}$$

$$f_3^{(3)}(\varphi_3) = \frac{1}{2\pi} \tag{7.43}$$

and the cumulative distribution

$$F_1^{(3)}(\varphi_1) = \frac{1}{\pi}\left(\varphi_1 - \frac{1}{2}\sin(2\,\varphi_1)\right) \ , \tag{7.44}$$

$$F_2^{(3)}(\varphi_2) = \frac{1 - \cos(\varphi_2)}{2} \ , \tag{7.45}$$

$$F_3^{(3)}(\varphi_3) = \frac{\varphi_3}{2\pi} \ . \tag{7.46}$$

Quantile functions are

$$Q_1^{(3)}(p_1) = \left\{ \varphi_1 \mid p_1 = \frac{1}{\pi}\left(\varphi_1 - \frac{1}{2}\sin(2\,\varphi_1)\right) \right\} \ , \tag{7.47}$$

$$Q_2^{(3)}(p_2) = \cos^{-1}(1 - 2 \cdot p_2) \ , \tag{7.48}$$

$$Q_3^{(3)}(p_3) = 2\pi \cdot p_3 \ , \tag{7.49}$$

where a 1D root finding method is used in Q_1 as described in 7.4.2. Back in Cartesian coordinates, this reads

$$T = \zeta^{(e)} \circ Q^{(e)} \colon [0,1]^e \to \mathbb{S}^e \ , \tag{7.50}$$

$$T(\underline{p}) = \begin{bmatrix} \cos(\varphi_1(p_1)) \\ \sin(\varphi_1(p_1)) \cdot (1 - 2 \cdot p_2) \\ \sin(\varphi_1(p_1)) \cdot 2 \cdot \sqrt{p_2 \cdot (1 - p_2)} \cdot \cos(2\pi \cdot p_3) \\ \sin(\varphi_1(p_1)) \cdot 2 \cdot \sqrt{p_2 \cdot (1 - p_2)} \cdot \sin(2\pi \cdot p_3) \end{bmatrix} \ , \tag{7.51}$$

where

$$\varphi_1(p_1) = Q_1^{(3)}(p_1) = \left\{ \varphi_1 \mid p_1 = \frac{1}{\pi}\left(\varphi_1 - \frac{1}{2}\sin(2\,\varphi_1)\right) \right\} \ . \tag{7.52}$$

7.2.4.D (Hypersphere $\mathbb{S}^s$) For $s \geq 3$, closed form solutions of the cumulative distributions $F_t^{(s)}$ do exist [178, p. 164], but not of all the quantile functions $Q_t^{(s)}$. Refer to Section 7.4 for efficient ways to compute them numerically.

7.2.5 Von Mises–Fisher Density

We have the vMF density function

$$f^{(s)}(\underline{x}) = c \cdot \exp\left\{ \kappa \cdot \underline{\mu}^\top \underline{x} \right\} \ , \tag{7.53}$$

$$\underline{x} \in \mathbb{S}^s \subset \mathbb{R}^{s+1} \tag{7.54}$$

with its normalization constant

$$c = \frac{\kappa^{\frac{s-1}{2}}}{(2\pi)^{\frac{s+1}{2}} I_{\frac{D-1}{2}}(\kappa)} \ , \tag{7.55}$$

where I_v denotes the modified Bessel function of the first kind [1, pp. 374–377] at order v. After centering to $\underline{\mu} = \underline{e}_1$ and transformation to spherical coordinates, this simplifies to

$$f^{(s)}(\underline{\varphi}) = c \cdot \exp\{\kappa \cdot \cos(\varphi_1)\} \ . \tag{7.56}$$

We get the cumulative distribution

$$F^{(s)}(\underline{\varphi}) = \int_{\underline{u}=\underline{0}}^{\underline{\varphi}} f^{(s)}(\underline{\varphi}) \, \mathrm{d}V \tag{7.57}$$

$$= \int_{\underline{u}=\underline{0}}^{\underline{\varphi}} c \cdot e^{\kappa \cdot \cos(u_1)} \cdot \prod_{t=1}^{s} \left(\sin^{s-t}(u_t) \, \mathrm{d}u_t\right) \tag{7.58}$$

$$= c \cdot \left(\int_{u_1=0}^{\varphi_1} e^{\kappa \cdot \cos(u_1)} \sin^{s-1}(u_1) \right) \cdot \prod_{t=2}^{s} \left(\int_{u_t=0}^{\varphi_t} \sin^{s-t}(u_t) \, \mathrm{d}u_t \right) \ . \tag{7.59}$$

The first marginal cumulative $F_1^{(s)}$ is

$$F_1^{(s)}(\varphi_1) = c_1 \int_{u_1=0}^{\varphi_1} e^{\kappa \cdot \cos(u_1)} \sin^{s-1}(u_1) \, \mathrm{d}u_1 \ , \tag{7.60}$$

$$c_1 = \frac{\Gamma\left(\frac{s+1}{2}\right)}{\sqrt{\pi} \cdot \Gamma\left(\frac{s}{2}\right) \cdot {}_0F_1\left(;\, \frac{s+1}{2};\, \frac{\kappa^2}{4}\right)} \ , \tag{7.61}$$

where $\Gamma(z)$ is the Euler gamma function [1, pp. 255–258], and ${}_0F_1(;\, a;\, z)$ is the confluent hypergeometric limit function [134, Chap. 3]. As described in Section 7.4, the quantile $Q_1^{(s)}$, i.e., the inverse of $F_1^{(s)}$, can, e.g., be obtained as the solution of the initial value problem

$$y' = \frac{1}{c_1 \cdot e^{\kappa \cdot \cos(y)} \cdot \sin^{s-1}(y)} \ , \tag{7.62}$$

$$y(0) = 0 \ . \tag{7.63}$$

The other marginal cumulative distributions,

$$F_t^{(s)}(\varphi_t) = c_t \cdot \int_{u_t=0}^{\varphi_t} \sin^{s-t}(u_t) \, \mathrm{d}u_t, \quad t \in \{2, 3, \ldots, s\} \ , \tag{7.64}$$

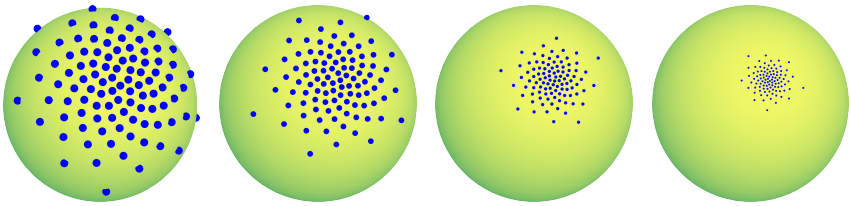

(a) $\kappa = 5$ **(b)** $\kappa = 10$ **(c)** $\kappa = 30$ **(d)** $\kappa = 80$

Figure 7.3: Sets of 100 vMF samples with different concentration parameters κ, produced by orthogonal inverse transform of a Fibonacci–Kronecker lattice.

are the same as those we have already seen for the uniform distribution (7.23).

7.2.5.A (Circle $\mathbb{S}^1$) The vMF distribution on the $\mathbb{S}^1$ circle is identical to the von Mises distribution

$$f^{(1)}(\varphi) = c \cdot e^{\kappa \cdot \cos(\varphi)} \, \mathrm{d}\varphi \ . \tag{7.65}$$

Cumulative and quantile functions are not available in closed form; therefore, one of the methods in Section 7.4 should be applied directly to $f^{(1)}$.

7.2.5.B (Sphere $\mathbb{S}^2$) For the vMF density on $\mathbb{S}^2$, we do obtain closed-form solutions for the separable cumulative distribution

$$F_1^{(2)}(\varphi_1) = \frac{1}{e^{\kappa} - e^{-\kappa}} \cdot \left(e^{\kappa} - e^{\kappa \cdot \cos(\varphi_1)} \right) \ , \tag{7.66}$$

$$F_2^{(2)}(\varphi_2) = \frac{\varphi_2}{2\pi} \ , \tag{7.67}$$

as well as the quantile function

$$Q_1^{(2)}(p) = \cos^{-1}\left(\frac{1}{\kappa} \log\left(e^{\kappa} - p \cdot \left(e^{\kappa} - e^{-\kappa} \right) \right) \right) \ , \tag{7.68}$$

$$= \cos^{-1}\left(1 + \frac{1}{\kappa} \cdot \mathrm{log1p}(p \cdot \mathrm{expm1}(-2\kappa)) \right) \ , \tag{7.69}$$

$$Q_2^{(2)}(q) = 2\pi \cdot q \ , \tag{7.70}$$

where (7.69) is a numerically more stable variant of (7.68) by using the often available functions

$$\operatorname{log1p}(x) = \log(1+x) \tag{7.71}$$

$$\operatorname{expm1}(x) = e^x - 1 \tag{7.72}$$

that avoid cancellation errors from floating point operations. Note that this result is very similar to [103, Sec. II.A] and [80, Sec. 3.2]. Thus, we obtain the complete quantile function

$$Q^{(2)} \;:\; [0,1]^2 \to \mathcal{R}^{(2)}_{\mathrm{SC}} \tag{7.73}$$

$$Q^{(2)}(\underline{p}) = \begin{bmatrix} Q^{(2)}_1(p_1) \\ Q^{(2)}_2(q_2) \end{bmatrix} \;, \tag{7.74}$$

that transforms uniform samples to vMF samples in spherical coordinates (φ_1, φ_2). Finally, with the orthogonal mapping

$$T = \zeta^{(2)} \circ Q^{(2)} \colon \mathbb{R}^2 \to \mathbb{S}^2, \tag{7.75}$$

we can turn any 2D low-discrepancy (or, trivially, random) sequence $\underline{x}^{\mathrm{u}}_i$ into vMF distributed samples $\underline{x}^{f}_i$ in Cartesian coordinates

$$\underline{x}^{f}_i = T(\underline{x}^{\mathrm{u}}_i) \;, \tag{7.76}$$

$$\underline{x}^{f}_i \sim f(\underline{x}) \;. \tag{7.77}$$

In particular, choosing the centered Fibonacci–Kronecker lattice (3.41) as the uniform reference point set, we obtain [O7]

$$\underline{x}^{f}_i = \begin{bmatrix} w \\ \sqrt{1-w^2} \cdot \cos\!\left(\frac{2\pi i}{\Phi}\right) \\ \sqrt{1-w^2} \cdot \sin\!\left(\frac{2\pi i}{\Phi}\right) \end{bmatrix} \;, \tag{7.78}$$

$$w = 1 + \frac{1}{\kappa} \cdot \operatorname{log1p}\!\left(\frac{2i-1}{2L} \cdot \operatorname{expm1}(-2\kappa) \right) \;, \tag{7.79}$$

$$i \in \{1, 2, \ldots, L\} \;. \tag{7.80}$$

See Figure 7.3 for a visualization. Note that this inverse transform is orthogonal but has a singularity which, for small L, deteriorates the dispersion near it, see Section 6.7.

The possibility mapping Fibonacci lattices to non-uniform spherical densities, yielding locally homogeneous point sets, has been recognized before [167] (see Figure 7.2 c).

7.3 Acceptance-Rejection Sampling

Acceptance-rejection sampling is a widely used technique to generate random samples from probability distributions that are difficult to sample directly. The basic idea behind it is to generate random samples from a simpler, known distribution (referred to as the "proposal" or "envelope" distribution) and then accept or reject these samples based on their relationship to the target distribution. If the rejection operation is done deterministically and not probabilistically as usual, it is an orthogonal mapping, however with a discontinuity at the boundary region between acceptance and rejection. Furthermore, one dimension of the reference grid is collapsed, which leads to some deterioration of the discrepancy and disparity.

Suppose $f(\underline{x})$ is a complicated density difficult to sample from. However, there is a proposal density $f_{\mathrm{pp}}(\underline{x})$ that we can easily draw samples from, e.g., uniform or Gaussian, and positive constant c such that

$$f(\underline{x}) \leq c \cdot f_{\mathrm{pp}}(\underline{x}) \; \forall \underline{x} \quad . \tag{7.81}$$

We then draw proposal samples $\underline{x}_{\mathrm{pp}} \sim f_{\mathrm{pp}}(\underline{x})$ and accept them with probability

$$P_a = \frac{f(\underline{x}_{\mathrm{pp}})}{c \cdot f_{\mathrm{pp}}(\underline{x}_{\mathrm{pp}})} \quad , \tag{7.82}$$

respectively, yielding samples $\underline{x} \sim f(\underline{x})$.

According to [45], this can be shown as follows.

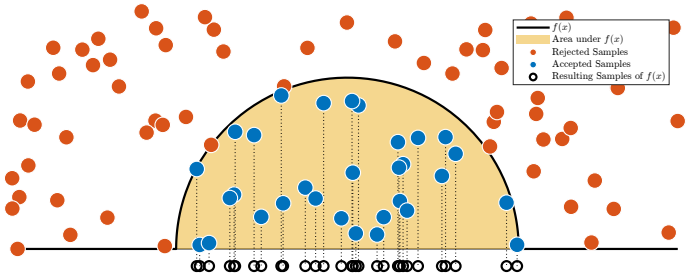

(a) Random proposal samples.

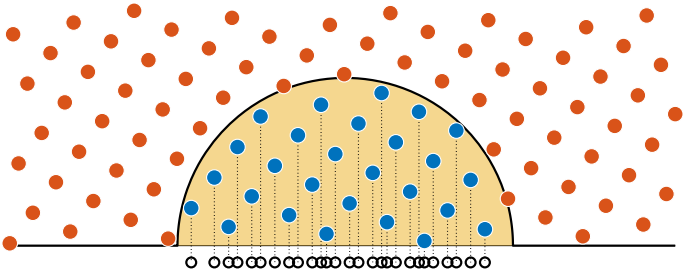

(b) Quasi-Random proposal samples.

Figure 7.4: Rejection sampling of Gaussian mixture (black line) with uniform proposal density. Augmented proposal samples (union of red and blue points) are divided into rejected (red points) and accepted samples (blue points). Marginalizing out the auxiliary y-coordinate yields the final samples (black points). Quasi-random proposal yields more locally homogeneous samples (b). Modified from [O5, Fig. 2].

Lemma 7.1. *For random variable* $\underline{\boldsymbol{x}} \sim f_{\mathrm{pp}}(\underline{x})$, $\underline{x} \in \mathbb{R}^s$, *constant* $c > 0$, *and random variable* $\boldsymbol{y}$ *with*

$$f_{\mathrm{pp}}(y|\underline{x}) = \begin{cases} \frac{1}{c \cdot f_{\mathrm{pp}}(\underline{x})} & , \quad 0 < y < c \cdot f_{\mathrm{pp}}(\underline{x}) \\ 0 \ , & \quad \textit{otherwise} \end{cases} \tag{7.83}$$

i.e., $\boldsymbol{y}$ *conditioned on a specific* $\underline{x}$ *is uniform in the interval* $(0,\ c \cdot f_{\mathrm{pp}}(\underline{x}))$, *the joint density* $f_{\mathrm{pp}}(\underline{x}, y)$ *is uniform in the set*

$$\mathcal{A} = \{\underline{x} \in \mathbb{R}^s,\ 0 < y < c \cdot f_{\mathrm{pp}}(\underline{x})\} \ . \tag{7.84}$$

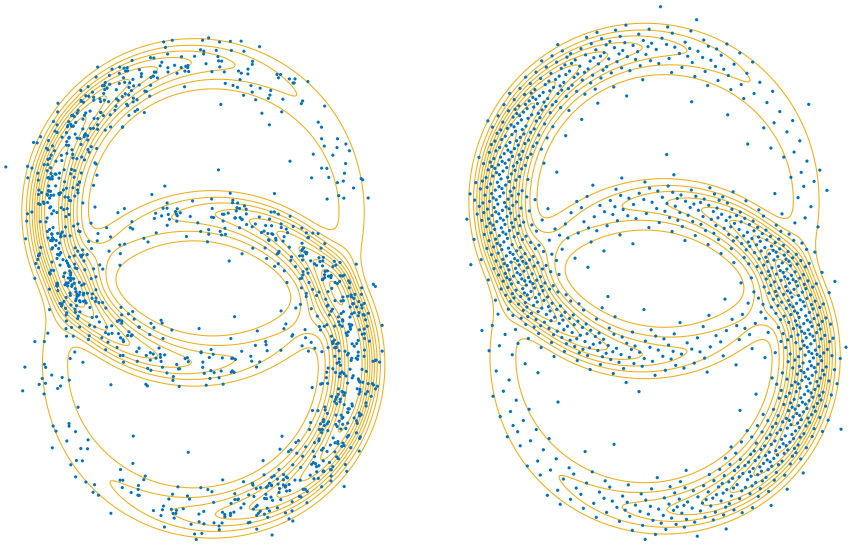

(a) Random proposal. **(b)** Extended Fibonacci proposal.

Figure 7.5: Rejection sampling (blue points) of complicated 2D density (yellow contour lines). Uniform proposal samples drawn randomly (a) and based on extended Fibonacci-Frolov lattices (b). Taken from [O5, Fig. 4].

Proof.

$$f_{\mathrm{pp}}(y,x) = f(y \,|\, x) \cdot f(x) \tag{7.85}$$

$$= \begin{cases} f_{\mathrm{pp}}(x) \cdot \frac{1}{c \cdot f_{\mathrm{pp}}(\underline{x})} & , \quad 0 < y < c \cdot f_{\mathrm{pp}}(\underline{x}) \\ 0 \ , & \text{otherwise} \end{cases} \tag{7.86}$$

$$= \begin{cases} \frac{1}{c} & , \quad 0 < y < c \cdot f_{\mathrm{pp}}(\underline{x}) \\ 0 \ , & \text{otherwise} \ . \end{cases} \tag{7.87}$$

□

Lemma 7.2. *Let random variable $\underline{\boldsymbol{x}}$ be uniformly distributed in $\mathcal{A} \subset \mathbb{R}^s$. Then the conditional density $f(\underline{x} \,|\, \underline{x} \in \mathcal{B})$, where $\mathcal{B} \subset \mathcal{A}$, is uniform in $\mathcal{B}$. ($\mathcal{A}$ and $\mathcal{B}$ should have non-zero volumes.)*

Proof. The proof is obvious. □

Lemma 7.3. *Given* $(s+1)$*-dimensional random variable* $[\underline{\boldsymbol{x}}, \boldsymbol{y}]^\top$ *uniformly distributed in*

$$\mathcal{B} = \{\underline{x} \in \mathbb{R}^s,\ 0 < y < c \cdot f(\underline{x})\}\ ,$$

then for the marginal random variable holds $\underline{\boldsymbol{x}} \sim f(\underline{x})$.

Proof.

$$\int_0^{f(\underline{x})} f(y, \underline{x})\,\mathrm{d}y = \int_0^{f(\underline{x})} \frac{1}{c}\,\mathrm{d}y = f(\underline{x})\ .$$

□

In summary, we start with the proposal samples and augment them with an extra coordinate y that is uniformly distributed in $0 < y < c \cdot f_{\mathrm{pp}}(\underline{x})$, yielding samples uniformly distributed in

$$\mathcal{A} = \{\underline{x} \in \mathbb{R}^s,\ 0 < y < c \cdot f_{\mathrm{pp}}(\underline{x})\}$$

according to Lemma 7.1. Then we "cut out" the set

$$\mathcal{B} = \{\underline{x} \in \mathbb{R}^s,\ 0 < y < c \cdot f(\underline{x})\} \subset \mathcal{A}\ ,$$

yielding samples uniform in $\mathcal{B}$ according to Lemma 7.2. Finally, a marginalization (removal of the augmented coordinate y) yields the desired samples $\underline{x} \sim f(\underline{x})$ according to Lemma 7.3. See Figure 7.4a for an intuitive visualization.

Rejection sampling is traditionally performed with iid random proposal samples, yielding likewise iid samples for the desired density. Low discrepancy or quasi-random point sets exhibit more local homogeneity. As in rejection sampling, they can often be used as drop-in replacements of iid random samples. Using a Fibonacci lattice for proposal sampling, we obtain much more locally homogeneous samples [O5] (see Figure 7.4b).

For 2D densities, the augmented proposal is 3D. Fibonacci lattices are well-known only in two dimensions, but a higher-dimensional generalization

of Fibonacci-type Frolov lattices has been proposed recently [140] and further formalized and evaluated (see Figure 7.5).

- Advantages
  - Requires density function handle only. No integral needed.
  - No numerical optimization needed.
- Disadvantages
  - Suitable proposal density needed.
  - Overhead increases exponentially with dimension.
  - Somewhat inferior dispersion due to marginalization.

7.4 Numerical Computation of 1D Inverse Transform

In orthogonal inverse transform sampling, we often compute inverse cumulative distributions of 1D density functions. Here, we describe various ways to do this efficiently.

First of all, $f(x)$ should be normalized such that

$$\int_{-\infty}^{\infty} f(x) = 1 \ . \tag{7.88}$$

1D integrals on a fixed domain can efficiently be computed numerically [152], so obtaining the normalization constant is never a problem.

7.4.1 Analytic Expression of $Q(p)$

If the quantile function $Q(p)$ can be expressed in closed form, it can be used directly as inverse transform. This is the case, e.g., for the Gaussian density, using the inverse error function.

7.4.2 Analytic Expression of $F(x)$

The cumulative $F(x)$ is available in closed form but not $Q(p)$. Then, the inverse function evaluation

$$x_i^f = F^{-1}(x_i^{\mathrm{u}}) \tag{7.89}$$

can be done with a nested intervals algorithm like bisection or the one-dimensional Newton-Raphson method [138, Sec. 9.1+9.4], [103, Sec. II.C].

7.4.3 Inverse Interpolation

The cumulative distribution $F(x)$

$$F'(x) = f(x) \ , \qquad F(-\infty) = 0 \ , \tag{7.90}$$

can also be computed directly with a numerical ODE solver like ODE45

$$y'(t) = f(t) \ , \qquad y(-\infty) = 0 \ , \tag{7.91}$$

yielding a series of (t, y)-tuples that can be used to interpolate $F(x)$. Interchanging the coordinates, i.e., interpolating the (y, t)-tuples, yields an approximation of the wanted quantile function and can propagate the uniform samples through the inverse of $F(x)$. Note that this is effectively a tabulation of the quantile function and can be used repeatedly.

7.4.4 Inverse ODE

The quantile function $Q(p)$ can also directly be stated as an ordinary differential equation (ODE) [128] given only $f(x)$, without having to compute the cumulative $F(x)$ as an intermediate result

$$y'(t) = \frac{1}{f(y(t))} \ , \tag{7.92}$$

where $y(t)$ here directly represents $Q(p)$. This is an application of the inverse function theorem and can be proven as follows:

$$F(Q(p)) = p \qquad | \frac{\partial}{\partial p} \tag{7.93}$$

$$F'(Q(p)) \cdot Q'(p) = 1 \qquad | F'(x) = f(x) \tag{7.94}$$

$$f(Q(p)) \cdot Q'(p) = 1 \qquad | \text{ solve for } Q' \tag{7.95}$$

$$Q'(p) = \frac{1}{f(Q(p))} \ . \tag{7.96}$$

However, one must choose the initial condition more carefully in some cases to avoid numerical problems. For example, for the Gaussian density, the initial condition would be

$$Q(0) = -\infty \ . \tag{7.97}$$

Also the derivative y' may be infinite at the initial condition, causing numerical problems. This can be resolved by starting from some $p \in (0, 1)$ instead of $p = 0$ and integrating the ODE to the right and the left, respectively.

7.4.5 ODE Event Locations

ODE solvers can detect the exact time when a specific event occurs, e.g., a moon completes one orbit in an astrophysical simulation. This functionality can be used to evaluate $Q(p)$ while simulating $F(x)$ via

$$y'(t) = f(t) \ . \tag{7.98}$$

To do this, define L event functions $\mathrm{ev}_i(t, y)$

$$\mathrm{ev}_i(t, y) = y - x_i^{\mathrm{u}} \ , \qquad i \in \{1, 2, \ldots, L\} \ , \tag{7.99}$$

such that L event locations $(t_i^{\mathrm{ev}}, y_i^{\mathrm{ev}})$ are identified and returned. The event locations t_i^{ev} are then the transformed samples

$$x_i^f = Q(x_i^{\mathrm{u}}) = t_i^{\mathrm{ev}} \ , \qquad i \in \{1, 2, \ldots, L\} \ . \tag{7.100}$$

This has the advantage that initial conditions are never a problem: in the Gaussian case, we would have $y(-\infty) = 0$, compare to (7.97).

7.4.6 Fast Approximation

In environments where solving ODEs is too computationally expensive, simple interpolation methods can be used [63, Sec. 4].

7.5 Summary

We presented specific formulas for low-dispersion sampling from various densities: multivariate product-type and Gaussian densities, hyperspherical uniform and von Mises–Fisher densities, and arbitrary densities via acceptance-rejection. Since these formulas often contain evaluations of scalar inverse cumulative distributions, we also assembled some ideas to compute these efficiently using ODE solvers.

CHAPTER 8

Evaluation

Contents

> Measure what is measurable,
> and make measurable what is not so.
>
> Galileo Galilei (1564–1642)

The sampling methods described in this work have been implemented in the Julia language [10], using the package Distributions [9], [113]. In this chapter, sampling methods are evaluated with respect to dispersion and

worst-case integration error. The comparative plots are generated via the Makie package [31].

8.1 Dispersion, Uniform Periodic

8.1.1 Equidistant Points

In the 1D case, the point set with minimal dispersion is simply the equidistant point set with

$$\mathring{\text{dispr}}(\mathcal{P}_L) = \frac{1}{2 \cdot L} \quad . \tag{8.1}$$

This marks the lower bound that is achievable.

8.1.2 Cubic or Regular Lattice

8.1.2.A ($s = 2$) For regular or square point configurations (with samples located at the corners of the squares), the point farthest from all samples is at the center of the square, so the dispersion is half the diagonal. Each square cell has a quarter of a sample at each of the four corners, respectively, i.e., one sample per square cell. With side length a, cell area $A = a^2$, relation to the number of samples $A = \frac{1}{L}$, and diagonal $a \cdot \sqrt{2}$, we obtain

$$\mathring{\text{dispr}}(\mathcal{P}_L) = \frac{1}{\sqrt{2}} \cdot \frac{1}{\sqrt{L}} \tag{8.2}$$

$$\approx 0.707106 \cdot \frac{1}{\sqrt{L}} \quad . \tag{8.3}$$

8.1.2.B (Arbitrary s) Extending this to (hyper-)cubic arrangements in higher dimensions s, we have

$$\mathring{\text{dispr}}(\mathcal{P}_L) = \frac{\sqrt{s}}{2} \cdot \left(\frac{1}{L}\right)^{\frac{1}{s}} \quad . \tag{8.4}$$

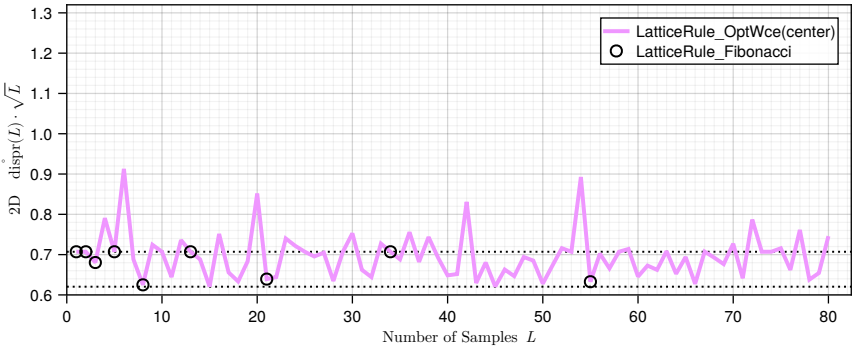

(a) Dispersion of wce-optimal rank-1 lattices in $s = 2$, from Section 5.2.2.B.

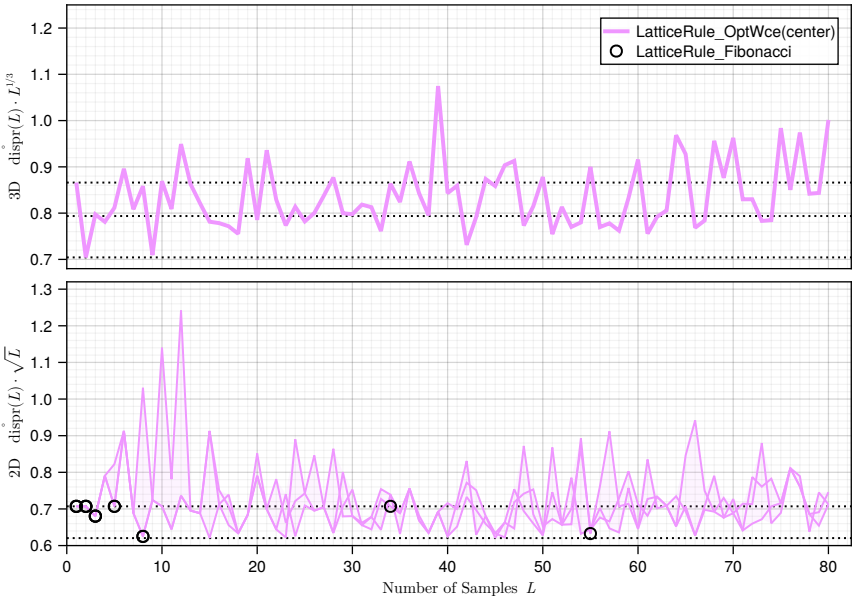

(b) Dispersion of wce-optimal rank-1 lattices in $s = 3$, from Section 5.2.2.C (top). Dispersion of their three 2D projections is also shown (bottom).

Figure 8.1: Dispersion of rank-1 lattice points with optimal wce. Dashed lines indicate cubic lattice (8.4), FCC and HCP system (8.8), and BCC lattice (8.10) in 3D and square (8.2) and equilateral configuration (8.5) in 2D case. Fibonacci–rank-1 point sets are additionally marked with black circles.

8.1.3 Closest Packing

8.1.3.A ($s = 2$) The densest possible arrangement of equal circles is the hexagonal packing, a tiling of equilateral triangles. We have a sixth sample at each of the three corners, respectively, hence $A = \frac{1}{2 \cdot L}$. The point farthest from all samples is the geometric center of the triangle; therefore, the dispersion is equivalent to the exradius $\frac{a}{\sqrt{3}}$. With $A = \frac{\sqrt{3}}{4} \cdot a^2$, we obtain

$$\mathring{\text{dispr}}(\mathcal{P}_L) = \sqrt{2} \cdot 3^{-\frac{3}{4}} \cdot \frac{1}{\sqrt{L}} \tag{8.5}$$

$$\approx 0.620403 \cdot \frac{1}{\sqrt{L}} \ . \tag{8.6}$$

See also [26, p. 110].

8.1.3.B ($s = 3$) In three dimensions, the face-centered cubic closest packing (FCC or CCP) and the hexagonal closest packing (HCP) achieve the most effective packing. Their dispersion can be calculated from the lattice determinant det and the covering radius R according to

$$\mathring{\text{dispr}}(\mathcal{P}_L) = \frac{R}{\left(\sqrt{\det}\right)^{\frac{1}{s}}} \cdot L^{-\frac{1}{s}} \ . \tag{8.7}$$

For the FCC lattice [26, p. 112] as well as for the HCP system [26, p. 114], we obtain

$$\mathring{\text{dispr}}(\mathcal{P}_L) = 2^{-\frac{1}{3}} \cdot L^{-\frac{1}{3}} \tag{8.8}$$

$$\approx 0.793700 \cdot L^{-\frac{1}{3}} \ . \tag{8.9}$$

Another important arrangement is the body-centered cubic lattice (BCC). Unlike FCC and HCP, the BCC is not a closest packing but has a smaller dispersion [26, p. 116]

$$\mathring{\text{dispr}}(\mathcal{P}_L) = \sqrt{5} \cdot 2^{\frac{5}{3}} \cdot L^{-\frac{1}{3}} \tag{8.10}$$

$$\approx 0.704317 \cdot L^{-\frac{1}{3}} \ . \tag{8.11}$$

8.1.4 Rank-1 Lattices from WCE Optimization

8.1.4.A ($s = 1$) For $s = 1$, the equidistant point set has the smallest discrepancy and also the smallest dispersion (Section 5.2.2.A). The higher-dimensional wce-optimal rank-1 lattices that we evaluate in the following all have equidistant 1D marginals.

8.1.4.B ($s = 2$) We evaluate the periodic dispersion of the 2D rank-1 lattices with globally optimal worst-case error (Section 5.2.2.B). Note that every other Fibonacci–rank-1 lattice, $L \in \{5, 13, 34, \ldots\}$, has a rotated square arrangement (3.28) and therefore the periodic dispersion of the square configuration (8.2). The other Fibonacci–rank-1 lattices, $L \in \{3, 8, 21, 55, \ldots\}$, have a dispersion between the ones of the square and the equilateral configuration. The alternating square and approximately equilateral triangular configurations are also clearly visible in Figure B.1. The 1D marginals are not shown as they all are precisely the equidistant point set.

Results: Figures 8.1 a and A.2.

8.1.4.C ($s = 3$) Likewise we evaluate 3D wce-optimal rank-1 lattices (Section 5.2.2.C) and their three 2D projections xy, xz, yz. 1D marginals are all equidistant, so we do not need to plot them.

Results: Figures 8.1 b and A.3.

8.1.5 Kronecker Sequences

8.1.5.A ($s = 1$) We evaluate the dispersion of 1D Kronecker sequences (Section 3.3.2). They are based on the inverse golden ratio ($0.618033\ldots$), the wce-optimal Kronecker generator component for $s = 2$ ($0.580100\ldots$) (5.43), the silver ratio or square root of two ($0.414213\ldots$), the square root of three ($0.732050\ldots$), the inverse plastic ratio ($0.754877\ldots$), and the inverse square plastic ratio ($0.569840\ldots$), respectively.

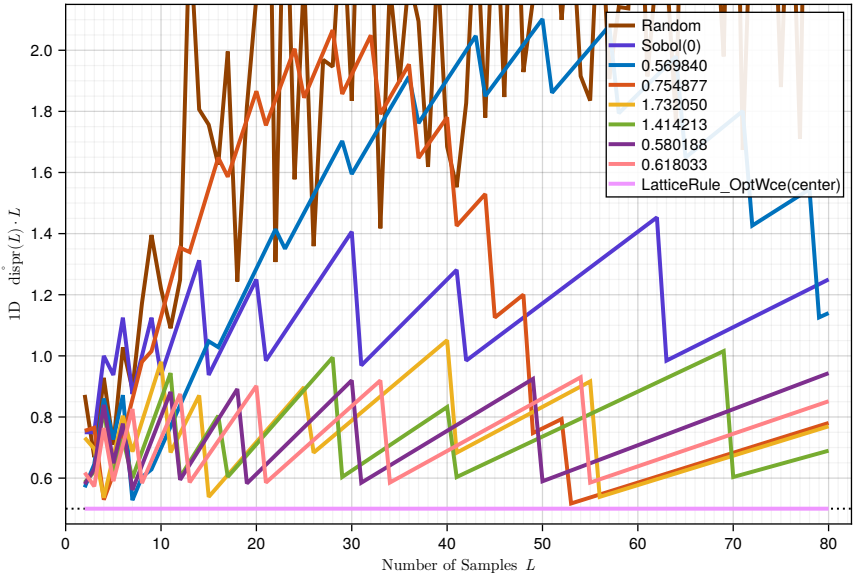

Figure 8.2: Dispersion of 1D Kronecker sequences. Dashed line indicates dispersion of equidistant points, in this case, identical to wce-optimal and equidistant lattice.

We notice that the two plastic ratio-based Kronecker sequences achieve a better-than-random dispersion only after a "burn-in" phase of about $L = 50$ and $L = 100$, respectively. The best results are achieved by the golden sequence and the wce-optimal generator from $s = 2$, closely followed by the roots of primes. The equidistant point set has a lower dispersion than all Kronecker sequences. However, it is a closed point set, while Kronecker sequences are open.

Results: Figures 8.2 and A.1.

8.1.5.B ($s = 2$) We compare 2D Kronecker sequences that are based on the plastic ratio (Section 3.3.2.B), the square roots of primes (Section 3.3.2.D), and the Kronecker wce optimization (Section 5.3.2.B), with respect to their periodic dispersions.

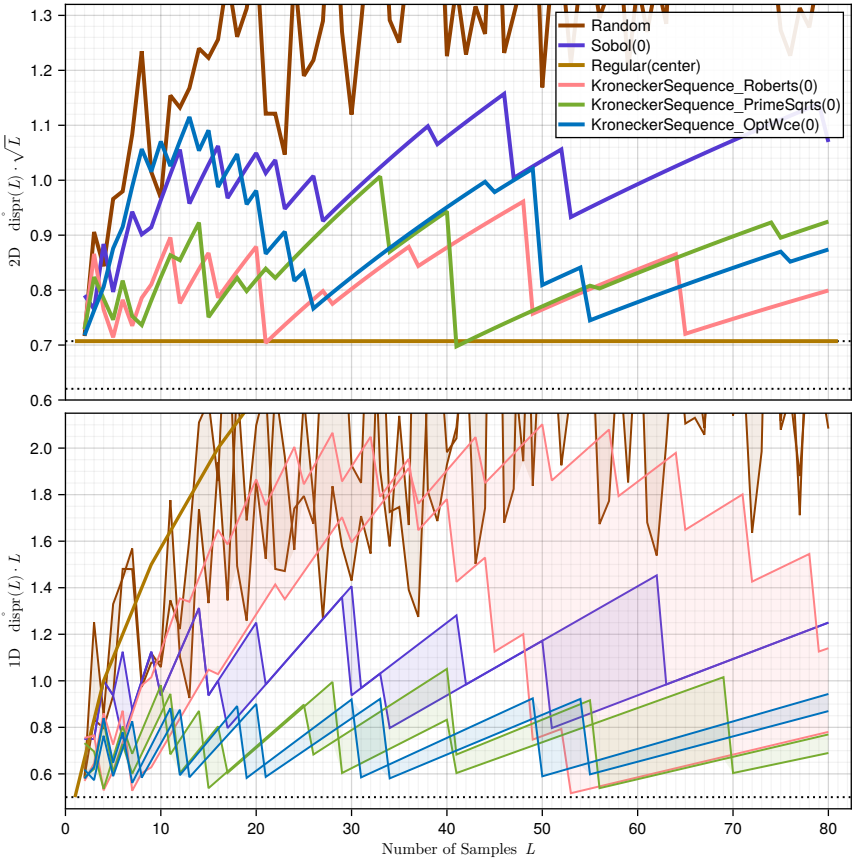

Figure 8.3: Dispersion of 2D Kronecker sequences (top) and their two 1D marginals (bottom), respectively. Dashed lines indicate dispersion of square and hexagonal lattice (2D) and equidistant points (1D).

We notice that the plastic ratio-based Kronecker sequence has the best 2D discrepancy but the worst 1D marginals; this is again the "burn-in" problem from Section 8.1.5.A. The wce-optimal and roots-of-primes Kronecker sequences are very similar. The wce-optimal Kronecker sequence

has slightly worse 2D discrepancy and slightly better 1D discrepancy than roots-of-primes.

Results: Figures 8.3 and A.2.

8.1.5.C ($s = 3$) We also compare the dispersions of the 3D Kronecker sequences based on the R_3 sequence (Section 3.3.2.C), the square roots of primes (Section 3.3.2.D), and the wce-optimal Kronecker sequence (Section 5.3.2.C), along with all their 2D and one-dimensional marginals, respectively.

We notice again that the R_3 sequence has the best 3D but worst 1D dispersion. The wce-optimal Kronecker sequence has slightly better dispersion in 3D, 2D, and 1D than the roots-of-primes sequence.

Results: Figures 8.4 and A.3.

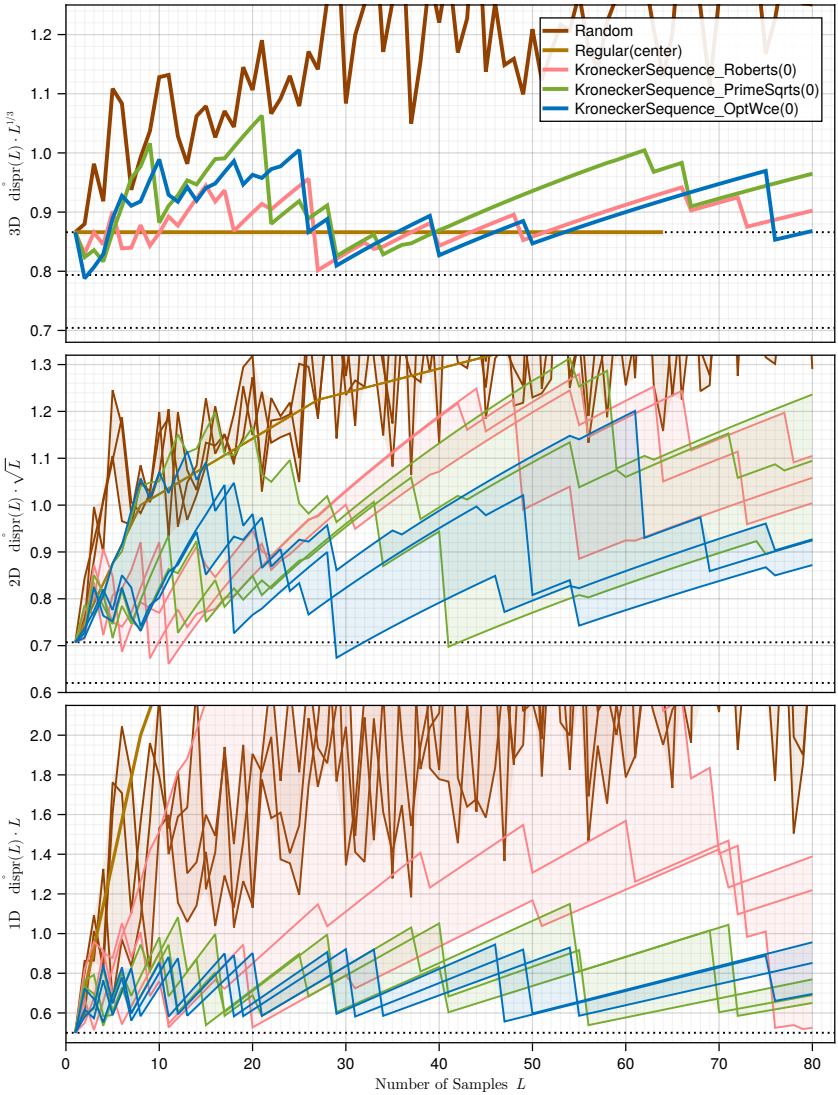

Figure 8.4: Dispersion of 3D Kronecker sequences and their 2D and 1D marginals. Dashed lines indicate dispersion of cubic, FCC, and BCC lattice (3D), square and hexagonal (2D), and equidistant points (1D).

8.2 Dispersion, Non-Uniform

We apply the novel *non-uniform* dispersion measure (Section 6.3) to evaluate various Gaussian sampling methods. As a practical approximation, we compute the dispersion of point set $\mathcal{P}_L$ with respect to density $f(\cdot)$ as

$$\operatorname{dispr}(\mathcal{P}_L; f) = \max_{\underline{x} \in \mathcal{P}_{\mathrm{cc}}} \left\{ \left[\frac{\int_{B(\underline{x}, r(\underline{x}))} f(\underline{u}) \, \mathrm{d}\underline{u}}{\lambda(B(\underline{x}, r(\underline{x})))} \right]^{\frac{1}{s}} \cdot \, r(\underline{x}) \right\} , \tag{8.12}$$

where $\mathcal{P}_{\mathrm{cc}}$ are the incenters of the simplices of the Delaunay triangulation of $\mathcal{P}_L$ with corresponding circumradius $r(\underline{x})$. This simplification neglects, however, the possibility that, for non-uniform densities, some spheres smaller than a circumsphere (and touching less than $(s+1)$ points) may produce higher values in the argument of the maximization (8.12). Furthermore, spheres outside the convex hull should ideally be incorporated as well. The integrals are computed numerically using [106] for the scalar case and [47] for $s \geq 2$, where the integrals over the interior of the circumspheres are formulated in polar ($s = 2$) and spherical ($s = 3$) coordinates.

Among others, we compare against the state-of-art LCD-based Gaussian samples. Thereby `LCD_StdNormal` uses the C++ implementation from the nonlinearestimation toolbox [160] that computes SND samples only [164] that are then transformed to arbitrary Gaussians via the Cholesky decomposition of the covariance, resulting in increased dispersion. `LCD_Gauss` employs a Julia implementation of [59]. For SND samples, both implementations should give nearly identical results, differing only due to different quadrature and nonlinear optimization algorithms, parameters, and initial guesses, and the additional symmetry constraint in `LCD_StdNormal`.

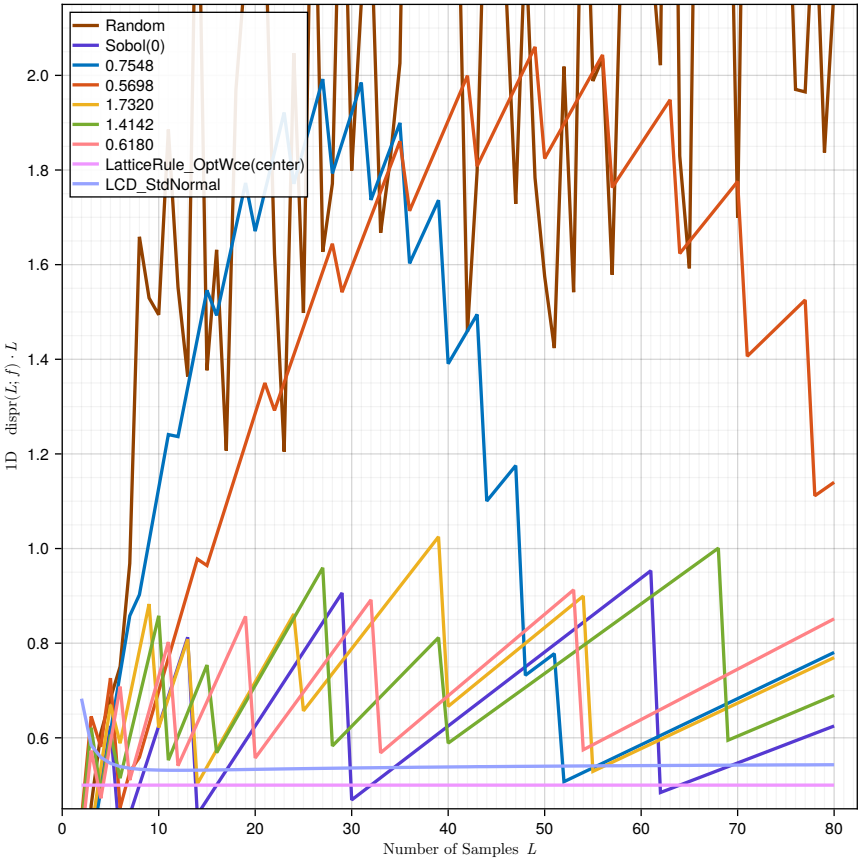

Figure 8.5: Non-uniform dispersion, SND, $s = 1$.

8.2.1 Isotropic Gaussian

8.2.1.A ($s = 1$) Evaluating non-uniform dispersion for the 1D SND, $\mathbf{C} = 1$, over the number of samples L for various sampling methods. Note that the non-uniform dispersion of a 1D point set that has been obtained via inverse transform sampling is identical to the uniform dispersion of the respective uniform point set (Lemma 6.4 and Figure 8.2).

Results: Figure 8.5.

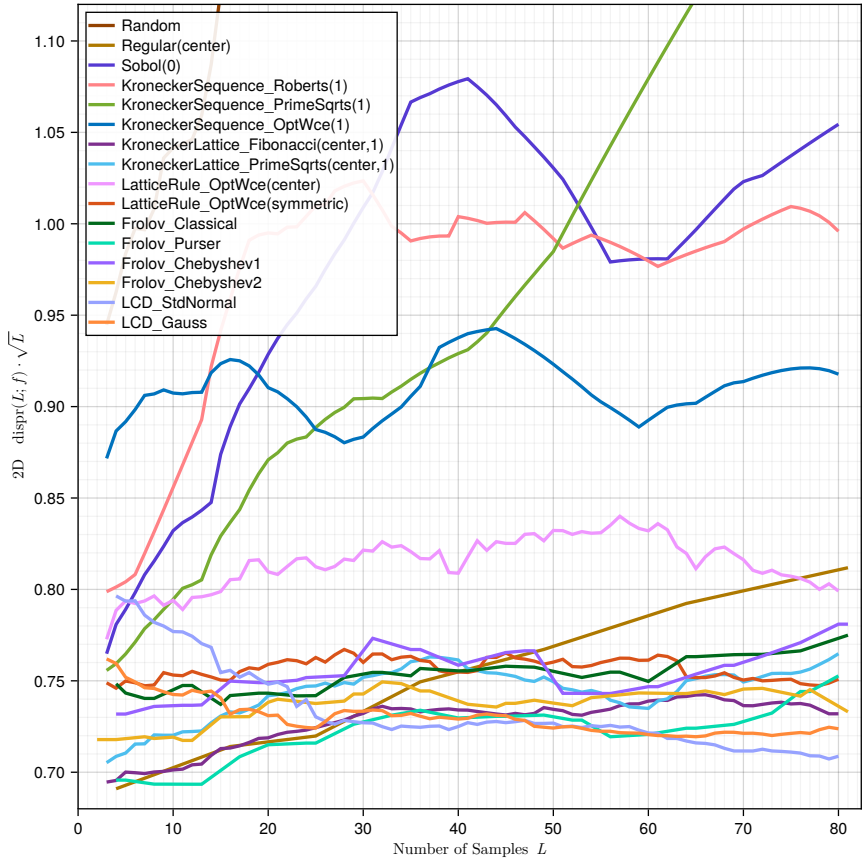

Figure 8.6: Non-uniform dispersion, SND, $s = 2$. Moving average with window $(L-10) \le L \le (L+10)$ for better readability. Sample arrangements in Figure 8.7.

8.2.1.B ($s = 2$) Evaluating non-uniform dispersion for a 2D SND, $\mathbf{C} = \mathrm{diag}(1, 1)$. For small L, the best dispersion is achieved by the Purser or Fibonacci–Frolov method until it is overhauled by the LCD method for higher L.

Results: Figures 8.6 and A.4. Samples: Figures 8.7 and A.5.

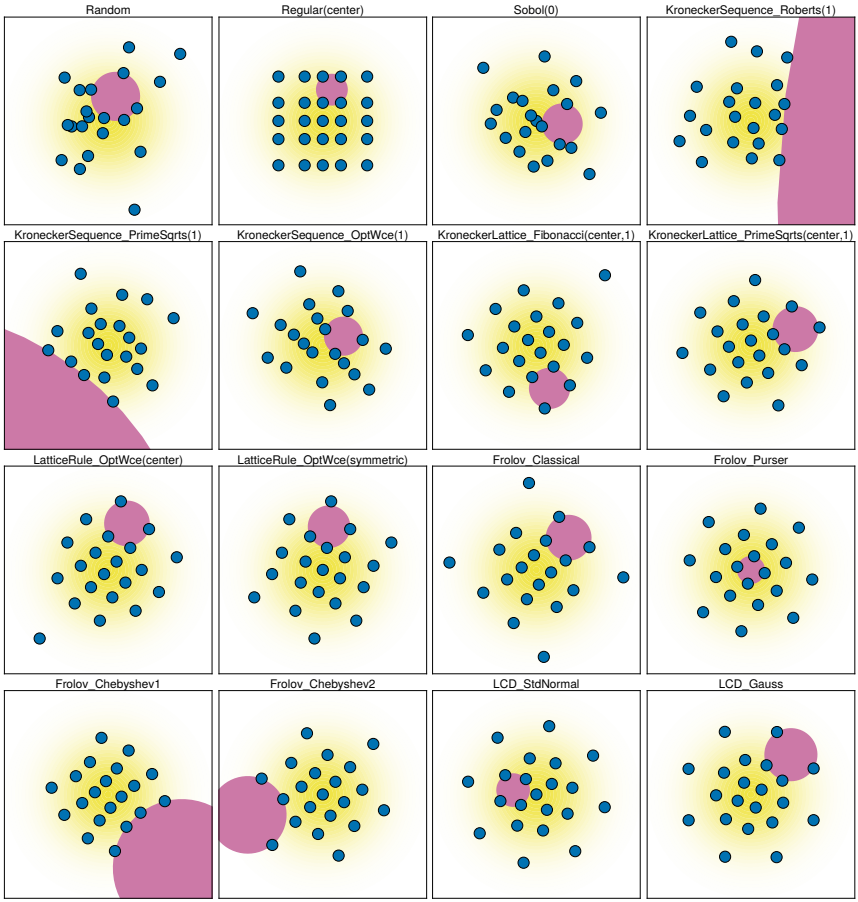

Figure 8.7: SND (yellow) with $L \approx 21$ samples (blue) from various sampling methods, $s = 2$. Circumcircle defining the non-uniform dispersion (8.12) shown in purple.

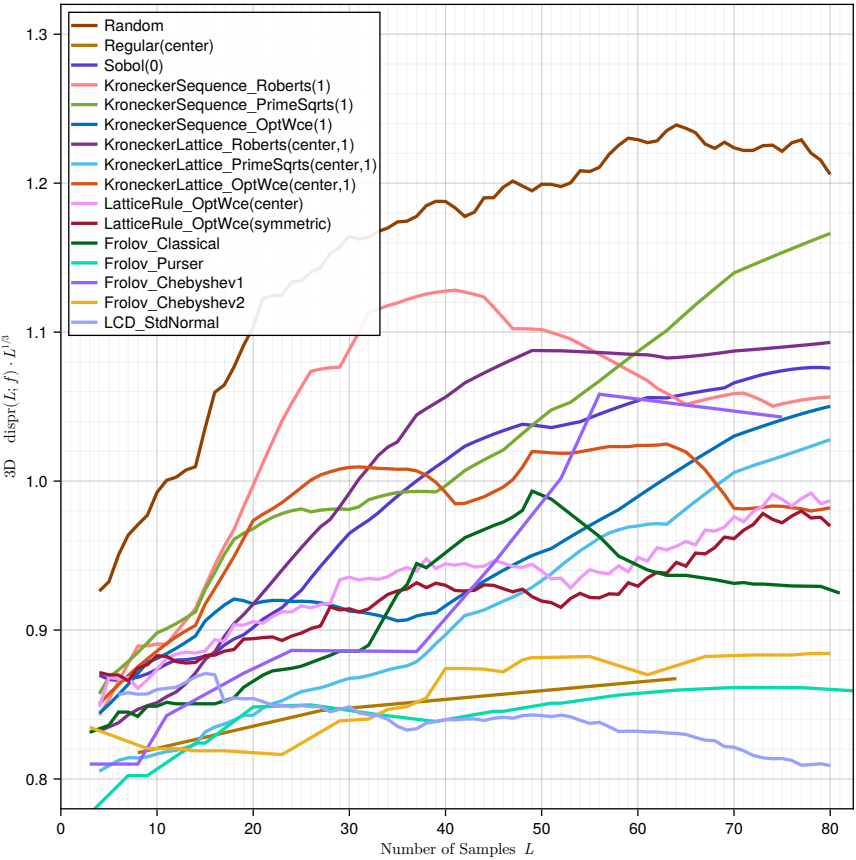

Figure 8.8: Non-uniform dispersion, SND, $s = 3$. Moving average with window $(L - 10) \leq L \leq (L + 10)$ for better readability.

8.2.1.C ($s = 3$) Evaluating non-uniform dispersion for the 3D SND, $\mathbf{C} = \text{diag}(1, 1, 1)$. For smaller L, the best dispersion is achieved by the Chebyshev2–Frolov method, and for higher L again by the LCD method.

Results: Figures 8.8 and A.6. Samples: Figures 8.9 and A.7.

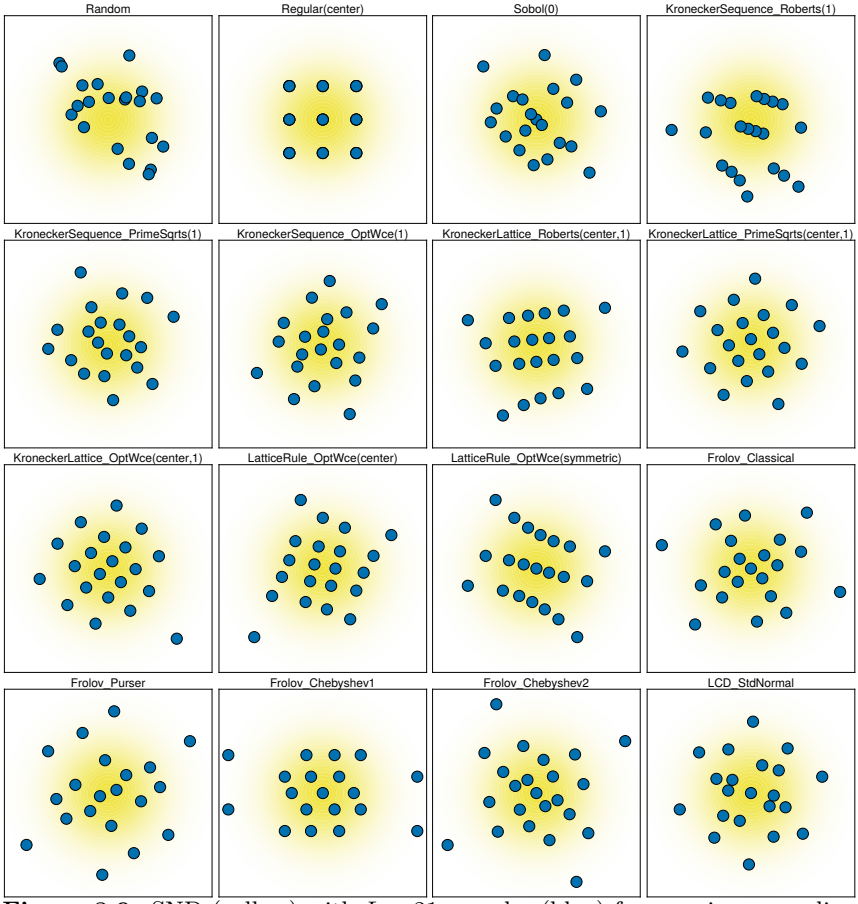

Figure 8.9: SND (yellow) with $L \approx 21$ samples (blue) from various sampling methods, $s = 3$. Projection along first two dimensions, x, y.

8.2.2 Non-Isotropic Gaussian

8.2.2.A ($s = 2$) We define a non-standard Gaussian density with a 1:2 ratio of standard deviations along the independent marginals (not aligned with the standard coordinate system) and compute the non-uniform dispersions. Purser or Fibonacci–Frolov lattice and Fibonacci–Kronecker lattice achieve the best dispersion, closely followed by the classical Frolov lattice, the Chebyshev2–Frolov lattice, and the roots-of-primes Kronecker lattice.

Results: Figures 8.10 and A.8. Samples: Figures 8.11 and A.9.

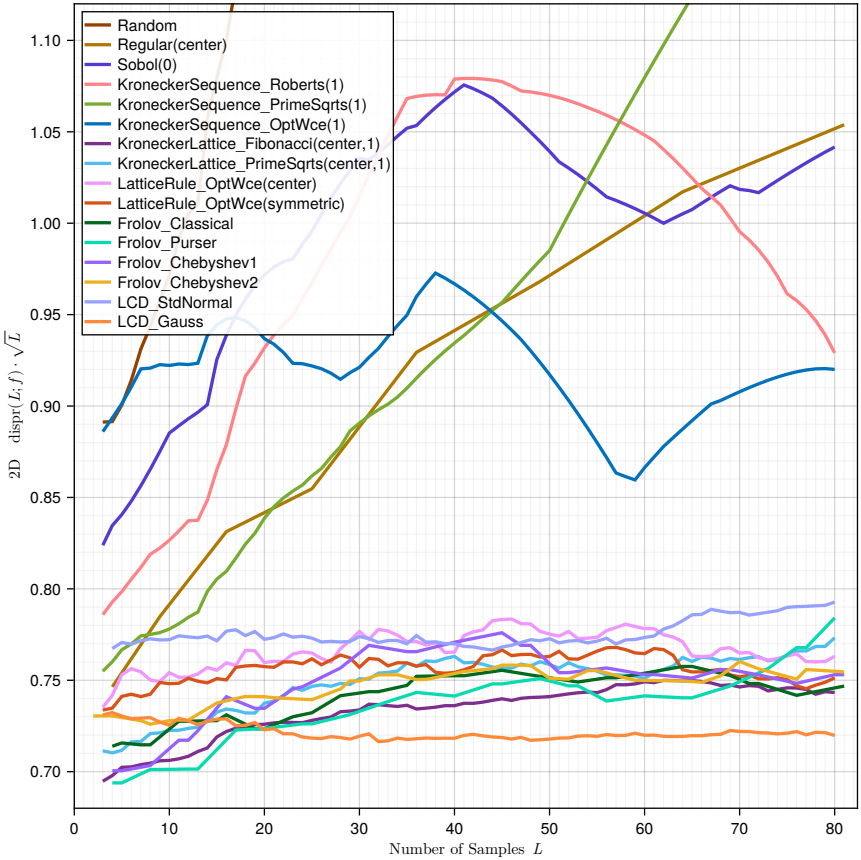

Figure 8.10: Non-uniform dispersion, non-standard Gaussian, with 2:1 standard deviation of singular axes, $s = 2$. Moving average with window $(L - 10) \leq L \leq (L + 10)$ for better readability. Sample arrangements in Figure 8.11.

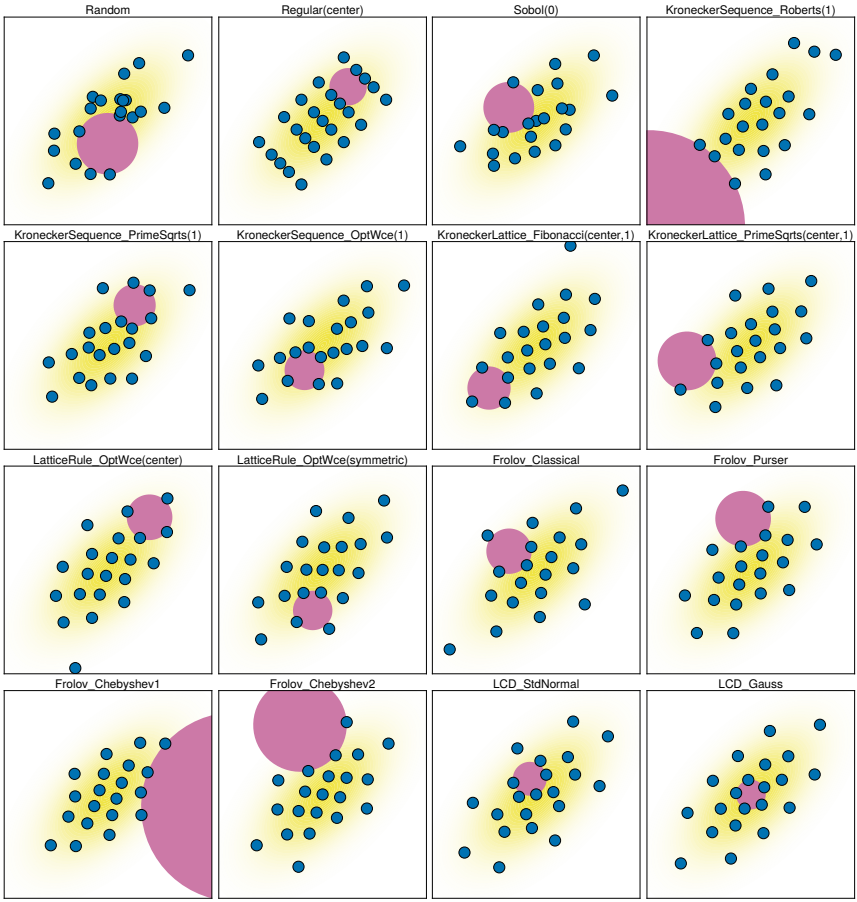

Figure 8.11: Anisotropic Gaussian density (yellow) with $L \approx 21$ samples (blue) from various sampling methods, $s = 2$. Circumcircle defining the non-uniform dispersion (8.12) shown in purple.

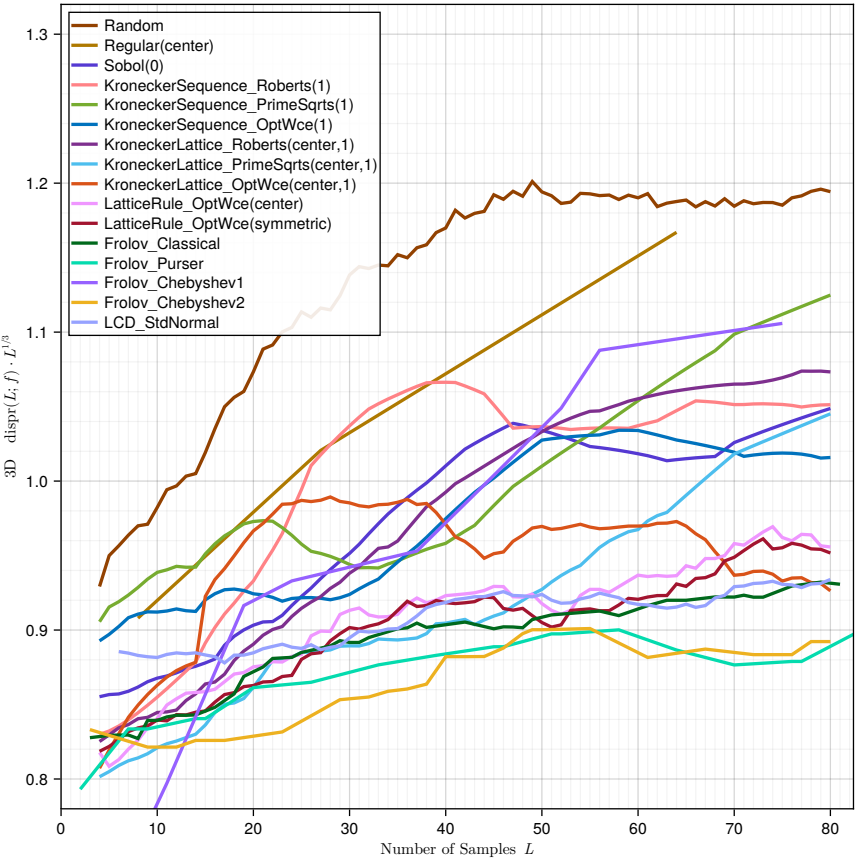

Figure 8.12: Non-uniform dispersion, non-standard Gaussian, with 4:2:1 standard deviation of singular axes, $s = 3$. Moving average with window $(L - 10) \leq L \leq (L + 10)$ for better readability.

8.2.2.B ($s = 3$) Similarly, we compare the non-uniform dispersion for various sampling methods for a Gaussian density with a 1:2:4 ratio of standard deviations in $s = 3$. Chebyshev2–Frolov and Purser–Frolov achieve the best discrepancy, followed by classical Frolov, LCD, and symmetric wce-optimal rank-1 lattice.

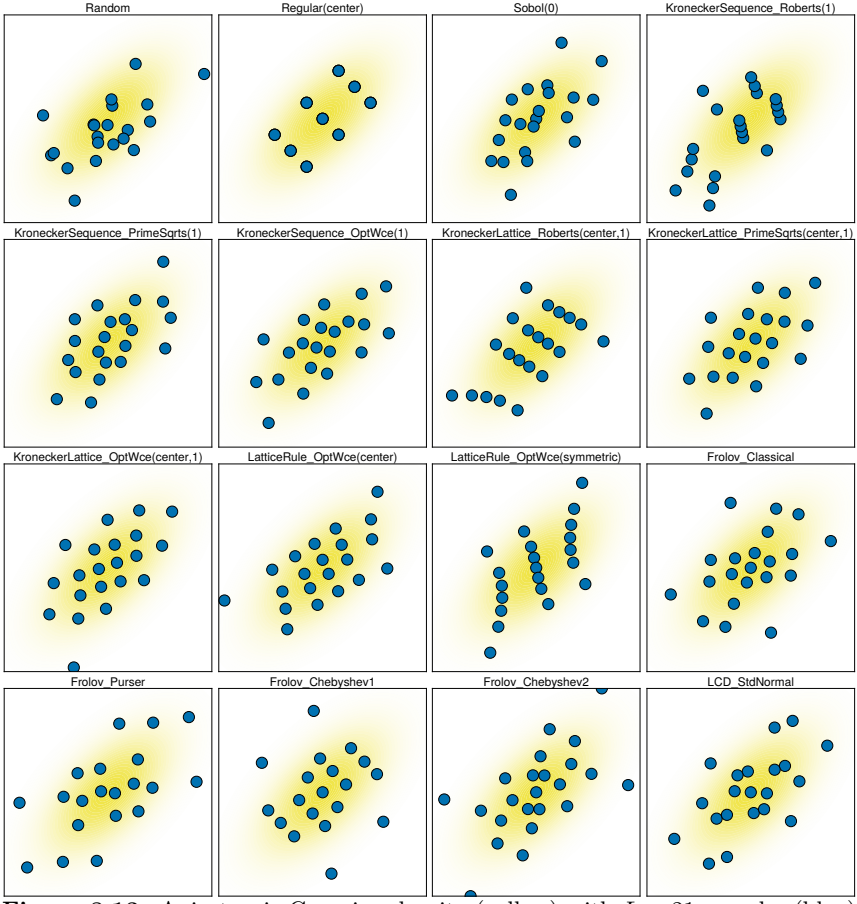

Figure 8.13: Anisotropic Gaussian density (yellow) with $L \approx 21$ samples (blue) from various sampling methods, $s = 3$. Projection along first two dimensions, x, y.

Results: Figures 8.12 and A.11. Samples: Figures 8.13 and A.12.

8.3 Worst Case Error, Periodic

We evaluate various point sets with respect to the worst-case integration error in a periodic Hilbert space (5.31).

8.3.1 Uniform Point Sets

8.3.1.A ($s = 1$) Evaluating the wce of 1D uniform point sets. From the open point sets, the best wce is achieved by the golden sequence, closely followed by the other component of the 2D wce-optimal Kronecker sequence and the roots-of-primes. The components of the plastic ratio-based sequence yield inferior results. The best rate of exactly $1/L$ is achieved by the wce-optimal and equidistant point set, which is, however, closed.

Results: Figures 8.14 and A.14.

8.3.1.B ($s = 2$) Evaluating the periodic wce of 2D uniform point sets. From open point sets, wce-optimal Kronecker, Sobol, and roots-of-primes Kronecker sequences yield the lowest wce, and the plastic ratio-based sequence is inferior. Random samples have the same rate as the square regular lattice. The best overall rate of nearly $1/L$ is achieved by the wce-optimal rank-1 lattices that include the Fibonacci rank-1 lattices.

Results: Figures 8.15 and A.15.

8.3.1.C ($s = 3$) Evaluating the wce of 3D periodic uniform point sets. Open point set with lowest wce is the wce-optimized Kronecker sequence, followed by Sobol and roots-of-primes. R_3 sequence is inferior. Cubic lattice is even worse than random. Best overall rate again by the closed wce-optimized rank-1 lattice.

Results: Figures 8.16 and A.16.

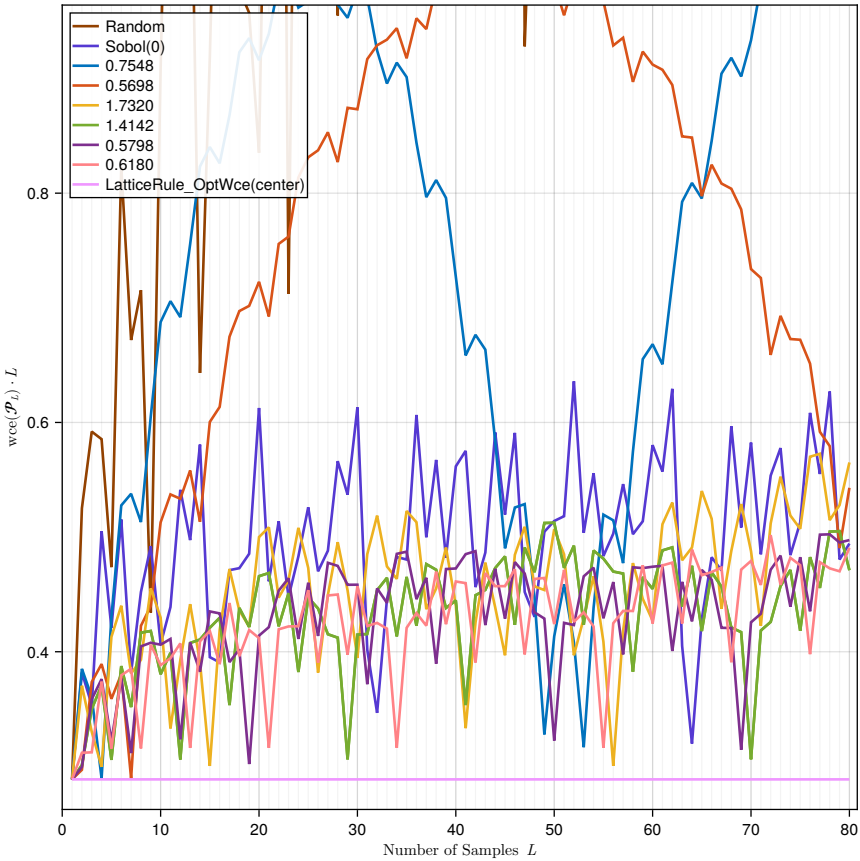

Figure 8.14: Worst-case integration error, periodic, $s = 1$.

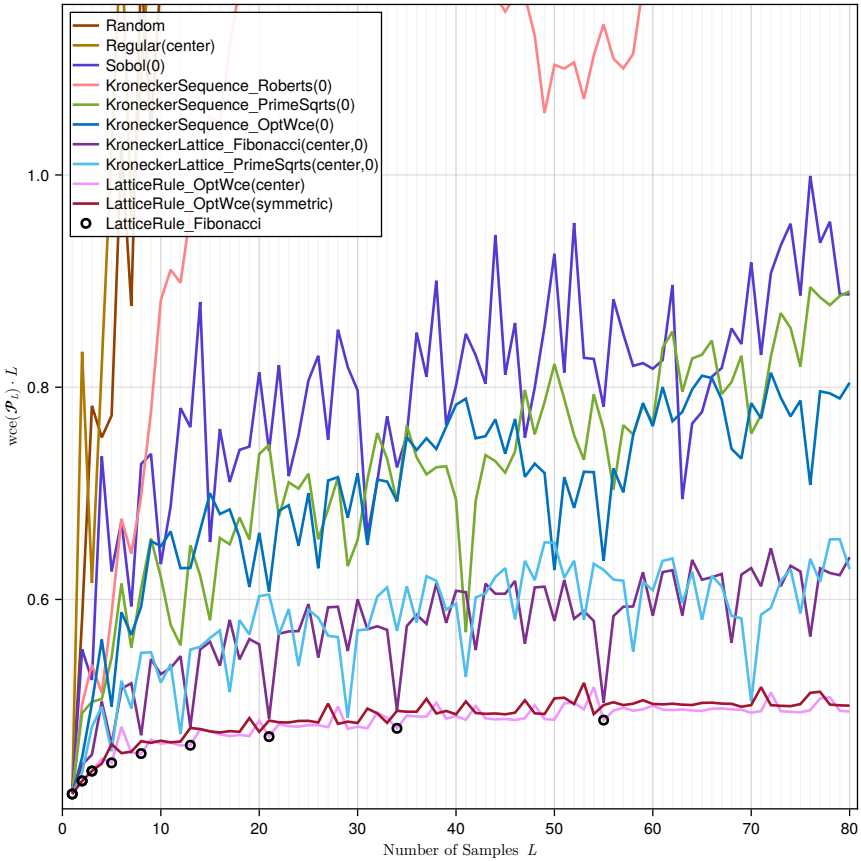

Figure 8.15: Worst-case integration error, periodic, $s = 2$. Black dots indicate Fibonacci–rank-1 lattice.

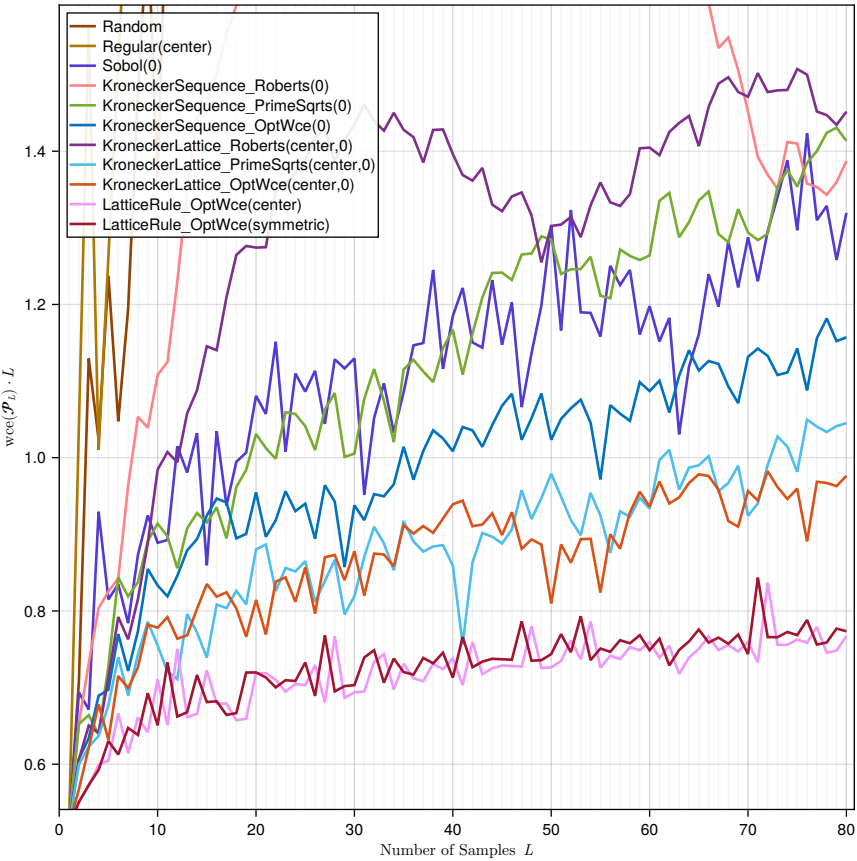

Figure 8.16: Worst-case integration error, periodic, $s = 3$.

8.4 Worst Case Error, Aperiodic

We evaluate various point sets with respect to the worst-case integration error in an aperiodic Hilbert space (5.32).

8.4.1 Uniform Point Sets

8.4.1.A ($s = 1$) Evaluating the aperiodic wce of 1D uniform point sets. From the open point sets, the best wce is achieved by the golden sequence, closely followed by the other component of the 2D wce-optimal Kronecker sequence and the roots-of-primes. The plastic ratio-based sequence yields inferior results. The best rate of exactly $1/L$ is achieved by the wce-optimal and equidistant point set, which is, however, closed.

Results: Figures 8.17 and A.18.

8.4.1.B ($s = 2$) Evaluating the wce of 2D periodic uniform point sets. From open point sets, wce-optimal Kronecker sequence and Sobol sequence seem to give the lowest wce. Random samples have the same rate as the square regular lattice. The best overall rate of nearly $1/L$ is achieved by the wce-optimal rank-1 lattices that include the Fibonacci rank-1 lattices.

Results: Figures 8.18 and A.19.

8.4.1.C ($s = 3$) Evaluating the wce of 3D periodic uniform point sets. Open point set with lowest wce seems to be wce-optimized Kronecker sequence, Sobol sequence, and roots-of-primes. The cubic lattice is even worse than random. Best overall rate by the closed Porser–Frolov and Chebyshev2–Frolov lattice.

Results: Figures 8.19 and A.20.

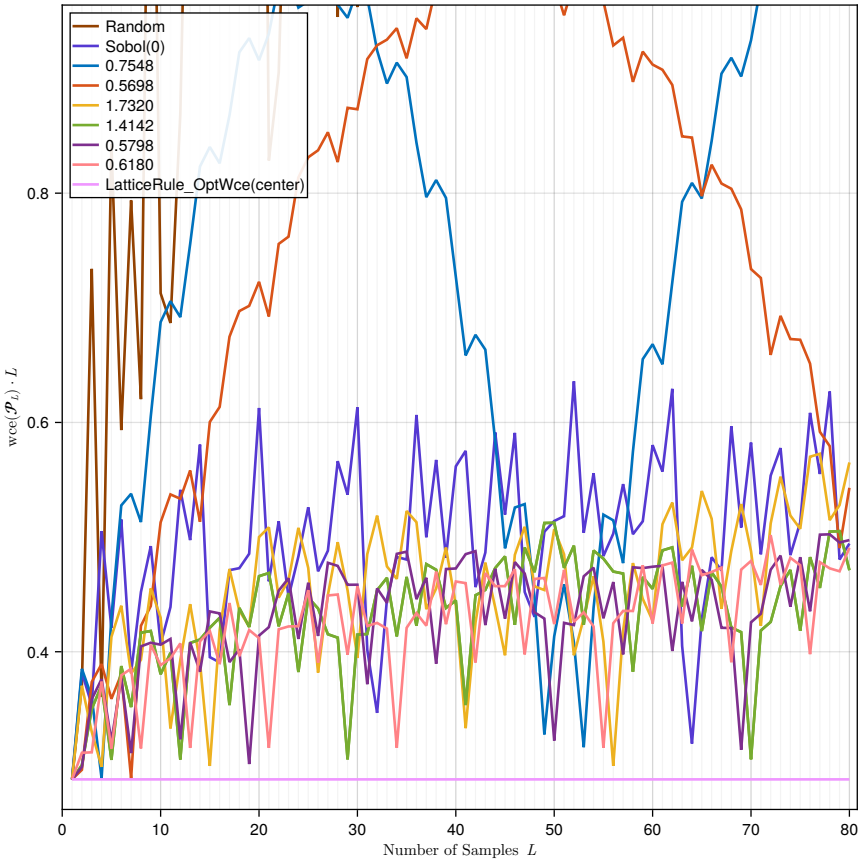

Figure 8.17: Worst-case integration error, aperiodic, $s = 1$.

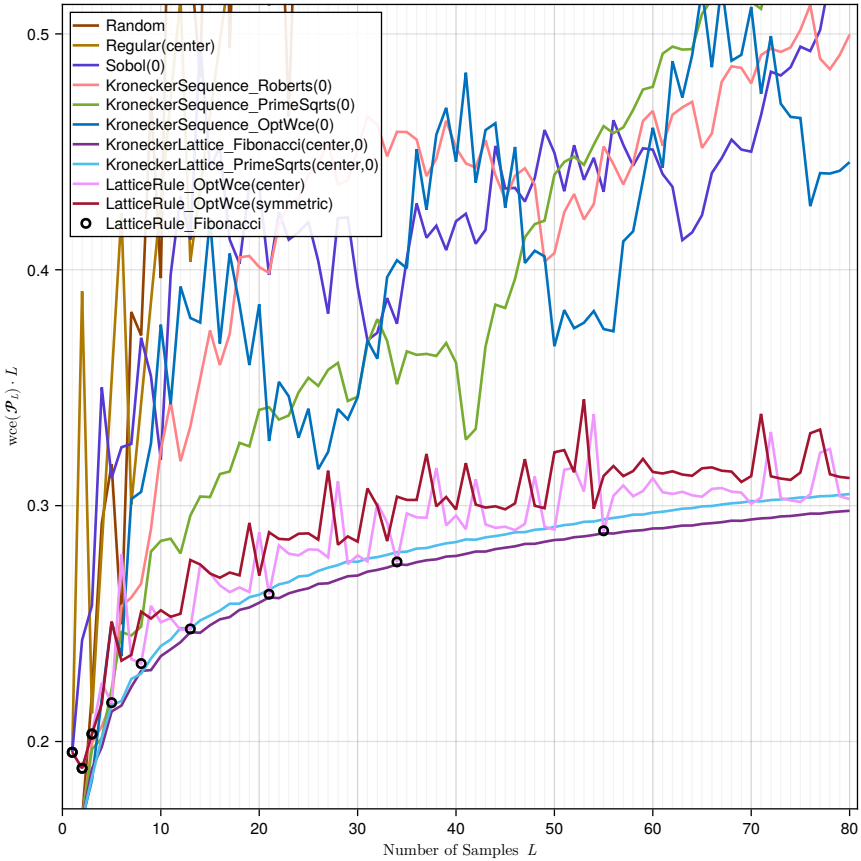

Figure 8.18: Worst-case integration error, aperiodic, $s = 2$. Black dots indicate Fibonacci–rank-1 lattice.

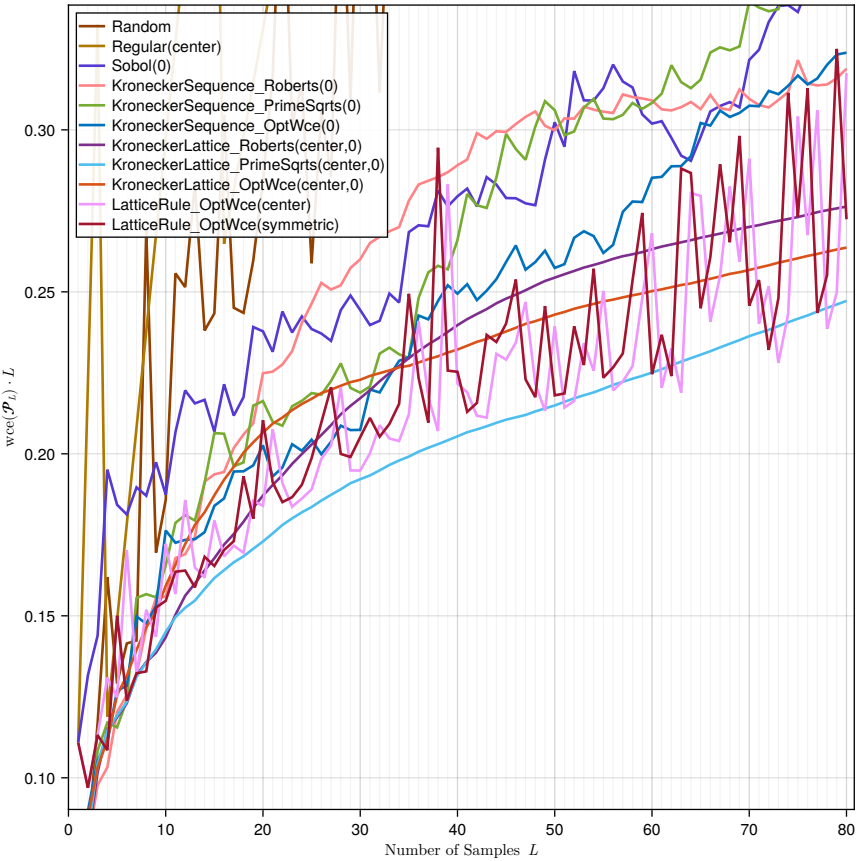

Figure 8.19: Worst-case integration error, aperiodic, $s = 3$.

8.5 Discussion

Out of all the available point sets, which one is now the very best that we should use? This depends on the metric, the number of samples, the dimension, and the affordable computational complexity. Based a somewhat subjective review of the figures in Appendix A, two tables are compiled listing the point sets with lowest dispersion and the lowest wce in certain scenarios.

Sampling methods are thereby abbreviated as follows, where the colors correspond to the charts and also help to identify methods that are particularly often among the best. `LCD`: Gaussian sampling based on minimizing a distance of LCDs [59]; `Sobol`: Sobol sequence, a well-known and widely available method for reference [83], [158]; `LR_Fib`: Fibonacci–rank-1 lattice (Section 3.3.1.D); `LR_OptWCE`: Lattice rule optained from wce minimization (Section 5.2.2); `KS_OptWCE`: Kronecker sequence obtained from wce minimization (Section 5.3.2); `KS_Roberts`: R_s Kronecker sequence due to Martin Roberts (Section 3.3.2.C); `KS_PrmSqrt`: Kronecker sequence from roots of primes (Section 3.3.2.D); `KS_Fib`: Fibonacci–Kronecker sequence or golden sequence (Section 3.3.2.A); `KL_Fib`: Fibonacci–Kronecker lattice (Section 3.3.3.B); `KL_OptWCE`: Kronecker lattice (Section 3.3.3.A) based on the $(s-1)$-dimensional `KS_OptWCE`; `Fr_Purser`: Purser–Frolov lattice (Section 3.3.4.D and Chapter 4); `Fr_Cheb1`: Frolov lattice from Chebyshev polynomials of the first kind (Section 3.3.4.B); `Fr_Cheb2`: Frolov lattice from Chebyshev polynomials of the second kind (Section 3.3.4.C).

We distinguish between *all* point sets (including the closed ones), and *open* point sets, i.e., Kronecker sequences, the Sobol sequence, and iid samples, where more samples can be added while keeping the old ones in place.

s	Lowest Dispersion Point Sets					
	all			open		
	Uniform	SND	Gauss	Uniform	SND	Gauss
1D	LR_-OptWCE =equidist	LR_-OptWCE =equidist	LR_-OptWCE =equidist	KS_-Roberts =KS_Fib	KS_-Roberts =KS_Fib	KS_-Roberts =KS_Fib
2D	LR_-OptWCE =**LR_Fib** (for $L = F_k$)	LCD, Fr_-Purser	LCD, Fr_-Purser, KL_Fib	KS_-Roberts	KS_-OptWCE	KS_-OptWCE
3D	LR_-OptWCE, KS_-Roberts, KS_-OptWCE	LCD, Fr_-Purser	Fr_-Cheb2, Fr_-Purser	KS_-Roberts, KS_-OptWCE	KS_-OptWCE, Sobol, KS_-PrmSqrt	KS_-OptWCE, Sobol, KS_-Roberts, KS_-PrmSqrt

Table 8.1: Point sets with lowest dispersion, from inspection of Appendices A.1 to A.3.

s	Lowest WCE Point Sets			
	all		open	
	periodic wce	aperiodic wce	periodic wce	aperiodic wce
1D	LR_OptWCE =equidist	LR_OptWCE =equidist	KS_Roberts =KS_Fib	KS_Roberts =KS_Fib
2D	LR_OptWCE =LR_Fib (for $L = F_k$)	KL_Fib	KS_OptWCE	KS_OptWCE, Sobol
3D	LR_OptWCE	Fr_Purser, Fr_Cheb2	KS_OptWCE, Sobol, KS_PrmSqrt	KS_OptWCE, Sobol, KS_PrmSqrt, KS_Roberts
4D	LR_OptWCE	Fr_Cheb1, KL_OptWCE	KS_OptWCE, Sobol	Sobol, KS_OptWCE

Table 8.2: Point sets with lowest wce, from inspection of Appendices A.4 and A.5.

We see that in 1D, the equidistant point set is always the best closed and the golden sequence the best open point set regarding any measure, dispersion or wce. Low-dispersion uniform samples in any dimension are best drawn via LR_OptWCE (closed), and KS_Roberts (open). Low-dispersion Gaussian samples are best drawn via LCD or Fr_Purser (closed), and KS_OptWCE (open). Low-discrepancy / low-wce samples are best produced via LR_OptWCE (closed, periodic), or KS_OptWCE and Sobol (open).

It is very interesting to see that the point sets yielding lowest aperiodic wce are in general the same ones that also yield Gaussian samples with the lowest dispersion, just as predicted in Section 6.7. In particular, this is

- 2D, closed: KL_Fib,
- 3D, closed: Fr_Purser, Fr_Cheb2,
- 2D, open: KS_OptWCE,

- 3D, open: KS_OptWCE, Sobol, KS_PrmSqrt, KS_Roberts.

8.6 Summary

We evaluated the quality of sampling methods developed in this work, comparing them to state of art methods. Some standard arrangements like equidistant points, cubic lattice, and hexagonal packing were reiterated and included in the evaluation plots for orientation. We saw that the Fibonacci–rank-1 lattice has a dispersion alternating between the one of a square lattice and close to the one of a hexagonal packing. Furthermore, we used the novel non-uniform dispersion to compare Gaussian sampling methods. We also compared low-discrepancy point sets based on their periodic and aperiodic worst-case error. Finally, we compiled two tables with the best low-dispersion and low-wce point sets in various scenarios and identified the "multiple winners".

CHAPTER 9

Conclusion

Contents

> In literature and in life we ultimately pursue, not conclusions, but beginnings.
>
> Literature Unbound, 1986
> Sam Tanenhaus (*1955)

In this thesis, we have addressed various methods to obtain deterministic samples of non-uniform densities. Deterministic sampling allows, e.g., more efficient numerical integration and filtering. In addition to the Euclidean space $\mathbb{R}^s$, we considered sampling on the hypersphere $\mathbb{S}^s$.

9.1 Contributions

This thesis dealt with a range of better-than-random sampling methods. State of the art was extended by some improvements in LCD sampling and acceptance-rejection sampling, by adding a few missing puzzle pieces

concerning the highly interesting and long-studied Fibonacci lattices, by defining a non-uniform dispersion measure, by a method to obtain non-uniform low-dispersion samples for various densities, and by some low-discrepancy point sets that have been obtained via a brute force search.

9.1.1 Direct Non-Uniform Sampling

The already known LCD-based sample reduction method in $\mathbb{R}^s$ has been extended to the $\mathbb{S}^2$ sphere. Furthermore, the state-of-art LCD-based Gaussian sampling has been modified to produce "somewhat-transformable" samples, enabling caching of SND reference samples that can quickly be transformed to arbitrary Gaussians with less quality loss than before. Furthermore, a deterministic and optimization-based variant of acceptance-rejection sampling for arbitrary densities has been proposed.

9.1.2 Low-Discrepancy Samples

Relationships between the 2D Fibonacci–rank-1, Fibonacci–Kronecker, and Fibonacci–Frolov lattices have been worked out. Little-known properties of the Fibonacci–Frolov lattice were presented in detail formally as well as intuitively. A number of rank-1 lattices and Kronecker sequences with globally optimal worst-case integration error have been computed. Both belong to the "multiple winners" in an evaluation with various metrics and settings (Tables 8.1 and 8.2).

9.1.3 Orthogonal Inverse Transform Sampling

The well-known dispersion measure has been generalized to non-uniform densities. The well-known inequality between dispersion and discrepancy has been generalized to non-uniform densities. Based on this, we obtained a non-uniform low-dispersion sampling method via orthogonal inverse transforms of low-discrepancy point sets. Concrete formulas are given for the multivariate Gaussian, the hyperspherical uniform, and the hyperspherical von Mises–Fisher density.

9.1.4 List of Contributions

It follows a concise summary of key contributions brought forward in this work, including cross-references.

- **Non-uniform dispersion** measure (Section 6.3).
- Effect of **mappings** on relation between dispersion and discrepancy (Section 6.6.4).
- Multivariate non-uniform low-dispersion sampling via **orthogonal inverse transform** of low-discrepancy points (Section 6.7).
  - Multivariate **Gaussian** low-dispersion samples (Section 7.1.2), [O8], [O3].
  - **Hyperspherical** uniform low-dispersion samples (Section 7.2.4).
  - **Von Mises–Fisher** low-dispersion samples (Section 7.2.5), [O7].
- **Fibonacci** Lattices
  - Identify connection between square unit cell configuration [123, Theorem 3] of Fibonacci–rank-1 lattice and two-dimensional Fibonacci–Frolov lattice [140] by taking the limit (3.65).
  - Identify previously uncrecognized work about a higher-dimensional extension of two-dimensional Fibonacci–Frolov lattice [140]. Formalize details about its inner working (4.21), (Figure 4.3).
- Point sets with globally **optimal worst-case error**
  - Expand global search for two-dimensional rank-1 lattice rules [68] to higher numbers of samples and to higher dimensions (Section 5.2.2 and Appendix C.1).
  - Adapt quality measure for fixed L [68] to variable L (5.42), enabling global search for Kronecker sequences (Appendix C.2).
  - Both yield superior results in a variety of settings (Tables 8.1 and 8.2).
- Advancements in **LCD** sampling
  - Improve transformability of Gaussian LCD samples by conditional or component-by-component sampling (Section 2.2.2), [O1].
  - Define LCD directly on $\mathbb{S}^2$ without linearization (Section 2.2.1). Exploit symmetry and find closed form distance measure for

Dirac mixture densities (2.27). Apply to spherical sample reduction [O9].

- **Acceptance-Rejection** sampling
  - Acceptance-rejection sampling with low-discrepancy point sets (Section 7.3), [O5].
  - Starting from acceptance-rejection sampling, derive Packing-of-Volume-Under-Density sampling (Section 7.3), [O6].
- Linear **proposal mapping** to fully exploit the advantages of low-discrepancy sampling (Section 6.8.3.B).

APPENDIX A

Evaluation

Contents

Figures don't lie,
but liars do figure.

Carroll D. Wright
(1840–1909)

This appendix contains the evaluation plots from Chapter 8 but with a greater range of L.

A.1 Uniform Dispersion

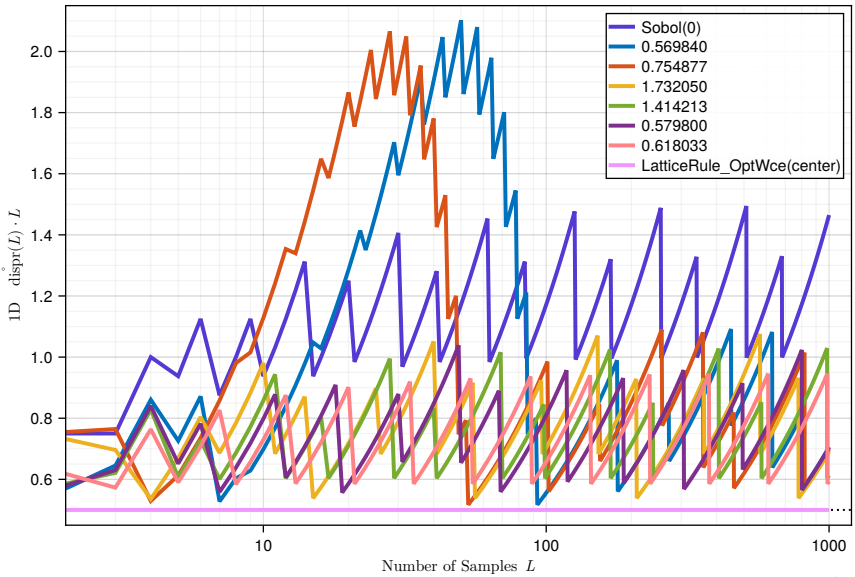

Figure A.1: Uniform dispersion of 1D Kronecker sequences, Section 8.1.5.A. The wce-optimal Kronecker sequence generator component from 2D, 0.579800 . . ., is optimized up to $L_{\max} = 177$.

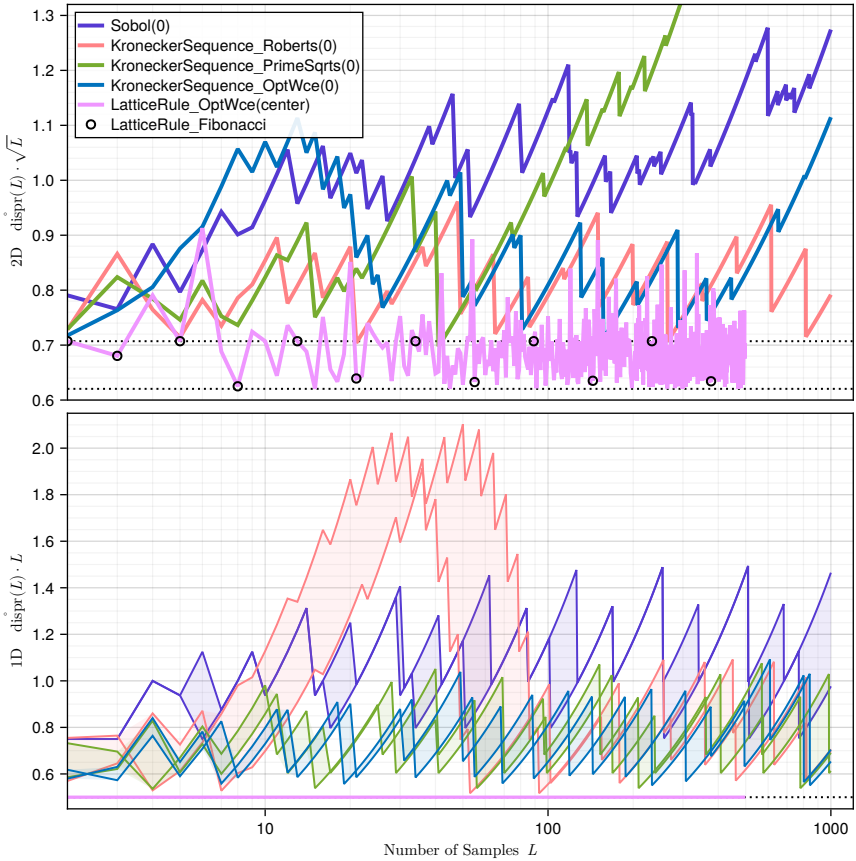

Figure A.2: Uniform dispersion of 2D Kronecker sequences, Section 8.1.5.B. The wce-optimal Kronecker sequence generator is optimized up to $L_{\max} = 177$.

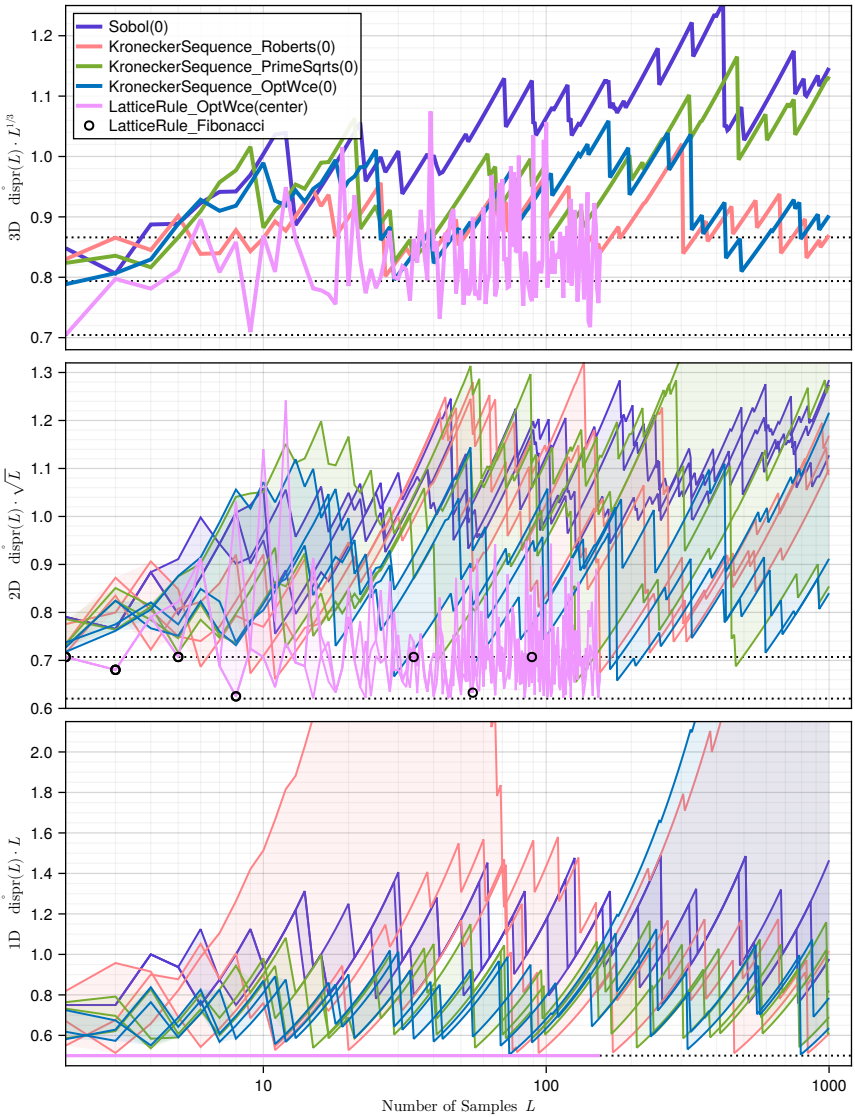

Figure A.3: Uniform dispersion of 3D Kronecker sequences, Section 8.1.5.C. The wce-optimal Kronecker sequence generator is optimized up to $L_{\max} = 73$.

A.2 Standard Normal Dispersion

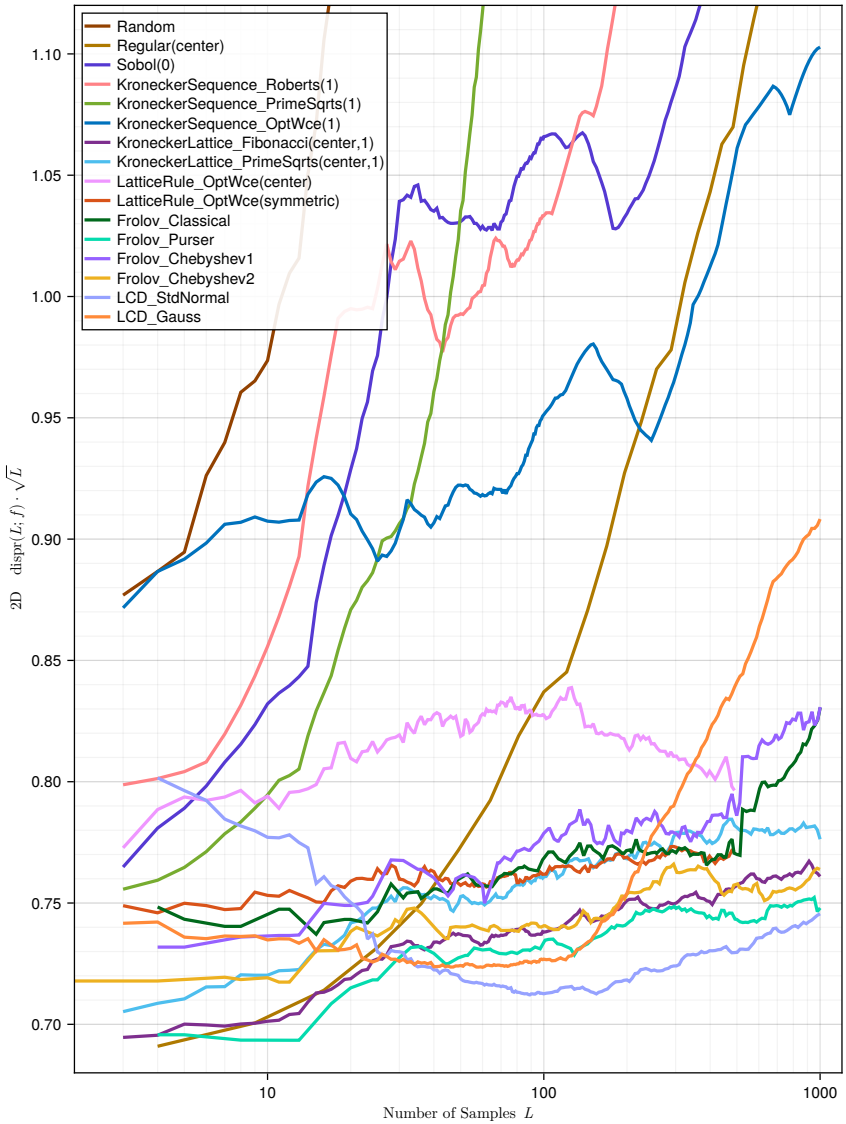

Figure A.4: 2D SND dispersion, Section 8.2.1.B. `KroneckerSequence_OptWce` with $L_{\max} = 177$. Smoothing for better readability.

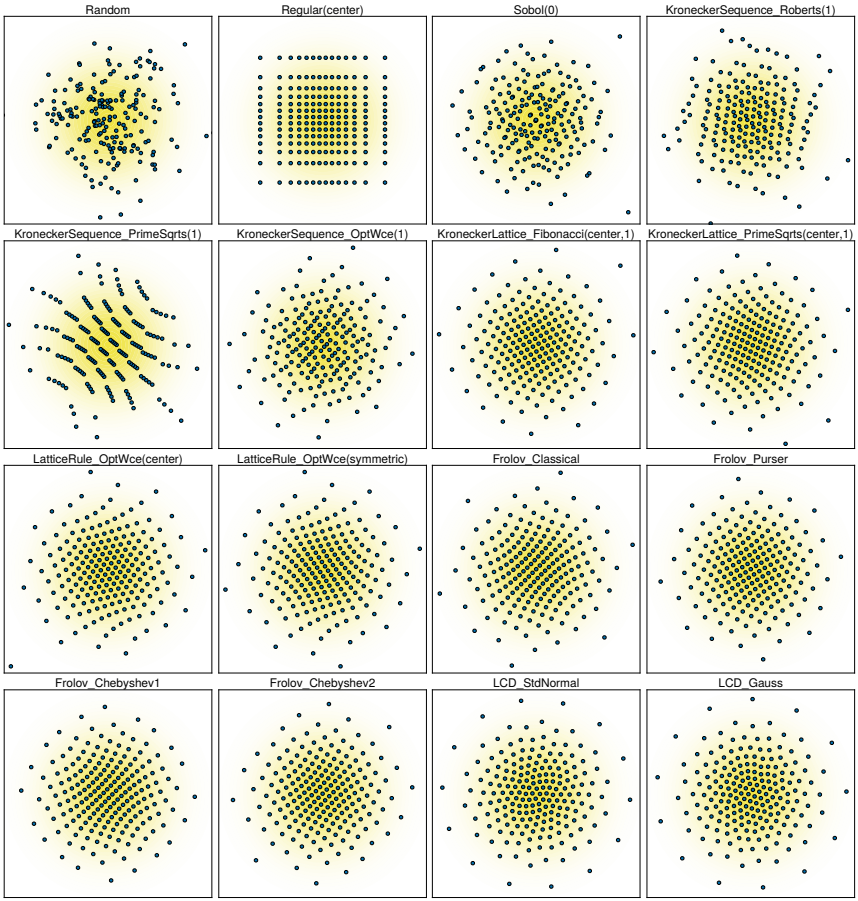

Figure A.5: 2D SND (yellow) with $L \approx 200$ samples (blue).

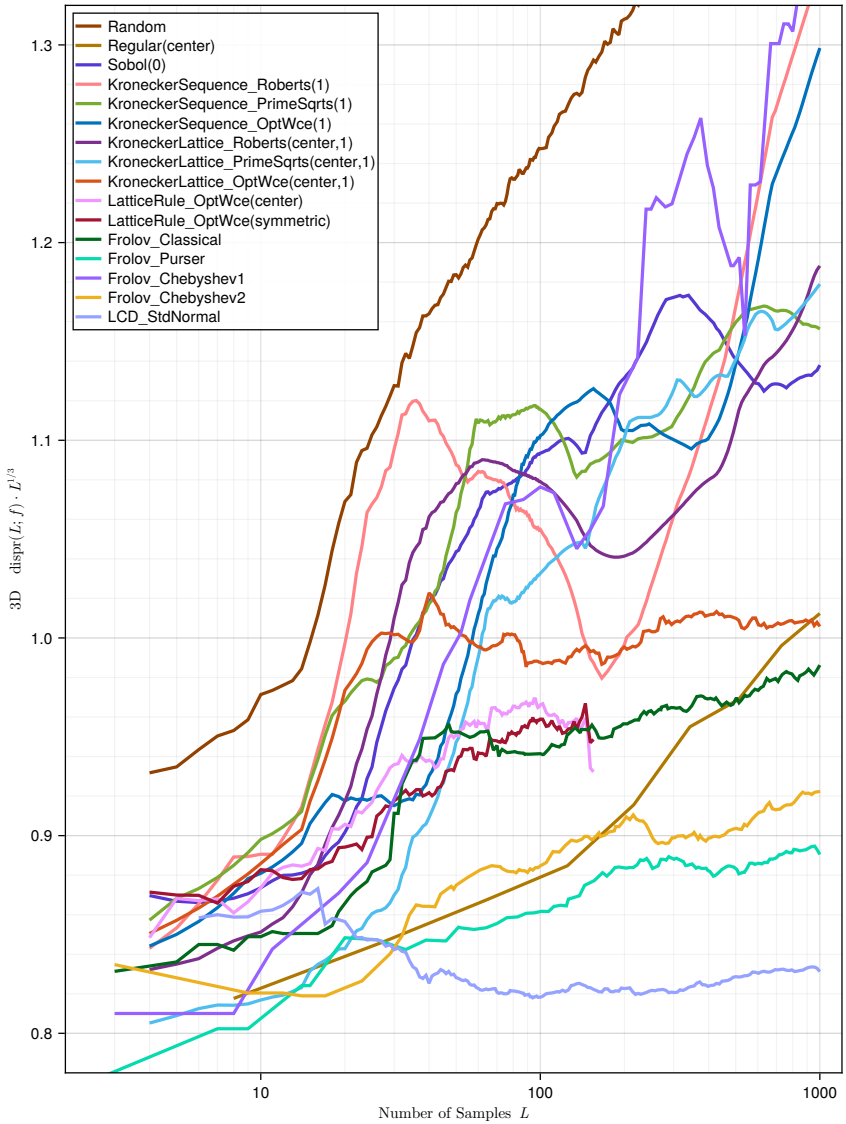

Figure A.6: 3D SND dispersion, Section 8.2.1.C. `KroneckerSequence_OptWce` with $L_{\max} = 73$. Smoothing for better readability.

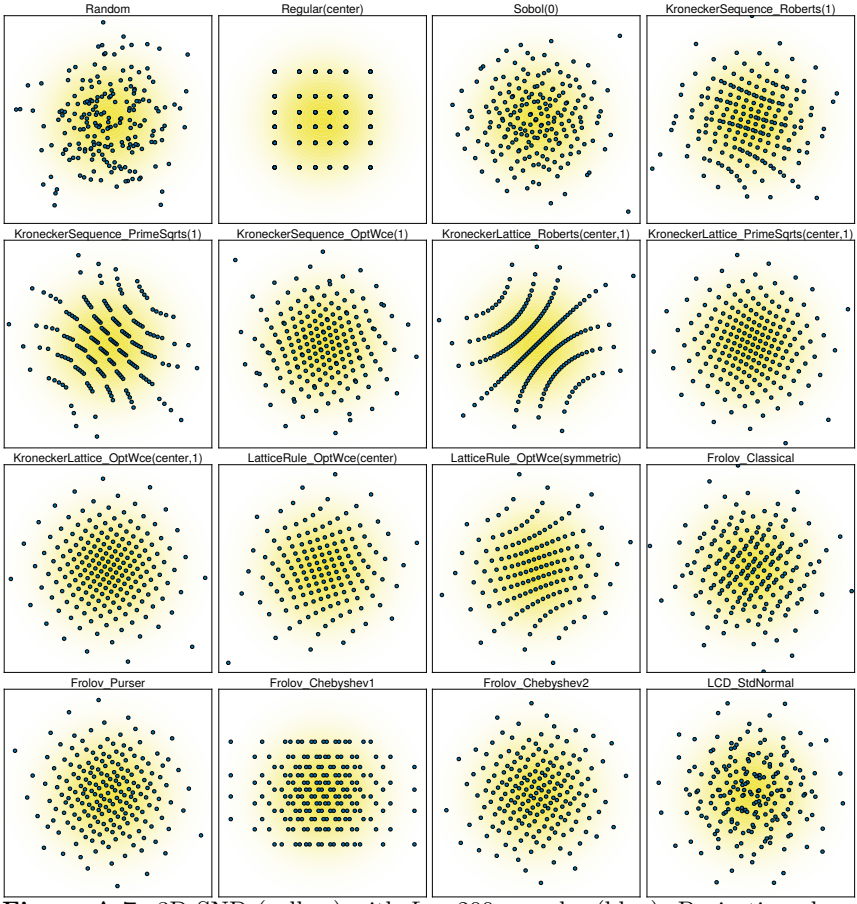

Figure A.7: 3D SND (yellow) with $L \approx 200$ samples (blue). Projection along first two dimensions, x, y.

A.3 Anisotropic Gaussian Dispersion

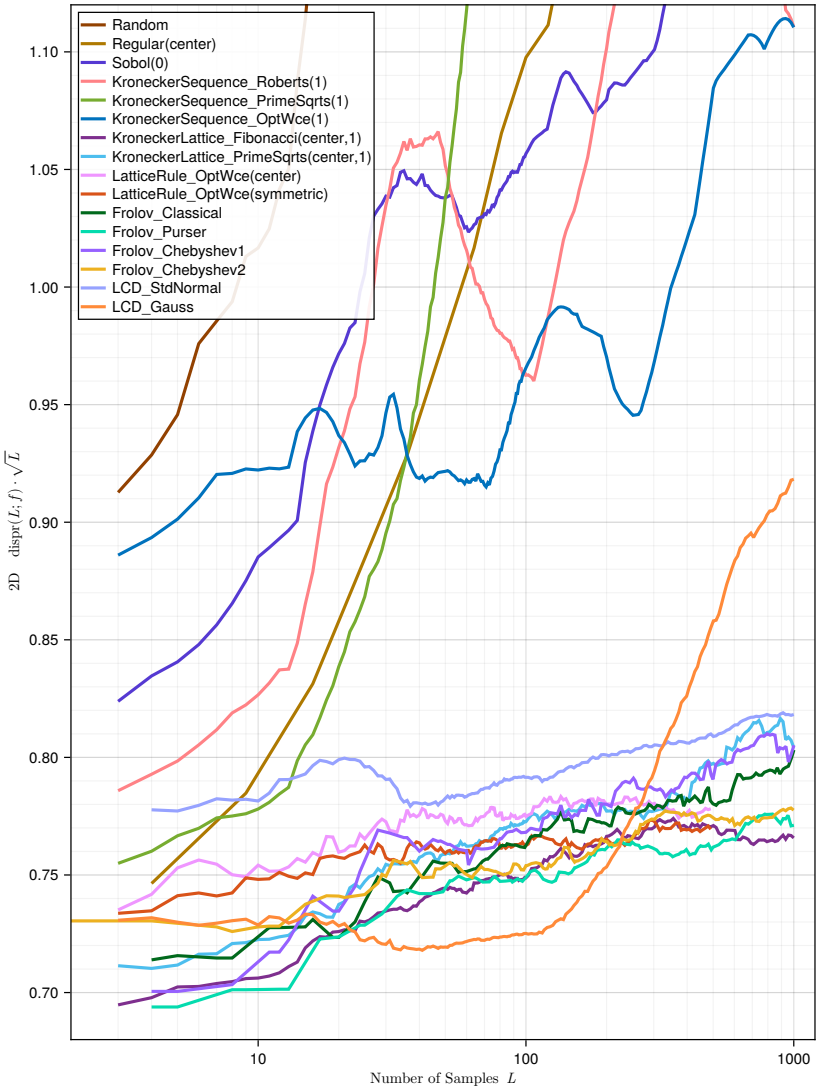

Figure A.8: 2D anisotropic Gaussian dispersion, Section 8.2.2.A. `KroneckerSequence_OptWce` with $L_{\max} = 177$. Smoothing for better readability (unsmoothed in Figure A.10).

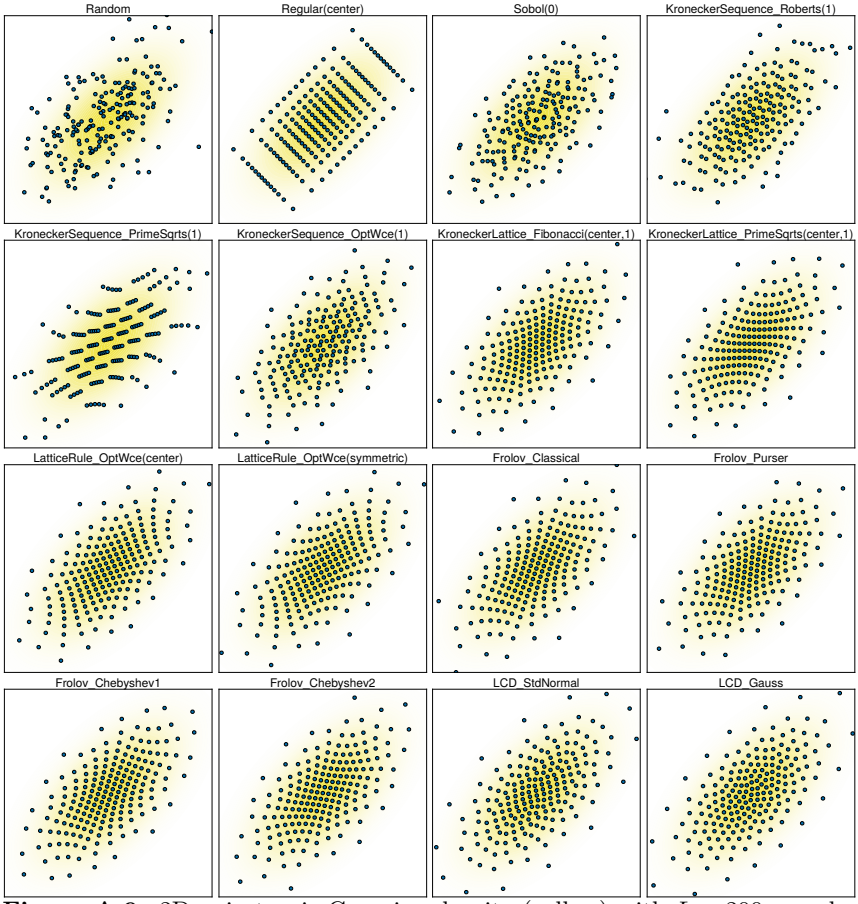

Figure A.9: 2D anisotropic Gaussian density (yellow) with $L \approx 200$ samples (blue).

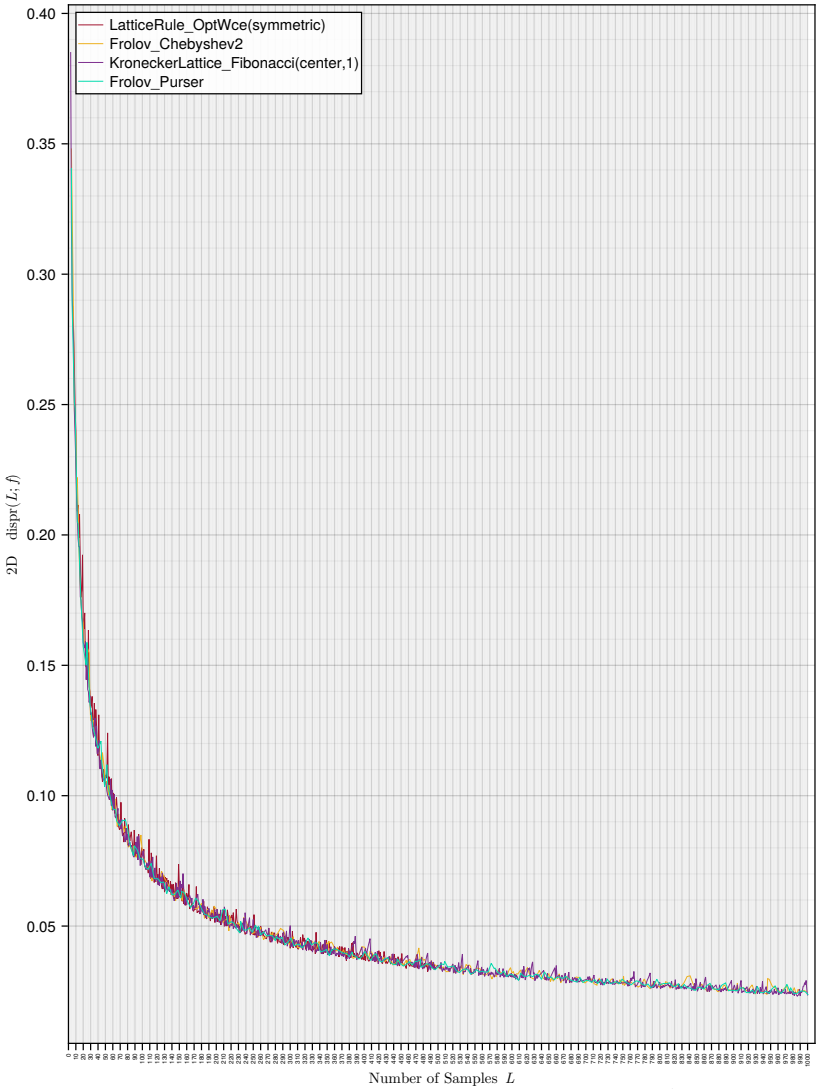

Figure A.10: 2D anisotropic Gaussian dispersion, Section 8.2.2.A. Best methods only, except `LCD_Gauss` due to computation time. No smoothing, zoom in to read.

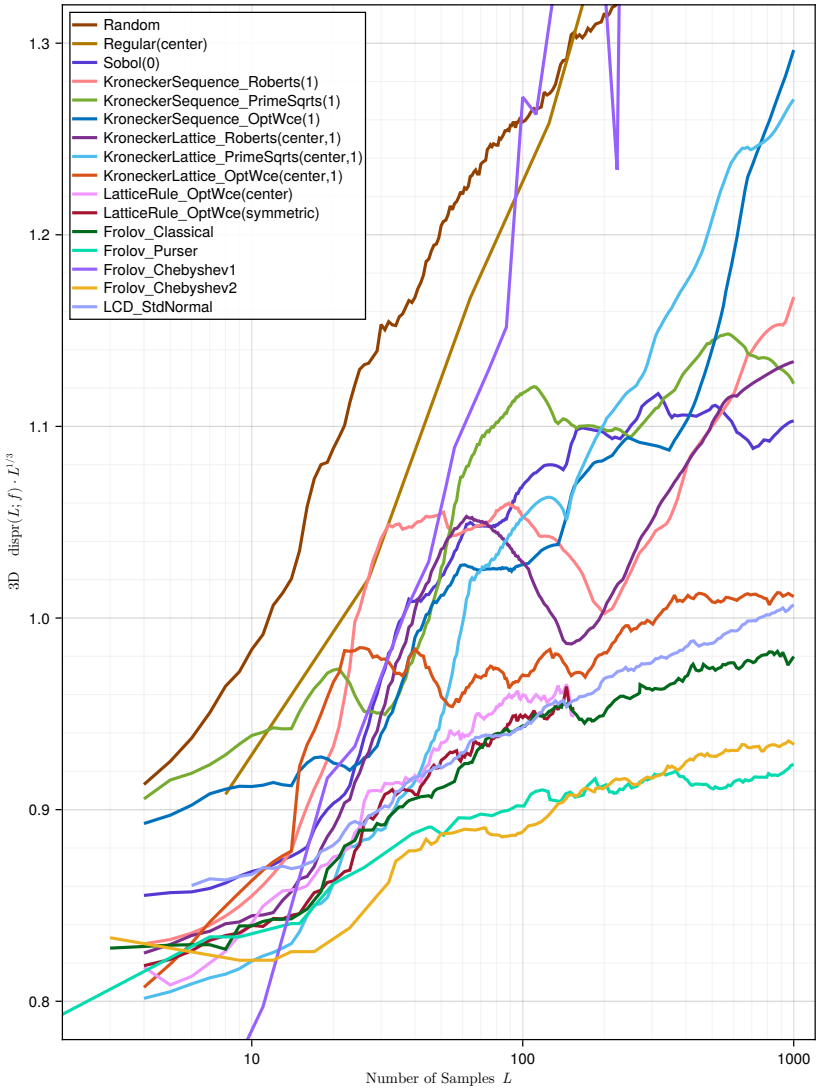

Figure A.11: 3D anisotropic Gaussian dispersion, Section 8.2.2.B. `KroneckerSequence_OptWce` with $L_{\max} = 73$. Smoothing for better readability (unsmoothed in Figure A.13).

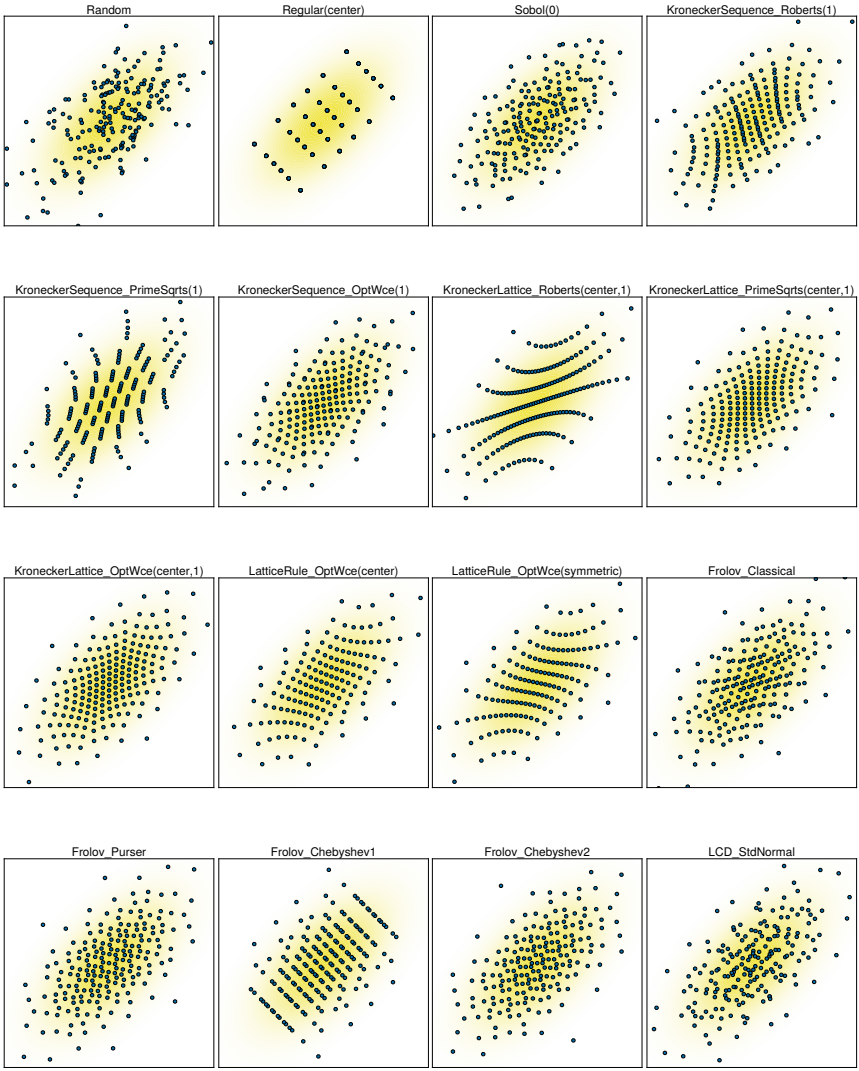

Figure A.12: 3D anisotropic Gaussian density (yellow) with $L \approx 200$ samples (blue). Projection along first two dimensions, x, y.

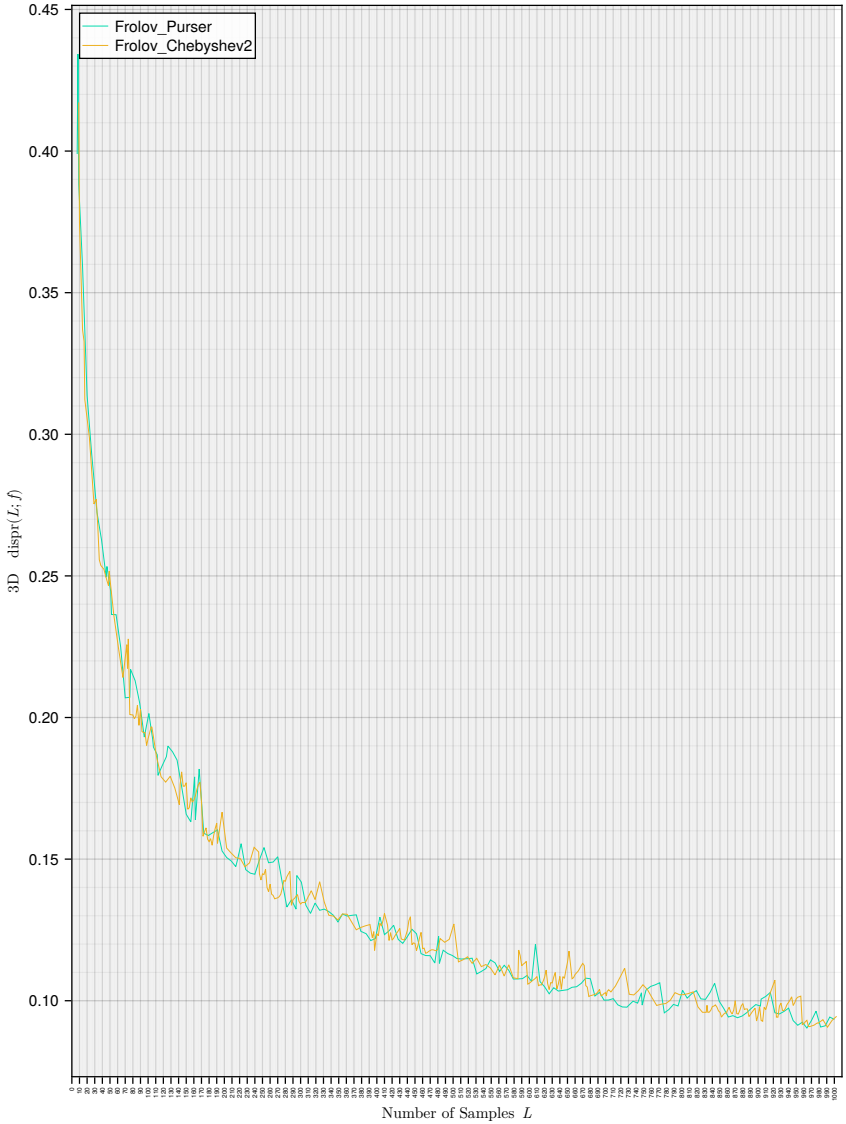

Figure A.13: 3D anisotropic Gaussian dispersion, Section 8.2.2.B. Best methods only. No smoothing, zoom in to read.

A.4 Periodic Worst-Case Error

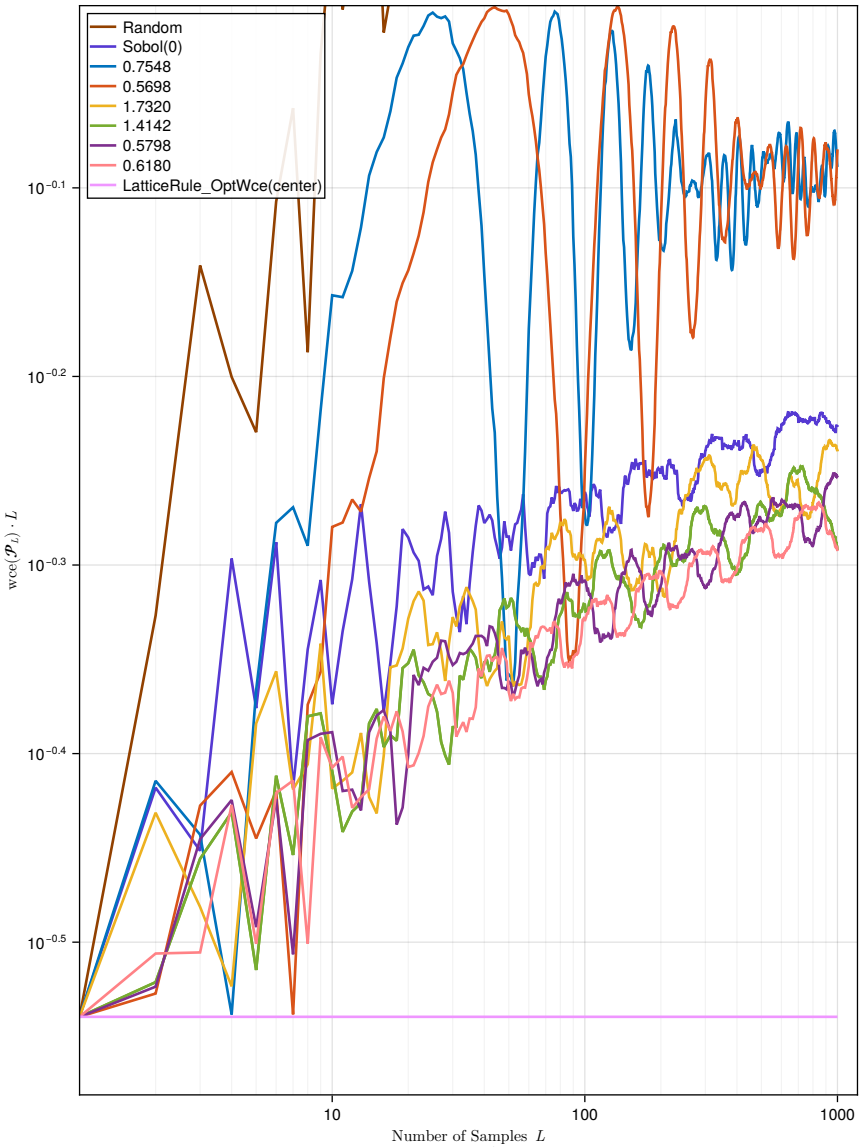

Figure A.14: 1D periodic wce, Section 8.3.1.A. Smoothing for better readability.

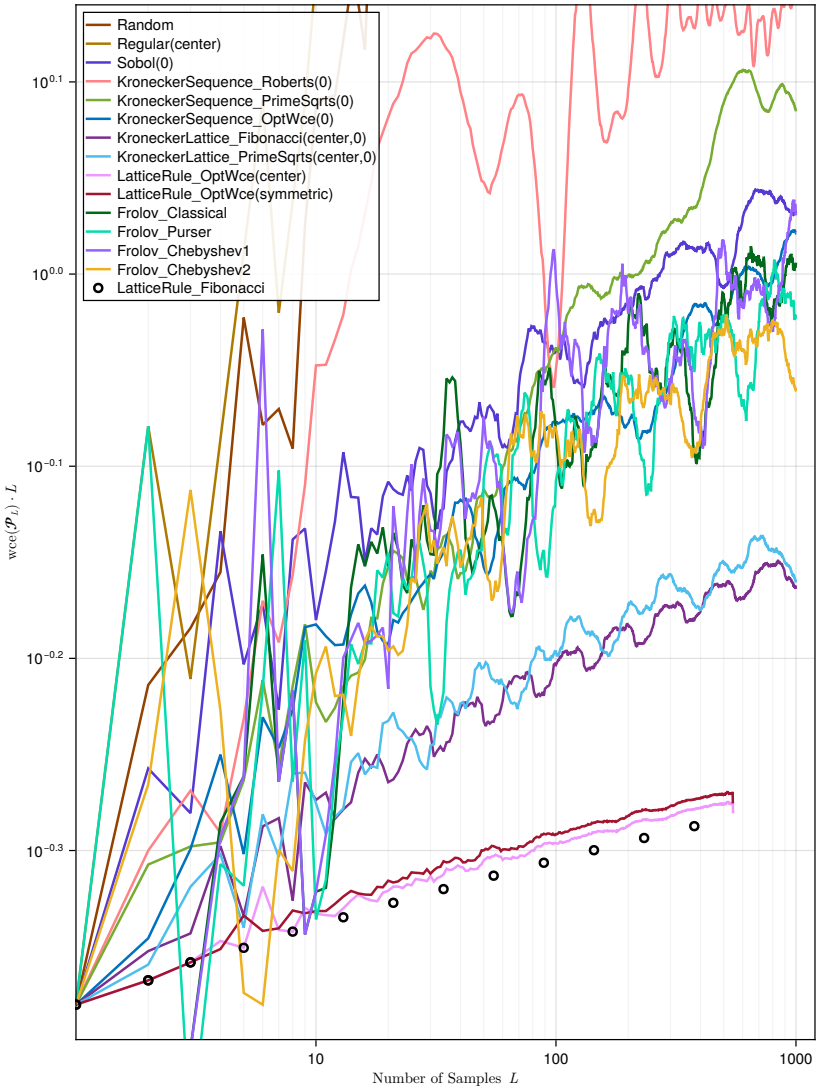

Figure A.15: 2D periodic wce, Section 8.3.1.B. Black dots indicate Fibonacci–rank-1 lattice. `KroneckerSequence_OptWce` with $L_{\max} = 177$. Smoothing for better readability.

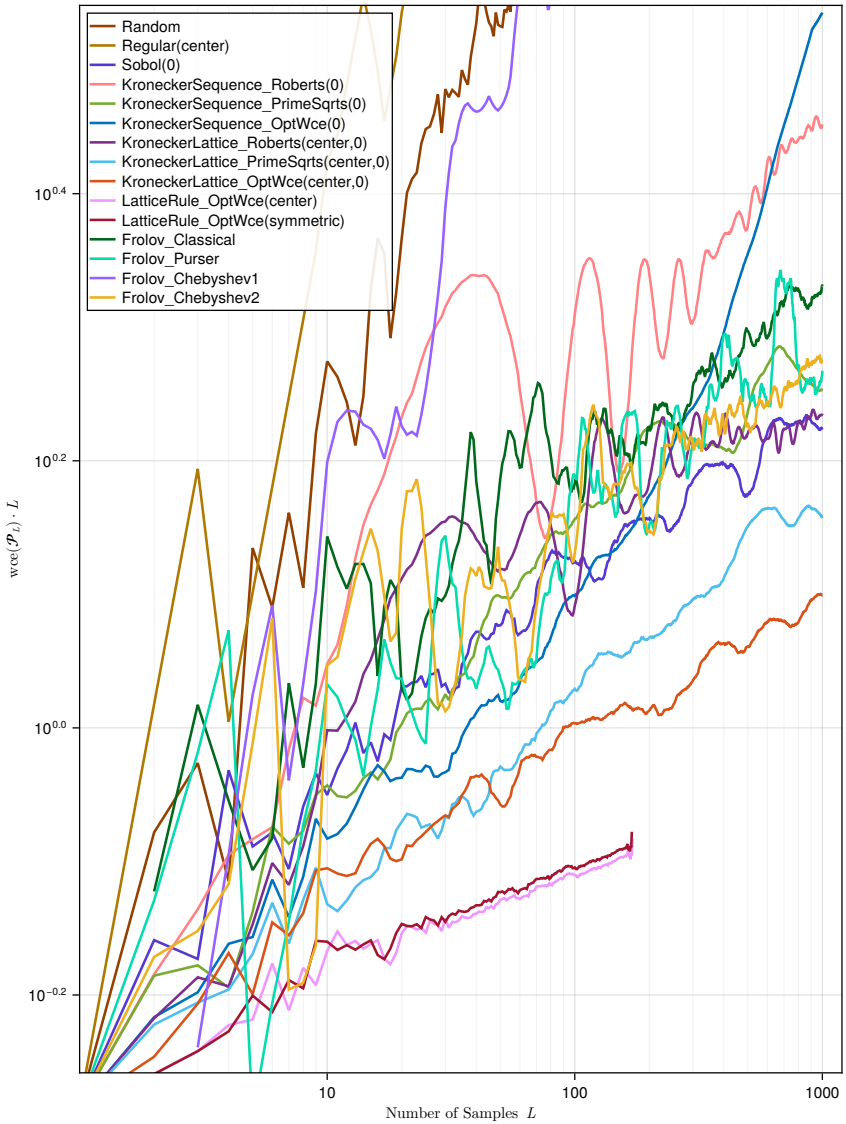

Figure A.16: 3D periodic wce, Section 8.3.1.C. `KroneckerSequence_OptWce` with $L_{\max} = 73$. Smoothing for better readability.

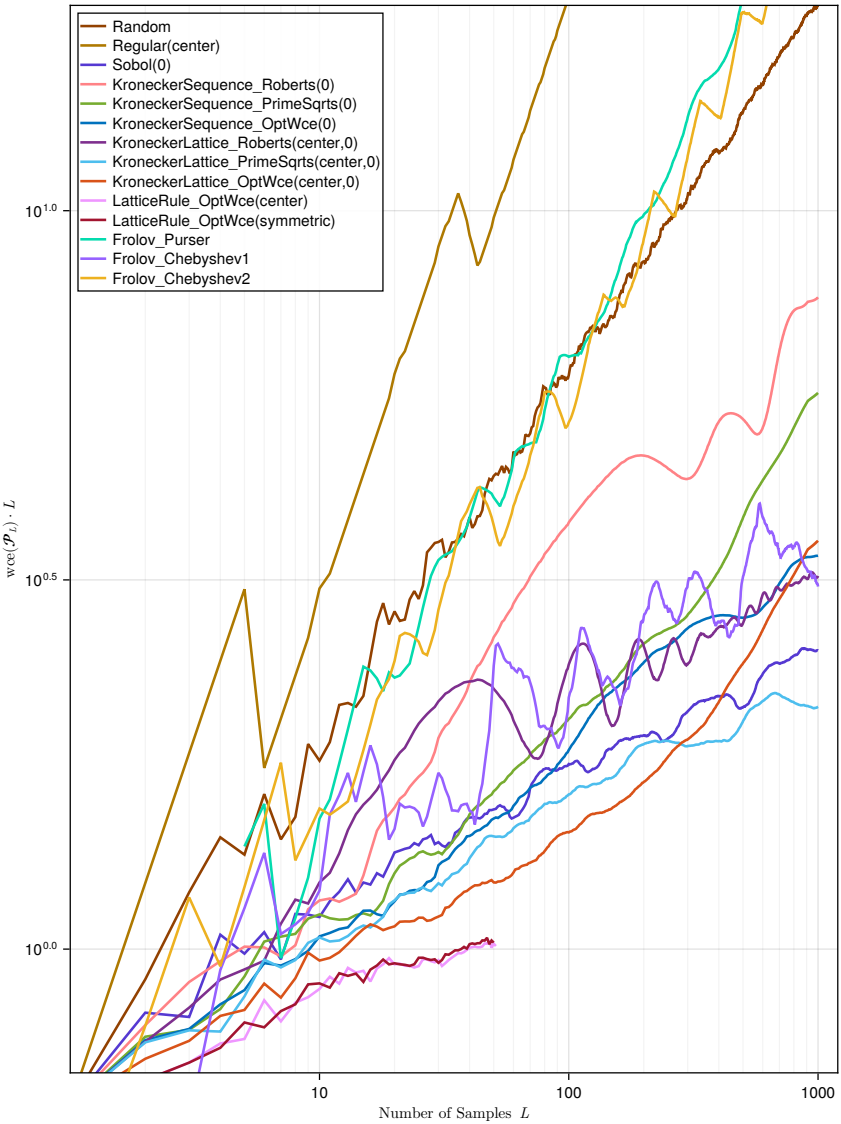

Figure A.17: 4D periodic wce. `KroneckerSequence_OptWce` with $L_{\max} = 31$. Smoothing for better readability.

A.5 Aperiodic Worst-Case Error

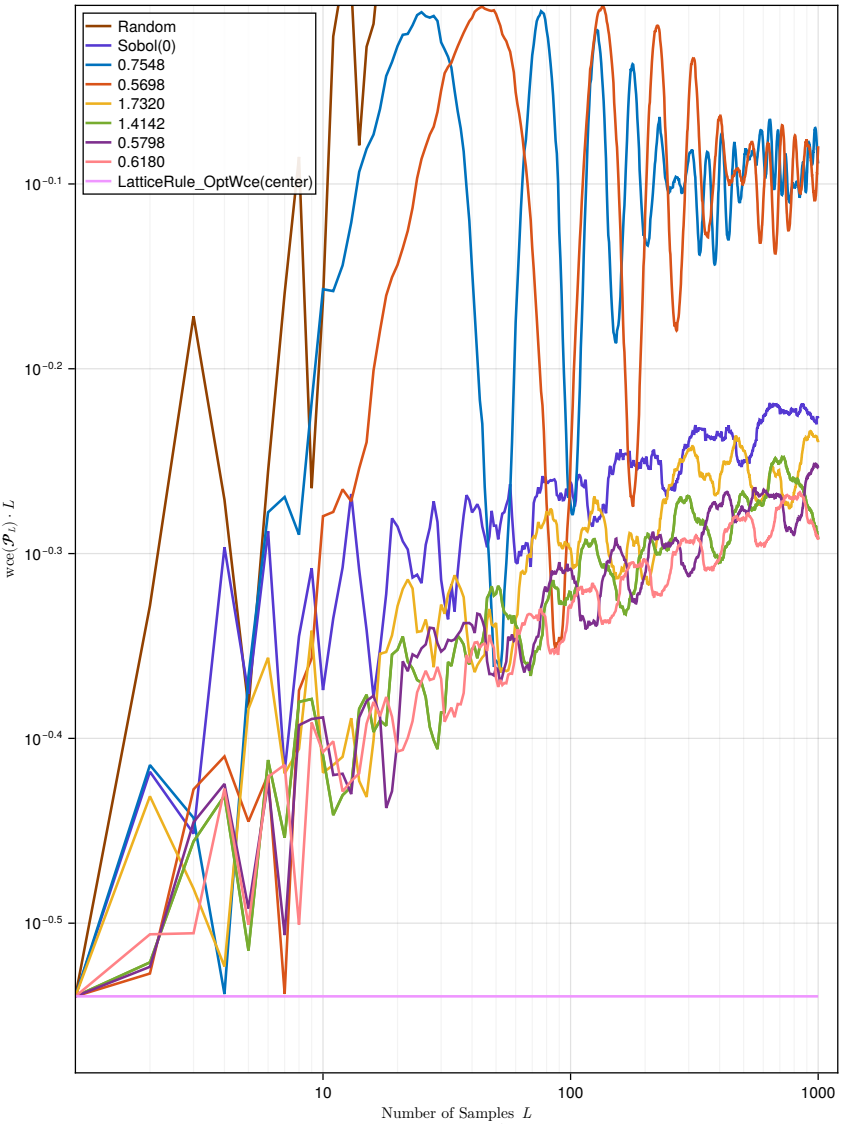

Figure A.18: 1D aperiodic wce, Section 8.4.1.A. Smoothing for better readability.

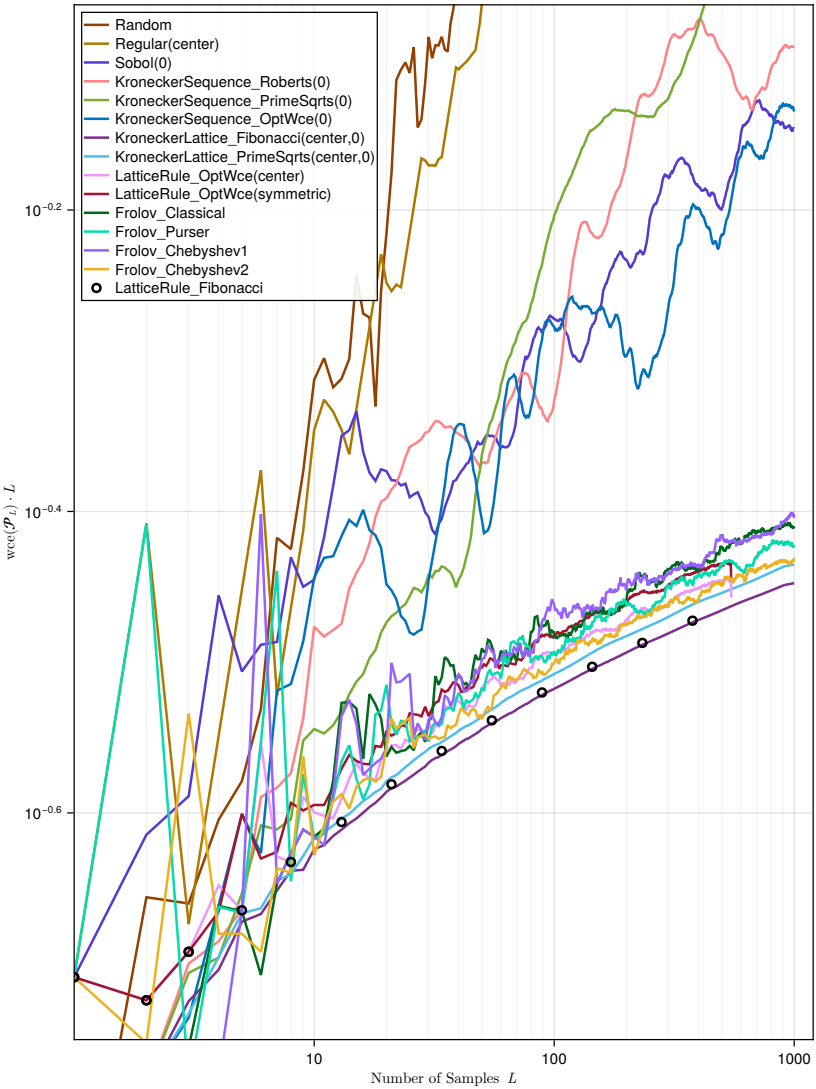

Figure A.19: 2D aperiodic wce, Section 8.4.1.B. Black dots indicate Fibonacci–rank-1 lattice. `KroneckerSequence_OptWce` with $L_{\max} = 177$. Smoothing for better readability.

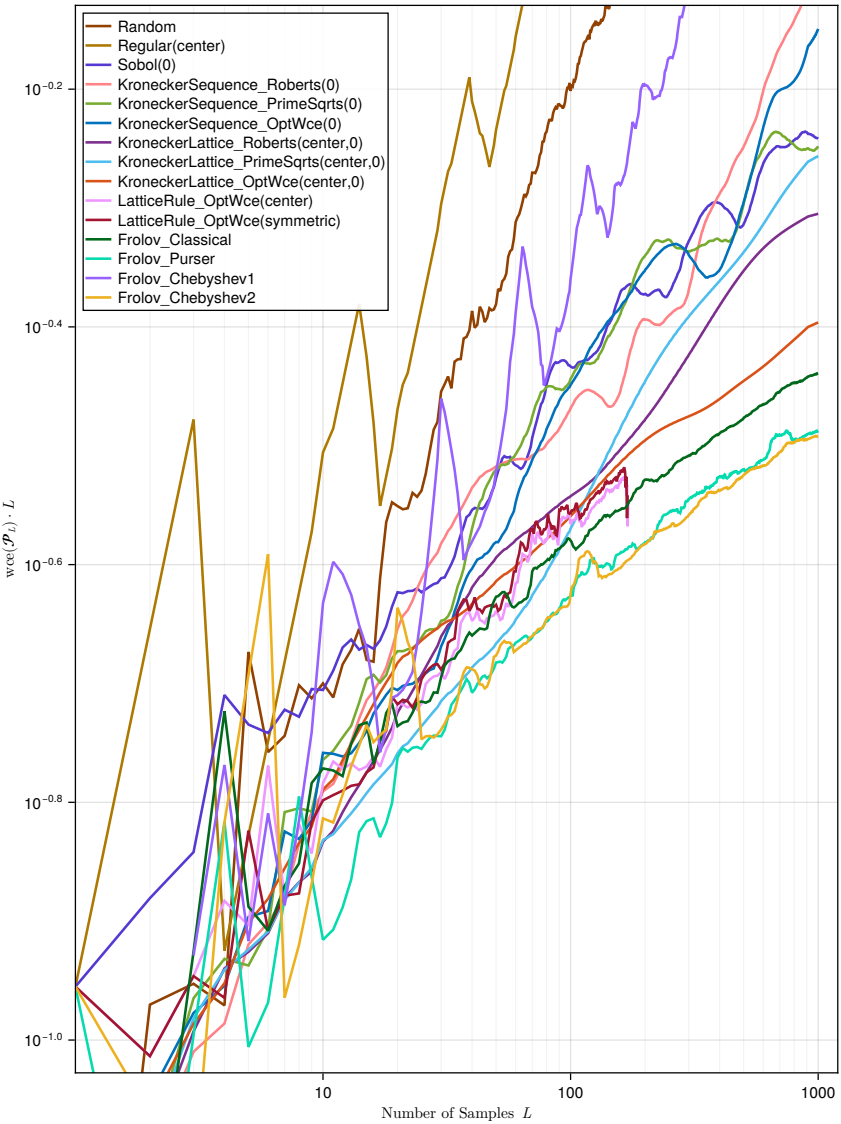

Figure A.20: 3D aperiodic wce, Section 8.4.1.C. `KroneckerSequence_OptWce` with $L_{\max} = 73$. Smoothing for better readability.

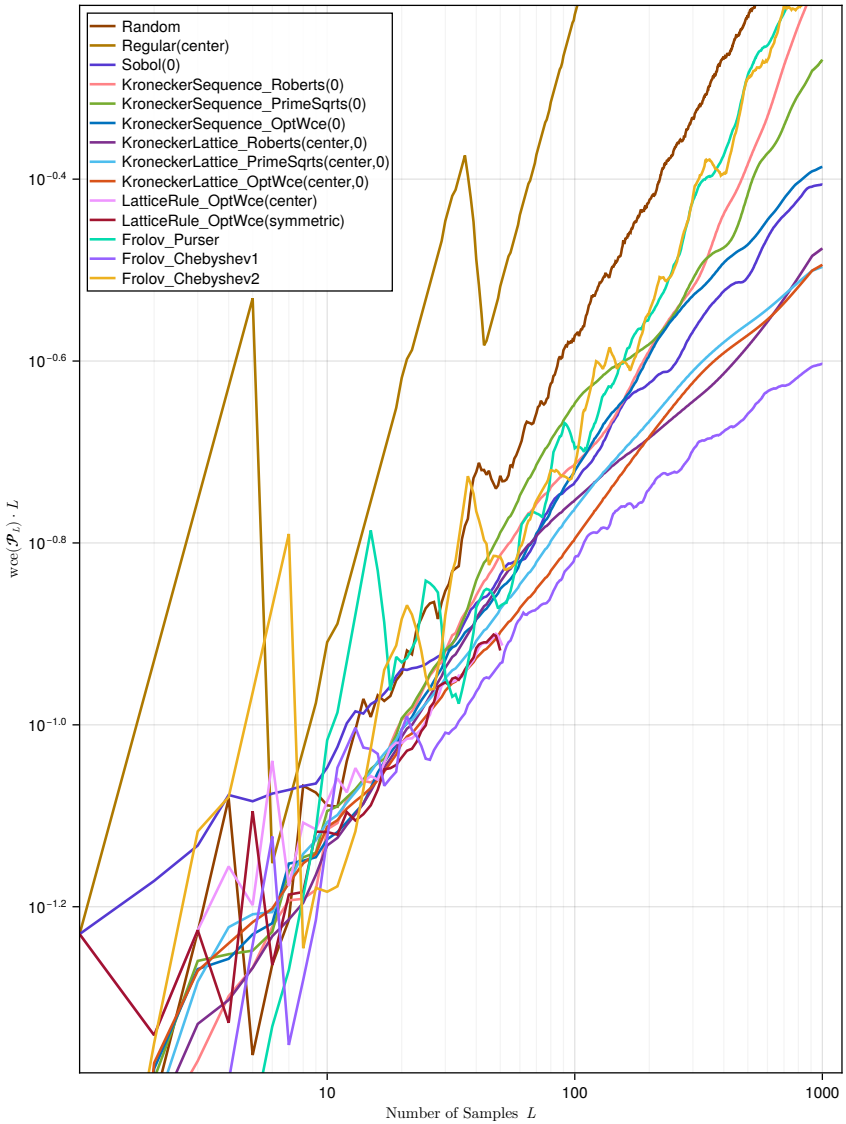

Figure A.21: 4D aperiodic wce. `KroneckerSequence_OptWce` with $L_{\max} = 31$. Smoothing for better readability.

APPENDIX B

Visualization of Point Sets

Contents

> Use a picture.
> It's worth a thousand words.
>
> Arthur Brisbane (1864–1936)

B.1 2D Uniform Point Sets

For each construction method of uniform point sets in $s = 2$, we show a matrix of figures with different numbers of samples L. Unless stated otherwise, L increases with a fixed increment $\Delta L = 5$ between two entries from left to right and top to bottom, varying from $L = 5$ to $L = 100$.

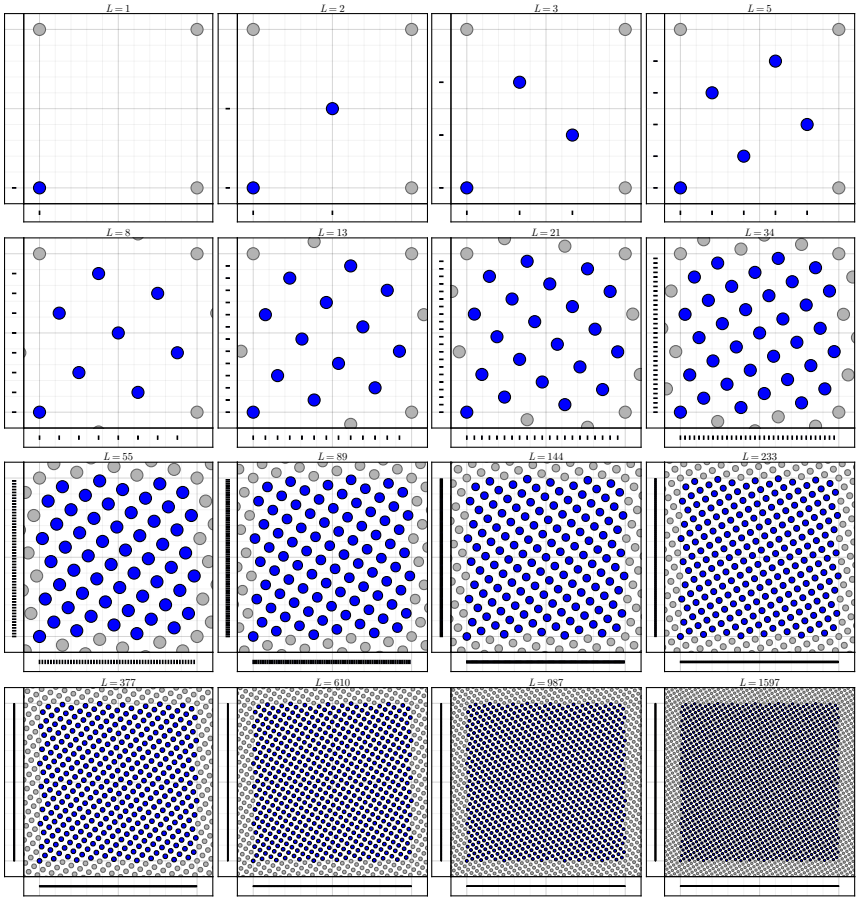

Figure B.1: Fibonacci–rank 1 lattice (3.27), $L = \{1, 2, 3, 5, 8, 13, 21, 34, 55, 89, 144, 233, 377, 610, 987, 1597\}$.

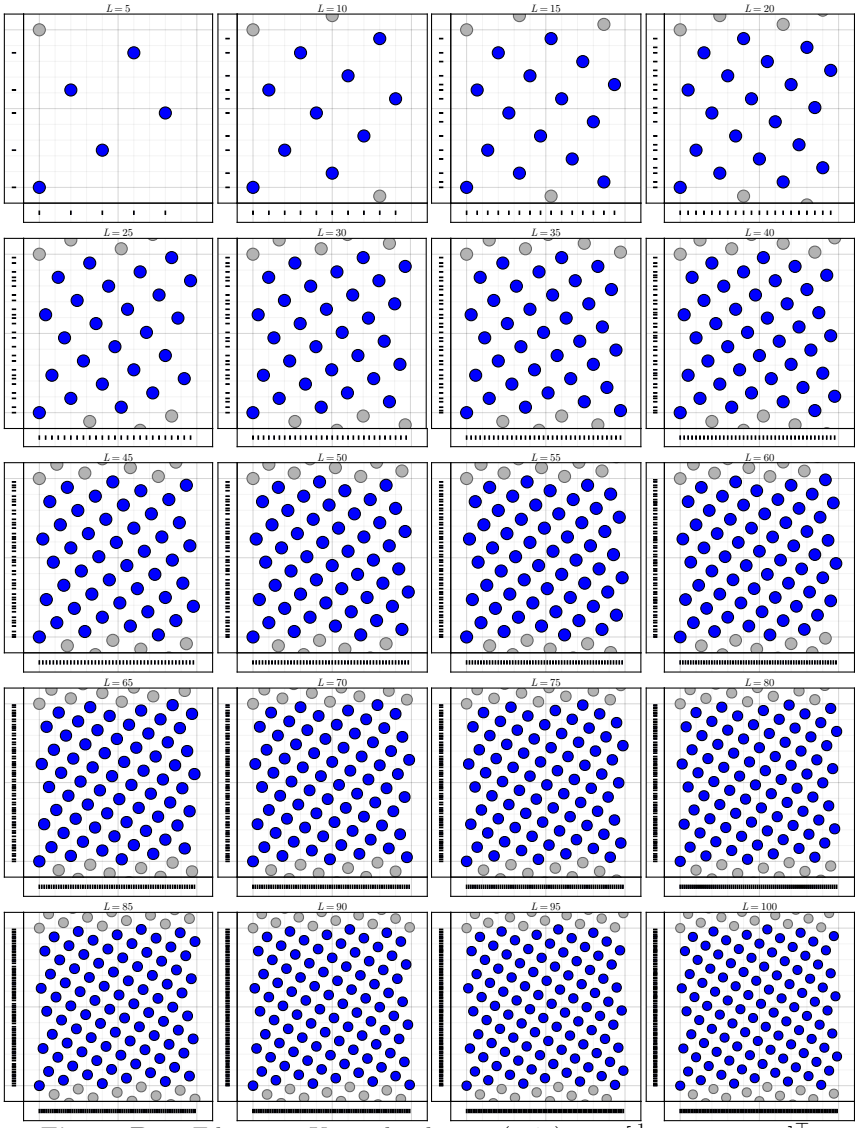

Figure B.2: Fibonacci–Kronecker lattice (3.41), $\underline{g} = [\frac{1}{L}, 0.618033\ldots]^\top$.

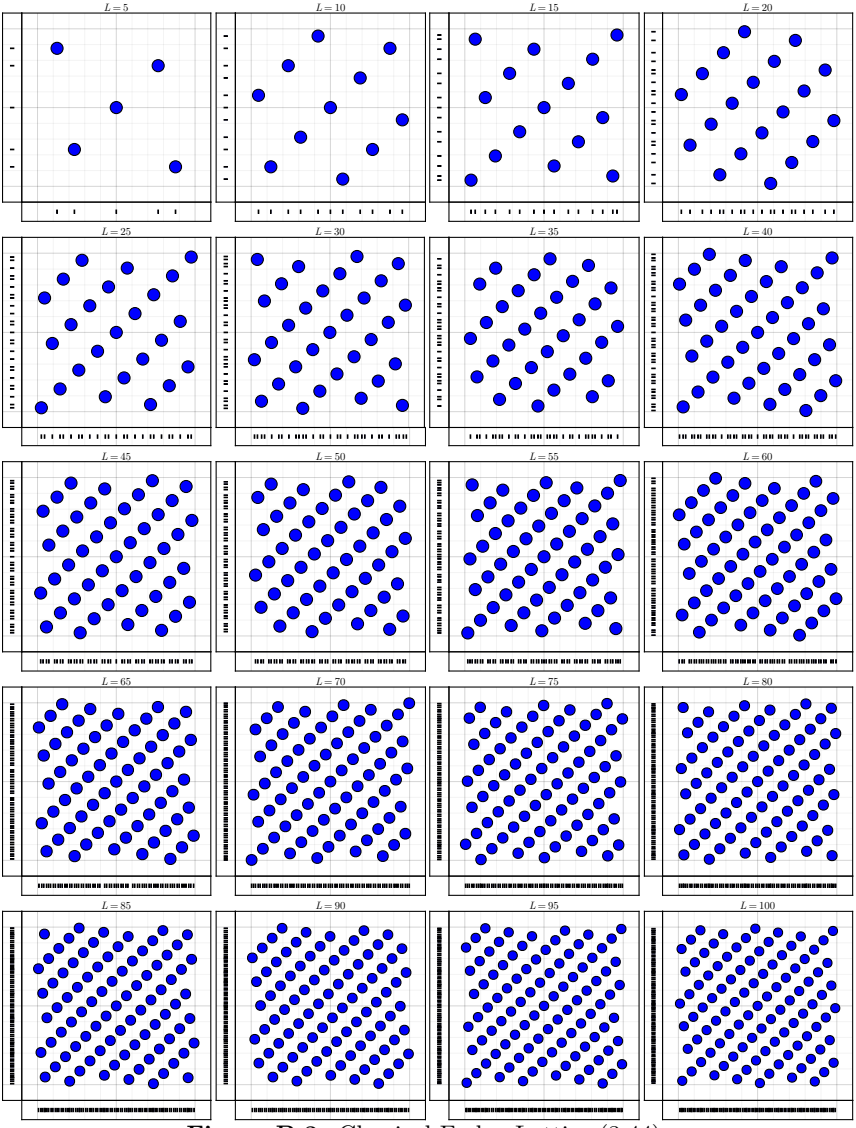

Figure B.3: Classical Frolov Lattice (3.44).

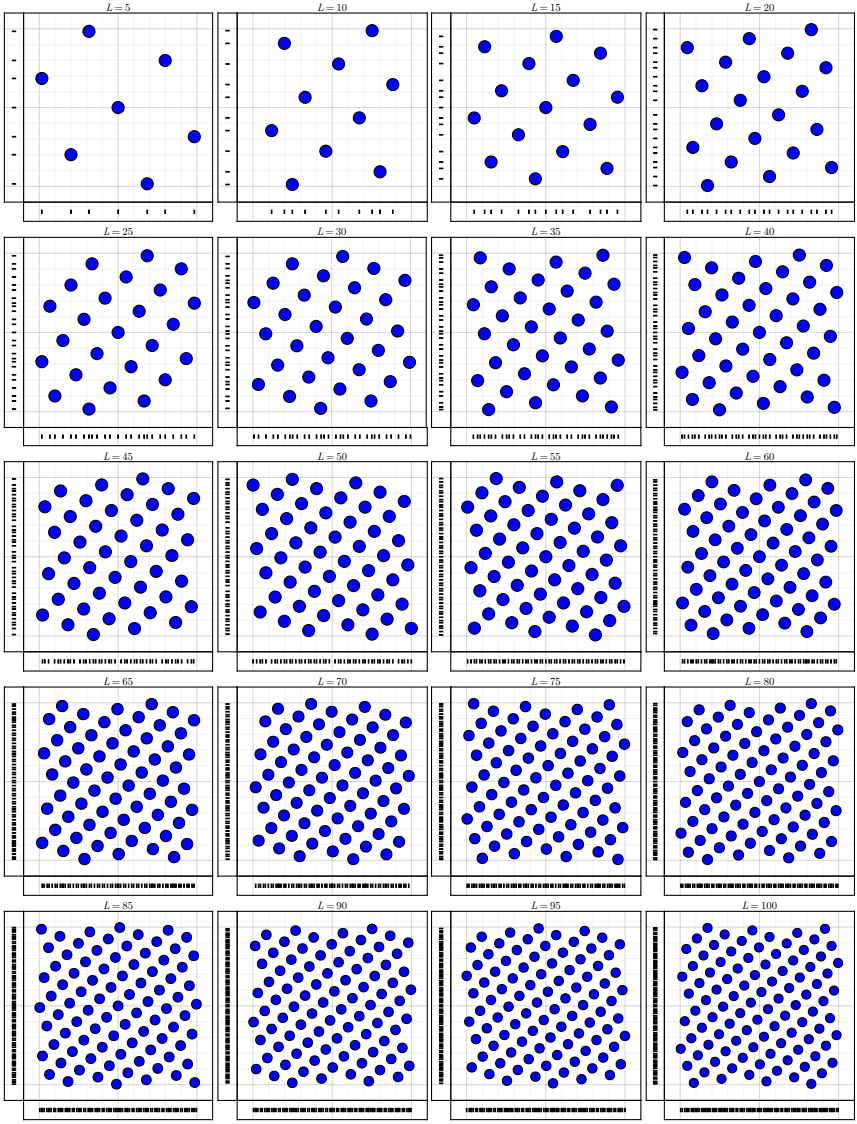

Figure B.4: Frolov Lattice from Chebyshev polynomials of second kind (3.59).

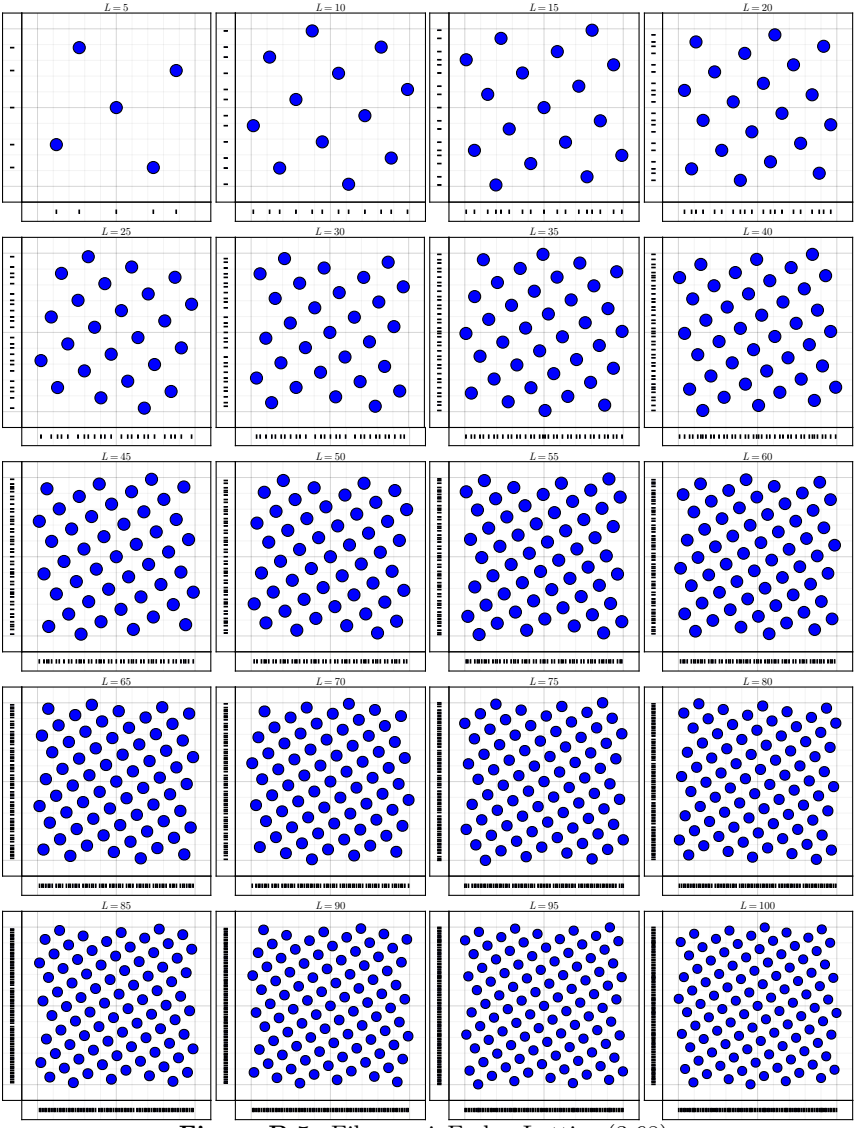

Figure B.5: Fibonacci–Frolov Lattice (3.68).

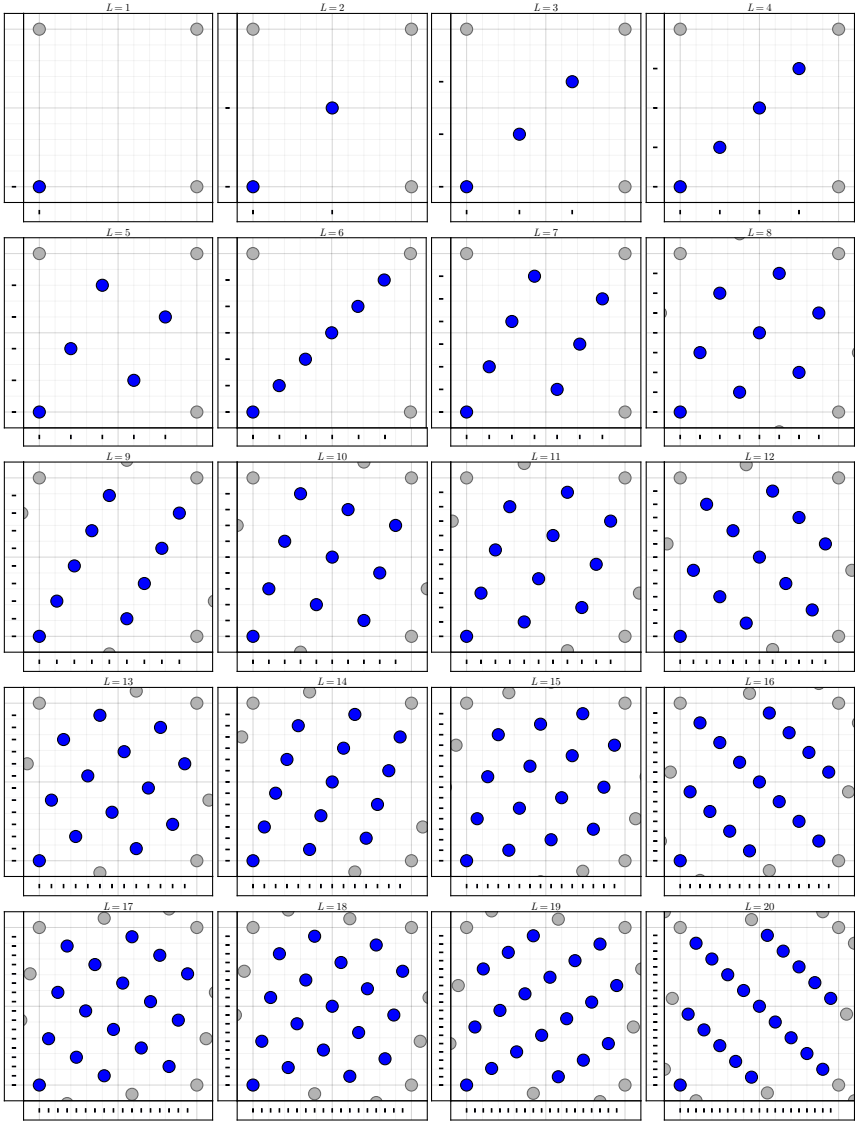

Figure B.6: Rank-1 lattices (5.40) with globally minimal wce (5.31). $L \in [1, 20]$, $\Delta L = 1$.

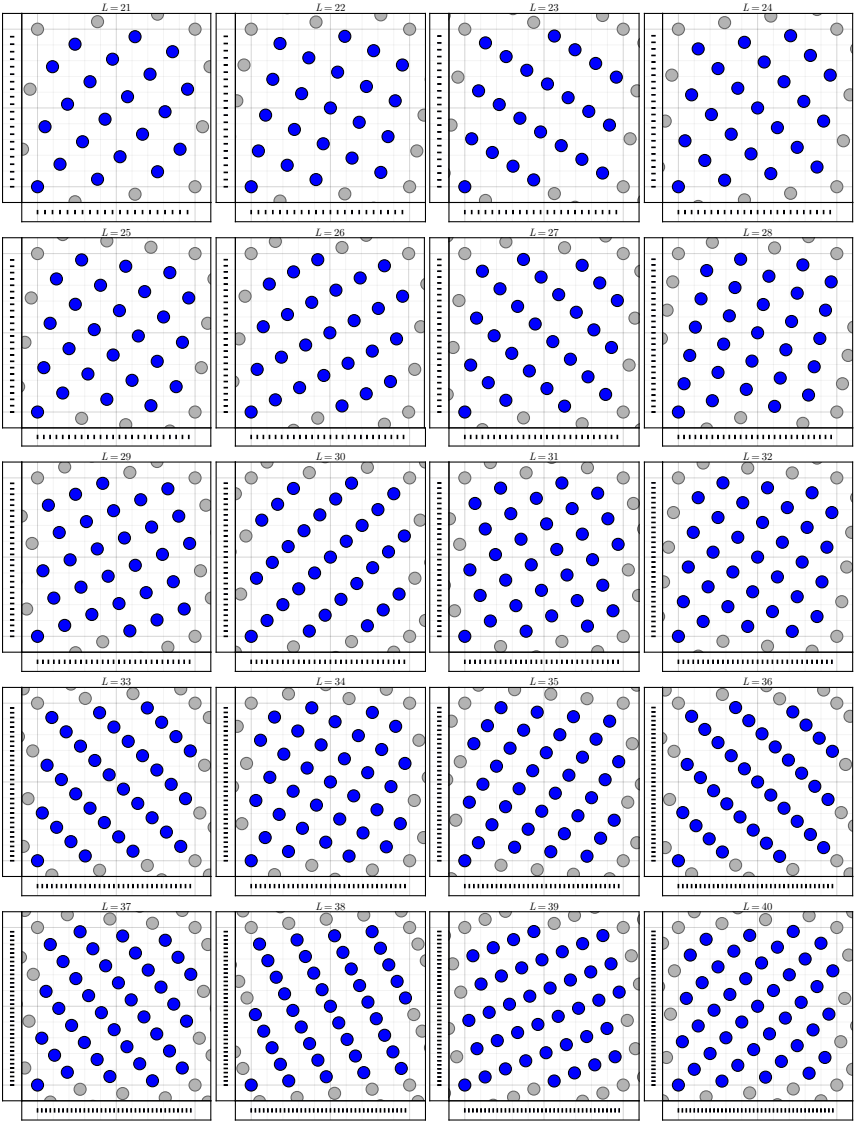

Figure B.7: Rank-1 lattices (5.40) with globally minimal wce (5.31). $L \in [21, 40]$, $\Delta L = 1$.

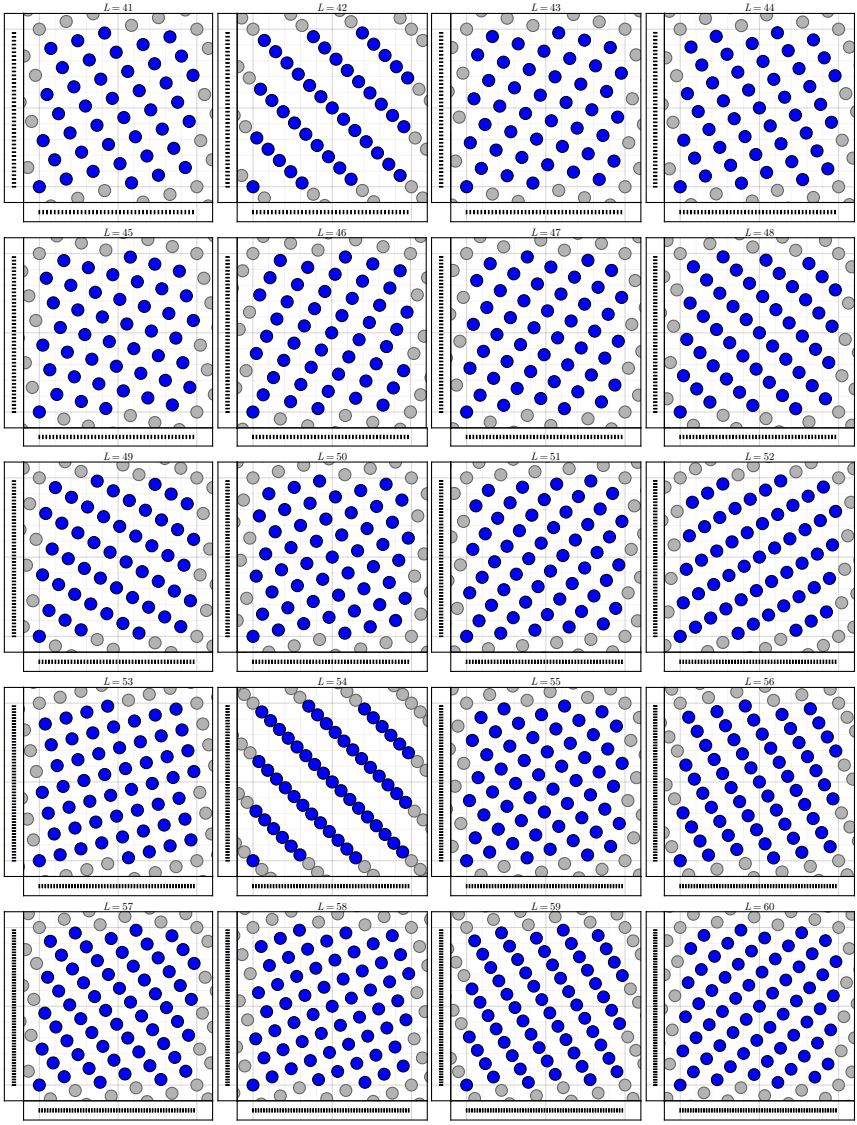

Figure B.8: Rank-1 lattices (5.40) with globally minimal wce (5.31). $L \in [41, 60]$, $\Delta L = 1$.

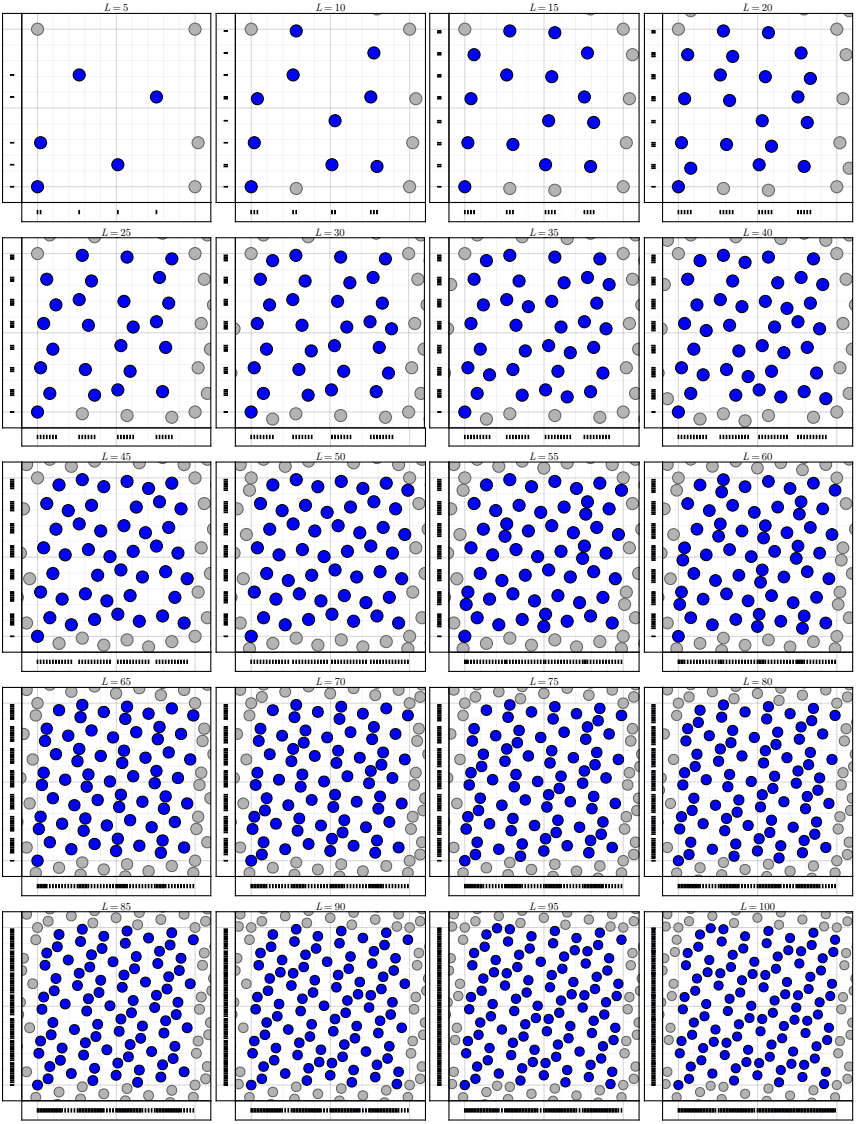

Figure B.9: Plastic ratio / R_2 Kronecker sequence (3.38), $\underline{a} = [0.754877\ldots, 0.569840\ldots]^\top$.

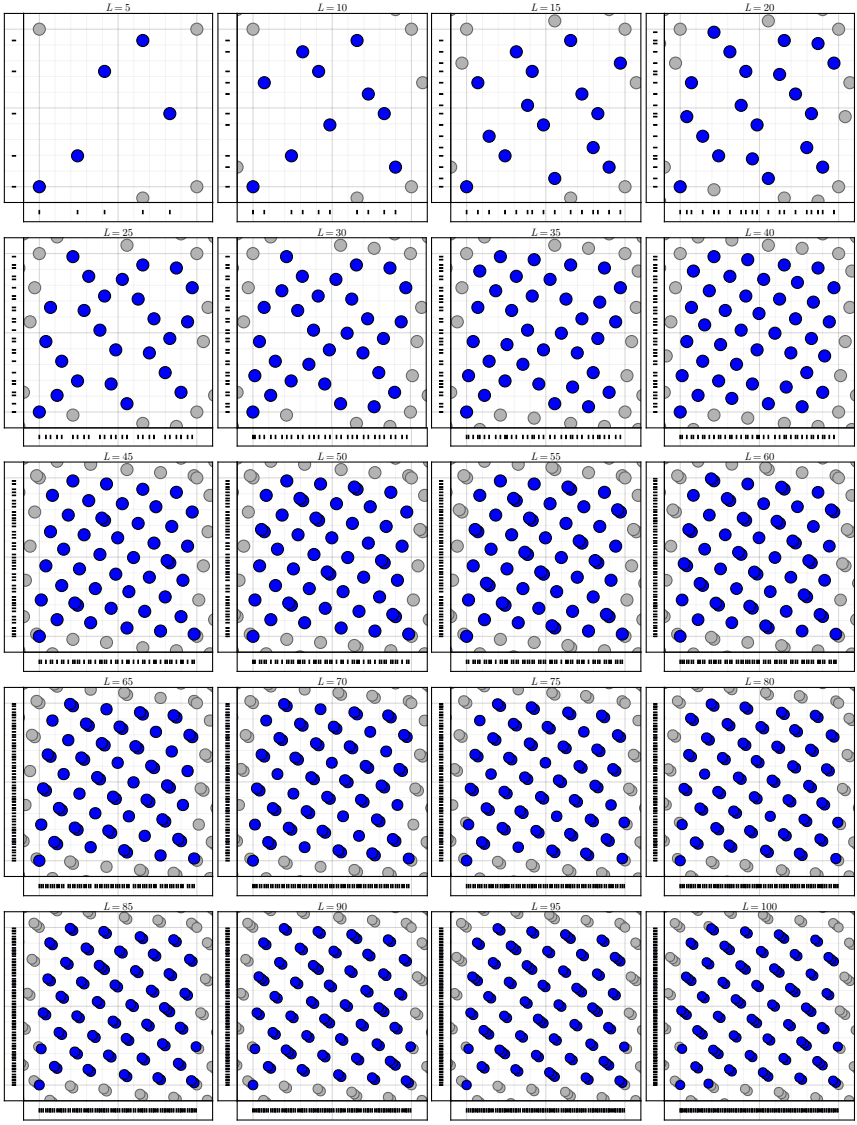

Figure B.10: Square of Primes Kronecker sequence (3.39), $\underline{a} = [1.414213\ldots, 1.732050\ldots]^\top$.

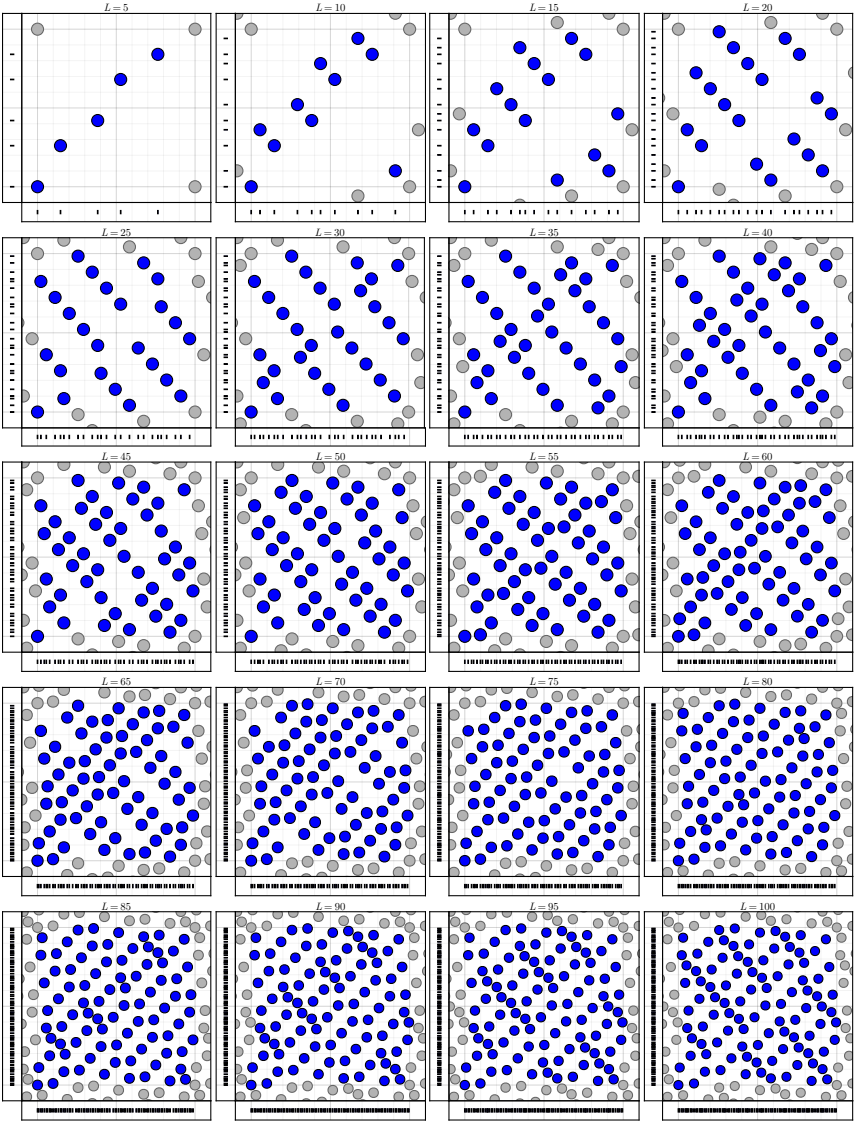

Figure B.11: Optimized wce Kronecker sequence (5.43), $\underline{a} = [0.579800\ldots, 0.618030\ldots]^\top$. $L_{\max} = 177$.

B.2 3D Uniform Point Sets

For each construction method of uniform point sets in $s = 3$, we show a matrix of 2D marginals with different numbers of samples L. Each row from left to right shows the $(x, y), (x, z)$, and (y, z)-marginal. From top to bottom, we show increasing numbers of samples $L = \{20, 40, 60, 80, 100\}$.

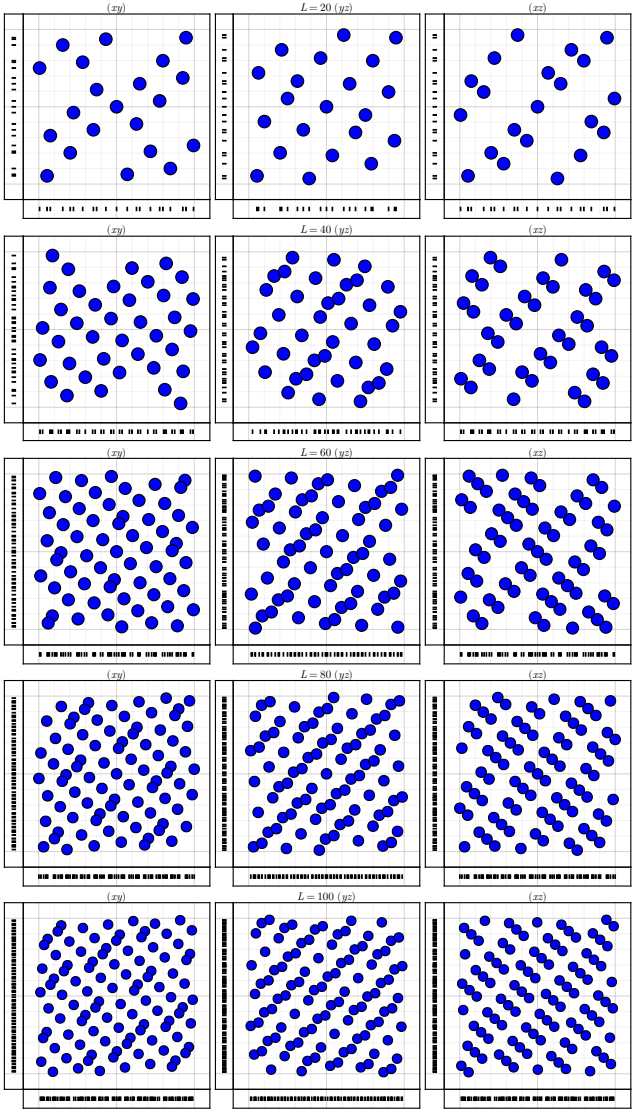

Figure B.12: Classical Frolov Lattice (3.45).

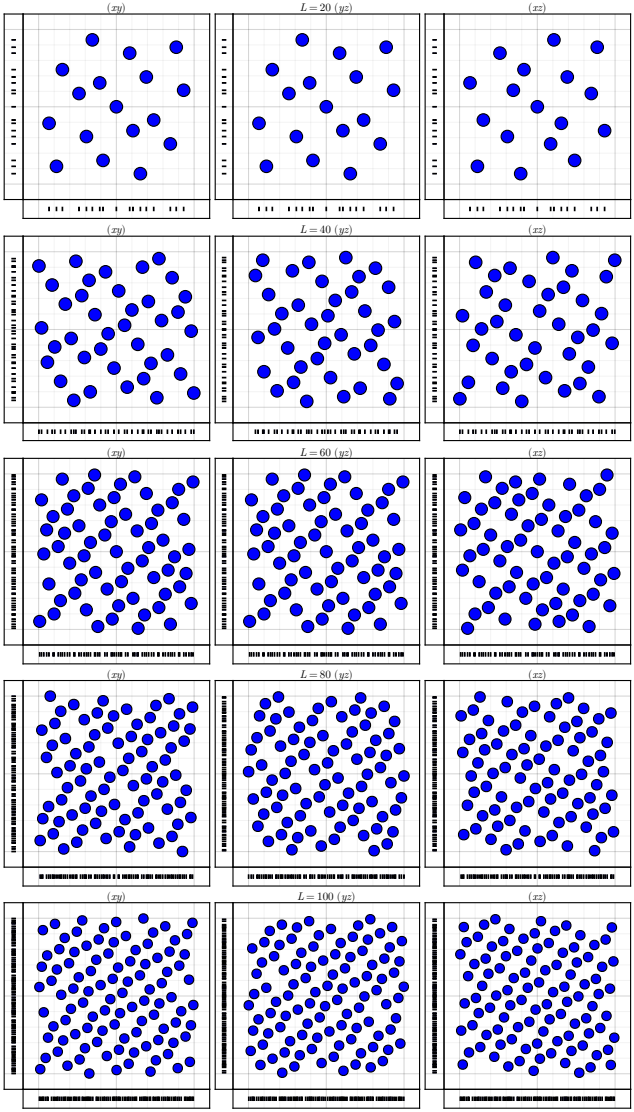

Figure B.13: Frolov Lattice from Chebyshev polynomials of second kind (3.60).

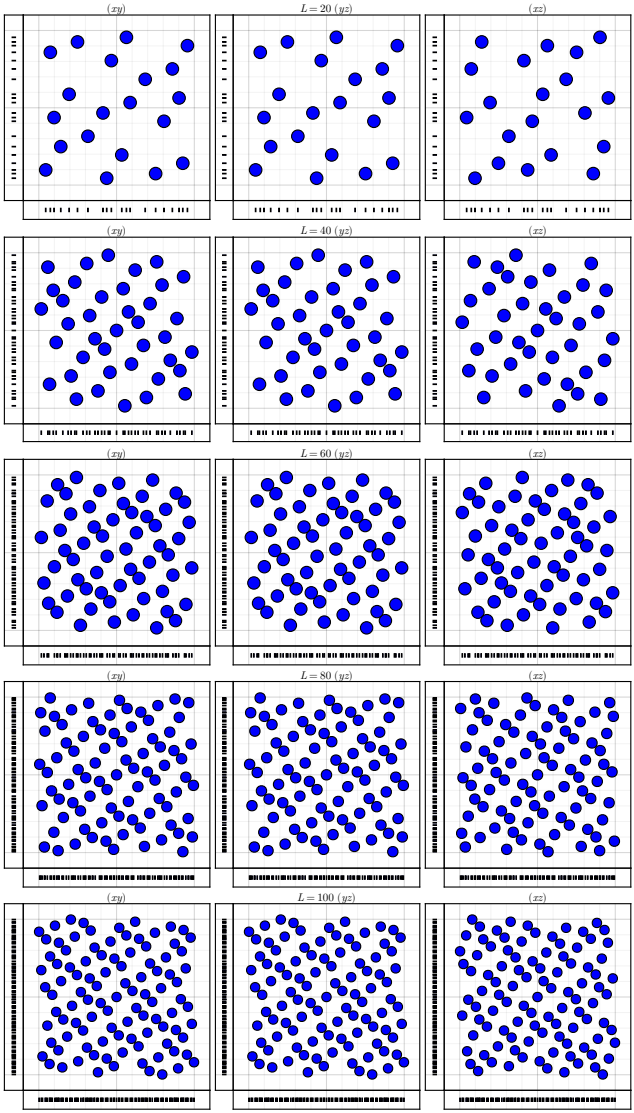

Figure B.14: Fibonacci–Frolov Lattice (4.29).

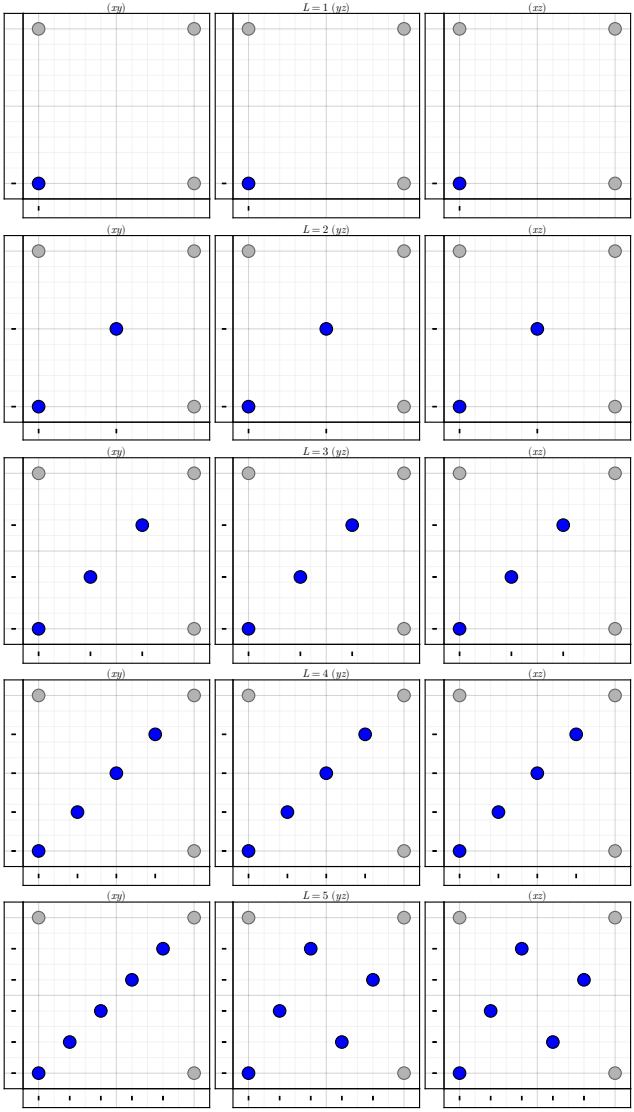

Figure B.15: Rank-1 lattices (5.41) with globally minimal wce (5.31). $L \in [1, 5]$, $\Delta L = 1$.

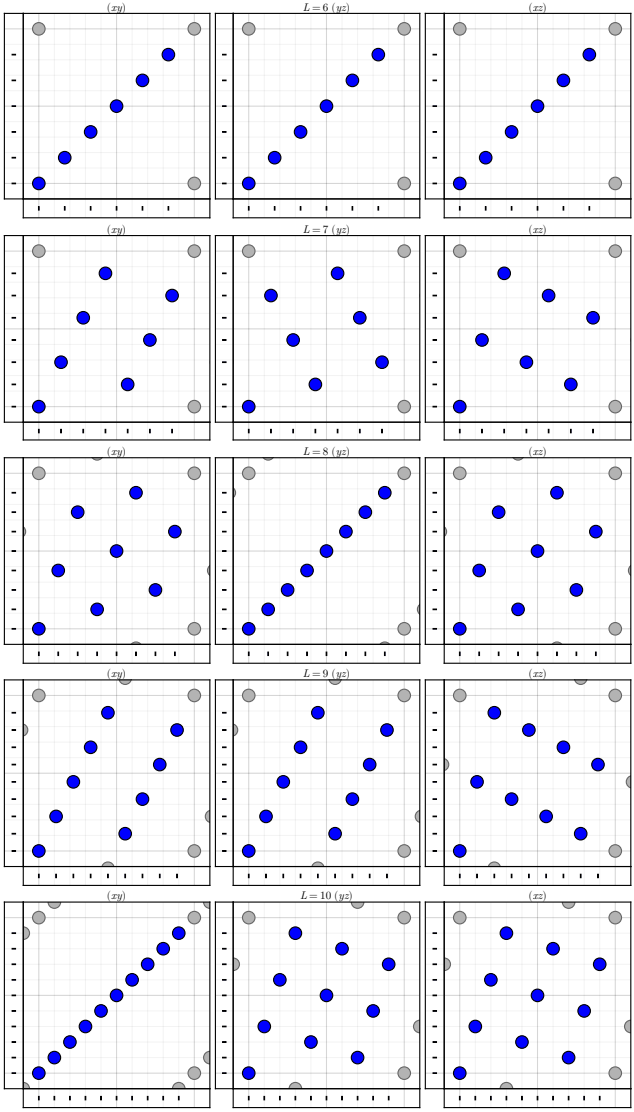

Figure B.16: Rank-1 lattices (5.41) with globally minimal wce (5.31). $L \in [6, 10]$, $\Delta L = 1$.

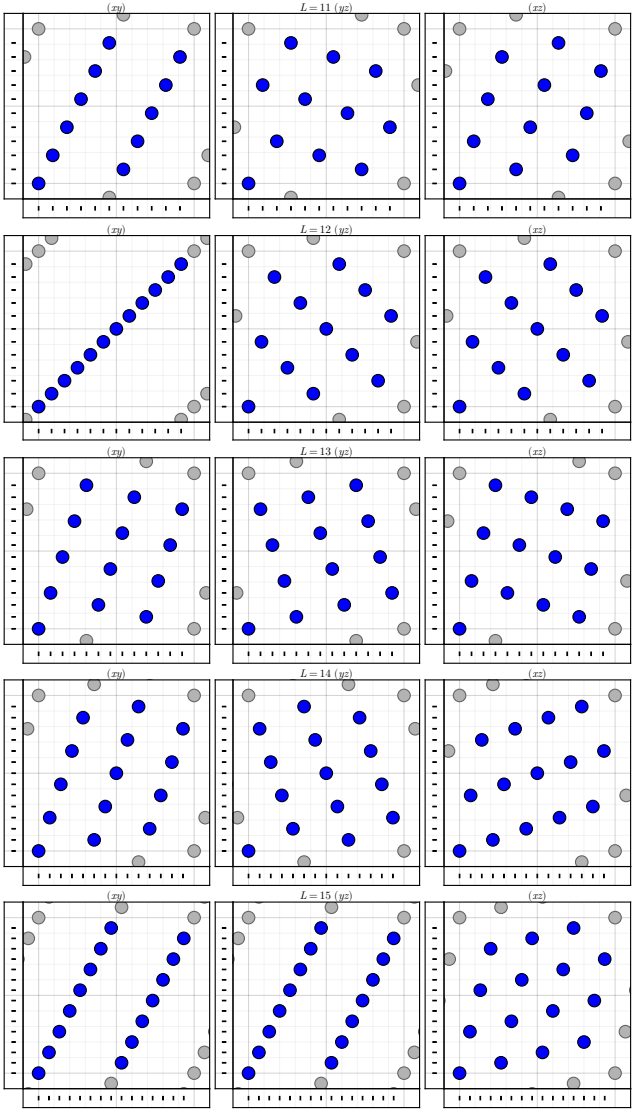

Figure B.17: Rank-1 lattices (5.41) with globally minimal wce (5.31). $L \in [11, 15]$, $\Delta L = 1$.

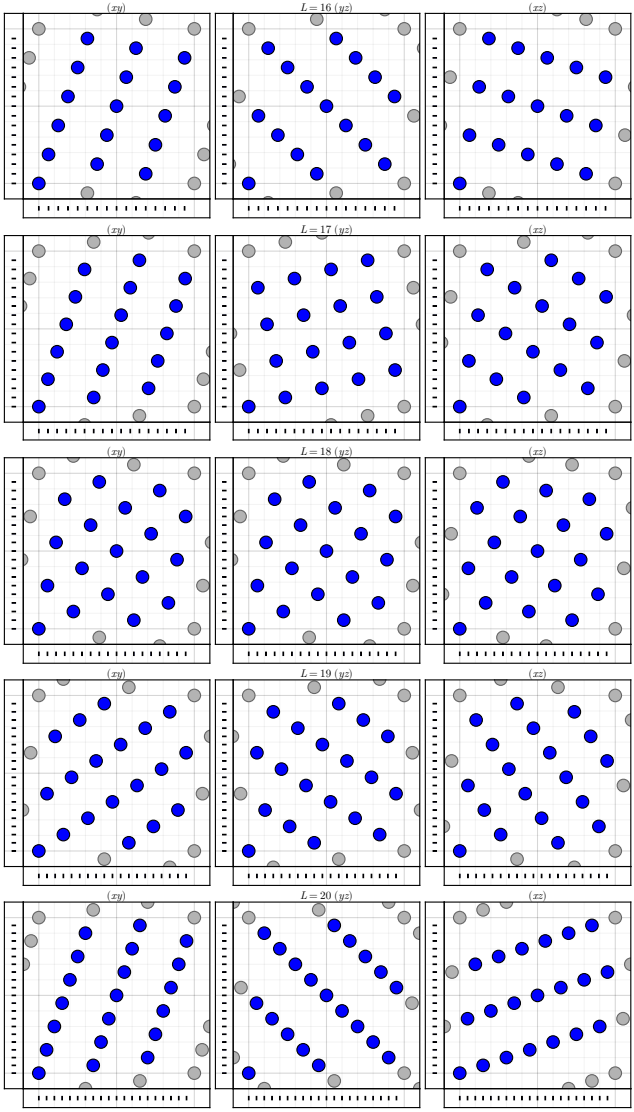

Figure B.18: Rank-1 lattices (5.41) with globally minimal wce (5.31). $L \in [16, 20]$, $\Delta L = 1$.

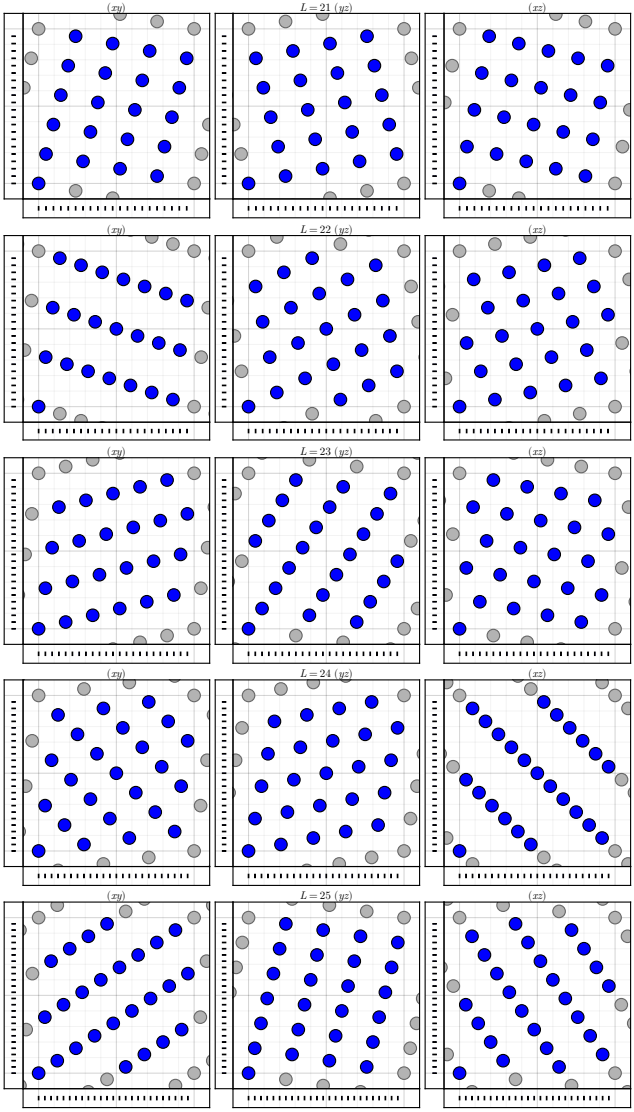

Figure B.19: Rank-1 lattices (5.41) with globally minimal wce (5.31). $L \in [21, 25]$, $\Delta L = 1$.

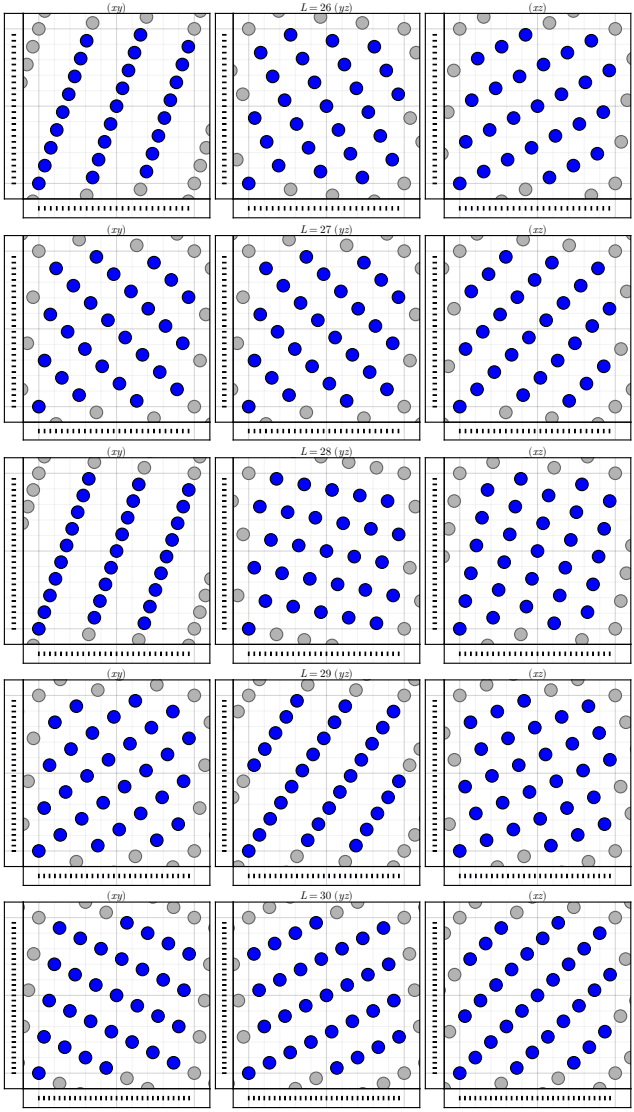

Figure B.20: Rank-1 lattices (5.41) with globally minimal wce (5.31). $L \in [26, 30]$, $\Delta L = 1$.

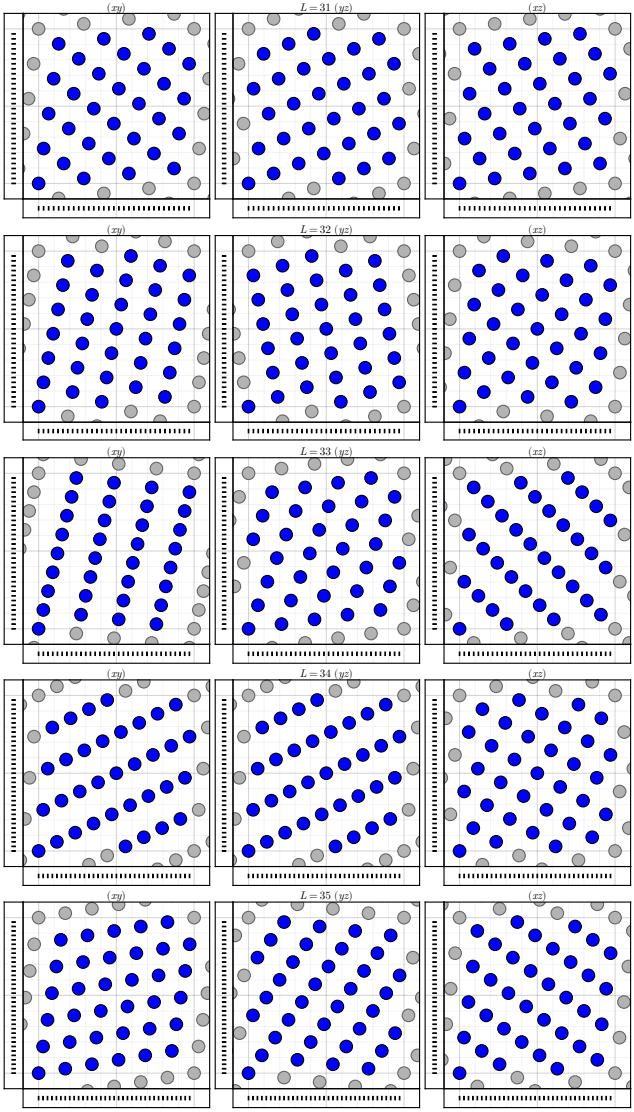

Figure B.21: Rank-1 lattices (5.41) with globally minimal wce (5.31). $L \in [31, 35]$, $\Delta L = 1$.

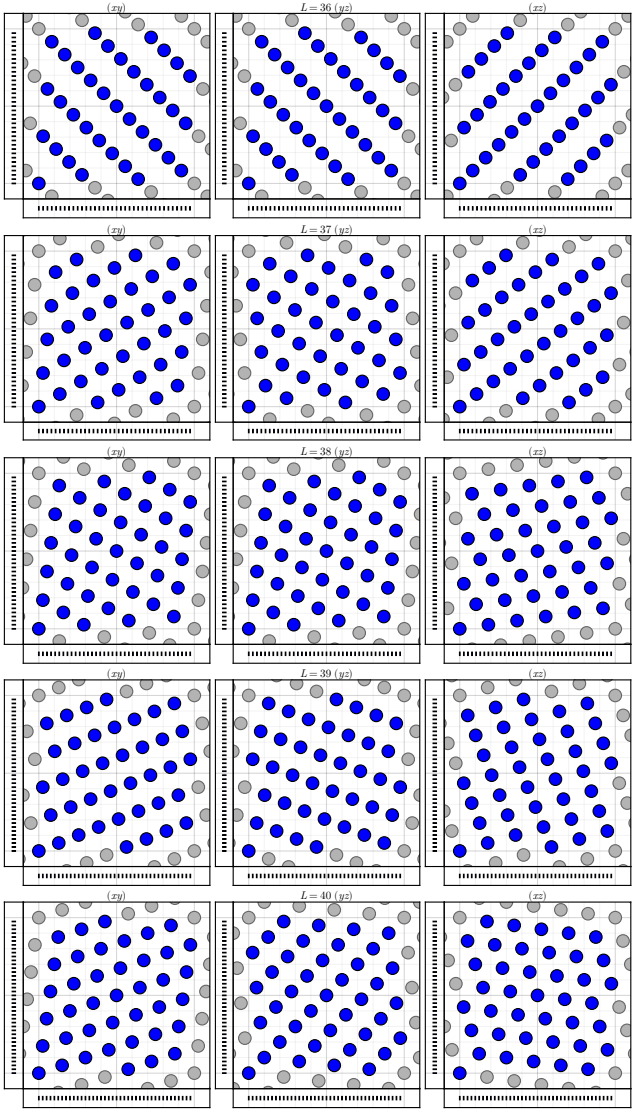

Figure B.22: Rank-1 lattices (5.41) with globally minimal wce (5.31). $L \in [36, 40]$, $\Delta L = 1$.

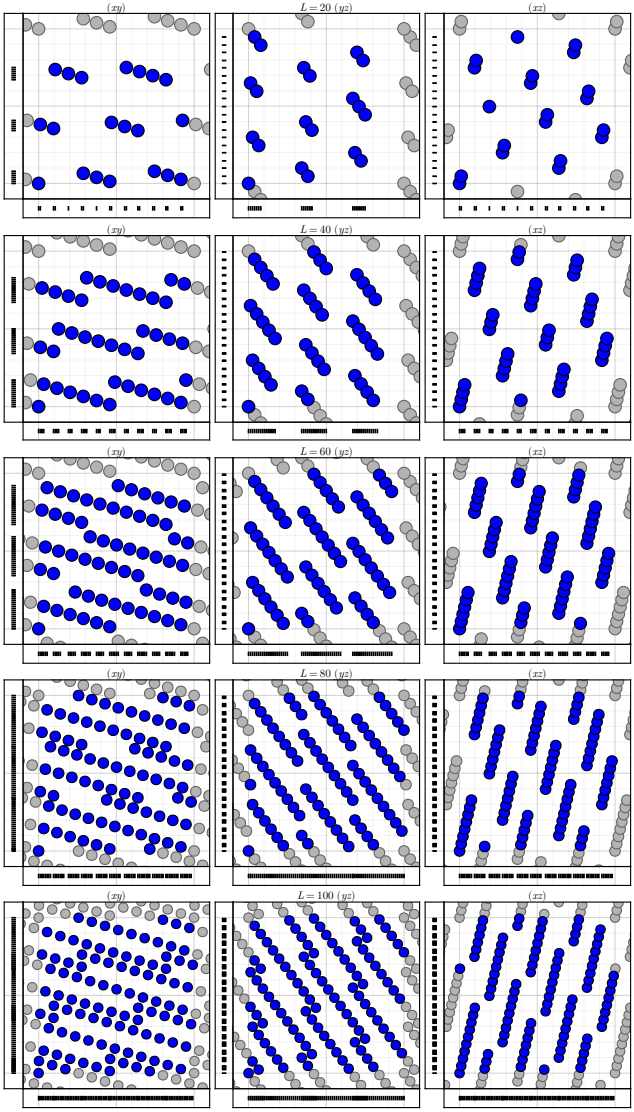

Figure B.23: Martin Roberts / R_3 Kronecker sequence (3.38), $\underline{a} = [0.819172\ldots, 0.671043\ldots, 0.549700\ldots]^\top$.

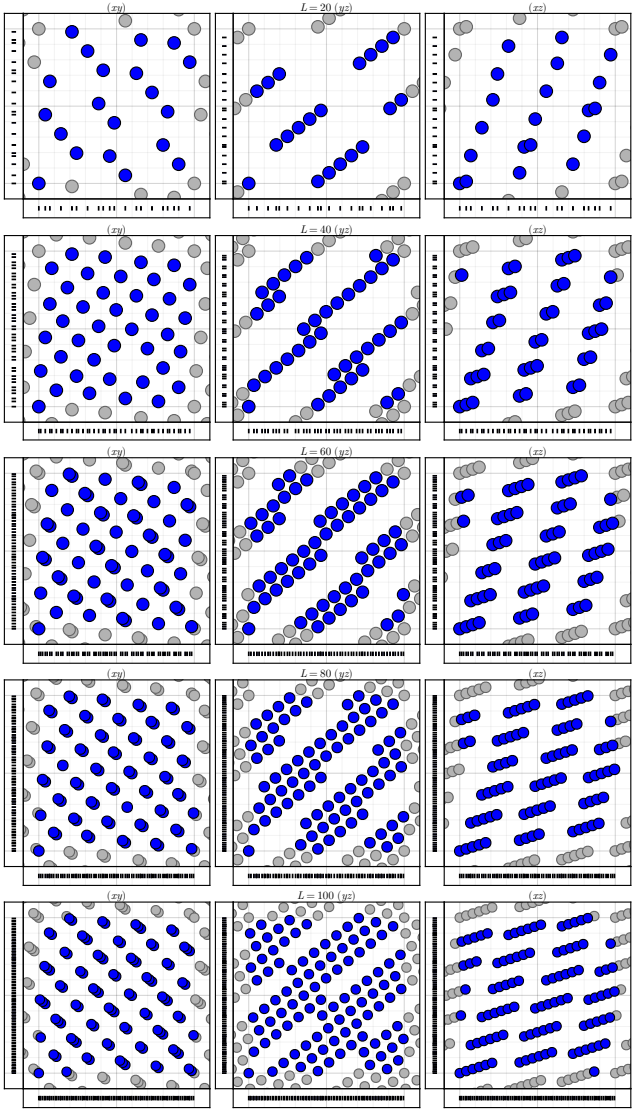

Figure B.24: Roots-of-primes Kronecker sequence (3.39), $\underline{a} = [1.414213\ldots, 1.732050\ldots, 2.236067\ldots]^\top$.

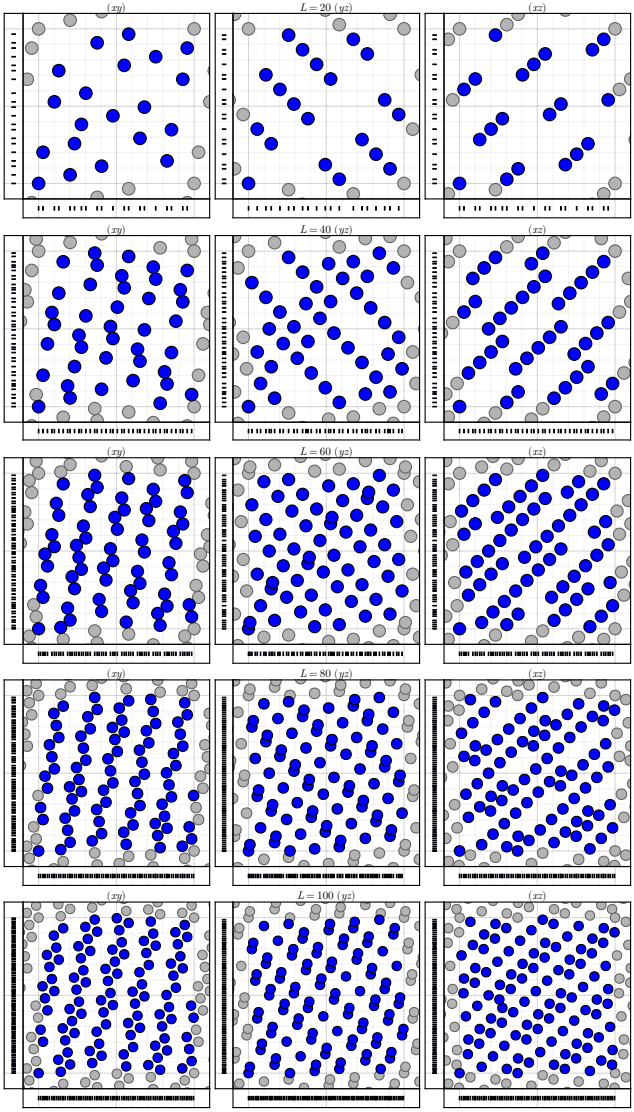

Figure B.25: Optimized wce Kronecker sequence (5.44), $\underline{a} = [0.724686\ldots, 0.618020\ldots, 0.581078\ldots]^\top$, $L_{\max} = 73$.

APPENDIX C

Numeric Representations of Point Sets

Contents

> Numbers constitute the only universal language.
>
> Nathanael West (1903–1940)

Lists of lattice rules and Kronecker sequences obtained by brute force computation. Can be copy-pasted directly into program code from most PDF viewers. The author acknowledges support by the state of Baden-Württemberg through bwHPC.

C.1 Rank-1 Lattices with Optimal wce

Rank-1 lattices, Section 5.2.2, with globally minimal wce (5.31). Format: in each vector, the first element is the number of samples L, and the remaining entries are the generating vector g_L^{opt}. For example, vector `[21, 1, 8]` encodes the 2D point set

$$\underline{x}_i = \frac{i}{21} \cdot \begin{bmatrix} 1 \\ 8 \end{bmatrix} \mod 1 \ , \qquad i \in \{0, 1, \ldots, 20\} \ . \tag{C.1}$$

C.1.1 $s = 2$

```
[2, 1, 1],
[3, 1, 1],
[4, 1, 1],
[5, 1, 2],
[6, 1, 1],
[7, 1, 2],
[8, 1, 3],
[9, 1, 2],
[10, 1, 3],
[11, 1, 3],
[12, 1, 5],
[13, 1, 5],
[14, 1, 3],
[15, 1, 4],
[16, 1, 7],
[17, 1, 5],
[18, 1, 5],
[19, 1, 7],
[20, 1, 9],
[21, 1, 8],
[22, 1, 5],
[23, 1, 7],
[24, 1, 7],
[25, 1, 7],
[26, 1, 7],
[27, 1, 8],
[28, 1, 5],
[29, 1, 12],
[30, 1, 11],
[31, 1, 13],
[32, 1, 7],
[33, 1, 10],
[34, 1, 13],
[35, 1, 13],
[36, 1, 11],
[37, 1, 11],
[38, 1, 17],
[39, 1, 16],
[40, 1, 11],
[41, 1, 12],
[42, 1, 13],
[43, 1, 12],
[44, 1, 13],
[45, 1, 19],
[46, 1, 17],
[47, 1, 13],
[48, 1, 11],
[49, 1, 19],
[50, 1, 19],
[51, 1, 14],
[52, 1, 11],
[53, 1, 23],
[54, 1, 17],
[55, 1, 21],
[56, 1, 17],
[57, 1, 13],
[58, 1, 17],
[59, 1, 18],
[60, 1, 13],
[61, 1, 17],
[62, 1, 23],
[63, 1, 17],
[64, 1, 19],
[65, 1, 19],
[66, 1, 25],
[67, 1, 18],
[68, 1, 25],
[69, 1, 19],
[70, 1, 29],
[71, 1, 21],
[72, 1, 19],
[73, 1, 27],
[74, 1, 31],
[75, 1, 29],
[76, 1, 21],
[77, 1, 18],
[78, 1, 17],
[79, 1, 30],
[80, 1, 31],
[81, 1, 31],
[82, 1, 23],
[83, 1, 30],
[84, 1, 19],
[85, 1, 23],
[86, 1, 25],
[87, 1, 19],
[88, 1, 19],
[89, 1, 34],
[90, 1, 17],
[91, 1, 27],
[92, 1, 21],
[93, 1, 25],
[94, 1, 39],
[95, 1, 39],
[96, 1, 29],
[97, 1, 35],
[98, 1, 27],
[99, 1, 29],
[100, 1, 41],
[101, 1, 39],
[102, 1, 23],
[103, 1, 37],
[104, 1, 29],
[105, 1, 31],
[106, 1, 31],
[107, 1, 47],
[108, 1, 29],
[109, 1, 45],
[110, 1, 31],
[111, 1, 41],
[112, 1, 31],
[113, 1, 35],
[114, 1, 25],
[115, 1, 34],
[116, 1, 45],
[117, 1, 43],
[118, 1, 35],
[119, 1, 44],
[120, 1, 49],
[121, 1, 46],
[122, 1, 33],
[123, 1, 34],
[124, 1, 29],
[125, 1, 27],
[126, 1, 55],
[127, 1, 29],
[128, 1, 47],
[129, 1, 49],
[130, 1, 47],
[131, 1, 50],
[132, 1, 35],
[133, 1, 39],
[134, 1, 39],
[135, 1, 41],
[136, 1, 53],
[137, 1, 31],
[138, 1, 37],
[139, 1, 39],
[140, 1, 41],
[141, 1, 59],
[142, 1, 31],
[143, 1, 59],
[144, 1, 55],
[145, 1, 44],
[146, 1, 41],
[147, 1, 41],
[148, 1, 41],
[149, 1, 44],
[150, 1, 61],
[151, 1, 56],
[152, 1, 41],
[153, 1, 55],
[154, 1, 45],
[155, 1, 46],
[156, 1, 37],
[157, 1, 46],
[158, 1, 57],
[159, 1, 44],
[160, 1, 43],
[161, 1, 61],
[162, 1, 43],
[163, 1, 62],
[164, 1, 67],
[165, 1, 46],
[166, 1, 49],
[167, 1, 46],
[168, 1, 71],
[169, 1, 70],
[170, 1, 47],
[171, 1, 50],
[172, 1, 63],
[173, 1, 64],
[174, 1, 71],
[175, 1, 47],
[176, 1, 65],
[177, 1, 49],
[178, 1, 49],
[179, 1, 74],
[180, 1, 41],
[181, 1, 70],
[182, 1, 53],
[183, 1, 67],
[184, 1, 43],
[185, 1, 68],
[186, 1, 55],
[187, 1, 71],
[188, 1, 69],
[189, 1, 55],
[190, 1, 53],
[191, 1, 74],
[192, 1, 71],
[193, 1, 81],
[194, 1, 75],
[195, 1, 59],
[196, 1, 75],
[197, 1, 71],
[198, 1, 53],
[199, 1, 55],
[200, 1, 59],
[201, 1, 56],
[202, 1, 73],
[203, 1, 46],
[204, 1, 89],
[205, 1, 76],
[206, 1, 63],
[207, 1, 76],
[208, 1, 79],
[209, 1, 80],
[210, 1, 59],
[211, 1, 64],
[212, 1, 81],
[213, 1, 62],
[214, 1, 65],
[215, 1, 58],
[216, 1, 49],
[217, 1, 64],
[218, 1, 59],
[219, 1, 64],
[220, 1, 93],
[221, 1, 62],
[222, 1, 91],
[223, 1, 68],
[224, 1, 97],
[225, 1, 62],
[226, 1, 69],
[227, 1, 94],
[228, 1, 61],
[229, 1, 94],
[230, 1, 83],
[231, 1, 50],
[232, 1, 85],
```

```
[233, 1, 89],
[234, 1, 71],
[235, 1, 63],
[236, 1, 65],
[237, 1, 98],
[238, 1, 93],
[239, 1, 70],
[240, 1, 71],
[241, 1, 105],
[242, 1, 65],
[243, 1, 94],
[244, 1, 55],
[245, 1, 88],
[246, 1, 95],
[247, 1, 68],
[248, 1, 91],
[249, 1, 76],
[250, 1, 67],
[251, 1, 70],
[252, 1, 73],
[253, 1, 74],
[254, 1, 75],
[255, 1, 92],
[256, 1, 75],
[257, 1, 71],
[258, 1, 71],
[259, 1, 100],
[260, 1, 79],
[261, 1, 100],
[262, 1, 61],
[263, 1, 109],
[264, 1, 109],
[265, 1, 74],
[266, 1, 79],
[267, 1, 79],
[268, 1, 99],
[269, 1, 75],
[270, 1, 97],
[271, 1, 80],
[272, 1, 103],
[273, 1, 100],
[274, 1, 81],
[275, 1, 76],
[276, 1, 73],
[277, 1, 81],
[278, 1, 85],
[279, 1, 65],
[280, 1, 107],
[281, 1, 109],
[282, 1, 109],
[283, 1, 104],
[284, 1, 105],
[285, 1, 83],
[286, 1, 79],
[287, 1, 106],
[288, 1, 119],
[289, 1, 80],
[290, 1, 81],
[291, 1, 85],
[292, 1, 111],
[293, 1, 81],
[294, 1, 89],
[295, 1, 108],
[296, 1, 83],
[297, 1, 109],
[298, 1, 91],
[299, 1, 116],
```

```
[300, 1, 89],
[301, 1, 89],
[302, 1, 111],
[303, 1, 116],
[304, 1, 113],
[305, 1, 112],
[306, 1, 65],
[307, 1, 119],
[308, 1, 117],
[309, 1, 70],
[310, 1, 71],
[311, 1, 115],
[312, 1, 131],
[313, 1, 121],
[314, 1, 129],
[315, 1, 92],
[316, 1, 69],
[317, 1, 121],
[318, 1, 113],
[319, 1, 139],
[320, 1, 93],
[321, 1, 94],
[322, 1, 89],
[323, 1, 94],
[324, 1, 95],
[325, 1, 141],
[326, 1, 99],
[327, 1, 97],
[328, 1, 71],
[329, 1, 136],
[330, 1, 89],
[331, 1, 129],
[332, 1, 89],
[333, 1, 101],
[334, 1, 129],
[335, 1, 123],
[336, 1, 127],
[337, 1, 128],
[338, 1, 129],
[339, 1, 100],
[340, 1, 101],
[341, 1, 104],
[342, 1, 101],
[343, 1, 131],
[344, 1, 105],
[345, 1, 143],
[346, 1, 105],
[347, 1, 134],
[348, 1, 103],
[349, 1, 106],
[350, 1, 93],
[351, 1, 80],
[352, 1, 97],
[353, 1, 149],
[354, 1, 131],
[355, 1, 99],
[356, 1, 147],
[357, 1, 109],
[358, 1, 147],
[359, 1, 105],
[360, 1, 133],
[361, 1, 100],
[362, 1, 107],
[363, 1, 134],
[364, 1, 135],
[365, 1, 101],
[366, 1, 143],
```

```
[367, 1, 99],
[368, 1, 107],
[369, 1, 80],
[370, 1, 133],
[371, 1, 144],
[372, 1, 109],
[373, 1, 109],
[374, 1, 155],
[375, 1, 103],
[376, 1, 105],
[377, 1, 144],
[378, 1, 139],
[379, 1, 111],
[380, 1, 141],
[381, 1, 140],
[382, 1, 141],
[383, 1, 106],
[384, 1, 139],
[385, 1, 102],
[386, 1, 141],
[387, 1, 104],
[388, 1, 163],
[389, 1, 115],
[390, 1, 109],
[391, 1, 145],
[392, 1, 149],
[393, 1, 116],
[394, 1, 117],
[395, 1, 142],
[396, 1, 109],
[397, 1, 151],
[398, 1, 111],
[399, 1, 121],
[400, 1, 117],
[401, 1, 119],
[402, 1, 157],
[403, 1, 119],
[404, 1, 169],
[405, 1, 157],
[406, 1, 109],
[407, 1, 119],
[408, 1, 169],
[409, 1, 121],
[410, 1, 173],
[411, 1, 89],
[412, 1, 173],
[413, 1, 121],
[414, 1, 97],
[415, 1, 152],
[416, 1, 115],
[417, 1, 154],
[418, 1, 159],
[419, 1, 155],
[420, 1, 89],
[421, 1, 164],
[422, 1, 161],
[423, 1, 131],
[424, 1, 153],
[425, 1, 157],
[426, 1, 119],
[427, 1, 163],
[428, 1, 133],
[429, 1, 131],
[430, 1, 119],
[431, 1, 128],
[432, 1, 179],
[433, 1, 179],
```

```
[434, 1, 121],
[435, 1, 133],
[436, 1, 129],
[437, 1, 169],
[438, 1, 121],
[439, 1, 136],
[440, 1, 129],
[441, 1, 167],
[442, 1, 137],
[443, 1, 186],
[444, 1, 97],
[445, 1, 163],
[446, 1, 165],
[447, 1, 130],
[448, 1, 131],
[449, 1, 165],
[450, 1, 97],
[451, 1, 105],
[452, 1, 167],
[453, 1, 172],
[454, 1, 99],
[455, 1, 173],
[456, 1, 191],
[457, 1, 192],
[458, 1, 123],
[459, 1, 140],
[460, 1, 129],
[461, 1, 140],
[462, 1, 179],
[463, 1, 179],
[464, 1, 141],
[465, 1, 128],
[466, 1, 129],
[467, 1, 193],
[468, 1, 181],
[469, 1, 131],
[470, 1, 193],
[471, 1, 193],
[472, 1, 185],
[473, 1, 181],
[474, 1, 131],
[475, 1, 196],
[476, 1, 109],
[477, 1, 196],
[478, 1, 175],
[479, 1, 145],
[480, 1, 209],
[481, 1, 134],
[482, 1, 177],
[483, 1, 128],
[484, 1, 135],
[485, 1, 178],
[486, 1, 205],
[487, 1, 144],
[488, 1, 181],
[489, 1, 106],
[490, 1, 187],
[491, 1, 145],
[492, 1, 143],
[493, 1, 191],
[494, 1, 147],
[495, 1, 188],
[496, 1, 133],
[497, 1, 152],
[498, 1, 193],
```

C.1.2 $s = 3$

```
[2, 1, 1, 1],
[3, 1, 1, 1],
[4, 1, 1, 1],
[5, 1, 1, 2],
[6, 1, 1, 1],
[7, 1, 2, 3],
[8, 1, 3, 3],
[9, 1, 2, 4],
[10, 1, 1, 3],
[11, 1, 2, 3],
[12, 1, 1, 5],
[13, 1, 3, 4],
[14, 1, 3, 5],
[15, 1, 2, 4],
```

```
[16, 1, 3, 5],
[17, 1, 3, 5],
[18, 1, 5, 7],
[19, 1, 7, 8],
[20, 1, 3, 7],
[21, 1, 4, 5],
[22, 1, 7, 9],
[23, 1, 6, 9],
[24, 1, 7, 11],
[25, 1, 9, 11],
[26, 1, 3, 7],
[27, 1, 8, 10],
[28, 1, 3, 5],
[29, 1, 8, 12],
[30, 1, 7, 11],
```

```
[31, 1, 7, 9],
[32, 1, 5, 7],
[33, 1, 4, 10],
[34, 1, 9, 13],
[35, 1, 6, 8],
[36, 1, 11, 13],
[37, 1, 8, 10],
[38, 1, 7, 11],
[39, 1, 16, 17],
[40, 1, 7, 17],
[41, 1, 12, 16],
[42, 1, 5, 13],
[43, 1, 9, 12],
[44, 1, 7, 13],
[45, 1, 8, 17],
```

```
[46, 1, 13, 17],
[47, 1, 10, 18],
[48, 1, 5, 17],
[49, 1, 13, 19],
[50, 1, 11, 19],
[51, 1, 11, 16],
[52, 1, 9, 23],
[53, 1, 19, 22],
[54, 1, 7, 17],
[55, 1, 12, 21],
[56, 1, 9, 15],
[57, 1, 13, 20],
[58, 1, 11, 17],
[59, 1, 14, 18],
[60, 1, 11, 13],
```

```
[61, 1, 13, 19],
[62, 1, 13, 17],
[63, 1, 17, 26],
[64, 1, 19, 23],
[65, 1, 17, 19],
[66, 1, 17, 29],
[67, 1, 14, 18],
[68, 1, 19, 21],
[69, 1, 16, 19],
[70, 1, 13, 27],
[71, 1, 15, 21],
[72, 1, 7, 19],
[73, 1, 19, 30],
[74, 1, 11, 29],
[75, 1, 16, 29],
[76, 1, 27, 31],
[77, 1, 24, 30],
[78, 1, 17, 29],
[79, 1, 15, 24],
[80, 1, 17, 31],
[81, 1, 11, 31],
[82, 1, 23, 31],
[83, 1, 30, 36],
[84, 1, 25, 37],
[85, 1, 23, 26],
```

```
[86, 1, 15, 25],
[87, 1, 13, 19],
[88, 1, 13, 17],
[89, 1, 20, 32],
[90, 1, 17, 19],
[91, 1, 19, 32],
[92, 1, 15, 35],
[93, 1, 14, 22],
[94, 1, 35, 39],
[95, 1, 28, 36],
[96, 1, 23, 29],
[97, 1, 21, 36],
[98, 1, 27, 29],
[99, 1, 23, 41],
[100, 1, 27, 29],
[101, 1, 22, 37],
[102, 1, 19, 23],
[103, 1, 18, 29],
[104, 1, 25, 31],
[105, 1, 32, 44],
[106, 1, 41, 45],
[107, 1, 31, 41],
[108, 1, 23, 29],
[109, 1, 19, 25],
[110, 1, 19, 29],
```

```
[111, 1, 34, 46],
[112, 1, 31, 47],
[113, 1, 30, 43],
[114, 1, 25, 43],
[115, 1, 24, 52],
[116, 1, 35, 49],
[117, 1, 34, 43],
[118, 1, 25, 33],
[119, 1, 16, 36],
[120, 1, 43, 49],
[121, 1, 38, 50],
[122, 1, 23, 51],
[123, 1, 32, 38],
[124, 1, 23, 35],
[125, 1, 23, 29],
[126, 1, 19, 55],
[127, 1, 45, 55],
[128, 1, 37, 49],
[129, 1, 35, 49],
[130, 1, 47, 51],
[131, 1, 30, 39],
[132, 1, 35, 47],
[133, 1, 39, 58],
[134, 1, 29, 37],
[135, 1, 41, 56],
```

```
[136, 1, 25, 41],
[137, 1, 37, 43],
[138, 1, 31, 43],
[139, 1, 21, 30],
[140, 1, 19, 41],
[141, 1, 25, 61],
[142, 1, 33, 41],
[143, 1, 40, 54],
[144, 1, 43, 55],
[145, 1, 34, 46],
[146, 1, 27, 41],
[147, 1, 23, 43],
[148, 1, 35, 41],
[149, 1, 45, 55],
[150, 1, 47, 59],
[151, 1, 35, 56],
[152, 1, 53, 63],
[153, 1, 35, 55],
[154, 1, 23, 43],
[155, 1, 36, 56],
[156, 1, 35, 47],
```

C.1.3 $s = 4$

```
[2, 1, 1, 1, 1],
[3, 1, 1, 1, 1],
[4, 1, 1, 1, 1],
[5, 1, 1, 2, 2],
[6, 1, 1, 1, 1],
[7, 1, 1, 2, 3],
[8, 1, 1, 3, 3],
[9, 1, 1, 2, 4],
[10, 1, 1, 3, 3],
[11, 1, 2, 3, 4],
[12, 1, 1, 5, 5],
[13, 1, 4, 5, 6],
[14, 1, 1, 3, 5],
[15, 1, 2, 4, 7],
[16, 1, 3, 5, 7],
[17, 1, 3, 4, 5],
```

```
[18, 1, 1, 5, 7],
[19, 1, 3, 4, 5],
[20, 1, 3, 7, 9],
[21, 1, 2, 5, 8],
[22, 1, 3, 5, 7],
[23, 1, 4, 5, 7],
[24, 1, 5, 7, 11],
[25, 1, 4, 6, 9],
[26, 1, 3, 5, 7],
[27, 1, 4, 7, 11],
[28, 1, 3, 5, 11],
[29, 1, 8, 9, 12],
[30, 1, 7, 11, 13],
[31, 1, 8, 11, 12],
[32, 1, 7, 9, 15],
[33, 1, 4, 7, 10],
```

```
[34, 1, 9, 13, 15],
[35, 1, 6, 8, 13],
[36, 1, 5, 11, 13],
[37, 1, 8, 11, 14],
[38, 1, 5, 7, 9],
[39, 1, 4, 14, 17],
[40, 1, 7, 9, 17],
[41, 1, 9, 12, 15],
[42, 1, 11, 13, 17],
[43, 1, 9, 12, 15],
[44, 1, 3, 7, 13],
[45, 1, 8, 17, 19],
[46, 1, 9, 13, 17],
[47, 1, 7, 11, 17],
```

C.2 Kronecker Sequences with Optimal wce

Kronecker sequences, Section 5.3.2, with globally minimal wce (5.31). Format: in each vector, the first element is the maximum number of samples $L_{\max}$ the worst case error is optimized for, and the remaining entries are the generator $\underline{\alpha}^{\text{opt}}_{L_{\max}}$. For example, vector `[100, 0.381988, 0.419810]` encodes the point set

$$\underline{x}_i = i \cdot \begin{bmatrix} 0.381988 \\ 0.419810 \end{bmatrix} \mod 1 \ , \quad i \in \{0, 1, \ldots, L\} \ , \quad L \leq 100 \ . \qquad \text{(C.2)}$$

C.2.1 $s = 1$

```
[  5, 0.39533333333333331],
[  6, 0.38745098039215686],
[  7, 0.38387806250319678],
[  8, 0.38102439955574069],
[  9, 0.38115688707044815],
[ 10, 0.38213146888384986],
[ 11, 0.38245622173144145],
[ 12, 0.38294017203301495],
[ 13, 0.38328934785663543],
[ 14, 0.38315010508369096],
[ 15, 0.38292238518811539],
[ 16, 0.38257089314556847],
[ 17, 0.38234750508114762],
[ 18, 0.38220664403977656],
[ 19, 0.38202629427083223],
[ 20, 0.38188998149396836],
[ 21, 0.38176458810846731],
[ 22, 0.38172085014686724],
[ 23, 0.38173701814744138],
[ 24, 0.38175863037711483],
[ 25, 0.38181045122160218],
[ 26, 0.38187414839420186],
[ 27, 0.38191524441225816],
[ 28, 0.38195057984226044],
[ 29, 0.38197161536209773],
[ 30, 0.38199999921243982],
[ 31, 0.38203347428545559],
[ 32, 0.38205813402475952],
[ 33, 0.38208380225307753],
[ 34, 0.38210657387834446],
[ 35, 0.38211565105217044],
[ 36, 0.38211754358512096],
[ 37, 0.38210976839135130],
[ 38, 0.38210126493531799],
[ 39, 0.38209217134804663],
[ 40, 0.38207756130345266],
[ 41, 0.38206191121817623],
[ 42, 0.38204405498129740],
[ 43, 0.38202947933161019],
[ 44, 0.38201828509522995],
[ 45, 0.38200725639432132],
[ 46, 0.38199891945521525],
[ 47, 0.38199225673144704],
[ 48, 0.38198405416704173],
[ 49, 0.38197579245054042],
[ 50, 0.38196642789464774],
[ 51, 0.38195839474056759],
[ 52, 0.38195160674380529],
[ 53, 0.38194431030303749],
[ 54, 0.38193775641273542],
[ 55, 0.38193140430779154],
[ 56, 0.38192702342583629],
[ 57, 0.38192462580881675],
[ 58, 0.38192301307553911],
[ 59, 0.38192303949028072],
[ 60, 0.38192429120835275],
[ 61, 0.38192547806470534],
[ 62, 0.38192707429981143],
[ 63, 0.38192859155882342],
[ 64, 0.38193093501586578],
[ 65, 0.38193403965687334],
[ 66, 0.38193714290895237],
[ 67, 0.38194071989102796],
[ 68, 0.38194450913320194],
[ 69, 0.38194771728965504],
[ 70, 0.38195062811125319],
[ 71, 0.38195294458824552],
[ 72, 0.38195524152795962],
[ 73, 0.38195750346875007],
[ 74, 0.38195927444767963],
[ 75, 0.38196087938001033],
[ 76, 0.38196217959536810],
[ 77, 0.38196368101773348],
[ 78, 0.38196542586021071],
[ 79, 0.38196710240519277],
[ 80, 0.38196898682239167],
[ 81, 0.38197098936451934],
[ 82, 0.38197274045298313],
[ 83, 0.38197439766807256],
[ 84, 0.38197582171625660],
[ 85, 0.38197731522782136],
[ 86, 0.38197888037388916],
[ 87, 0.38198028459739042],
[ 88, 0.38198169896360046],
[ 89, 0.38198305080194495],
[ 90, 0.38198407659657646],
[ 91, 0.38198487708933809],
[ 92, 0.38198535083080903],
[ 93, 0.38198570607368465],
[ 94, 0.38198594552006304],
[ 95, 0.38198590788352044],
[ 96, 0.38198571608278137],
[ 97, 0.38198532285745096],
[ 98, 0.38198492547623530],
[ 99, 0.38198455008785637],
[100, 0.38198408440765391],
[101, 0.38198364317471878],
[102, 0.38198319913136314],
[103, 0.38198261000932204],
[104, 0.38198194211688646],
[105, 0.38198114184194748],
[106, 0.38198033679510546],
[107, 0.38197953318917899],
[108, 0.38197863759741868],
[109, 0.38197772503268562],
[110, 0.38197676798325048],
[111, 0.38197588659294457],
[112, 0.38197509798861651],
[113, 0.38197433385665569],
[114, 0.38197366428447066],
[115, 0.38197307214947529],
[116, 0.38197246794127621],
[117, 0.38197189076511423],
[118, 0.38197130485031583],
[119, 0.38197078800172202],
[120, 0.38197034232098664],
[121, 0.38196990642743828],
[122, 0.38196952541056878],
[123, 0.38196917932929136],
[124, 0.38196879365610409],
[125, 0.38196839301840702],
[126, 0.38196794550300506],
[127, 0.38196750737111179],
[128, 0.38196707754332981],
[129, 0.38196660634784907],
[130, 0.38196612691923237],
[131, 0.38196562256109562],
[132, 0.38196515067978543],
[133, 0.38196471846242330],
[134, 0.38196429020950856],
[135, 0.38196390026189747],
[136, 0.38196353926774579],
[137, 0.38196316053819701],
[138, 0.38196278319997340],
[139, 0.38196238798174897],
[140, 0.38196201482906117],
[141, 0.38196166484847854],
[142, 0.38196130570935583],
[143, 0.38196096108529087],
[144, 0.38196062051178081],
[145, 0.38196032417087811],
[146, 0.38196007787737857],
[147, 0.38195985767465368],
[148, 0.38195968774794425],
[149, 0.38195956203755399],
[150, 0.38195944827106743],
[151, 0.38195935970736844],
[152, 0.38195928276199553],
[153, 0.38195924520543656],
[154, 0.38195924769022327],
[155, 0.38195926722286544],
[156, 0.38195932012516476],
[157, 0.38195939864164569],
[158, 0.38195947401027935],
[159, 0.38195955469308596],
[160, 0.38195962761355889],
[161, 0.38195971364714010],
[162, 0.38195981186752131],
[163, 0.38195990221668202],
[164, 0.38195999694521904],
[165, 0.38196008880358367],
[166, 0.38196020012652343],
[167, 0.38196033359145359],
[168, 0.38196047454114929],
[169, 0.38196063658647245],
```

[170, 0.381960815744555393],		[265, 0.381968488410454501],		[360, 0.381965543744150041],
[171, 0.381960992511322371],		[266, 0.381968464866552821],		[361, 0.381965523199007061],
[172, 0.381961174293514121],		[267, 0.381968441337194321],		[362, 0.381965502026616611],
[173, 0.381961352648814151],		[268, 0.381968414481547841],		[363, 0.381965480726579271],
[174, 0.381961543861319701],		[269, 0.381968385374529261],		[364, 0.381965458997749991],
[175, 0.381961748202454541],		[270, 0.381968352465021701],		[365, 0.381965437798267301],
[176, 0.381961951749828001],		[271, 0.381968318388543231],		[366, 0.381965417280967831],
[177, 0.381962164216976821],		[272, 0.381968283132236191],		[367, 0.381965396838693961],
[178, 0.381962380890457921],		[273, 0.381968244232390561],		[368, 0.381965377096761041],
[179, 0.381962584262744541],		[274, 0.381968203290181501],		[369, 0.381965357915148301],
[180, 0.381962779349920681],		[275, 0.381968159430021661],		[370, 0.381965338431082931],
[181, 0.381962958093846561],		[276, 0.381968111563207061],		[371, 0.381965318987363191],
[182, 0.381963133200236671],		[277, 0.381968072383559231],		[372, 0.381965299198179341],
[183, 0.381963304148351721],		[278, 0.381968027860612241],		[373, 0.381965279836999291],
[184, 0.381963458634659801],		[279, 0.381967983988655001],		[374, 0.381965260944433391],
[185, 0.381963604221305151],		[280, 0.381967940361300161],		[375, 0.381965241868315261],
[186, 0.381963736486263081],		[281, 0.381967894410094491],		[376, 0.381965223091395631],
[187, 0.381963869377781761],		[282, 0.381967847207059701],		[377, 0.381965204398703681],
[188, 0.381964004761813691],		[283, 0.381967797639663821],		[378, 0.381965186667397941],
[189, 0.381964133698710071],		[284, 0.381967748050642651],		[379, 0.381965170073415571],
[190, 0.381964264882850731],		[285, 0.381967698582253771],		[380, 0.381965154129210841],
[191, 0.381964396056633351],		[286, 0.381967647330775481],		[381, 0.381965139417261961],
[192, 0.381964515164441961],		[287, 0.381967595755579041],		[382, 0.381965125852375351],
[193, 0.381964627029431621],		[288, 0.381967543250986311],		[383, 0.381965112717561561],
[194, 0.381964726496417271],		[289, 0.381967492404911019],		[384, 0.381965100343442051],
[195, 0.381964824061456041],		[290, 0.381967443745996561],		[385, 0.381965088424079061],
[196, 0.381964922144311051],		[291, 0.381967395843401611],		[386, 0.381965077662322061],
[197, 0.381965006115942311],		[292, 0.381967350398807081],		[387, 0.381965068120989961],
[198, 0.381965088377614061],		[293, 0.381967307161153121],		[388, 0.381965059256711871],
[199, 0.381965161419395081],		[294, 0.381967264066629791],		[389, 0.381965051514550511],
[200, 0.381965244625549321],		[295, 0.381967222081031291],		[390, 0.381965044729328631],
[201, 0.381965331754357431],		[296, 0.381967180338509571],		[391, 0.381965038157836221],
[202, 0.381965419153392441],		[297, 0.381967140857455311],		[392, 0.381965032024714321],
[203, 0.381965513897258751],		[298, 0.381967103812678231],		[393, 0.381965025972039801],
[204, 0.381965614631677971],		[299, 0.381967067661042101],		[394, 0.381965020574484001],
[205, 0.381965712405887951],		[300, 0.381967033668310471],		[395, 0.381965015820783571],
[206, 0.381965811194360351],		[301, 0.381967001367230001],		[396, 0.381965011144160371],
[207, 0.381965907252734881],		[302, 0.381966968675350181],		[397, 0.381965006891728301],
[208, 0.381966008881894641],		[303, 0.381966936242915831],		[398, 0.381965002851226371],
[209, 0.381966116596490931],		[304, 0.381966903087651351],		[399, 0.381964999691570771],
[210, 0.381966223871026861],		[305, 0.381966870831737911],		[400, 0.381964997519495311],
[211, 0.381966335781568021],		[306, 0.381966839452988591],		[401, 0.381964995908284201],
[212, 0.381966450272485551],		[307, 0.381966807394283961],		[402, 0.381964995295354271],
[213, 0.381966588378925411],		[308, 0.381966775635690481],		[403, 0.381964995581378971],
[214, 0.381966664121118021],		[309, 0.381966743608219921],		[404, 0.381964996157684201],
[215, 0.381966762206193081],		[310, 0.381966713163647331],		[405, 0.381964997262469461],
[216, 0.381966859590992411],		[311, 0.381966684595393791],		[406, 0.381964998620880741],
[217, 0.381966956149745301],		[312, 0.381966656740187821],		[407, 0.381965000775110631],
[218, 0.381967045747089511],		[313, 0.381966630795820051],		[408, 0.381965003751560451],
[219, 0.381967132282949261],		[314, 0.381966606491838171],		[409, 0.381965007086701891],
[220, 0.381967213565383931],		[315, 0.381966582185166661],		[410, 0.381965011118342081],
[221, 0.381967296796313971],		[316, 0.381966558533121171],		[411, 0.381965015691213271],
[222, 0.381967383040865251],		[317, 0.381966534807010701],		[412, 0.381965020181716021],
[223, 0.381967467780836571],		[318, 0.381966512475173661],		[413, 0.381965024751661661],
[224, 0.381967555571701701],		[319, 0.381966491610788331],		[414, 0.381965029091007271],
[225, 0.381967645320306251],		[320, 0.381966470980928621],		[415, 0.381965033647915401],
[226, 0.381967773080664231],		[321, 0.381966451495788621],		[416, 0.381965038396023861],
[227, 0.381967814540330801],		[322, 0.381966432748460371],		[417, 0.381965042857879861],
[228, 0.381967893828493051],		[323, 0.381966413098866851],		[418, 0.381965047299723191],
[229, 0.381967974785891541],		[324, 0.381966392959434771],		[419, 0.381965051926679521],
[230, 0.381968055840221491],		[325, 0.381966371640992731],		[420, 0.381965056090233071],
[231, 0.381968134264159881],		[326, 0.381966350234922171],		[421, 0.381965061043504531],
[232, 0.381968212827305141],		[327, 0.381966328722219031],		[422, 0.381965066033455201],
[233, 0.381968292005030819],		[328, 0.381966305871757561],		[423, 0.381965071405121091],
[234, 0.381968360021522961],		[329, 0.381966282400477641],		[424, 0.381965077066778291],
[235, 0.381968424472868161],		[330, 0.381966257838920021],		[425, 0.381965082511162791],
[236, 0.381968480631685661],		[331, 0.381966233581774841],		[426, 0.381965087922652101],
[237, 0.381968533251964321],		[332, 0.381966208911228651],		[427, 0.381965093261779191],
[238, 0.381968581211466061],		[333, 0.381966185666547735],		[428, 0.381965098379143391],
[239, 0.381968621217585291],		[334, 0.381966161988999521],		[429, 0.381965103872277941],
[240, 0.381968655593310671],		[335, 0.381966138573767661],		[430, 0.381965109159826571],
[241, 0.381968682791296531],		[336, 0.381966114132912931],		[431, 0.381965114511174101],
[242, 0.381968707797288141],		[337, 0.381966089156285381],		[432, 0.381965119792697871],
[243, 0.381968731357358651],		[338, 0.381966063064235811],		[433, 0.381965125505268011],
[244, 0.381968754032872301],		[339, 0.381966036978804101],		[434, 0.381965131744887941],
[245, 0.381968776833802021],		[340, 0.381966010945666571],		[435, 0.381965138826172531],
[246, 0.381968783327763791],		[341, 0.381965983998740041],		[436, 0.381965145269413721],
[247, 0.381968792267420981],		[342, 0.381965956834245221],		[437, 0.381965152833256831],
[248, 0.381968796492976661],		[343, 0.381965929128553541],		[438, 0.381965160489178281],
[249, 0.381968794125836841],		[344, 0.381965902151544021],		[439, 0.381965168424799441],
[250, 0.381968789059570211],		[345, 0.381965876147718211],		[440, 0.381965176455677181],
[251, 0.381968781504491931],		[346, 0.381965850396651101],		[441, 0.381965184989247921],
[252, 0.381968768284048351],		[347, 0.381965825736042211],		[442, 0.381965194059049441],
[253, 0.381968751813835441],		[348, 0.381965802031924261],		[443, 0.381965203342084451],
[254, 0.381968731084902591],		[349, 0.381965778235862751],		[444, 0.381965213096732811],
[255, 0.381968710370135581],		[350, 0.381965754821618321],		[445, 0.381965223222274801],
[256, 0.381968690495766151],		[351, 0.381965731340740971],		[446, 0.381965233277890061],
[257, 0.381968669112262681],		[352, 0.381965708805156011],		[447, 0.381965243390687441],
[258, 0.381968648996057651],		[353, 0.381965687299102691],		[448, 0.381965253345362851],
[259, 0.381968629718183291],		[354, 0.381965666032767661],		[449, 0.381965263478633911],
[260, 0.381968607895661951],		[355, 0.381965645441411161],		[450, 0.381965273781127491],
[261, 0.381968585112314021],		[356, 0.381965625891763311],		[451, 0.381965283913200061],
[262, 0.381968559962502951],		[357, 0.381965605702847991],		[452, 0.381965294077951271],
[263, 0.381968535373681828],		[358, 0.381965585401059351],		[453, 0.381965304146203331],
[264, 0.381968512721383661],		[359, 0.381965564472778461],		[454, 0.381965314511441007],

```
| [455, 0.38196532524522531], |
| [456, 0.38196533608255079], |
| [457, 0.38196534728693365], |
| [458, 0.38196535879842514], |
| [459, 0.38196537025101152], |
| [460, 0.38196538178624095], |
| [461, 0.38196539323766154], |
| [462, 0.38196540493061187], |
| [463, 0.38196541688093621], |
| [464, 0.38196542880872703], |
| [465, 0.38196544091749313], |
| [466, 0.38196545311330582], |
| [467, 0.38196546501798950], |
| [468, 0.38196547672833353], |
| [469, 0.38196548805502867], |
| [470, 0.38196549926918522], |
| [471, 0.38196551035436538], |
| [472, 0.38196552101915854], |
| [473, 0.38196553142477718], |
| [474, 0.38196554145584449], |
| [475, 0.38196555143594829], |
| [476, 0.38196556141084054], |
| [477, 0.38196557116042623], |
| [478, 0.38196558089636706], |
| [479, 0.38196559056306495], |
| [480, 0.38196559984918144], |
| [481, 0.38196560886785491], |
```

C.2.2 $s = 2$

```
| [  5, 0.39494530979186898, 0.39494530979186898],
| [  6, 0.38721156902859027, 0.38721156902859027],
| [  7, 0.38364421343670080, 0.38364421343670080],
| [  8, 0.38087753864434121, 0.38087753864434121],
| [  9, 0.38106319363905422, 0.38106319363905422],
| [ 10, 0.38049366379916577, 0.41796974341472143],
| [ 11, 0.38090258865886817, 0.41794044649375001],
| [ 12, 0.38146809942068910, 0.41791489802883525],
| [ 13, 0.38189558437643339, 0.41839111036588472],
| [ 14, 0.38185239270511140, 0.41902528431483316],
| [ 15, 0.38172870011694915, 0.41941282842471533],
| [ 16, 0.38843394307659927, 0.41953755471577481],
| [ 17, 0.38842705375860380, 0.41970019840840778],
| [ 18, 0.38844550208273674, 0.41989006712033233],
| [ 19, 0.38844280286118603, 0.42006071042967219],
| [ 20, 0.38853470443376785, 0.42010500439517218],
| [ 21, 0.38868958964940668, 0.42009616412145995],
| [ 22, 0.38797288571840686, 0.41999918799250874],
| [ 23, 0.38782010611984173, 0.41991162976106805],
| [ 24, 0.36918163137514237, 0.41983523279089650],
| [ 25, 0.36932235854190915, 0.41977447375614106],
| [ 26, 0.36945169785492088, 0.41973818250762923],
| [ 27, 0.36956030210826896, 0.41969373022117273],
| [ 28, 0.36962615873724802, 0.41965559653181667],
| [ 29, 0.36966904948184959, 0.41961189641287211],
| [ 30, 0.36968656891302182, 0.41957968820115410],
| [ 31, 0.36970112063752708, 0.41955315347611161],
| [ 32, 0.36712398788399303, 0.41953035927103521],
| [ 33, 0.36710216161832437, 0.41953940805135370],
| [ 34, 0.38195988285199872, 0.41969023238102349],
| [ 35, 0.38198288688808046, 0.41969827726338615],
| [ 36, 0.38199680671159469, 0.41970760902912835],
| [ 37, 0.38199939681293804, 0.41972449485875918],
| [ 38, 0.38199961309121616, 0.41974583313852892],
| [ 39, 0.38199781418272827, 0.41976347436794226],
| [ 40, 0.38198954606594981, 0.41977976501223602],
| [ 41, 0.38198632592591381, 0.41979112974172340],
| [ 42, 0.38196643070406722, 0.41980215683188898],
| [ 43, 0.38195601788747546, 0.41981093798624214],
| [ 44, 0.38194848591076341, 0.41982192475468666],
| [ 45, 0.38194080845808059, 0.41983454727221886],
| [ 46, 0.38193560908069324, 0.41984516418087359],
| [ 47, 0.38193191208931515, 0.41985533340703307],
| [ 48, 0.38192654022666467, 0.41986336749399772],
| [ 49, 0.38192101277202001, 0.41987165146617389],
| [ 50, 0.38191432139544884, 0.41987958732474318],
| [ 51, 0.38190902709042784, 0.41988454675978493],
| [ 52, 0.38190499979664877, 0.41988751400940677],
| [ 53, 0.38190041491210236, 0.41988738293095568],
| [ 54, 0.38189650336516745, 0.41988582724855567],
| [ 55, 0.38189271809861525, 0.41988253657044483],
| [ 56, 0.38189090568673667, 0.41987947722303010],
| [ 57, 0.38189103714256178, 0.41987660132409893],
| [ 58, 0.38189184261615733, 0.41987258437833269],
| [ 59, 0.38189415028753654, 0.41986813965459724],
| [ 60, 0.38189754728707626, 0.41986270381578289],
| [ 61, 0.38190075309214033, 0.41985732268237347],
| [ 62, 0.38190422995504392, 0.41985179119158950],
| [ 63, 0.38190748189797635, 0.41984719528523379],
| [ 64, 0.38191139083557213, 0.41984352134322772],
| [ 65, 0.38191590739703141, 0.41983994563445631],
| [ 66, 0.38192030042429570, 0.41983686762777034],
| [ 67, 0.38192504423521312, 0.41983386910613585],
| [ 68, 0.38192989074667089, 0.41983154128329331],
| [ 69, 0.38193408641774573, 0.41982970279427978],
| [ 70, 0.38193792974988433, 0.41982762983138971],
| [ 71, 0.38194113915406108, 0.41982552831347980],
| [ 72, 0.38194429011664532, 0.41982301253405657],
| [ 73, 0.38194737012667329, 0.41982049092096835],
| [ 74, 0.38194993623952461, 0.41981780470755592],
| [ 75, 0.38195232867446371, 0.41981547271697767],
| [ 76, 0.38195441141285535, 0.41981346828362465],
| [ 77, 0.38195670255117475, 0.41981132648491837],
| [ 78, 0.38195923706097773, 0.41980924208083509],
| [ 79, 0.38196170002085733, 0.41980699856736436],
| [ 80, 0.38196436925953359, 0.41980492532129110],
| [ 81, 0.38196715198789039, 0.41980294382354777],
| [ 82, 0.38196964964483532, 0.41980145463637547],
| [ 83, 0.38197201562008459, 0.41980045012469053],
| [ 84, 0.38197410807477905, 0.41979962891179173],
| [ 85, 0.38197622894897210, 0.41979913681818920],
| [ 86, 0.38197838155866415, 0.41979881784043771],
| [ 87, 0.38198032929593345, 0.41979889551576410],
| [ 88, 0.38198247753042356, 0.41980031485699010],
| [ 89, 0.38198403935620212, 0.41979975209026238],
| [ 90, 0.38198547753042356, 0.41980031485699010],
| [ 91, 0.38198665675413723, 0.41980083375960342],
| [ 92, 0.38198747866052890, 0.41980145604042596],
| [ 93, 0.38198814769145834, 0.41980210777110050],
| [ 94, 0.38198866999855552, 0.41980297935386279],
| [ 95, 0.38198889417521736, 0.41980405456385778],
| [ 96, 0.38198894630726243, 0.41980514851873962],
| [ 97, 0.38198878220100713, 0.41980633018666047],
| [ 98, 0.38198859642052474, 0.41980749535613598],
| [ 99, 0.38198841766396774, 0.41980876724477073],
| [100, 0.38198813887160810, 0.41981010504561622],
| [101, 0.38198788157057351, 0.41981133292615813],
| [102, 0.38198761918102531, 0.41981248996207116],
| [103, 0.38198720671238706, 0.41981347228437010],
| [104, 0.38198671037167115, 0.41981437267018262],
| [105, 0.38198607790413441, 0.41981515109634204],
| [106, 0.38198544248006772, 0.41981594056632321],
| [107, 0.38198480922888628, 0.41981673679824499],
| [108, 0.38198407856059796, 0.41981742368242347],
| [109, 0.38198332386603651, 0.41981805098598279],
| [110, 0.38198251751930246, 0.41981856247208993],
| [111, 0.38198178143652756, 0.41981904988748053],
| [112, 0.38198113171029269, 0.41981949290130000],
| [113, 0.38198049638932430, 0.41981999979780251],
| [114, 0.38197994338870583, 0.41982057007515783],
| [115, 0.38197945665125957, 0.41982113053772585],
| [116, 0.38197894625625245, 0.41982172334616069],
| [117, 0.38197845383377194, 0.41982230689720423],
| [118, 0.38197794268691604, 0.41982294776671414],
| [119, 0.38197748817747390, 0.41982363137848994],
| [120, 0.38197709330630986, 0.41982427646788073],
| [121, 0.38197669964395708, 0.41982490496738956],
| [122, 0.38197635269486335, 0.41982546962799844],
| [123, 0.38197603456554423, 0.41982601698956967],
| [124, 0.38197567007394106, 0.41982652453755381],
| [125, 0.38197528897757566, 0.41982705676510607],
| [126, 0.38197485980056933, 0.41982761257528423],
| [127, 0.38197565777643805, 0.42017643964830004],
| [128, 0.38197523625952029, 0.42017705576900116],
| [129, 0.38197477428351523, 0.42017764349706971],
| [130, 0.38197430480531741, 0.42017824022298966],
| [131, 0.38197381154469595, 0.42017882292838826],
| [132, 0.38197335499043134, 0.42017946654124455],
| [133, 0.38197294139066290, 0.42018014989157582],
| [134, 0.38197253350876698, 0.42018083118290961],
| [135, 0.38197216458229072, 0.42018153001890529],
| [136, 0.38197182513976968, 0.42018222090778823],
| [137, 0.38197146728866233, 0.42018294078002610],
| [138, 0.38197110939281875, 0.42018367923491462],
| [139, 0.38197073064033621, 0.42018438789885532],
| [140, 0.38197036969670523, 0.42018507692662443],
| [141, 0.38197002794988766, 0.42018571862797882],
| [142, 0.38196967357486789, 0.42018633842167979],
| [143, 0.38196932983334070, 0.42018692295022747],
| [144, 0.38196898603199753, 0.42018750693572726],
| [145, 0.38196868095913888, 0.42018808860564372],
| [146, 0.38196842129472292, 0.42018863486861247],
| [147, 0.38196818401110283, 0.42018915916895128],
| [148, 0.38196799342406978, 0.42018964216341786],
```

```
| [149, 0.38196784369180259, 0.42019010788022659]|,
| [150, 0.38196770382747430, 0.42019054900087816]|,
| [151, 0.38196758815933268, 0.42019099817213640]|,
| [152, 0.38196748362038530, 0.42019145721965762]|,
| [153, 0.38196741877617379, 0.42019189927412098]|,
| [154, 0.38196739413727854, 0.42019233765258135]|,
| [155, 0.38196738707693340, 0.42019275889585100]|,
| [156, 0.38196741428831421, 0.42019318580135528]|,
| [157, 0.38196746812126842, 0.42019361436780156]|,
| [158, 0.38196751790523858, 0.42019401519492139]|,
| [159, 0.38196757184107366, 0.42019439566327837]|,
| [160, 0.38196761686009767, 0.42019474018505582]|,
| [161, 0.38196767377027463, 0.42019506561114056]|,
| [162, 0.38196774172729031, 0.42019536542213087]|,
| [163, 0.38196779975352485, 0.42019566330652269]|,
| [164, 0.38196785975464825, 0.42019595931190967]|,
| [165, 0.38196791439447741, 0.42019623403133666]|,
| [166, 0.38196798556544215, 0.42019649699852146]|,
| [167, 0.38196807614743211, 0.42019673759439968]|,
| [168, 0.38196817151474322, 0.42019697172043530]|,
| [169, 0.38196828496436247, 0.42019719537927402]|,
| [170, 0.38196841254063774, 0.42019742885757072]|,
| [171, 0.38196853568384920, 0.42019767402788166]|,
| [172, 0.38196866215900649, 0.42019791567519704]|,
| [173, 0.38196878378154647, 0.42019816248274472]|,
| [174, 0.38196891661614590, 0.42019840582229867]|,
| [175, 0.38196906109997680, 0.42019865958911878]|,
| [176, 0.38196920397696804, 0.42019892140454557]|,
| [177, 0.38196935570538115, 0.42019917392673339]|
```

C.2.3 $s = 3$

```
| [  5, 0.39461632031689775, 0.39461632031689775, 0.39461632031689775],
| [  6, 0.38699962830010370, 0.38699962830010370, 0.38699962830010370],
| [  7, 0.38199135243447396, 0.38199135243447396, 0.41750051233943497],
| [  8, 0.37923440992012819, 0.37923440992012819, 0.41928208483826696],
| [  9, 0.37945223984825738, 0.37945223984825738, 0.41995527942530442],
| [ 10, 0.29427108420410197, 0.38178037978427370, 0.41790025959999927],
| [ 11, 0.27671699329248989, 0.38161687252915660, 0.41758087402281879],
| [ 12, 0.27624494433630975, 0.38207911523277893, 0.41751679611329340],
| [ 13, 0.27636237937567271, 0.38243621762997942, 0.41796076596234416],
| [ 14, 0.27660341634517627, 0.38234950785311189, 0.41857396732068214],
| [ 15, 0.27663693342963209, 0.38220066077997606, 0.41894894437559721],
| [ 16, 0.27674167242269643, 0.38193218224072756, 0.41927602277784703],
| [ 17, 0.27689109847590559, 0.38177893897832399, 0.41946605111933616],
| [ 18, 0.27698192582885611, 0.38170067395862278, 0.41967875559388462],
| [ 19, 0.27692107771620478, 0.38157526820217069, 0.41986877350834489],
| [ 20, 0.27684083166537199, 0.38148746067404860, 0.41993711279601825],
| [ 21, 0.27675147282934415, 0.38140656730458022, 0.41995191802598569],
| [ 22, 0.27661593397465939, 0.38140420558136051, 0.41989114185776000],
| [ 23, 0.27650925941186544, 0.38145770100326043, 0.41982310964565217],
| [ 24, 0.27643988105512834, 0.38151339117240196, 0.41973981026489737],
| [ 25, 0.27638285898074533, 0.38159751591068819, 0.41968865300044517],
| [ 26, 0.27630930602158682, 0.38169176018741136, 0.41966024378934830],
| [ 27, 0.27625205077848303, 0.38175847717447248, 0.41961887014398069],
| [ 28, 0.27620932352361371, 0.38181492097429914, 0.41958013856552662],
| [ 29, 0.27616733932739496, 0.38185366666447973, 0.41953343888897071],
| [ 30, 0.27614844412375789, 0.38189869512981373, 0.41949919563200899],
| [ 31, 0.27615247260590098, 0.38194737939184203, 0.41947134862523106],
| [ 32, 0.27616927529349977, 0.38198576386362415, 0.41946394312480517],
| [ 33, 0.27618471799492350, 0.38202371440856375, 0.41947286037419407],
| [ 34, 0.27620841326422324, 0.38205697135523647, 0.41948373044599663],
| [ 35, 0.27623968801025034, 0.38207558671899261, 0.41950096148223126],
| [ 36, 0.27627207851480406, 0.38208598082233036, 0.41951874119925670],
| [ 37, 0.27629606870578638, 0.38208551966710419, 0.41954395728404675],
| [ 38, 0.27631786033800260, 0.38208297200319968, 0.41957338672493472],
| [ 39, 0.27633760879273489, 0.38207865163164551, 0.41959909083285587],
| [ 40, 0.27635650495593778, 0.38206443940713897, 0.41908601220910396],
| [ 41, 0.27637159390919702, 0.38205240955284592, 0.41905216956033919],
| [ 42, 0.27638867406705225, 0.38203775741737217, 0.41902216217297350],
| [ 43, 0.27640570369637729, 0.38202569657696395, 0.41899462530128112],
| [ 44, 0.27641868511362072, 0.38201657209374912, 0.41897386008156939],
| [ 45, 0.27643114350426556, 0.38200726534837598, 0.41895906945031525],
| [ 46, 0.27644344156784628, 0.38200029973009908, 0.41894642893295186],
| [ 47, 0.27645396141586170, 0.38199474992736737, 0.41893715321274738],
| [ 48, 0.27645969826913569, 0.38198731823737492, 0.41892919357430675],
| [ 49, 0.27646305161950369, 0.38197955481634488, 0.41892458580226349],
| [ 50, 0.27646430147727269, 0.38197056733283896, 0.41892247772822916],
| [ 51, 0.27646175942641960, 0.38196683156230210, 0.41979452129642891],
| [ 52, 0.27645906244363000, 0.38196062787011686, 0.41980176767562638],
| [ 53, 0.27645621475002163, 0.38195394523048143, 0.41980569890927122],
| [ 54, 0.27645267075530544, 0.38194799169856231, 0.41980796427215761],
| [ 55, 0.27644711329267180, 0.38194221997168637, 0.41980823470024992],
| [ 56, 0.27644118512567972, 0.38193847272851095, 0.41980850290688027],
| [ 57, 0.27643509138136979, 0.38193671074917412, 0.41980874220784886],
| [ 58, 0.27642812714156811, 0.38193568915609544, 0.41980765555891775],
| [ 59, 0.27642185358680577, 0.38193628745349123, 0.41980600400511159],
| [ 60, 0.27641669022901927, 0.38193807933192242, 0.41980324781917044],
| [ 61, 0.27641226745697761, 0.38193981558688184, 0.41980040611253988],
| [ 62, 0.27640768551975814, 0.38194196308175848, 0.41979727456158633],
| [ 63, 0.27640386101783981, 0.38194398598085416, 0.41979497568357110],
| [ 64, 0.27640086156685550, 0.38194672012871744, 0.41979349478450317],
| [ 65, 0.27532170234365461, 0.38195416571893409, 0.41891589374330224],
| [ 66, 0.27532128091494706, 0.38195774228232676, 0.41891688624590662],
| [ 67, 0.27532100665902709, 0.38196168352004389, 0.41891748177231475],
| [ 68, 0.27532095064797629, 0.38196573887058938, 0.41891839507811168],
| [ 69, 0.27532072627404203, 0.38196916921902324, 0.41891958274404900],
| [ 70, 0.27531963206292465, 0.38197228991481663, 0.41892036439368652],
```

```
[ 71, 0.27531812628462377, 0.38197481545321499, 0.41892104034156658],
[ 72, 0.27531622372249309, 0.38197729281407694, 0.41892130974072822],
[ 73, 0.27531362369944623, 0.38197970715429153, 0.41892163502513285],
```

C.2.4 $s = 4$

```
[  5, 0.39433833701411702, 0.39433833701411702, 0.39433833701411702, 0.39433833701411702],
[  6, 0.38681077758540555, 0.38681077758540555, 0.38681077758540555, 0.38681077758540555],
[  7, 0.28589528613951148, 0.38237830455697441, 0.41692374560755463, 0.41692374560755463],
[  8, 0.28066427020961648, 0.38064198852675069, 0.38064198852675063, 0.41954189636240014],
[  9, 0.27848681346860943, 0.38053699690224840, 0.38053699690224840, 0.41984762886107285],
[ 10, 0.27736888273673715, 0.38135471592200065, 0.38135471592200065, 0.41917009126153987],
[ 11, 0.27619711654145068, 0.38162657996343224, 0.38162657996343224, 0.41903488182554599],
[ 12, 0.27589736910354495, 0.38210409367756037, 0.38210409367756037, 0.41890651101651394],
[ 13, 0.27612485726474717, 0.38247239226773055, 0.38247239226773055, 0.41925700853366710],
[ 14, 0.27663171140202941, 0.38263337292013649, 0.38263337292013649, 0.43739096250694975],
[ 15, 0.27672456736429057, 0.38250303005310410, 0.38250303005310410, 0.43747377882088850],
[ 16, 0.27687093855220296, 0.38224860184876736, 0.38224860184876736, 0.43755963049998453],
[ 17, 0.27705540651836907, 0.38211596596130604, 0.38211596596130604, 0.43783911532617886],
[ 18, 0.27718198127720856, 0.38205429914067945, 0.38205429914067945, 0.43819263337398107],
[ 19, 0.27713735169712822, 0.38193451059958233, 0.38193451059958233, 0.43843242627802526],
[ 20, 0.27705421557589099, 0.38183794754470379, 0.38183794754470379, 0.43863153924112802],
[ 21, 0.27695074366590816, 0.38174135824571492, 0.38174135824571492, 0.43875352319339994],
[ 22, 0.22769415905284338, 0.29542871842706298, 0.36887787490315682, 0.41996015812205040],
[ 23, 0.22766320742004423, 0.29554486892257154, 0.36903536946010063, 0.41989399212882966],
[ 24, 0.22768788611894886, 0.29561993106345713, 0.36920208507845320, 0.41981639802494380],
[ 25, 0.22774835890809755, 0.29570336986901868, 0.36933286296830503, 0.41977324523509829],
[ 26, 0.22781370681567950, 0.29579418075409220, 0.36945277576158769, 0.41975330123604843],
[ 27, 0.22785253898873323, 0.29587189864942742, 0.36955348693567736, 0.41972204806381685],
[ 28, 0.22789492557306146, 0.29591076852877490, 0.36961024972797957, 0.41969529084005930],
[ 29, 0.22794277831301582, 0.29593264934238839, 0.36964309685987767, 0.41966210484391298],
[ 30, 0.22798817553470974, 0.29593981597036229, 0.36965120672040880, 0.41963833531392741],
[ 31, 0.22801700052067958, 0.29592285473973451, 0.36965836916613093, 0.41961804860504126],
```

APPENDIX
D

Visual Examples

> The best way to understanding
> is a few good examples.
>
> Isaac Newton (1643–1727)

A few visual examples explaining Gaussian sampling via orthogonally transforming uniform low-discrepancy samples.

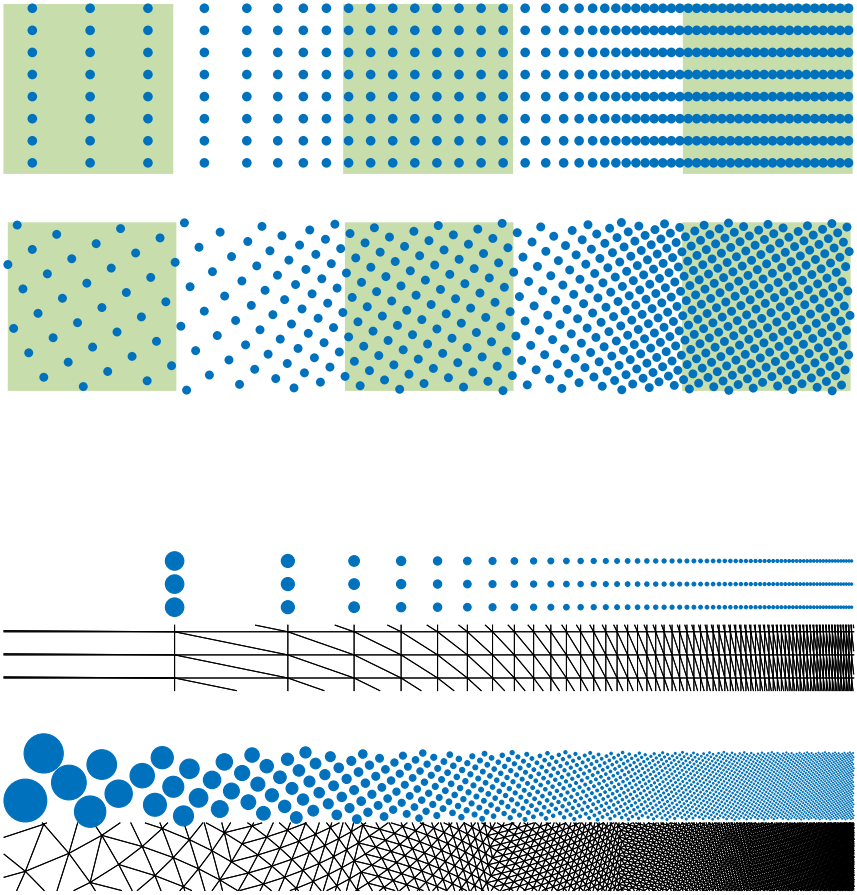

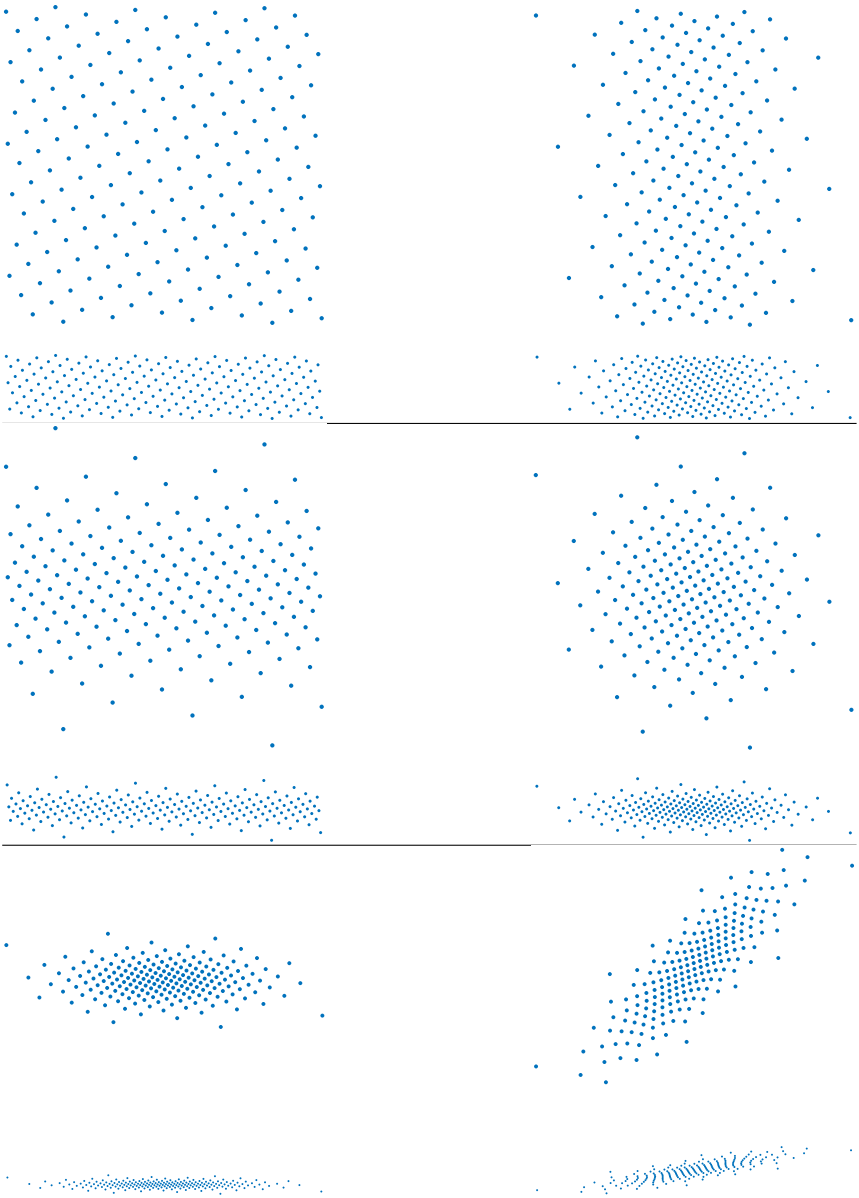

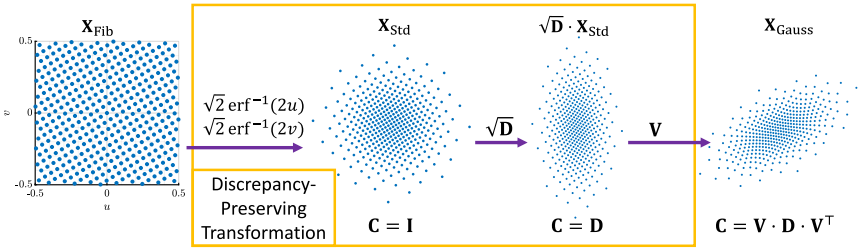
$\mathbf{X}_{\text{Fib}}$
$\mathbf{X}_{\text{Std}}$
$\sqrt{\mathbf{D}} \cdot \mathbf{X}_{\text{Std}}$
$\mathbf{X}_{\text{Gauss}}$
$\sqrt{2}\,\text{erf}^{-1}(2u)$
$\sqrt{2}\,\text{erf}^{-1}(2v)$
$\sqrt{\mathbf{D}}$
$\mathbf{V}$
Discrepancy-Preserving Transformation
$\mathbf{C} = \mathbf{I}$
$\mathbf{C} = \mathbf{D}$
$\mathbf{C} = \mathbf{V} \cdot \mathbf{D} \cdot \mathbf{V}^{\top}$

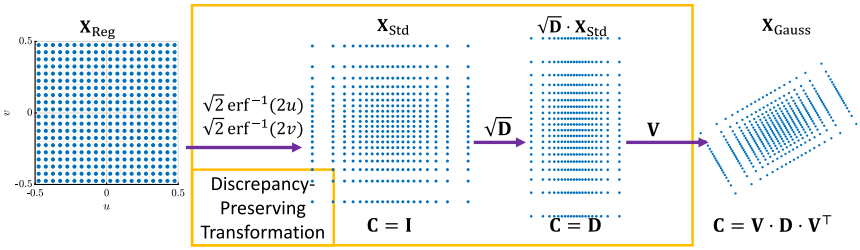
$\mathbf{X}_{\text{Reg}}$
$\mathbf{X}_{\text{Std}}$
$\sqrt{\mathbf{D}} \cdot \mathbf{X}_{\text{Std}}$
$\mathbf{X}_{\text{Gauss}}$
$\sqrt{2}\,\text{erf}^{-1}(2u)$
$\sqrt{2}\,\text{erf}^{-1}(2v)$
$\sqrt{\mathbf{D}}$
$\mathbf{V}$
Discrepancy-Preserving Transformation
$\mathbf{C} = \mathbf{I}$
$\mathbf{C} = \mathbf{D}$
$\mathbf{C} = \mathbf{V} \cdot \mathbf{D} \cdot \mathbf{V}^{\top}$

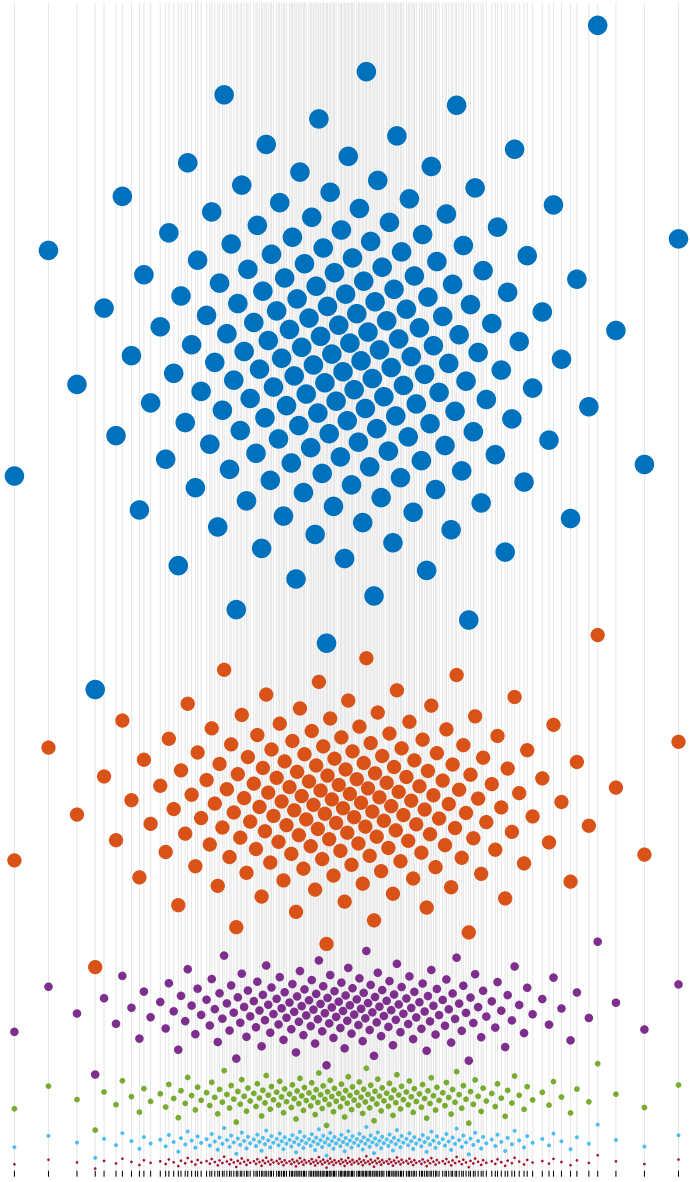

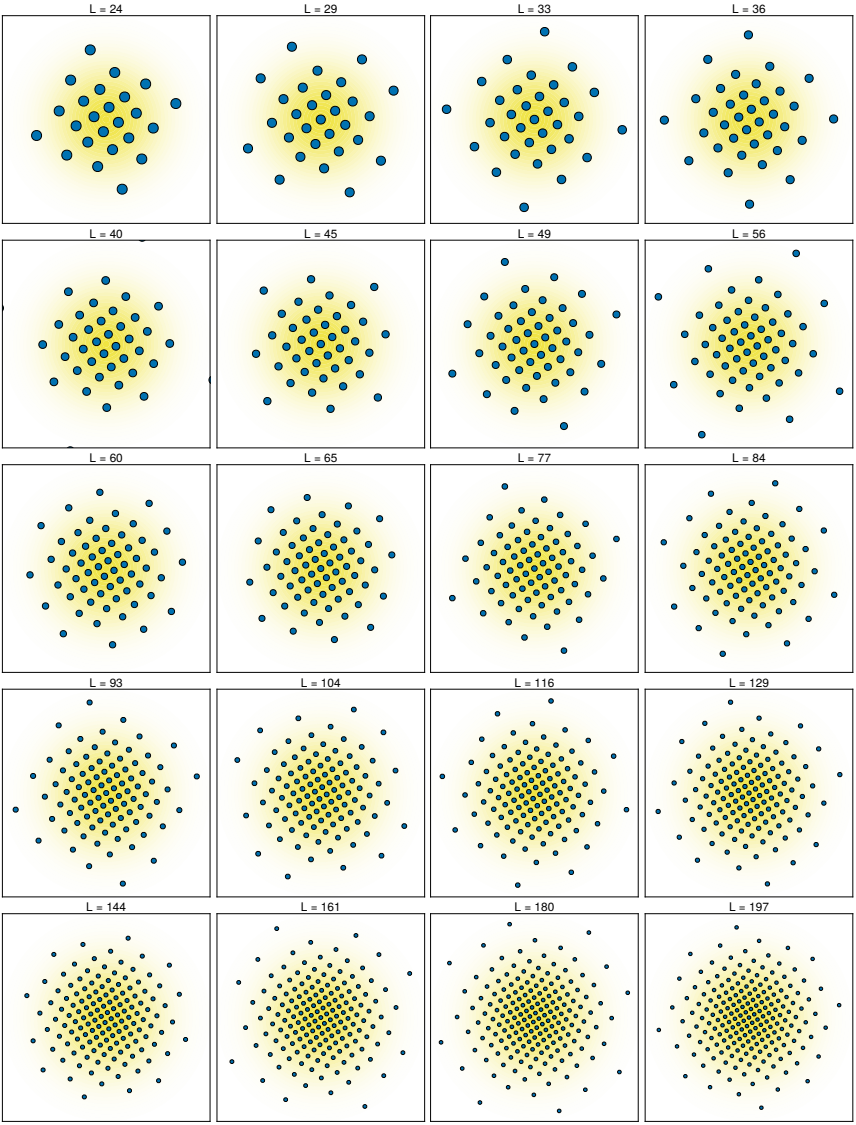
L = 24
L = 29
L = 33
L = 36
L = 40
L = 45
L = 49
L = 56
L = 60
L = 65
L = 77
L = 84
L = 93
L = 104
L = 116
L = 129
L = 144
L = 161
L = 180
L = 197

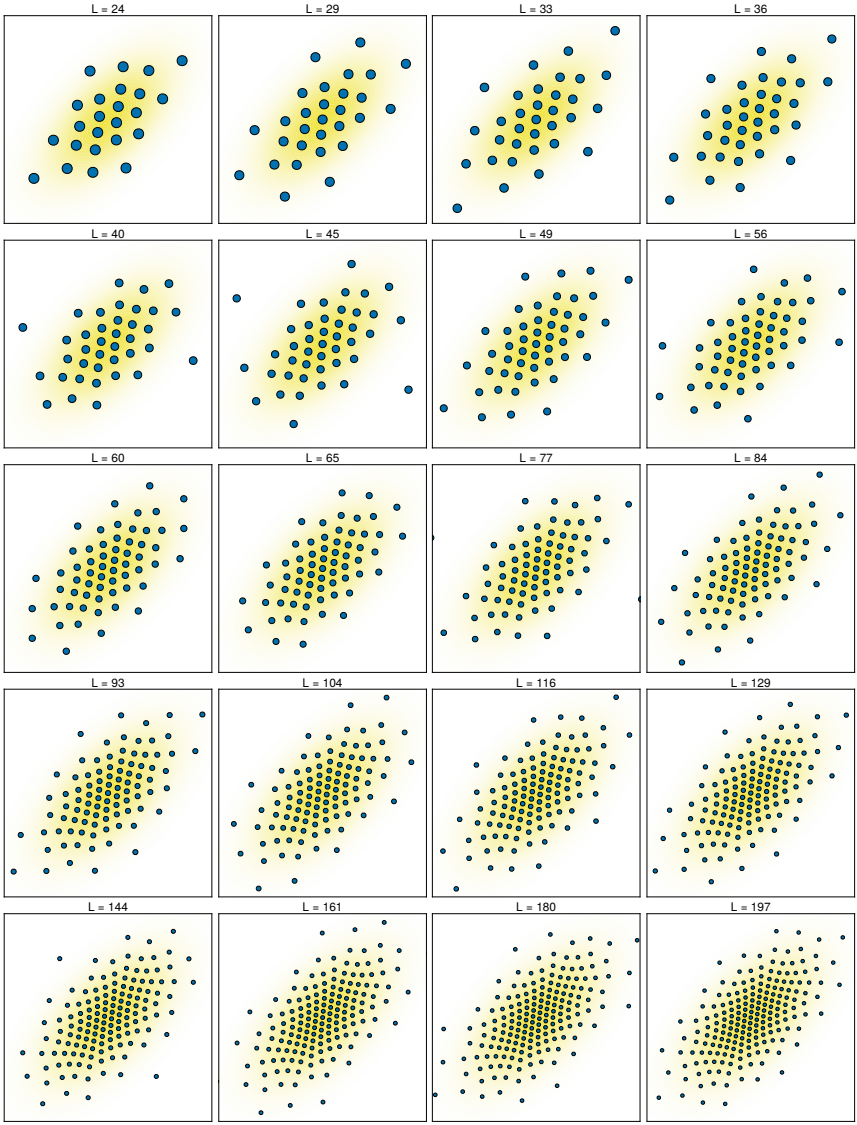
L = 24
L = 29
L = 33
L = 36
L = 40
L = 45
L = 49
L = 56
L = 60
L = 65
L = 77
L = 84
L = 93
L = 104
L = 116
L = 129
L = 144
L = 161
L = 180
L = 197

Bibliography

[1] M. Abramowitz and I. A. Stegun, eds. *Handbook of Mathematical Functions with Formulas, Graphs, and Mathematical Tables*. Dover Publications, 1972. ISBN: 0486612724 (cit. on pp. 155, 160).

[2] Christoph Aistleitner, Dmitriy Bilyk, and Aleksandar Nikolov. "Tusnády's Problem, the Transference Principle, and Non-Uniform QMC Sampling". In: *Monte Carlo and Quasi-Monte Carlo Methods*. Ed. by Art B. Owen and Peter W. Glynn. Cham: Springer International Publishing, 2018, pp. 169–180. ISBN: 978-3-319-91436-7 (cit. on pp. 89, 117).

[3] Christoph Aistleitner and Josef Dick. "Functions of Bounded Variation, Signed Measures, and a General Koksma-Hlawka Inequality". English. In: *Acta Arithmetica* 167.2 (2015), pp. 143–171. ISSN: 0065-1036 (cit. on pp. 18, 116, 117, 122, 123, 144, 152).

[4] Stuart Anderson and Dani Novak. *The Generalized Binet Formula for Calculating Fibonacci Vectors*. researchgate, May 2008 (cit. on p. 82).

[5] Ienkaran Arasaratnam and Simon Haykin. "Cubature Kalman Filters". In: *IEEE Transactions on Automatic Control* 54.6 (2009), pp. 1254–1269. DOI: 10.1109/TAC.2009.2019800 (cit. on p. 13).

[6] Emanouil I. Atanassov. "Efficient CPU-Specific Algorithm for Generating the Generalized Faure Sequences". In: *Large-Scale Scientific Computing*. Ed. by Ivan Lirkov et al. Berlin, Heidelberg: Springer Berlin Heidelberg, 2004, pp. 121–127. ISBN: 978-3-540-24588-9 (cit. on p. 17).

[7] Nikolai Sergeevich Bakhvalov. "On the Approximate Calculation of Multiple Integrals". In: *Journal of Complexity* 31.4 (2015), pp. 502–516. ISSN: 0885-064X. DOI: https://doi.org/10.1016/j.jco.2014.12.003 (cit. on p. 10).

[8] Jérémy Berthomieu, Christian Eder, and Mohab Safey El Din. "msolve: A Library for Solving Polynomial Systems". In: *2021 International Symposium on Symbolic and Algebraic Computation*. 46th International Symposium on Symbolic and Algebraic Computation. Saint Petersburg, Russia:

ACM, July 2021, pp. 51–58. DOI: 10.1145/3452143.3465545 (cit. on p. 103).

[9] Mathieu Besançon et al. “Distributions.jl: Definition and Modeling of Probability Distributions in the JuliaStats Ecosystem”. In: *Journal of Statistical Software* 98.16 (2021), pp. 1–30. ISSN: 1548-7660. DOI: 10.18637/jss.v098.i16 (cit. on p. 171).

[10] Jeff Bezanson et al. “Julia: A Fresh Approach to Numerical Computing”. In: *SIAM review* 59.1 (2017), pp. 65–98 (cit. on pp. 100, 171).

[11] Dmitriy Bilyk. “On Roth’s Orthogonal Function Method in Discrepancy Theory”. In: *Unif. Distrib. Theory* 6.1 (2011), pp. 143–184 (cit. on pp. 11, 90).

[12] G. E. P. Box and Mervin E. Muller. “A Note on the Generation of Random Normal Deviates”. In: *The Annals of Mathematical Statistics* 29.2 (1958), pp. 610–611. DOI: 10.1214/aoms/1177706645 (cit. on pp. 11, 139).

[13] David W. Boyd. “Pisot and Salem Numbers in Intervals of the Real Line”. In: *Mathematics of Computation* 32.144 (1978), pp. 1244–1260. ISSN: 00255718, 10886842 (cit. on p. 62).

[14] Mark Briers, Simon Maskell, and Robert Wright. “A rao-blackwellised unscented Kalman filter”. In: *Sixth International Conference of Information Fusion, 2003. Proceedings of the.* Vol. 1. 2003, pp. 55–61. DOI: 10.1109/ICIF.2003.177426 (cit. on p. 17).

[15] Alexander Buchholz, Florian Wenzel, and Stephan Mandt. “Quasi-Monte Carlo Variational Inference”. In: *Proceedings of the 35th International Conference on Machine Learning*. Ed. by Jennifer Dy and Andreas Krause. Vol. 80. Proceedings of Machine Learning Research. PMLR, July 2018, pp. 668–677 (cit. on p. 140).

[16] Russel E. Caflisch. “Monte Carlo and Quasi-Monte Carlo Methods”. en. In: *Acta Numerica* 7 (Jan. 1998). Publisher: Cambridge University Press, pp. 1–49. ISSN: 1474-0508, 0962-4929. DOI: 10.1017/S0962492900002804 (cit. on p. 10).

[17] Sylvain Calinon. “Gaussians on Riemannian Manifolds: Applications for Robot Learning and Adaptive Control”. In: *IEEE Robotics & Automation Magazine* 27.2 (2020), pp. 33–45. DOI: 10.1109/MRA.2020.2980548 (cit. on p. 15).

[18] Mathieu Cambou, Marius Hofert, and Christiane Lemieux. "Quasi-random Numbers for Copula Models". In: *Statistics and Computing* 27.5 (2017), pp. 1307–1329. ISSN: 1573-1375. DOI: 10.1007/s11222-016-9688-4 (cit. on p. 151).

[19] Pravin Chandra and Eric W. Weisstein. *Fibonacci Number. From MathWorld–A Wolfram Web Resource.* Online. Visited on 31/05/2023 (cit. on p. 71).

[20] Paul Otto Chelson. *Quasi-random techniques for Monte Carlo methods.* The Claremont Graduate University, Thesis (Ph.D.) ProQuest Dissertations Publishing, 1976. ISBN: 9781082949227 (cit. on p. 123).

[21] Keewhan Choi and W. G. Bulgren. "An Estimation Procedure for Mixtures of Distributions". In: *Journal of the Royal Statistical Society* (1968). ISSN: 0035-9246 (cit. on p. 25).

[22] Wikimedia Commons. *File:Bayer pattern on sensor.svg — Wikimedia Commons, the free media repository.* [Online; accessed 4-October-2023]. 2020 (cit. on p. 4).

[23] Wikimedia Commons. *File:CIExy1931 MacAdam.png — Wikimedia Commons, the free media repository.* [Online; accessed 28-September-2023]. 2020 (cit. on p. 4).

[24] Wikimedia Commons. *File:50 MW molten-salt power tower in hami.jpg — Wikimedia Commons, the free media repository.* [Online; accessed 4-October-2023]. 2023 (cit. on p. 4).

[25] Wikimedia Commons. *Probably Polistes, Paper Wasp. Heathcote National Park, NSW Australia, April 2009.* [Online; accessed 8-November-2023]. 2023 (cit. on p. 7).

[26] J. H. Conway and N. J. A. Sloane. "Certain Important Lattices and Their Properties". In: *Sphere Packings, Lattices and Groups.* Vol. Sphere Packings, Lattices and Groups. New York, NY: Springer New York, 1999, pp. 94–135. ISBN: 978-1-4757-6568-7. DOI: 10.1007/978-1-4757-6568-7_4 (cit. on p. 174).

[27] J. H. Conway and N. J. A. Sloane. "Coverings, Lattices and Quantizers". In: *Sphere Packings, Lattices and Groups.* Vol. Sphere Packings, Lattices and Groups. New York, NY: Springer New York, 1999, pp. 31–62. ISBN: 978-1-4757-6568-7. DOI: 10.1007/978-1-4757-6568-7_2 (cit. on p. 91).

[28] Ronald Cools, Frances Y. Kuo, and Dirk Nuyens. "Constructing Embedded Lattice Rules for Multivariate Integration". In: *SIAM Journal on Scientific Computing* 28.6 (2006), pp. 2162–2188. DOI: 10.1137/06065074X (cit. on p. 107).

[29] Ronald Cools and Philip Rabinowitz. “Monomial Cubature Rules Since “Stroud”: A Compilation”. In: *Journal of Computational and Applied Mathematics* 48.3 (1993), pp. 309–326. ISSN: 0377-0427. DOI: 10.1016/0377-0427(93)90027-9 (cit. on p. 13).

[30] Ronald Cools et al. “Fast Component-by-Component Construction of Lattice Algorithms for Multivariate Approximation with POD and SPOD Weights”. In: *Mathematics of Computation* 90.328 (2021), pp. 787–812 (cit. on p. 56).

[31] Simon Danisch and Julius Krumbiegel. “Makie.jl: Flexible high-performance data visualization for Julia”. In: *Journal of Open Source Software* 6.65 (2021), p. 3349. DOI: 10.21105/joss.03349 (cit. on p. 172).

[32] D. A. Darling. “The Kolmogorov-Smirnov, Cramér-von Mises Tests”. In: *The Annals of Mathematical Statistics* 28.4 (1957), pp. 823–838. ISSN: 0003-4851 (cit. on p. 25).

[33] Josef Dick, Aicke Hinrichs, and Friedrich Pillichshammer. “A Note on the Periodic L_2-Discrepancy of Korobov’s p-Sets”. In: *Archiv der Mathematik* 115.1 (2020), pp. 67–78. ISSN: 1420-8938. DOI: 10.1007/s00013-020-01460-5 (cit. on p. 127).

[34] Josef Dick, Peter Kritzer, and Friedrich Pillichshammer. “Introduction”. In: *Lattice Rules: Numerical Integration, Approximation, and Discrepancy*. Cham: Springer International Publishing, 2022, pp. 1–54. ISBN: 978-3-031-09951-9. DOI: 10.1007/978-3-031-09951-9_1 (cit. on p. 48).

[35] Josef Dick, Frances Y. Kuo, and Ian H. Sloan. “High-Dimensional Integration: The Quasi-Monte Carlo Way”. In: *Acta Numerica* 22 (2013), pp. 133–288. DOI: 10.1017/S0962492913000044 (cit. on pp. 10, 11, 16, 49, 57, 58, 64, 88, 89, 94–97, 140, 144).

[36] Josef Dick et al. “Lattice-Based Integration Algorithms: Kronecker Sequences and Rank-1 Lattices”. In: *Annali di Matematica Pura ed Applicata (1923 -)* 197.1 (Feb. 2018), pp. 109–126. ISSN: 1618-1891. DOI: 10.1007/s10231-017-0670-3 (cit. on pp. 50–52, 69).

[37] Benjamin Doerr et al. “Component-by-Component Construction of Low-Discrepancy Point Sets of Small Size”. In: *Monte Carlo Methods and Applications* 14.2 (July 2008), pp. 129–149. DOI: doi:10.1515/MCMA.2008.007 (cit. on p. 56).

[38] Dinh Dũng and Tino Ullrich. “Lower Bounds for the Integration Error for Multivariate Functions with Mixed Smoothness and Optimal Fibonacci Cubature for Functions on the Square”. en. In: *Mathematische Nachrichten* 288.7 (2015), pp. 743–762. ISSN: 1522-2616. DOI: 10.1002/mana.201400048 (cit. on p. 58).

[39] Adrian Ebert et al. “Digit-by-Digit and Component-by-Component Constructions of Lattice Rules for Periodic Functions With Unknown Smoothness”. In: *Journal of Complexity* 66 (2021), p. 101555. ISSN: 0885-064X. DOI: 10.1016/j.jco.2021.101555 (cit. on p. 56).

[40] Henri Faure. “Discrépance de suites associées à un système de numération (en dimension s)”. fre. In: *Acta Arithmetica* 41.4 (1982), pp. 337–351 (cit. on p. 17).

[41] Willliam Feller. *An Introduction to Probability Theory and Its Applications: Volume I*. John Wiley & Sons, 1968 (cit. on p. 10).

[42] Michael Fennel, Antonio Zea, and Uwe D. Hanebeck. “Optimization-Driven Design of a Kinesthetic Haptic Interface with Human-Like Capabilities”. In: *IEEE Transactions on Haptics* (2021). DOI: 10.1109/TOH.2021.3137938 (cit. on p. 15).

[43] Fernando Llorente Fernández et al. “Adaptive Quadrature Schemes for Bayesian Inference via Active Learning”. In: *IEEE Access* 8 (2020), pp. 208462–208483. DOI: 10.1109/ACCESS.2020.3038333 (cit. on p. 91).

[44] Daniel Fink. *A Compendium of Conjugate Priors*. Tech. rep. Bozeman, MT 59717: Montana State Univeristy, May 1997 (cit. on p. 16).

[45] Bernard D. Flury. “Acceptance–Rejection Sampling Made Easy”. In: *SIAM Review* 32.3 (1990), pp. 474–476 (cit. on p. 163).

[46] Konstantin Konstantinovich Frolov. “Upper Error Bounds for Quadrature Formulas on Function Classes”. In: *Doklady Akademii Nauk* 231.4 (1976), pp. 818–821 (cit. on p. 66).

[47] Alan C. Genz and Aftab Ahmad Malik. “Remarks on Algorithm 006: An Adaptive Algorithm for Numerical Integration Over an N-Dimensional Rectangular Region”. In: *Journal of Computational and Applied mathematics* 6.4 (1980), pp. 295–302 (cit. on p. 180).

[48] Igor Gilitschenski and Uwe D. Hanebeck. “Efficient Deterministic Dirac Mixture Approximation of Gaussian Distributions”. In: *Proceedings of the 2013 American Control Conference (ACC 2013)*. Washington D.C., USA, June 2013. DOI: 10.1109/acc.2013.6580197 (cit. on p. 13).

[49] Christophe Godin, Christophe Golé, and Stéphane Douady. “Phyllotaxis as Geometric Canalization During Plant Development”. In: *Development* 147.19 (Oct. 2020) (cit. on p. 59).

[50] Henry W. Gould. “A History of the Fibonacci Q-Matrix and a Higher-Dimensional Problem”. In: *Fibonacci Quart* 19.3 (1981), pp. 250–257 (cit. on p. 74).

[51] Eugene Gover and Nishan Krikorian. “Determinants and the Volumes of Parallelotopes and Zonotopes”. In: *Linear Algebra and its Applications* 433.1 (2010), pp. 28–40. ISSN: 0024-3795. DOI: https://doi.org/10.1016/j.laa.2010.01.031 (cit. on p. 51).

[52] Dong Guo and Xiaodong Wang. “Quasi-Monte Carlo Filtering in Nonlinear Dynamic Systems”. In: *IEEE Transactions on Signal Processing* 54.6 (2006), pp. 2087–2098. DOI: 10.1109/TSP.2006.873585 (cit. on p. 140).

[53] Philipp A. Guth et al. *A quasi-Monte Carlo Method for an Optimal Control Problem Under Uncertainty*. 2019 (cit. on p. 5).

[54] Philipp A. Guth et al. “A Quasi-Monte Carlo Method for Optimal Control Under Uncertainty”. In: *SIAM/ASA Journal on Uncertainty Quantification* 9.2 (2021), pp. 354–383. DOI: 10.1137/19M1294952 (cit. on p. 5).

[55] J. M. Hammersley and K. W. Morton. “A new Monte Carlo Technique: Antithetic Variates”. In: *Mathematical Proceedings of the Cambridge Philosophical Society* 52.3 (1956), pp. 449–475. DOI: 10.1017/S0305004100031455 (cit. on p. 16).

[56] Hee Han et al. “Domain structures and piezoelectric properties of Pb(Zr0.2Ti0.8)O3 nanocapacitors”. In: *Journal of Applied Physics* 108.4 (Aug. 2010), p. 044102. ISSN: 0021-8979. DOI: 10.1063/1.3475476 (cit. on p. 4).

[57] Uwe D. Hanebeck. “Optimal Reduction of Multivariate Dirac Mixture Densities”. In: *at – Automatisierungstechnik* 63.4 (Apr. 2015), pp. 265–278. DOI: 10.1515/auto-2015-0005 (cit. on p. 27).

[58] Uwe D. Hanebeck. “Deterministic Sampling of Multivariate Densities based on Projected Cumulative Distributions”. In: *Proceedings of the 54th Annual Conference on Information Sciences and Systems (CISS 2020)*. Princeton, New Jersey, USA, Mar. 2020. DOI: 10.1109/CISS48834.2020.1570617413 (cit. on pp. 16, 37, 38).

[59] Uwe D. Hanebeck, Marco F. Huber, and Vesa Klumpp. "Dirac Mixture Approximation of Multivariate Gaussian Densities". In: *Proceedings of the 2009 IEEE Conference on Decision and Control (CDC 2009)*. Shanghai, China, Dec. 2009. DOI: 10.1109/CDC.2009.5400649 (cit. on pp. 12, 13, 16, 27, 180, 200).

[60] Uwe D. Hanebeck and Vesa Klumpp. "Localized Cumulative Distributions and a Multivariate Generalization of the Cramér-von Mises Distance". In: *Proceedings of the 2008 IEEE International Conference on Multisensor Fusion and Integration for Intelligent Systems (MFI 2008)*. Seoul, Republic of Korea, Aug. 2008, pp. 33–39. DOI: 10.1109/MFI.2008.4648104 (cit. on pp. 13, 16, 26, 27).

[61] Uwe D. Hanebeck and Martin Pander. "Progressive Bayesian Estimation with Deterministic Particles". In: *Proceedings of the 19th International Conference on Information Fusion (Fusion 2016)*. Heidelberg, Germany, July 2016 (cit. on p. 34).

[62] Hansgrohe Deutschland Vertriebs GmbH. *Raindance Select S Handbrause 150 3jet EcoSmart*. [Online; accessed 25-October-2023]. 2023 (cit. on p. 4).

[63] Jürgen Hartinger and Reinhold Kainhofer. "Non-Uniform Low-Discrepancy Sequence Generation and Integration of Singular Integrands". In: *Monte Carlo and Quasi-Monte Carlo Methods 2004*. Ed. by Harald Niederreiter and Denis Talay. Berlin, Heidelberg: Springer Berlin Heidelberg, 2006, pp. 163–179. ISBN: 978-3-540-31186-7 (cit. on p. 170).

[64] Stefan Heinrich. "Some Open Problems Concerning the Star-Discrepancy". In: *Journal of Complexity* 19.3 (2003). Oberwolfach Special Issue, pp. 416–419. ISSN: 0885-064X. DOI: https://doi.org/10.1016/S0885-064X(03)00014-1 (cit. on p. 18).

[65] Ernst Hellinger. "Neue Begründung der Theorie Quadratischer Formen von Unendlichvielen Veränderlichen." de. In: *Journal für die reine und angewandte Mathematik* 1909.136 (1909), pp. 210–271 (cit. on p. 24).

[66] Guillermo Henry and Daniela Rodriguezs. "Robust Estimators in Partly Linear Regression Models on Riemannian Manifolds". In: *Communications in Statistics-Theory and Methods* (2022), pp. 1–17 (cit. on p. 14).

[67] Doug Hensley and Francis Edward Su. “Random Walks with Badly Approximable Numbers”. In: *Unusual Applications of Number Theory: DIMACS Workshop, Unusual Applications of Number Theory, January 10-14, 2000, DIMACS Center*. Vol. 64. DIMACS Series in Discrete Mathematics and Theoretical Computer Science. American Mathematical Soc. 2004, p. 95 (cit. on p. 61).

[68] Aicke Hinrichs and Jens Oettershagen. “Optimal Point Sets for Quasi-Monte Carlo Integration of Bivariate Periodic Functions with Bounded Mixed Derivatives”. en. In: *Monte Carlo and Quasi-Monte Carlo Methods*. Ed. by Ronald Cools and Dirk Nuyens. Springer Proceedings in Mathematics & Statistics. Cham: Springer International Publishing, 2016, pp. 385–405. ISBN: 978-3-319-33507-0. DOI: 10.1007/978-3-319-33507-0_19 (cit. on pp. 58, 59, 97, 98, 103, 207).

[69] E. Hlawka and R. Mück. “Über eine Transformation von gleichverteilten Folgen II”. In: *Computing* 9.2 (1972), pp. 127–138. ISSN: 1436-5057. DOI: 10.1007/BF02236962 (cit. on p. 117).

[70] Edmund Hlawka. “Funktionen von beschränkter Variation in der Theorie der Gleichverteilung”. de. In: *Annali di Matematica Pura ed Applicata* 54.1 (1961), pp. 325–333. ISSN: 1618-1891. DOI: 10.1007/BF02415361 (cit. on p. 90).

[71] P. F. Hokayem and C. T. Abdallah. “Quasi-Monte Carlo Methods in Robust Control Design”. In: *42nd IEEE International Conference on Decision and Control (IEEE Cat. No.03CH37475)*. Vol. 3. 2003, pp. 2435–2440. DOI: 10.1109/CDC.2003.1272985 (cit. on p. 5).

[72] Ross Honsberger. “A Second Look at the Fibonacci and Lucas Numbers”. In: vol. 9. Dolciani Mathematical Expositions. The Mathematical Association of America, 1985. Chap. 8, pp. 102–138. ISBN: 0-88385-318-3 (cit. on p. 71).

[73] Wolfgang Hörmann, Josef Leydold, and Gerhard Derflinger. “General Principles in Random Variate Generation”. In: *Automatic Nonuniform Random Variate Generation*. Berlin, Heidelberg: Springer Berlin Heidelberg, 2004, pp. 13–41. ISBN: 978-3-662-05946-3. DOI: 10.1007/978-3-662-05946-3_2 (cit. on p. 40).

[74] Scott Hotton et al. “The Possible and the Actual in Phyllotaxis: Bridging the Gap between Empirical Observations and Iterative Models”. In: *Journal of Plant Growth Regulation* 25.4 (Dec. 2006), pp. 313–323. ISSN: 1435-8107 (cit. on p. 59).

[75] Marco F. Huber and Uwe D. Hanebeck. “Gaussian Filter based on Deterministic Sampling for High Quality Nonlinear Estimation”. In: *Proceedings of the 17th IFAC World Congress (IFAC 2008)*. Vol. 17. 2. Seoul, Republic of Korea, July 2008. DOI: 10.3182/20080706-5-KR-1001.02291 (cit. on p. 12).

[76] Marco F. Huber and Uwe D. Hanebeck. “Gaussian Filter based on Deterministic Sampling for High Quality Nonlinear Estimation”. In: *IFAC Proceedings Volumes* 41.2 (2008). 17th IFAC World Congress, pp. 13527–13532. ISSN: 1474-6670. DOI: https://doi.org/10.3182/20080706-5-KR-1001.02291 (cit. on pp. 12, 35).

[77] G. van (Gerrit) Iterson. *Mathematische und Mikroskopisch-Anatomische Studien über Blattstellungen nebst Betrachtungen über den Schalenbau der Miliolinen.* Jena: Fischer, 1907 (cit. on p. 59).

[78] K. Ito and K. Xiong. “Gaussian Filters for Nonlinear Filtering Problems”. In: *IEEE Transactions on Automatic Control* 45.5 (2000), pp. 910–927. DOI: 10.1109/9.855552 (cit. on p. 12).

[79] Peter Jäckel. “A Note on Multivariate Gauss-Hermite Quadrature”. In: *London: ABN-Amro. Re* (2005) (cit. on p. 12).

[80] Wenzel Jakob. “Numerically Stable Sampling of the von Mises-Fisher Distribution on S^2 (and Other Tricks)”. In: *Interactive Geometry Lab, ETH Zürich, Tech. Rep* (2012), p. 6 (cit. on p. 162).

[81] Lucas Janson, Brian Ichter, and Marco Pavone. “Deterministic Sampling-Based Motion Planning: Optimality, Complexity, and Performance”. In: *The International Journal of Robotics Research* 37.1 (2018), pp. 46–61. DOI: 10.1177/0278364917714338 (cit. on p. 5).

[82] Bin Jia, Ming Xin, and Yang Cheng. “High-Degree Cubature Kalman Filter”. In: *Automatica* 49.2 (2013), pp. 510–518. ISSN: 0005-1098 (cit. on p. 13).

[83] Stephen Joe and Frances Y. Kuo. “Remark on Algorithm 659: Implementing Sobol’s Quasirandom Sequence Generator”. In: *ACM Trans. Math. Softw.* 29.1 (Mar. 2003), pp. 49–57. ISSN: 0098-3500. DOI: 10.1145/641876.641879 (cit. on pp. 17, 200).

[84] S. J. Julier. “The Scaled Unscented Transformation”. In: *Proceedings of the 2002 American Control Conference (IEEE Cat. No.CH37301)*. Vol. 6. May 2002, pp. 4555–4559 (cit. on p. 13).

[85] S. J. Julier and J. K. Uhlmann. "Reduced Sigma Point Filters for the Propagation of Means and Covariances through Nonlinear Transformations". In: *Proceedings of the 2002 American Control Conference (IEEE Cat. No.CH37301)*. Vol. 2. 2002, pp. 887–892. DOI: 10.1109/ACC.2002.1023128 (cit. on p. 13).

[86] S. J. Julier and J. K. Uhlmann. "Unscented Filtering and Nonlinear Estimation". In: *Proceedings of the IEEE* 92.3 (2004), pp. 401–422. DOI: 10.1109/JPROC.2003.823141 (cit. on p. 16).

[87] Simon J. Julier and Jeffrey K. Uhlmann. "New Extension of the Kalman Filter to Nonlinear Systems". In: *Signal Processing, Sensor Fusion, and Target Recognition VI*. Vol. 3068. International Society for Optics and Photonics. July 1997, pp. 182–193 (cit. on pp. 13, 15, 16).

[88] Bjarne Junge and V. E. Hoggatt. "Polynomials Arising from Reflections across Multiple Plates". en. In: *Fibonacci Quarterly* 11.3 (1973), p. 7 (cit. on p. 82).

[89] Christopher Kacwin, Jens Oettershagen, and Tino Ullrich. "On the Orthogonality of the Chebyshev-Frolov Lattice and Applications". In: *Monatshefte für Mathematik* 184.3 (2017), pp. 425–441. ISSN: 1436-5081. DOI: 10.1007/s00605-017-1078-2 (cit. on pp. 54, 68).

[90] Christopher Kacwin et al. "Numerical Performance of Optimized Frolov Lattices in Tensor Product Reproducing Kernel Sobolev Spaces". en. In: *Foundations of Computational Mathematics* 21.3 (June 2021), pp. 849–889. ISSN: 1615-3383. DOI: 10.1007/s10208-020-09463-y (cit. on pp. 51, 54, 58, 66, 68, 69, 98).

[91] Toni Karvonen, Chris Oates, and Mark Girolami. "Integration in Reproducing Kernel Hilbert Spaces of Gaussian Kernels". en. In: *Mathematics of Computation* 90.331 (Sept. 2021), pp. 2209–2233. ISSN: 0025-5718, 1088-6842. DOI: 10.1090/mcom/3659 (cit. on p. 91).

[92] J. F. Koksma. "The Theory of Asymptotic Distribution Modulo One". en. In: *Compositio Mathematica* 16 (1964), pp. 1–22 (cit. on p. 90).

[93] Jurjen Ferdinand Koksma. "A General Theorem from the Theory of Uniform Distribution Modulo 1". In: *Mathematica B (Zutphen)* 11 (1942), pp. 7–11 (cit. on p. 90).

[94] A. N. Korobov. "The Approximate Computation of Multiple Integrals". In: *Dokl. Akad. Nauk SSSR*. Vol. 124. 1959, pp. 1207–1210 (cit. on p. 49).

[95] Leopold Kronecker. “Näherungsweise Ganzzahlige Auflösung Linearer Gleichungen”. In: *Leopold Kronecker's Werke*. Ed. by Kurt Hensel. Vol. III. Leipzig : Druck und Verlag von B.G. Teubner, 1895-1931, 1884. DOI: https://doi.org/10.3931/e-rara-17875 (cit. on p. 49).

[96] Jörg Krüger et al. “Laser micromachining of barium aluminium borosilicate glass with pulse durations between 20 fs and 3 ps”. In: *Applied Surface Science* 127-129 (1998), pp. 892–898. ISSN: 0169-4332. DOI: https://doi.org/10.1016/S0169-4332(97)00763-0 (cit. on p. 6).

[97] Lauwerens Kuipers and Harald Niederreiter. *Uniform Distribution of Sequences*. A Wiley-Interscience publication. John Wiley & Sons, Inc., 1974. ISBN: 0-471-51045-9 (cit. on p. 89).

[98] S. Kullback and R. A. Leibler. “On Information and Sufficiency”. In: *The Annals of Mathematical Statistics* 22.1 (1951), pp. 79–86. ISSN: 0003-4851 (cit. on p. 24).

[99] F. Y. Kuo et al. “Quasi-Monte Carlo for Highly Structured Generalised Response Models”. In: *Methodology and Computing in Applied Probability* 10.2 (2008), pp. 239–275. ISSN: 1573-7713. DOI: 10.1007/s11009-007-9045-3 (cit. on p. 147).

[100] Frances Y. Kuo, Weiwen Mo, and Dirk Nuyens. *Constructing Embedded Lattice-based Algorithms for Multivariate Function Approximation with a Composite Number of Points*. 2022 (cit. on p. 107).

[101] Frances Y. Kuo and Dirk Nuyens. “Application of Quasi-Monte Carlo Methods to Elliptic PDEs with Random Diffusion Coefficients: A Survey of Analysis and Implementation”. In: *Foundations of Computational Mathematics* 16.6 (2016), pp. 1631–1696. ISSN: 1615-3383. DOI: 10.1007/s10208-016-9329-5 (cit. on p. 5).

[102] Gerhard Kurz, Igor Gilitschenski, and Uwe D. Hanebeck. “Unscented von Mises–Fisher Filtering”. In: *IEEE Signal Processing Letters* 23.4 (Apr. 2016), pp. 463–467. DOI: 10.1109/LSP.2016.2529854 (cit. on pp. 12, 15).

[103] Gerhard Kurz and Uwe D. Hanebeck. “Stochastic Sampling of the Hyperspherical von Mises–Fisher Distribution Without Rejection Methods”. In: *Proceedings of the IEEE ISIF Workshop on Sensor Data Fusion: Trends, Solutions, Applications (SDF 2015)*. Bonn, Germany, Oct. 2015. DOI: 10.1109/SDF.2015.7347705 (cit. on pp. 162, 168).

[104] Gerhard Kurz et al. “Directional Statistics and Filtering Using libDirectional”. In: *Journal of Statistical Software* 89.4 (2019), pp. 1–31. DOI: 10.18637/jss.v089.i04 (cit. on p. 32).

[105] Johann Heinrich Lambert. *Anmerkungen und Zusätze zur Entwerfung der Land- und Himmelscharten*. Beyträge zum Gebrauche der MATHEMATIK und deren Anwendung durch J. H. Lambert 3. Berlin: Verlag der Buchhandlung der Realschule, 1772 (cit. on p. 153).

[106] Dirk Laurie. "Calculation of Gauss-Kronrod Quadrature Rules". In: *Mathematics of Computation* 66.219 (1997), pp. 1133–1145 (cit. on p. 180).

[107] Christiane Lemieux. "Variance Reduction Techniques". In: *Monte Carlo and Quasi-Monte Carlo Sampling*. New York, NY: Springer New York, 2009, pp. 1–52. ISBN: 978-0-387-78165-5. DOI: 10.1007/978-0-387-78165-5_4 (cit. on p. 16).

[108] Paul Leopardi. "A Partition of the Unit Sphere into Regions of Equal Area and Small Diameter". eng. In: *ETNA. Electronic Transactions on Numerical Analysis [electronic only]* 25 (2006), pp. 309–327 (cit. on p. 12).

[109] Kailai Li, Florian Pfaff, and Uwe D. Hanebeck. "Hyperspherical Deterministic Sampling Based on Riemannian Geometry for Improved Nonlinear Bingham Filtering". In: *Proceedings of the 22nd International Conference on Information Fusion (Fusion 2019)*. Ottawa, Canada, July 2019 (cit. on pp. 15, 28).

[110] Kailai Li, Florian Pfaff, and Uwe D. Hanebeck. "Nonlinear von Mises–Fisher Filtering Based on Isotropic Deterministic Sampling". In: *Proceedings of the 2020 IEEE International Conference on Multisensor Fusion and Integration for Intelligent Systems (MFI 2020)*. Virtual, Sept. 2020. DOI: 10.1109/MFI49285.2020.9235260 (cit. on p. 16).

[111] Kailai Li, Florian Pfaff, and Uwe D. Hanebeck. "Hyperspherical Dirac Mixture Reapproximation". In: *arXiv preprint arXiv:2110.10411* (Oct. 2021) (cit. on pp. 12, 16, 32).

[112] Kailai Li, Florian Pfaff, and Uwe D. Hanebeck. "Progressive von Mises–Fisher Filtering Using Isotropic Sample Sets for Nonlinear Hyperspherical Estimation". In: *Sensors* (Apr. 2021). DOI: 10.3390/s21092991 (cit. on pp. 12, 16).

[113] Dahua Lin et al. *JuliaStats/Distributions.jl: a Julia Package for Probability Distributions and Associated Functions*. July 2019. DOI: 10.5281/zenodo.2647458 (cit. on p. 171).

[114] M. M. Skriganov. "Constructions of uniform distributions in terms of geometry of numbers". In: *Algebra i Analiz* 6.3 (1994), pp. 200–230 (cit. on p. 51).

[115] David L. MacAdam. "Visual Sensitivities to Color Differences in Daylight". In: *J. Opt. Soc. Am.* 32.5 (May 1942), pp. 247–274. DOI: 10.1364/JOSA.32.000247 (cit. on p. 6).

[116] K. Mammasis and R. W. Stewart. "The FB5 Distribution and its Application in Wireless Communications". In: *2008 International ITG Workshop on Smart Antennas*. 2008, pp. 375–381. DOI: 10.1109/WSA.2008.4475585 (cit. on p. 14).

[117] Simon Maskell, Yifan Zhou, and Antonietta Mira. "Control Variates for Constrained Variables". In: *IEEE Signal Processing Letters* 29 (2022), pp. 2333–2337. DOI: 10.1109/LSP.2022.3221347 (cit. on p. 16).

[118] Henrique M. T. Menegaz et al. "A Systematization of the Unscented Kalman Filter Theory". In: *IEEE Transactions on Automatic Control* 60.10 (2015), pp. 2583–2598. DOI: 10.1109/TAC.2015.2404511 (cit. on p. 16).

[119] Michael R. Merrifield. *Hubble Space Telescope, Crystal Nebulae*. [Online; accessed 05-February-2024]. 2024 (cit. on p. 4).

[120] Microprocessor Standards Committee. "IEEE Standard for Floating-Point Arithmetic". In: *IEEE Std* 754-2019 (Revision of IEEE 754-2008) (2019), pp. 1–84. DOI: 10.1109/IEEESTD.2019.8766229 (cit. on pp. 53, 103).

[121] H. Niederreiter. "A Quasi-Monte Carlo Method for the Approximate Computation of the Extreme Values of a Function". In: *Studies in Pure Mathematics: To the Memory of Paul Turán*. Ed. by Paul Erdős et al. Basel: Birkhäuser Basel, 1983, pp. 523–529. ISBN: 978-3-0348-5438-2. DOI: 10.1007/978-3-0348-5438-2_45 (cit. on pp. 5, 91, 92, 125, 128).

[122] Harald Niederreiter. "Point Sets and Sequences with Small Discrepancy". In: *Monatshefte für Mathematik* 104.4 (1987), pp. 273–337. ISSN: 1436-5081. DOI: 10.1007/BF01294651 (cit. on p. 17).

[123] Harald Niederreiter and Ian H. Sloan. "Integration of Nonperiodic Functions of Two Variables by Fibonacci Lattice Rules". In: *Journal of computational and applied mathematics* 51.1 (1994), pp. 57–70 (cit. on pp. 58, 59, 70, 71, 207).

[124] Harald Niederreiter and Arne Winterhof. *Applied Number Theory*. en. Cham: Springer International Publishing, Sept. 2015. ISBN: 978-3-319-22321-6. DOI: 10.1007/978-3-319-22321-6 (cit. on pp. 61, 64).

[125] Cristiano Nisoli et al. "Annealing a Magnetic Cactus Into Phyllotaxis". In: *Phys. Rev. E* 81 (4 Apr. 2010), p. 046107 (cit. on p. 59).

[126] Dirk Nuyens. *Fast Construction of Good Lattice Rules*. Dissertation. Katholieke Universiteit Leuven – Faculteit Ingenieurswetenschappen, Apr. 2007. ISBN: 978-90-5682-804-2 (cit. on p. 90).

[127] OEIS Foundation, Inc. *The On-Line Encyclopedia of Integer Sequences*. Published electronically at `http://oeis.org`. 2023 (cit. on pp. 56, 61, 100).

[128] Hilary I. Okagbue, Muminu O. Adamu, and Timothy A. Anake. "Solutions of Chi-Square Quantile Differential Equation". In: *Proceedings of the World Congress on Engineering and Computer Science*. Vol. 2. 2017, pp. 813–818 (cit. on p. 168).

[129] Giray Ökten and Ahmet Göncü. "Generating Low-Discrepancy Sequences from the Normal Distribution: Box–Muller or Inverse Transform?" In: *Mathematical and Computer Modelling* 53.5 (2011), pp. 1268–1281. ISSN: 0895-7177. DOI: `https://doi.org/10.1016/j.mcm.2010.12.011` (cit. on pp. 143, 147).

[130] Konstantinos G. Papakonstantinou, Mariyam Amir, and Gordon P. Warn. "A Scaled Spherical Simplex Filter (S3F) with a Decreased $n + 2$ Sigma Points Set Size and Equivalent $2n + 1$ Unscented Kalman Filter (UKF) Accuracy". In: *Mechanical Systems and Signal Processing* 163 (2022), p. 107433. ISSN: 0888-3270. DOI: `10.1016/j.ymssp.2020.107433` (cit. on p. 13).

[131] Van L. Parsons. "Stratified Sampling". In: *Wiley StatsRef: Statistics Reference Online*. John Wiley & Sons, Ltd, 2017, pp. 1–11. ISBN: 9781118445112. DOI: `10.1002/9781118445112.stat05999.pub2` (cit. on p. 16).

[132] Mayur Patel. "Optimizing Kronecker Sequences for Multidimensional Sampling". In: *Journal of Computer Graphics Techniques (JCGT)* 11.1 (Mar. 2022), pp. 55–81. ISSN: 2331-7418 (cit. on pp. 61, 107).

[133] John A. Peacock. "Two-Dimensional Goodness-of-Fit Testing in Astronomy". In: *Monthly Notices of the Royal Astronomical Society* 202.3 (1983), pp. 615–627 (cit. on p. 26).

[134] Marko Petkovšek, Herbert S. Wilf, and Doron Zeilberger. *A=B*. AK Peters, Wellesley, MA, 1997. ISBN: 1568810636 (cit. on p. 160).

[135] Florian Pfaff, Kailai Li, and Uwe D. Hanebeck. "The Spherical Grid Filter for Nonlinear Estimation on the Unit Sphere". In: *Proceedings of the 1st Virtual IFAC World Congress (IFAC-V 2020)*. July 2020. DOI: `10.1016/j.ifacol.2020.12.031` (cit. on p. 12).

[136] G. M. Phillips. “A Survey of One-Dimensional and Multidimensional Numerical Integration”. In: *Computer Physics Communications* 20.1 (1980), pp. 17–27. ISSN: 0010-4655. DOI: 10.1016/0010-4655(80)90102-2 (cit. on p. 13).

[137] Tim Pillards and Ronald Cools. “Using Box-Muller with Low Discrepancy Points”. In: *Computational Science and Its Applications - ICCSA 2006*. Ed. by Marina L. Gavrilova et al. Berlin, Heidelberg: Springer Berlin Heidelberg, 2006, pp. 780–788. ISBN: 978-3-540-34080-5 (cit. on p. 139).

[138] William H. Press et al. *Numerical Recipes 3rd Edition: The Art of Scientific Computing*. Cambridge university press, 2007 (cit. on p. 168).

[139] Dominik Prossel and Uwe D. Hanebeck. “Dirac Mixture Reduction Using Wasserstein Distances on Projected Cumulative Distributions”. In: *Proceedings of the 25th International Conference on Information Fusion (Fusion 2022)*. Linköping, Sweden, July 2022. DOI: 10.23919/FUSION49751.2022.9841285 (cit. on pp. 16, 39).

[140] Robert James Purser. *Generalized Fibonacci Grids; A New Class of Structured, Smoothly Adaptive Multi-Dimensional Computational Lattices*. May 2008 (cit. on pp. 74, 75, 82–84, 86, 140, 167, 207).

[141] Abolfazl Rahimnejad, S. Andrew Gadsden, and Mohammad Al-Shabi. “Lattice Kalman Filters”. In: *IEEE Signal Processing Letters* 28 (2021). Conference Name: IEEE Signal Processing Letters, pp. 1355–1359. ISSN: 1558-2361. DOI: 10.1109/LSP.2021.3089935 (cit. on p. 140).

[142] George N. Raney. “Generalization of the Fibonacci Sequence to n Dimensions”. en. In: *Canadian Journal of Mathematics* 18 (1966). Publisher: Cambridge University Press, pp. 332–349. ISSN: 1496-4279. DOI: 10.4153/CJM-1966-036-0 (cit. on p. 82).

[143] J. Revels, M. Lubin, and T. Papamarkou. “Forward-Mode Automatic Differentiation in Julia”. In: *arXiv* (2016). ISSN: arXiv:1607.07892 [cs.MS] (cit. on p. 100).

[144] J. N. Ridley. “Packing Efficiency in Sunflower Heads”. In: *Mathematical Biosciences* 58.1 (1982), pp. 129–139. ISSN: 0025-5564 (cit. on p. 59).

[145] Branko Ristic, Sanjeev Arulampalam, and Neil J. Gordon. “Beyond the Kalman Filter: Particle Filters for Tracking Applications”. In: 2004 (cit. on p. 3).

[146] Martin Roberts. “The Unreasonable Effectiveness of Quasirandom Sequences”. In: *Extreme Learning* (2018), pp. 04–25 (cit. on p. 62).

[147] Claude Ambrose Rogers. “Packing and Covering”. In: *Cambridge Tracts in Mathematics and Mathematical Physics* 8.54 (1964), pp. 1–111. ISSN: 0068-6824 (cit. on pp. 92, 93).

[148] Murray Rosenblatt. “Remarks on a Multivariate Transformation”. In: *Selected Works of Murray Rosenblatt*. Ed. by Richard A. Davis, Keh-Shin Lii, and Dimitris N. Politis. Selected Works in Probability and Statistics book series (SWPS). New York, NY: Springer New York, 2011. Chap. 15, pp. 49–51. ISBN: 978-1-4419-8339-8. DOI: 10.1007/978-1-4419-8339-8_8 (cit. on p. 151).

[149] Michael Roth, Gustaf Hendeby, and Fredrik Gustafsson. “Nonlinear Kalman Filters Explained: A Tutorial on Moment Computations and Sigma Point Methods”. In: *Journal of Advances in Information Fusion* 11.1 (2016). Publisher: International society of information fusion, pp. 47–70 (cit. on p. 16).

[150] Reuven Y. Rubinstein and Ruth Marcus. “Efficiency of Multivariate Control Variates in Monte Carlo Simulation”. In: *Operations Research* 33.3 (1985), pp. 661–677. DOI: 10.1287/opre.33.3.661 (cit. on p. 16).

[151] József Sándor, Dragoslav S. Mitrinović, and Borislav Crstici. “Euler’s Φ-Function”. In: *Handbook of Number Theory I*. Vol. 351. Mathematics and Its Applications. Dordrecht: Springer Netherlands, 2006, pp. 9–37. ISBN: 978-1-4020-3658-3. DOI: 10.1007/1-4020-3658-2_1 (cit. on p. 56).

[152] Lawrence F. Shampine. “Matlab Program for Quadrature in 2D”. In: *Applied Mathematics and Computation* 202.1 (2008), pp. 266–274 (cit. on p. 167).

[153] George Shan and Mark J. van der Laan. “Targeted Estimation of L2 Distance Between Densities and its Application to Geo-Spatial Data”. In: *arXiv preprint* (2019). ISSN: arXiv:1905.13414 (cit. on p. 24).

[154] Peter Shirley. “Discrepancy as a Quality Measure for Sample Distributions”. In: *EG 1991-Technical Papers*. Eurographics Association, 1991. DOI: 10.2312/egtp.19911013 (cit. on p. 140).

[155] Paul B. Slater. “Numerical and Exact Analyses of Bures and Hilbert-Schmidt Separability and PPT Probabilities”. In: *Quantum Information Processing* 18.10 (2019), p. 312. ISSN: 1573-1332. DOI: 10.1007/s11128-019-2431-2 (cit. on p. 62).

[156] Ian H. Sloan. “Lattice Methods for Multiple Integration”. In: *Journal of Computational and Applied Mathematics* 12 (1985), pp. 131–143 (cit. on p. 16).

[157] John Parr Snyder. *Map Projections–A Working Manual*. Vol. 1395. U.S. Geological Survey Professional Paper. Washington, D.C.: US Government Printing Office, 1987. DOI: https://doi.org/10.3133/pp1395 (cit. on pp. 152–154).

[158] I.M. Sobol. "Uniformly Distributed Sequences with an Additional Uniform Property". In: *USSR Computational Mathematics and Mathematical Physics* 16.5 (1976), pp. 236–242. ISSN: 0041-5553. DOI: https://doi.org/10.1016/0041-5553(76)90154-3 (cit. on pp. 17, 200).

[159] N. M. Steen, G. D. Byrne, and E. M. Gelbard. "Gaussian Quadratures for the Integrals $\int_0^\infty \exp(-x^2) f(x)dx$ and $\int_0^b \exp(-x^2) f(x)dx$". In: *Mathematics of Computation* 23.107 (1969), pp. 661–671 (cit. on p. 12).

[160] Jannik Steinbring. *Nonlinear Estimation Toolbox* (cit. on p. 180).

[161] Jannik Steinbring and Uwe D. Hanebeck. "S2KF: The Smart Sampling Kalman Filter". In: *Proceedings of the 16th International Conference on Information Fusion (Fusion 2013)*. Istanbul, Turkey, July 2013 (cit. on p. 13).

[162] Jannik Steinbring and Uwe D. Hanebeck. "LRKF Revisited: The Smart Sampling Kalman Filter (S2KF)". In: *Journal of Advances in Information Fusion* 9.2 (Dec. 2014), pp. 106–123 (cit. on pp. 13, 16, 34).

[163] Jannik Steinbring and Uwe D. Hanebeck. "Progressive Gaussian Filtering Using Explicit Likelihoods". In: *Proceedings of the 17th International Conference on Information Fusion (Fusion 2014)*. Salamanca, Spain, July 2014 (cit. on p. 34).

[164] Jannik Steinbring, Martin Pander, and Uwe D. Hanebeck. "The Smart Sampling Kalman Filter with Symmetric Samples". In: *Journal of Advances in Information Fusion* 11.1 (June 2016), pp. 71–90 (cit. on pp. 13, 16, 34, 180).

[165] Universität Stuttgart. *Logo der Universität Stuttgart*. [Online; accessed 25-October-2023]. 2023 (cit. on p. 4).

[166] Kosuke Suzuki and Takehito Yoshiki. "Enumeration of the Chebyshev-Frolov Lattice Points in Axis-Parallel Boxes". In: *Hiroshima Mathematical Journal* 49.1 (2019), pp. 139–159. DOI: 10.32917/hmj/1554516041 (cit. on p. 55).

[167] Richard Swinbank and R. James Purser. “Fibonacci Grids: A Novel Approach to Global Modelling”. In: *Quarterly Journal of the Royal Meteorological Society* 132.619 (2006), pp. 1769–1793 (cit. on pp. 156, 158, 163).

[168] Jacek Szelazek. “Application of Subsurface Laser Engraving in Utrasonic Testing of Materials”. In: *11th European Conference on Non-Destructive Testing (ECNDT 2014)*. Vol. 19. e-Journal of Nondestructive Testing 12. Oct. 2014 (cit. on p. 6).

[169] Surya T. Tokdar and Robert E. Kass. “Importance Sampling: A Review”. In: *WIREs Computational Statistics* 2.1 (2010), pp. 54–60. DOI: 10.1002/wics.56 (cit. on p. 16).

[170] Ilan Vardi. *Computational Recreations in Mathematica*. Addison Wesley Longman Publishing Co., Inc., 1991 (cit. on p. 100).

[171] Eric A. Wan and Rudolph Van Der Merwe. “The Unscented Kalman Filter for Nonlinear Estimation”. In: *Proceedings of the IEEE 2000 Adaptive Systems for Signal Processing, Communications, and Control Symposium (Cat. No. 00EX373)*. Ieee. 2000, pp. 153–158 (cit. on p. 12).

[172] Tony T. Warnock. “Computational Investigations of Low-Discrepancy Point Sets”. In: *Applications of Number Theory to Numerical Analysis*. Ed. by S. K. Zaremba. Academic Press, 1972, pp. 319–343. ISBN: 978-0-12-775950-0. DOI: https://doi.org/10.1016/B978-0-12-775950-0.50015-7 (cit. on p. 90).

[173] Eric W. Weisstein. *Farey Sequence. From MathWorld–A Wolfram Web Resource*. Online. Visited on 07/06/2023 (cit. on p. 100).

[174] Hermann Weyl. “Über die Gleichverteilung von Zahlen mod. Eins”. In: *Mathematische Annalen* 77.3 (1916), pp. 313–352. ISSN: 1432-1807. DOI: 10.1007/BF01475864 (cit. on p. 49).

[175] Brian E. White. “On Optimal Extreme-Discrepancy Point Sets in the Square”. In: *Numerische Mathematik* 27.2 (1977), pp. 157–164. ISSN: 0945-3245. DOI: 10.1007/BF01396635 (cit. on p. 98).

[176] Jin Wu et al. “Fast Linear Quaternion Attitude Estimator Using Vector Observations”. In: *IEEE Transactions on Automation Science and Engineering* 15.1 (2018), pp. 307–319. DOI: 10.1109/TASE.2017.2699221 (cit. on p. 15).

[177] Stanisław K. Zaremba. “A Remarkable Lattice Generated by Fibonacci Numbers”. In: *Fibonacci Quarterly* 8.2 (1970), pp. 185–198 (cit. on p. 58).

[178] Eberhard Zeidler. “Wichtige Formeln, Graphische Darstellungen und Tabellen”. In: *Springer-Taschenbuch der Mathematik: Begründet von I.N. Bronstein und K.A. Semendjaew Weitergeführt von G. Grosche, V. Ziegler und D. Ziegler Herausgegeben von E. Zeidler*. Ed. by Eberhard Zeidler. Wiesbaden: Springer Fachmedien Wiesbaden, 2013, pp. 3–213. ISBN: 978-3-8348-2359-5. DOI: 10.1007/978-3-8348-2359-5_1 (cit. on p. 159).

Author's Publications

[O1] Daniel Frisch and Uwe D. Hanebeck. "Efficient Deterministic Conditional Sampling of Multivariate Gaussian Densities". In: *Proceedings of the 2020 IEEE International Conference on Multisensor Fusion and Integration for Intelligent Systems (MFI 2020)*. Virtual, Sept. 2020. DOI: 10.1109/MFI49285.2020.9235212 (cit. on pp. 33–35, 207).

[O2] Daniel Frisch and Uwe D. Hanebeck. "Progressive Bayesian Filtering with Coupled Gaussian and Dirac Mixtures". In: *Proceedings of the 23rd International Conference on Information Fusion (Fusion 2020)*. Virtual, July 2020. DOI: 10.23919/FUSION45008.2020.9190540 (cit. on p. 3).

[O3] Daniel Frisch and Uwe D. Hanebeck. "Deterministic Gaussian Sampling With Generalized Fibonacci Grids". In: *Proceedings of the 24th International Conference on Information Fusion (Fusion 2021)*. Sun City, South Africa, Nov. 2021. DOI: 10.23919/FUSION49465.2021.9626975 (cit. on pp. 12, 152, 207).

[O4] Daniel Frisch and Uwe D. Hanebeck. "Deterministic Sampling on the Circle Using Projected Cumulative Distributions". In: *Proceedings of the 25th International Conference on Information Fusion (Fusion 2022)*. Linköping, Sweden, July 2022. DOI: 10.23919/FUSION49751.2022.9841299 (cit. on pp. 38, 39).

[O5] Daniel Frisch and Uwe D. Hanebeck. "Rejection Sampling from Arbitrary Multivariate Distributions Using Generalized Fibonacci Lattices". In: *Proceedings of the 25th International Conference on Information Fusion (Fusion 2022)*. Linköping, Sweden, July 2022. DOI: 10.23919/FUSION49751.2022.9841322 (cit. on pp. 54, 164–166, 208).

[O6] Daniel Frisch and Uwe D. Hanebeck. "Deterministic Sampling of Arbitrary Densities Using Equal Sphere Packing of Volume under the Density (PoVuD)". In: *Proceedings of the 26th International Conference on Information Fusion (Fusion 2023)*. Charleston, USA, June 2023. DOI: 10.23919/FUSION52260.2023.10224093 (cit. on pp. 42, 208).

[O7] Daniel Frisch and Uwe D. Hanebeck. "Deterministic Von Mises-Fisher Sampling on the Sphere Using Fibonacci Lattices". In: *Proceedings of the combined IEEE 2023 Symposium Sensor Data Fusion and International Conference on Multisensor Fusion and Integration (SDF-MFI 2023)*. Bonn, Germany, Nov. 2023. DOI: 10.1109/SDF-MFI59545.2023.10361396 (cit. on pp. 162, 207).

[O8] Daniel Frisch and Uwe D. Hanebeck. "The Generalized Fibonacci Grid as Low-Discrepancy Point Set for Optimal Deterministic Gaussian Sampling". In: *Journal of Advances in Information Fusion* 18.1 (June 2023), pp. 16–34. ISSN: 1557-6418 (cit. on pp. 12, 54, 55, 152, 207).

[O9] Daniel Frisch, Kailai Li, and Uwe D. Hanebeck. "Optimal Reduction of Dirac Mixture Densities on the 2-Sphere". In: *Proceedings of the 1st Virtual IFAC World Congress (IFAC-V 2020)*. July 2020. DOI: 10.1016/j.ifacol.2020.12.1856 (cit. on pp. 16, 28–32, 208).

[O10] Kailai Li et al. "Geometry-Driven Deterministic Sampling for Nonlinear Bingham Filtering". In: *Proceedings of the 2019 European Control Conference (ECC 2019)*. Naples, Italy, June 2019. DOI: 10.23919/ECC.2019.8796102 (cit. on pp. 12, 15).